

Aus dem Institut für Molekular- und Zellbiologie der Hochschule Mannheim  
(Direktor: Prof. Dr. rer. nat. Mathias Hafner)

**Glyco-engineered HEK 293-F cell lines to produce therapeutic  
glycoproteins with human *N*-glycosylation and improved pharmacokinetics**

Inauguraldissertation  
zur Erlangung des Doctor scientiarum humanarum (Dr. sc. hum.)  
an der  
Medizinischen Fakultät Mannheim  
der  
Ruprecht-Karls-Universität  
zu  
Heidelberg

vorgelegt von  
Rico Uhler  
aus  
Sinsheim

2021

Dekan: Prof. Dr. med. Sergij Goerd

Referent: Prof. Dr. rer. nat. Mathias Hafner

## TABLE OF CONTENTS

|        |                                                                                         |    |
|--------|-----------------------------------------------------------------------------------------|----|
| 1      | ABBREVIATIONS.....                                                                      | 1  |
| 2      | INTRODUCTION.....                                                                       | 4  |
| 2.1    | Biopharmaceuticals .....                                                                | 4  |
| 2.2    | <i>N</i> -glycosylation .....                                                           | 4  |
| 2.3    | Receptor-mediated clearance of glycosylated proteins .....                              | 6  |
| 2.4    | Expression systems for recombinant protein therapeutics.....                            | 6  |
| 2.5    | The HEK 293-F expression system.....                                                    | 7  |
| 2.6    | Strategies to alter the <i>N</i> -glycosylation of HEK 293-F cell-derived proteins..... | 8  |
| 2.6.1  | Abolishing <i>N</i> -glycan GalNAc by gene knock-out.....                               | 8  |
| 2.6.2  | Increasing sialylation by gene knock-in .....                                           | 8  |
| 2.6.3  | Increasing sialylation by culture medium supplementation .....                          | 9  |
| 2.7    | Coagulation factors.....                                                                | 9  |
| 2.8    | Selection of model proteins FVII-alb, FVIII-BDD and FIX.....                            | 10 |
| 2.9    | Structure and PTMs of coagulation factor VII-albumin.....                               | 10 |
| 2.10   | Structure and PTMs of B domain deleted coagulation factor VIII.....                     | 11 |
| 2.11   | Structure and PTMs of coagulation factor IX .....                                       | 11 |
| 2.12   | Scientific question .....                                                               | 12 |
| 3      | MATERIALS AND METHODS .....                                                             | 13 |
| 3.1    | Materials.....                                                                          | 13 |
| 3.1.1  | Plasmids.....                                                                           | 13 |
| 3.1.2  | Gene constructs .....                                                                   | 15 |
| 3.1.3  | Oligonucleotides.....                                                                   | 16 |
| 3.1.4  | Bacteria and cell lines.....                                                            | 20 |
| 3.1.5  | Laboratory animals.....                                                                 | 24 |
| 3.1.6  | Standards .....                                                                         | 25 |
| 3.1.7  | Enzymes and proteins.....                                                               | 25 |
| 3.1.8  | Kits .....                                                                              | 26 |
| 3.1.9  | Chemicals .....                                                                         | 26 |
| 3.1.10 | Media and supplements .....                                                             | 27 |
| 3.1.11 | Buffers .....                                                                           | 28 |
| 3.1.12 | Consumables .....                                                                       | 29 |
| 3.1.13 | Devices .....                                                                           | 31 |
| 3.1.14 | Software.....                                                                           | 33 |
| 3.2    | Methods.....                                                                            | 33 |
| 3.2.1  | Microbiology and molecular biology methods.....                                         | 33 |
| 3.2.2  | Mammalian cell culture methods .....                                                    | 44 |
| 3.2.3  | Protein biochemistry methods .....                                                      | 47 |
| 3.2.4  | Pharmacokinetic rat experiment .....                                                    | 51 |
| 4      | RESULTS.....                                                                            | 53 |
| 4.1    | Generation of host cell lines overexpressing different sialyltransferases.....          | 53 |
| 4.1.1  | Characterization of the AAVS1 integration site.....                                     | 53 |
| 4.1.2  | Generation of pools stably overexpressing sialyltransferases .....                      | 54 |
| 4.1.3  | Characterization of pools stably overexpressing sialyltransferases.....                 | 56 |
| 4.1.4  | Generation of clones from <i>ST6GAL1</i> overexpressing pools.....                      | 58 |
| 4.1.5  | Characterization of clones overexpressing <i>ST6GAL1</i> .....                          | 59 |
| 4.2    | Generation and evaluation of cell lines expressing model proteins .....                 | 63 |
| 4.2.1  | Generation of cell lines expressing model proteins.....                                 | 63 |

|       |                                                                                            |     |
|-------|--------------------------------------------------------------------------------------------|-----|
| 4.2.2 | Characterization of cell lines expressing model proteins .....                             | 64  |
| 4.2.3 | Selection of cell lines for protein expression.....                                        | 65  |
| 4.3   | Production and purification of model proteins .....                                        | 67  |
| 4.3.1 | Production of model proteins .....                                                         | 67  |
| 4.3.2 | Purification of model proteins .....                                                       | 67  |
| 4.3.3 | Activation of FVII and FVII-alb for the pharmacokinetic rat experiment .....               | 69  |
| 4.4   | Establishment of the glycosylation analysis methods .....                                  | 70  |
| 4.4.1 | Identification of released monosaccharides.....                                            | 70  |
| 4.4.2 | Identification of <i>N</i> -glycans in <i>N</i> -glycan profiles .....                     | 71  |
| 4.4.3 | Matching identified <i>N</i> -glycans to HILIC fluorescence chromatogram peaks .....       | 81  |
| 4.4.4 | Reproducibility and comparability of glycosylation analysis methods .....                  | 86  |
| 4.5   | <i>N</i> -glycosylation analysis of glyco-engineered FVII-alb.....                         | 87  |
| 4.5.1 | Evaluation of GalNAc-transferase knock-out .....                                           | 88  |
| 4.5.2 | Evaluation of sialyltransferase overexpression .....                                       | 90  |
| 4.5.3 | Comparison of <i>ST6GALI</i> knock-in pools and clones.....                                | 94  |
| 4.5.4 | Evaluation of sialic acid metabolism precursor supplementation .....                       | 97  |
| 4.6   | Comparison of FVII-alb, FVIII-BDD and FIX <i>N</i> -glycans .....                          | 102 |
| 4.7   | Analysis of ASGP-R and MR binding of glyco-engineered FVII-alb .....                       | 106 |
| 4.7.1 | Reproducibility of glycan-receptor-binding experiments.....                                | 106 |
| 4.7.2 | Evaluation of GalNAc-transferase knock-out .....                                           | 107 |
| 4.7.3 | Evaluation of sialyltransferase overexpression .....                                       | 108 |
| 4.8   | Evaluation of pharmacokinetic properties of glyco-engineered FVII-alb .....                | 109 |
| 4.8.1 | Recovery.....                                                                              | 110 |
| 4.8.2 | Half-life .....                                                                            | 110 |
| 4.8.3 | Area under the curve .....                                                                 | 111 |
| 5     | DISCUSSION .....                                                                           | 112 |
| 5.1   | Evidence for sulfated GalNAc on FVII-alb <i>N</i> -glycans .....                           | 112 |
| 5.2   | The desired <i>N</i> -glycosylation of FVII-alb can be achieved by glyco-engineering ..... | 112 |
| 5.2.1 | Knock-out of <i>B4GALNT3</i> and <i>B4GALNT4</i> abolishes <i>N</i> -glycan GalNAc .....   | 112 |
| 5.2.2 | Knock-in of sialyltransferases improves sialylation.....                                   | 113 |
| 5.2.3 | The choice of clone can impact the <i>N</i> -glycosylation of the therapeutic protein..... | 115 |
| 5.2.4 | Sialic acid metabolism precursor supplementation does not improve sialylation.....         | 115 |
| 5.3   | The used glyco-engineering approach is applicable to other proteins.....                   | 116 |
| 5.4   | Sialyltransferase activity is the limiting factor for sialylation in HEK 293 cells .....   | 116 |
| 5.5   | Glyco-engineering can reduce <i>N</i> -glycan heterogeneity.....                           | 117 |
| 5.6   | Glyco-engineered FVII-albumin binds less to ASGP-R and MR .....                            | 117 |
| 5.7   | Glyco-engineered FVII-alb variants have improved pharmacokinetic properties.....           | 118 |
| 5.8   | Fused albumin improves pharmacokinetic properties by reducing receptor binding.....        | 118 |
| 5.9   | Conclusion.....                                                                            | 119 |
| 6     | SUMMARY .....                                                                              | 120 |
| 7     | ZUSAMMENFASSUNG .....                                                                      | 121 |
| 8     | REFERENCES .....                                                                           | 122 |
| 9     | ACKNOWLEDGEMENTS .....                                                                     | 143 |

## 1 ABBREVIATIONS

|                         |                                                                                       |
|-------------------------|---------------------------------------------------------------------------------------|
| <b>24-dwp</b>           | 24-deep-well plate                                                                    |
| <b>24-wp</b>            | 24-well plate                                                                         |
| <b>96-wp</b>            | 96-well plate                                                                         |
| <b>A230</b>             | absorption at wavelength 230 nm                                                       |
| <b>A260</b>             | absorption at wavelength 260 nm                                                       |
| <b>A280</b>             | absorption at wavelength 280 nm                                                       |
| <b>AA</b>               | amino acid                                                                            |
| <b>AAV</b>              | adeno-associated virus                                                                |
| <b>ASGP-R</b>           | asialoglycoprotein receptor                                                           |
| <b>AUC</b>              | area under the curve                                                                  |
| <b>B4GALNT3</b>         | beta 1,4- <i>N</i> -acetylgalactosaminyltransferase 3                                 |
| <b>B4GALNT4</b>         | beta 1,4- <i>N</i> -acetylgalactosaminyltransferase 4                                 |
| <b>BHK</b>              | baby hamster kidney                                                                   |
| <b>bis-GlcNAc</b>       | bisecting GlcNAc                                                                      |
| <b>c</b>                | cell                                                                                  |
| <b>cDNA</b>             | complementary DNA                                                                     |
| <b>CHO</b>              | chinese hamster ovary                                                                 |
| <b>CHST8</b>            | carbohydrate sulfotransferase 8                                                       |
| <b>CHST9</b>            | carbohydrate sulfotransferase 9                                                       |
| <b>CL</b>               | clone                                                                                 |
| <b>CMP-sialic acid</b>  | cytidine monophosphate <i>N</i> -acetylneuraminic acid                                |
| <b>CRISPR/Cas9</b>      | clustered regularly interspaced short palindromic repeats/CRISPR-associated protein 9 |
| <b>CSP</b>              | cell-specific productivity                                                            |
| <b>CT</b>               | C-terminal                                                                            |
| <b>Ct</b>               | cycle threshold                                                                       |
| <b>CV</b>               | column volume                                                                         |
| <b>Da</b>               | Dalton                                                                                |
| <b>dCt</b>              | delta Ct                                                                              |
| <b>ddCt</b>             | delta delta Ct                                                                        |
| <b>ddH<sub>2</sub>O</b> | laboratory grade water                                                                |
| <b>Div</b>              | divisions                                                                             |
| <b>DMB</b>              | 1,2-diamino-4,5-methylenedioxybenzene                                                 |
| <b>dPCR</b>             | digital PCR                                                                           |
| <b>DSB</b>              | double strand break                                                                   |
| <b>EDTA</b>             | ethylenediaminetetraacetic acid                                                       |
| <b>ELISA</b>            | enzyme-linked immunosorbent assay                                                     |
| <b>ER</b>               | endoplasmatic reticulum                                                               |
| <b>FAM</b>              | 6-carboxyfluorescein                                                                  |
| <b>FC</b>               | fold-change                                                                           |
| <b>FcRn</b>             | neonatal Fc receptor                                                                  |
| <b>FIX</b>              | coagulation factor IX                                                                 |
| <b>FucT</b>             | $\alpha$ 1,3/4-fucosyltransferase                                                     |
| <b>FUT10</b>            | fucosyltransferase 10                                                                 |
| <b>FUT11</b>            | fucosyltransferase 11                                                                 |
| <b>FUT4</b>             | fucosyltransferase 4                                                                  |
| <b>FUT8</b>             | fucosyltransferase 8                                                                  |

|                  |                                                                                                           |
|------------------|-----------------------------------------------------------------------------------------------------------|
| <b>FVII</b>      | coagulation factor VII                                                                                    |
| <b>FVIIa</b>     | activated coagulation factor VII                                                                          |
| <b>FVII-alb</b>  | FVII human serum albumin fusion protein                                                                   |
| <b>FVIII</b>     | coagulation factor VIII                                                                                   |
| <b>FVIII-BDD</b> | B-domain-deleted FVIII                                                                                    |
| <b>GalNAc</b>    | <i>N</i> -acetylgalactosamine                                                                             |
| <b>GalNAcT</b>   | GalNAc transferase                                                                                        |
| <b>GalT</b>      | galactosyltransferase                                                                                     |
| <b>GlcNAc</b>    | <i>N</i> -acetylglucosamine                                                                               |
| <b>GOI</b>       | gene of interest                                                                                          |
| <b>gRNA</b>      | guide RNA                                                                                                 |
| <b>GU</b>        | glucose units                                                                                             |
| <b>HA-L</b>      | left homology arm                                                                                         |
| <b>HA-R</b>      | right homology arm                                                                                        |
| <b>HC</b>        | heavy chain                                                                                               |
| <b>HCP</b>       | host cell protein                                                                                         |
| <b>HDR</b>       | homology directed repair                                                                                  |
| <b>HEK 293</b>   | human embryonic kidney 293                                                                                |
| <b>HEK 293-F</b> | human embryonic kidney FreeStyle 293-F                                                                    |
| <b>HEPES</b>     | 4-(2-hydroxyethyl)-1-piperazineethanesulfonic acid                                                        |
| <b>HILIC</b>     | hydrophobic interaction liquid chromatography                                                             |
| <b>HSA</b>       | human serum albumin                                                                                       |
| <b>HygR</b>      | hygromycin B resistance gene                                                                              |
| <b>indels</b>    | insertions or deletions                                                                                   |
| <b>kb</b>        | kilobasepairs                                                                                             |
| <b>kDa</b>       | kilodalton                                                                                                |
| <b>KI</b>        | knock-in                                                                                                  |
| <b>KO</b>        | knock-out                                                                                                 |
| <b>LC</b>        | light chain                                                                                               |
| <b>LC-MS</b>     | liquid chromatography mass spectrometry                                                                   |
| <b>M</b>         | DNA ladder                                                                                                |
| <b>m/z</b>       | mass per charge                                                                                           |
| <b>ManNAc</b>    | <i>N</i> -acetylmannosamine                                                                               |
| <b>MGAT1</b>     | <i>N</i> -acetylglucosaminyltransferase I                                                                 |
| <b>MGAT2</b>     | <i>N</i> -acetylglucosaminyltransferase II                                                                |
| <b>MGAT3</b>     | <i>N</i> -acetylglucosaminyltransferase III                                                               |
| <b>MGAT4</b>     | <i>N</i> -acetylglucosaminyltransferase IV                                                                |
| <b>MGAT5</b>     | <i>N</i> -acetylglucosaminyltransferase V                                                                 |
| <b>M-KI</b>      | integration of multiple donor plasmid copies in a single AAVS1 integration site                           |
| <b>MR</b>        | mannose receptor                                                                                          |
| <b>MW</b>        | molecular weight                                                                                          |
| <b>Neu5Ac</b>    | <i>N</i> -acetylneuraminic acid                                                                           |
| <b>Neu5Gc</b>    | <i>N</i> -glycolylneuraminic acid                                                                         |
| <b>NHEJ</b>      | non-homologous end joining                                                                                |
| <b>NT</b>        | <i>N</i> -terminal                                                                                        |
| <b>NTC</b>       | no-template control                                                                                       |
| <b>PAPAP</b>     | rigid linker consisting of six repeats of the amino acid sequence proline-alanine-proline-alanine-proline |

|                                |                                                                         |
|--------------------------------|-------------------------------------------------------------------------|
| <b>PCR</b>                     | polymerase chain reaction                                               |
| <b>PK</b>                      | pharmacokinetic                                                         |
| <b>pmol</b>                    | picomoles                                                               |
| <b>PTM</b>                     | post-translational modification                                         |
| <b>RI</b>                      | random integration                                                      |
| <b>RNP</b>                     | ribonucleoprotein particle                                              |
| <b>rpm</b>                     | revolutions per minute                                                  |
| <b>rSAP</b>                    | recombinant shrimp alkaline phosphatase                                 |
| <b>RT-qPCR</b>                 | quantitative reverse transcription real-time PCR                        |
| <b>SDS-PAGE</b>                | sodium dodecyl sulfate polyacrylamide gel electrophoresis               |
| <b>SiaT</b>                    | sialyltransferase                                                       |
| <b>S-KI</b>                    | integration of a single donor plasmid copy in an AAVS1 integration site |
| <b>SP</b>                      | stable pool                                                             |
| <b>SPR</b>                     | surface plasmon resonance                                               |
| <b>ST3GAL6</b>                 | ST3 beta-galactoside alpha-2,3-sialyltransferase 6                      |
| <b>ST3GAL6_sol</b>             | soluble version of ST6GAL1                                              |
| <b>ST6GAL1</b>                 | ST6 beta-galactoside alpha-2,6-sialyltransferase 1                      |
| <b>ST6GAL1_sol</b>             | soluble version of ST6GAL1                                              |
| <b>UHPLC</b>                   | ultra-high performance liquid chromatography                            |
| <b>v/v</b>                     | volume per volume                                                       |
| <b>VIC</b>                     | 2'-chloro-7'phenyl-1,4-dichloro-6-carboxy-fluorescein                   |
| <b>vit K</b>                   | vitamin K                                                               |
| <b>wt</b>                      | wild-type                                                               |
| <b>xg</b>                      | times gravity                                                           |
| <b><math>\alpha</math>-Gal</b> | Galactose- $\alpha$ -1,3-galactose                                      |

## 2 INTRODUCTION

### 2.1 Biopharmaceuticals

Biopharmaceuticals are drug products that are derived from biologic sources. They can be extracted from living systems (e.g. whole organs, tissues, cells, blood, or blood components) or produced by recombinant DNA technology (e.g. proteins, sugars, nucleic acids, gene therapies).

The market for biopharmaceuticals has been growing constantly for the past 30 years. While before 1995, there were only 25 approved products in the US and Europe, the number of newly approved products surged to more than 50 in each five-year period between 1995 and 2014.<sup>1</sup> And in only three and a half years from January 2015 to July 2018 it nearly doubled to 112 approvals.<sup>2</sup> Furthermore, from January 2014 to July 2018, 47% of the approved drugs with new molecular entities were biopharmaceuticals,<sup>2</sup> as compared to only 26% between January 2010 and July 2014.<sup>1</sup> These numbers emphasize the importance of the biopharmaceutical market, as does the total sales value of all biopharmaceutical products, which increased from \$94 billion in 2007<sup>3</sup> to \$140 billion in 2013<sup>1</sup> and to \$188 billion in 2017<sup>2</sup>, making it the fastest growing segment in the pharmaceutical industry. In this segment, protein therapeutics are the most important group, comprising the 20 top-selling biopharmaceuticals in 2017.<sup>2</sup>

The development and production of protein therapeutics is laborious and very cost-intensive.<sup>4</sup> Accordingly, as illustrated by the annual sales values of these products,<sup>2</sup> the therapies lead to high costs for patients and healthcare systems worldwide. For example, annual treatment costs for antibody therapeutics like Herceptin® or Remicade® can go up to \$35,000, making them some of the most expensive pharmaceuticals.<sup>4</sup> Similarly, hemophilia A treatment for a single patient costs between \$30,000 and several hundred thousand dollars per year, with lifetime costs in the millions.<sup>5</sup>

In some cases the cost of treatment is further increased by adverse events,<sup>6–10</sup> low efficacy or unfavorable pharmacokinetic (PK) properties of the protein,<sup>7,11–14</sup> all of which may result from unfavorable post-translational modifications (PTM). Therefore, developing therapeutic proteins with more favorable PTMs aims at providing safer and more efficacious therapeutic proteins to patients. Since PTMs are highly dependent on the expression system used to produce the therapeutic protein,<sup>15–18</sup> the development of more suitable expression systems paves the way for relieving patients and healthcare systems alike.

### 2.2 N-glycosylation

In that regard, *N*-glycosylation is an especially important PTM, since it is highly prevalent on therapeutic proteins<sup>19</sup> and can influence their biologic activity<sup>20–22</sup>, stability<sup>23,24</sup>, solubility<sup>25,26</sup>, immunogenicity<sup>7,27,28</sup>, and PK properties<sup>7,29,30</sup>. For therapeutic proteins such as tissue plasminogen activator and erythropoietin, for example, *N*-glycosylation can significantly influence activity and plasma half-life.<sup>29,31–33</sup>

*N*-glycosylation begins in the endoplasmic reticulum (ER)—in the presence of the amino acid (AA) recognition sequence asparagine-X-serine/threonine (X=any AA except proline)—by en-bloc transfer of an immature *N*-glycan (Figure 1A) from dolichol phosphate to the respective asparagine residue of the protein. During protein folding in the ER lumen, which is assisted by *N*-glycan-recognizing chaperones, the immature *N*-glycan is further processed (Figure 1B) and proceeds, upon correct folding of the protein, to the *cis*-Golgi.<sup>34</sup> In the *cis*-Golgi, mannosidases trim down the *N*-glycan. However, in some cases where the *N*-glycan is not accessible for the mannosidases (e.g. for human insulin receptor<sup>35</sup>), processing is incomplete, resulting in hybrid or high-mannose *N*-glycans (Figure 1B).<sup>36–38</sup> In the *medial*-Golgi, *N*-acetylglucosaminyltransferases I and II (MGAT1, MGAT2) add *N*-acetylglucosamine (GlcNAc) to one or both core mannose residues to initiate hybrid (Figure 1C) and complex *N*-glycan



formation, respectively (Figure 1D). Subsequently, in the *medial*-Golgi, *trans*-Golgi and *trans*-Golgi network, the *N*-glycan core structure and the GlcNAc antenna of hybrid *N*-glycans mature by the action of various glycosidases and glycosyltransferases.

In mammalian cells, there are several common *N*-glycan maturation steps. A so-called bisecting GlcNAc (bis-GlcNAc) residue can be transferred to the middle mannose of the trimannosyl core of complex *N*-glycans (Figure 1E) by the enzyme *N*-acetylglucosaminyltransferase III (MGAT3) or a fucose residue can be transferred to the asparagine-linked GlcNAc of the *N*-glycan core (so called “core fucose”; Figure 1E-H) by fucosyltransferase 8 (FUT8).<sup>34</sup> Furthermore, complex *N*-glycans can be branched by the enzymes *N*-acetylglucosaminyltransferase IV and V (MGAT4 and MGAT5), resulting in tri- and tetraantennary *N*-glycans (Figure 1E).<sup>34</sup> Antennary GlcNAcs are typically capped by galactose and sialic acid by various galactosyl- (GalT) and sialyltransferases (SiaT; Figure 1F). Sialic acids are predominantly added in  $\alpha$ 2,6-linkage—e.g. by ST6 beta-galactoside alpha-2,6-sialyltransferase 1 (ST6GAL1)—or in  $\alpha$ 2,3 linkage—e.g. by ST3 beta-galactoside alpha-2,3-sialyltransferase 6 (ST3GAL6).<sup>39</sup> In cells expressing beta-1,4-*N*-acetylgalactosaminyltransferase 3 (B4GALNT3) or beta-1,4-*N*-acetylgalactosaminyltransferase 4 (B4GALNT4), GlcNAc can be capped by *N*-acetylgalactosamine (GalNAc) instead of galactose (Figure 1G) if a peptide recognition motif is present on the protein.<sup>40–42</sup> GalNAc may then be processed by ST6GAL1,<sup>43,44</sup> or by either *N*-acetylgalactosamine-specific carbohydrate sulfotransferase 8 (CHST8) or 9 (CHST9),<sup>45</sup> resulting in sialylated or sulfated GalNAc (Figure 1G). Additionally, the subterminal GlcNAc of either Gal $\beta$ 4GlcNAc or GalNAc $\beta$ 4GlcNAc may get fucosylated (Figure 1H) by  $\alpha$ 1,3/4-fucosyltransferases (FucT).<sup>44,46</sup>

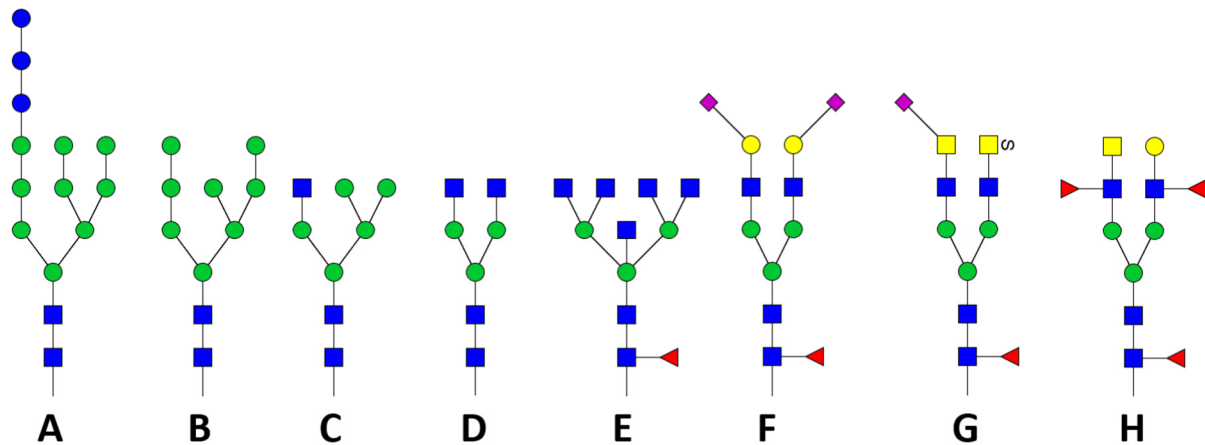


Figure 1: Immature *N*-glycans after en bloc transfer to the protein (A), before entering the *cis*-Golgi—which is also an example for a high-mannose *N*-glycan—(B) and before entering the *trans*-Golgi—which is also an example for a hybrid *N*-glycan (C). Biantennary *N*-glycan core structure (D) and tetraantennary, bisected, core-fucosylated *N*-glycan (E). Mature, core-fucosylated *N*-glycans capped with galactose and  $\alpha$ 2,3 and  $\alpha$ 2,6-linked sialic acids (F),  $\alpha$ 2,6 sialylated and sulfated GalNAc (G) and GalNAc and galactose as well as antennary fucose (H). Glucose: blue circle; Mannose: green circle; galactose: yellow circle; GlcNAc: blue square; GalNAc: yellow square; fucose: red triangle; Neu5Ac: purple diamond (facing left,  $\alpha$ 2,6-linked; facing right,  $\alpha$ 2,3-linked).

This maturation of *N*-glycans is species-<sup>15,16,47</sup> and cell-type-specific<sup>47–50</sup> due to differential expression of glycosidases, glycosyltransferases and glycan transporters,<sup>34</sup> but is also protein-<sup>47</sup> and site-specific<sup>36–38,47</sup> because some glycosyltransferases require a peptide recognition sequence for effective sugar transfer<sup>40–42</sup> or because the *N*-glycosylation site is not or only partially accessible<sup>36–38</sup>. Depending on the order of access of glycosidases and glycosyltransferases, *N*-glycans on a given protein molecule usually

vary, introducing a so-called microheterogeneity. This microheterogeneity also leads to a macroheterogeneity, meaning that different molecules of the same protein—even when produced at the same time in the same cell line—differ, which results in a heterogeneous mixture of molecules.<sup>34,47,49–51</sup> This so-called heterogeneity is the main challenge in *N*-glycan profiling approaches and is considered a risk for patients by regulatory authorities.<sup>51,52</sup>

### 2.3 Receptor-mediated clearance of glycosylated proteins

*N*-glycosylation can influence the PK properties of a therapeutic protein by facilitating receptor-mediated clearance.<sup>32,53–57</sup> The clearance thereby depends on the binding efficiency of the *N*-glycans to the clearance receptor and the abundance of the receptor. Two prominent examples for glycan-specific clearance receptors that are highly abundant in the liver are the asialoglycoprotein receptor (ASGP-R) and the mannose receptor (MR).<sup>30,58–60</sup> The ASGP-R efficiently clears proteins carrying *N*-glycans terminating with galactose and even more so those terminating with GalNAc<sup>61,62</sup>, while sialylation of galactose and GalNAc reduces clearance by the ASGP-R by masking these binding epitopes<sup>30,63,64</sup>. The MR displays a different substrate specificity and clears *N*-glycans with terminal mannose, fucose, GlcNAc,<sup>65–69</sup> and sulfated GalNAc<sup>69–72</sup>.

While *N*-glycan-mediated clearance is necessary for regulating the concentrations of endogenous proteins (e.g. regulating the hypothalamic-pituitary-gonad axis requires rapid clearance of luteinizing hormone via sulfated *N*-glycans<sup>59</sup>), it is usually not desired for therapeutic proteins because it limits the drug's bioavailability and thus its therapeutic effect. Too efficient drug clearance increases required doses and shortens intervals between administrations, which burdens patients and healthcare systems alike. To minimize *N*-glycan-mediated clearance, it is generally desirable to avoid terminal galactose, GalNAc, sulfated GalNAc, mannose, fucose, and GlcNAc residues and to promote sialic acid capping. There are exceptions, since for some proteins clearance is independent of *N*-glycosylation (e.g. certain IgGs<sup>73,74</sup> and coagulation factor VIII [FVIII]<sup>75,76</sup>) and because sialylation seems to impair the antibody-dependent cellular cytotoxicity of IgGs<sup>77</sup>. In any case, due to the manifold protein properties that are influenced by *N*-glycosylation, it is important to consider it as early as possible when developing *N*-glycosylated therapeutic proteins.

### 2.4 Expression systems for recombinant protein therapeutics

Since *N*-glycosylation is highly species-<sup>15,16,47</sup> and cell type-specific<sup>47–50</sup>, the most important variable affecting the *N*-glycosylation of a therapeutic protein is the choice of an expression system. While a range of options exists, they all come with particular strengths and weaknesses (reviewed in references<sup>15–17</sup>). However, most of them to date do not produce adequate *N*-glycosylation. The commonly used bacterial expression systems (e.g. *Escherichia coli*, *Lactobacillus lactis*, *Streptomyces lividans*, and *Pseudomonas aeruginosa*<sup>78</sup>) lack the glycosylation machinery.<sup>16,79,80</sup> Yeasts produce hypermannosylated *N*-glycans that are highly immunogenic in humans and reduce serum half-life through MR clearance.<sup>80–84</sup> Plant expression systems also produce immunogenic *N*-glycans, e.g. xylose as well as  $\alpha$ 1,3-linked fucose at the core GlcNAc, as well as high-mannose and unsialylated *N*-glycans, which are efficiently cleared by IgEs, the MR and the ASGP-R, respectively.<sup>16,80,85,86</sup> In insect cells, paucimannose-type *N*-glycans (Man<sub>3</sub>GlcNAc<sub>2</sub>) predominate and the proteins hence mostly lack galactose and sialic acids, but insect cells also produce the immunogenic fucose in  $\alpha$ 1,3 linkage to the core GlcNAc.<sup>80,87–91</sup> Lastly, transgenic animals produce the nonhuman, immunogenic sialic acid *N*-glycolylneuraminic acid (Neu5Gc) alongside the *N*-acetylneuraminic acid (Neu5Ac) found in humans and, in some cases, the immunogenic galactose- $\alpha$ -1,3-galactose ( $\alpha$ -Gal) epitope.<sup>16,92</sup>

Despite efforts to alter the *N*-glycosylation in those expression systems by glyco-engineering,<sup>79,93–95</sup> mammalian cell lines to date are the predominant expression system for biopharmaceuticals, comprising 79% of the approved products between 2015 and 2018.<sup>2</sup> The most used mammalian cell lines are all of rodent origin and include Chinese hamster ovary (CHO), baby hamster kidney (BHK) and murine myeloma NS0 and Sp2/0.<sup>16,96,97</sup>

However, the *N*-glycans they synthesize can differ from those in human cell lines. For example, CHO and BHK cells lack the enzymes to produce bis-GlcNAc or  $\alpha$ 2,6-linked sialic acids,<sup>98,99</sup> and CHO cells additionally lack  $\alpha$ 1,3/4-fucosyltransferases.<sup>47,100</sup> More significantly, in contrast to human cells,<sup>101,102</sup> the glycan epitopes  $\alpha$ -Gal and Neu5Gc were found on proteins produced in rodent cell lines.<sup>6,103–107</sup> Therefore, humans possess circulating antibodies against these two epitopes,<sup>108,109</sup> which can lead to inferior PK properties and immunologic adverse events when administering proteins carrying them.<sup>7,16,109,110</sup> The so-called “serum sickness” is one example for an immune reaction to Neu5Gc, where antibodies form precipitates with Neu5Gc-containing gangliosides, which results in vascular inflammation.<sup>111,112</sup> Also,  $\alpha$ -Gal-carrying Cetuximab, a monoclonal antibody against epidermal growth factors, caused hypersensitivity reactions against  $\alpha$ -Gal in some patients, which in some cases were even fatal.<sup>6,113</sup> Besides the immunogenicity of these epitopes themselves, they can also trigger the production of antibodies against the protein carrying them,<sup>108,114</sup> which is potentially a factor for the higher risk of anti-drug antibody formation seen in Hemophilia A patients treated with CHO and BHK cell-derived versus plasma- or FreeStyle 293-F (HEK 293-F) cell-derived FVIII.<sup>115–117</sup>

A further reason for using mammalian cell lines for therapeutic protein production is the need for other PTMs that are often required for adequate protein folding, stability, biological activity and PK properties.<sup>118–121</sup> Although PTMs generated by nonhuman mammalian cell lines are often sufficiently human-like, sometimes they are not (reviewed in references<sup>97,122</sup>). For example, coagulation factor IX (FIX) produced in human embryonic kidney 293 (HEK 293) cells had a higher  $\gamma$ -carboxylation and specific activity compared to FIX produced in BHK or CHO cells.<sup>12,123</sup> CHO cells are not able to fully cleave the FIX propeptide<sup>11</sup> and FIX produced in CHO cells had inferior PK properties compared to plasma-derived FIX<sup>14</sup>. Furthermore, protein C produced in CHO cells also lacks sufficient propeptide cleavage and  $\gamma$ -carboxylation for biologic activity, in contrast to the HEK 293-derived protein.<sup>124</sup> FVIII from plasma origin or produced in HEK 293-F cells—in contrast to FVIII produced in CHO and BHK cells—shows complete sulfation of tyrosine 1680,<sup>125</sup> which is required for von Willebrand factor binding<sup>13</sup> and positively affects FVIII half-life<sup>76</sup>.

The described adverse properties of nonhuman PTMs contribute to patients’ suffering and can increase healthcare costs, as showcased by the treatment of patients with FVIII inhibitors.<sup>5,126</sup> These additional costs could be reduced or even avoided by using human cell lines for the production of therapeutic proteins—especially for highly complex coagulation factors with multiple PTMs.<sup>120</sup>

## 2.5 The HEK 293-F expression system

The HEK 293 cell line is a human cell line that is extensively used in both academia and industry. It grows in serum-free suspension culture, is easy to transfect and efficient in transient and stable protein expression.<sup>17,97,127,128</sup> Furthermore, it is accepted by regulatory authorities for the production of marketed therapeutic proteins.<sup>97</sup> The HEK 293-F cell line is a commercially available clonal isolate of the HEK 293 cell line (branded FreeStyle 293-F by Thermo Fisher Scientific) with even faster suspension growth in serum-free medium and increased transfection efficiency as well as protein expression.<sup>97,129</sup> Therefore, the HEK 293-F expression system was used as a starting point for this study.

Besides their human PTMs, HEK 293 cells offer two more significant advantages over nonhuman mammalian cell lines. First, while the karyotype of independent HEK 293 lineages was found to vary notably, clonal cell lines are sufficiently stable<sup>130</sup> in contrast to those of other immortalized cell lines like HeLa or CHO<sup>131,132</sup>. Second, contaminating host cell proteins (HCP) are considered a potential risk in the World Health Organization's guideline for recombinant DNA technology products.<sup>133</sup> Even though HCPs are a problem in all cellular expression systems, nonhuman HCPs pose a greater risk to patients.<sup>9</sup>

However, so far, the *N*-glycosylation generated by HEK 293 cells exhibits two considerable disadvantages. First, GalNAc or sulfated GalNAc, which both cause efficient clearance of proteins by the ASGP-R and MR, respectively, were detected on multiple HEK 293 cell-derived glycoproteins including coagulation factor VII (FVII)<sup>49</sup>, FVIII<sup>125</sup>, low density lipoprotein receptor homolog SorLA/LR11<sup>134</sup>, protein C<sup>135</sup>, L-selectin<sup>136</sup>, erythropoietin<sup>137</sup> and tissue factor pathway inhibitor<sup>138</sup>. Furthermore, sialylation is lower in HEK 293 cell-derived FVII<sup>49</sup>, alpha(1)-proteinase inhibitor<sup>47</sup>, erythropoietin<sup>137</sup>, protein C<sup>135</sup> and cystatin F<sup>139</sup>, compared to the same proteins derived from CHO or BHK cells or from human plasma, which also results in increased ASGP-R-mediated clearance. Therefore, the HEK 293-F cell line was, until now, limited to the production of glycoproteins that are not prone to these *N*-glycan structures.

## **2.6 Strategies to alter the *N*-glycosylation of HEK 293-F cell-derived proteins**

### **2.6.1 Abolishing *N*-glycan GalNAc by gene knock-out**

A strategy to alter the *N*-glycosylation generated by HEK 293-F cells is cell line engineering—also referred to as glyco-engineering.<sup>140–148</sup> One approach to abolish *N*-glycan GalNAc could be a targeted gene knock-out (KO) of the GalNAc-transferases (GalNAcT) B4GALNT3 and B4GALNT4 responsible for the addition of GalNAc to *N*-glycans.<sup>40–42</sup>

Gene KO relies on targeted DNA double strand breaks (DSB), which can be induced by nuclease-based gene editing systems like the clustered regularly interspaced short palindromic repeats/CRISPR-associated protein 9 (CRISPR/Cas9) system.<sup>149</sup> When the DSBs are repaired by the error-prone non-homologous end joining (NHEJ) pathway, random insertions or deletions (indels) can occur, which frequently results in frame-shift mutations.<sup>149</sup> A resulting mRNA often contains premature stop codons and the AA sequence that will be translated from it is totally different to that of the actual protein, resulting in a non-functional protein.<sup>149</sup> After inducing a gene KO, the resulting pool of cells carries diverse indels but also wild-type (wt) alleles, which makes subsequent single-cell cloning necessary to obtain a cell line with the desired genotype. The clones are screened for those in which all alleles of the target gene carry mutations that, after transcription and translation, lead to disruption of the protein function, a so-called functional KO. To evaluate the phenotype exhibited by functional KO clones, model proteins are expressed in them and analyzed.

### **2.6.2 Increasing sialylation by gene knock-in**

The reason for the low sialylation of HEK 293 cell-derived proteins was not clear at the outset. However, in glyco-engineering studies with diverse cell lines, overexpression of SiaTs—which can for example be achieved by targeted gene knock-in (KI)—successfully increased sialylation,<sup>140,146,150–156</sup> indicating that the sialic acid transfer rate was limiting in the used cell lines.

Similar to gene KO, gene KI also relies on targeted DNA DSBs.<sup>149</sup> The homology-directed repair (HDR) pathway requires DNA sequences that are homologous to those near the DSB.<sup>149</sup> If the HDR pathway, instead of the NHEJ pathway, is used, the homologous DNA is inserted at the DSB.<sup>149</sup> By providing a

DNA repair template (e.g. a plasmid), in which the sequence that is to be integrated is flanked by sequences homologous to those near the DSB, the HDR machinery can be exploited for the targeted insertion of a transgene.<sup>157</sup> Selecting a suitable locus of insertion is essential since disruption of an important endogenous gene can harm the cell. Furthermore, selection of a suitable locus of insertion also enables long-term stable expression of the transgene. A suitable safe-harbor locus in human cells is the AAVS1 locus,<sup>158–160</sup> a hotspot for adeno-associated virus (AAV) integration.<sup>161</sup> After inducing a gene KI, cells in which neither targeted nor random integration (RI) of the transgene into the genome took place will not express the transgene, while cells where either took place will express it. Non-expressing cells can be removed from the cell pool by antibiotic selection if a selection marker was part of the DNA repair template.<sup>157</sup> Antibiotic selection then results in a heterogeneous pool of stably overexpressing cells with diverse expression levels.<sup>162–166</sup> While single-cell cloning is essential for the phenotypical assessment of gene KOs, it is dispensable for gene KI since all cells of the stable pool express the transgene to some extent.

### 2.6.3 Increasing sialylation by culture medium supplementation

*N*-glycan sialylation was successfully increased by medium supplementation with the sialic acid metabolism precursors ManNAc<sup>167–170</sup> or cytidine<sup>169</sup>, or by overexpression of genes involved in sialic acid transport and metabolism<sup>144,145,155,171</sup>. This indicates that in those cell lines, cytidine monophosphate *N*-acetylneuraminic acid (CMP-sialic acid)—the substrate of SiaTs<sup>172</sup>—was limiting in the Golgi.

With the strategies in place that induce the desired changes in *N*-glycosylation, the following chapters will deal with the selection of model proteins to test their resulting characteristics with respect to *N*-glycosylation.

## 2.7 Coagulation factors

An important group of biopharmaceuticals are coagulation factors, which are involved in hemostasis. Upon injury—in the first phase of hemostasis—platelets adhere to subendothelial collagen, where they are activated and aggregate into platelet plugs. The resulting procoagulant surface then triggers the coagulation cascade—the second phase of hemostasis. The coagulation cascade in turn is divided in three phases—initiation, amplification and propagation—in which serine proteases (coagulation factors II, VII, IX, X, XI and XII) and cofactors (tissue factor and coagulation factors V and VIII) act together to generate fibrin from fibrinogen, which spontaneously polymerizes to form an insoluble clot of fibrin and platelets. Subsequently, the transglutaminase coagulation factor XIII stabilizes the formed clot by covalently crosslinking fibrin, which ultimately stops the bleeding.<sup>173</sup>

FVIII and FIX are among the most relevant biopharmaceuticals with ten and six products approved in the US, only in the period between 2015 and 2018<sup>2</sup>. The underlying reason for their relevance is that the *FVIII* and *FIX* genes are located on the X chromosome, so that in males—who carry only a single X chromosome—a single mutation can reduce or abolish FVIII or FIX activity. This leads to a relatively high incidence of the X-linked, inherited diseases hemophilia A (1 in 5,000 male births<sup>174</sup>) and B (1 in 30,000 male births<sup>174</sup>) in the male population (compared to not X-linked inherited diseases). Hemophilia A and B are characterized by spontaneous and long-lasting hemorrhage, which is especially problematic when occurring on a regular basis in joints.<sup>174</sup> Plasma-derived or recombinant FVIII or FIX concentrates are used for on demand and long-term prophylactic treatment for hemophilia A and B and this ultimately explains the high number of FVIII and FIX products.<sup>174</sup>

One of the major challenges in the treatment of hemophilia A and B is inhibitor formation, which occurs in around 20-30% of hemophilia A and 1-5% of hemophilia B patients.<sup>175</sup> These inhibitors make patients

widely irresponsive to the treatment with FVIII and FIX,<sup>115,176</sup> and lead to high rates of morbidity and mortality in patients with an otherwise well-treatable disease.<sup>177</sup> To stop bleeding episodes in patients with inhibitors, activated coagulation factor VII (FVIIa) concentrates like NovoSeven®—the benchmark therapeutic which is produced in BHK cells—can be used.<sup>178</sup> Mechanistically, in high doses, FVIIa can by-pass the normal amplification loop in which FIXa and its cofactor FVIII activate FX and generate sufficient FXa for thrombin generation and subsequent fibrin clot formation.<sup>175,179</sup>

## 2.8 Selection of model proteins FVII-alb, FVIII-BDD and FIX

FVII was initially selected as the model protein for this study due to its importance as a by-passing agent in the treatment of hemophilia A and B with inhibitors, but also in the treatment of congenital FVII deficiency, acquired hemophilia and Glanzmann's thrombasthenia.<sup>178,180</sup> However, FVII exhibits a short *in vivo* half-life of 2.6 to 3.0 h,<sup>181–185</sup> which is a significant burden for patients due to the need of multiple intravenous injections,<sup>186</sup> and basically precludes prophylactic treatment regimens.

A strategy that can increase the terminal half-life of proteins is albumin fusion,<sup>187,188</sup> and a fusion of FVII to human serum albumin (FVII-alb) already showed promising half-life of around 6.1 to 9.7 h in clinical trials.<sup>189</sup> The reason for the extended half-life of albumin fusion proteins is the binding of albumin to the neonatal Fc receptor (FcRn).<sup>190–192</sup> When albumin fusion proteins are taken up from the bloodstream into cells, the FcRn binding prevents their degradation and leads to their recycling back into the bloodstream.<sup>190,191</sup> Due to the extended half-life of FVII-alb, this clinically more relevant molecule was selected over FVII as the main model protein for this study. In addition, FVII carries high levels of *N*-glycan GalNAc and little sialylation when produced in wt HEK 293 cells,<sup>49</sup> which gives ample opportunity for improvement via the planned glyco-engineering.

To confirm that the effect of the glyco-engineering is not specific to FVII-alb, but is applicable to other proteins, two additional model proteins—B domain-deleted FVIII (FVIII-BDD) and FIX—were expressed in a subset of the glyco-engineered host cell lines. FVIII-BDD and FIX were selected because they are important biopharmaceuticals, but also because their very different *N*-glycan profiles in comparison to FVII.<sup>48,50,125</sup>

## 2.9 Structure and PTMs of coagulation factor VII-albumin

FVII is a Ca<sup>2+</sup>-dependent serine protease that, in complex with its cofactor tissue factor, activates FX to generate FXa in the initiation phase of the coagulation cascade.<sup>193,194</sup> In the blood, the bulk of FVII exists in its zymogen form (FVII: ~50 kDa), which is activated to FVIIa upon vascular injury by the cleavage of the arginine 152–isoleucine 153 bond.<sup>195</sup> The resulting light chain (LC: ~20 kDa) and heavy chain (HC: ~30 kDa) are covalently linked by a single disulfide bond.<sup>195</sup> The marketed FVII product NovoSeven® contains FVII in its activated form. In the case of FVII-alb (~116 kDa) the HC is C-terminally fused to albumin via a rigid linker consisting of six repeats of the AA sequence proline-alanine-proline-alanine-proline (HC-PAPAP-albumin: ~100 kDa). The heavy chain of FVII can be further cleaved into an N-terminal (NT: ~18 kDa) and C-terminal (CT: ~12 kDa) fragment. An overview over the respective chains and fragments is given in Figure 2.



Figure 2: FVII and FVII-alb chain and fragment sizes. NT: N-terminal; CT: C-terminal; HC, heavy chain; LC, light chain.

FVII is heavily post-translationally modified by signal peptide cleavage and propeptide cleavage, disulfide bond formation,  $\gamma$ -carboxylation,  $\beta$ -hydroxylation, *O*-glycosylation and *N*-glycosylation.<sup>120,196</sup> Since  $\gamma$ -carboxylation is vitamin K (vit K) dependent,<sup>123</sup> FVII- and FVII-alb-expressing cell lines were cultured in medium supplemented with vit K. The FVII *N*-glycosylation sites at asparagine 145 and 322 are fully occupied.<sup>49,197–199</sup> When derived from human plasma, FVII carries bi- and triantennary, fully sialylated *N*-glycans, while CHO and BHK cell-derived FVII are less sialylated.<sup>49</sup> HEK 293 cell-derived FVII additionally carries GalNAc instead of galactose, a high degree of antenna fucosylation and even less sialic acid.<sup>49</sup> The albumin molecule is not glycosylated and therefore does not directly affect the glycosylation of the FVII-alb fusion protein.<sup>200</sup>

## 2.10 Structure and PTMs of B domain deleted coagulation factor VIII

FVIII is a divalent metal-ion-dependent cofactor that, in complex with FIXa, activates FX to generate FXa in the amplification phase of the coagulation cascade.<sup>201</sup> In the blood, the bulk of FVIII is present as a two-chain zymogen, which is activated to FVIIIa by thrombin, which results in the removal of the B and A3 domains.<sup>201,202</sup> Since the B domain is not relevant for coagulation activity<sup>203</sup>, reduces expression<sup>203,204</sup>, and precludes nanofiltration<sup>125</sup>, recombinant FVIII molecules often lack the B domain.<sup>120</sup> Therefore, a FVIII-BDD variant with the AA sequence of Nuwiq® (~168 kDa) was used in this study.<sup>9,125</sup>

FVIII-BDD is heavily post-translationally modified with signal peptide cleavage and propeptide cleavage, disulfide bond formation, tyrosine sulfation, serine and threonine phosphorylation, *O*-glycosylation and *N*-glycosylation.<sup>120,125</sup> The *N*-glycosylation sites at asparagine 60, 256, 1829 and 2137 (residues numbering based on plasma-derived FVIII) are occupied, while those at asparagine 601 and 1704 are not.<sup>50,125,205,206</sup> The B domain of plasma-derived FVIII carries 17 *N*- and 7 *O*-glycosylation sites which are not present in FVIII-BDD.<sup>125</sup> Hence, the *N*-glycosylation plasma-derived and recombinant FVIII-BDD differ markedly and cannot be directly compared. FVIII-BDD produced in CHO cells carries equal amounts of complex and high-mannose plus hybrid *N*-glycans.<sup>50</sup> The complex *N*-glycans are mainly biantennary with a high degree of sialylation, but carry the immunogenic Neu5Gc and  $\alpha$ -gal epitopes.<sup>50</sup> In comparison, HEK 293 cell-derived FVIII-BDD carries none of the immunogenic epitopes, but features GalNAc, high levels of antennary fucose and low levels of sialic acid on the complex *N*-glycans.<sup>125</sup>

## 2.11 Structure and PTMs of coagulation factor IX

The structure of FIX is very similar to that of FVII and it too is a  $\text{Ca}^{2+}$ -dependent serine protease. In complex with its cofactor FVIII, it activates FX to generate FXa both in the initiation and amplification phases of the coagulation cascade.<sup>207</sup> In the blood, the bulk of FIX is present in its zymogen form (~57 kDa), which is activated to FIXa by the cleavage of the arginine 145–alanine 146 and arginine 180–valine 181 bonds, releasing a 35 AA activation peptide.<sup>207</sup> The resulting LC and HC are covalently linked by a single disulfide bond.<sup>207</sup>

FIX is heavily post-translationally modified by signal peptide cleavage and propeptide cleavage, disulfide bond formation,  $\gamma$ -carboxylation,  $\beta$ -hydroxylation, tyrosine sulfation, serine and threonine phosphorylation *O*-glycosylation and *N*-glycosylation.<sup>120,207</sup> Since  $\gamma$ -carboxylation depends on vit K,<sup>123</sup> FIX expressing cell lines were cultured in medium supplemented with vit K. The *N*-glycosylation sites at asparagine 157 and 167 are fully occupied.<sup>48,207</sup> When derived from human plasma, FIX carries mainly tri- and tetraantennary, close to fully sialylated *N*-glycans with small amounts of antennary fucose.<sup>208</sup> The monosaccharide composition of CHO cell-derived FIX was similar to that of plasma-derived FIX, but sialylation was lower.<sup>48</sup> No *N*-glycosylation data of HEK 293 cell-derived FIX was available so far.

## 2.12 Scientific question

The ultimate goal of this study was to generate new host cell lines for the production of fully human proteins with *N*-glycans that do not carry GalNAc but a high level of sialic acids, in order to develop a human cell line-based production system for therapeutic proteins with improved PK properties.

Thus, the first target of the present study was to abolish terminal *N*-glycan GalNAc. The GalNAc-transferases (GalNAcT) B4GALNT3 and B4GALNT4, which are responsible for the addition of GalNAc to *N*-glycans,<sup>40–42</sup> were knocked-out at the genetic level at Transposagen Biopharmaceuticals using the CRISPR/Cas9 technology. Subsequently, clones with a functional KO of either *B4GALNT3*, or *B4GALNT4* or both, *B4GALNT3* as well as *B4GALNT4*, were selected for phenotype analysis.

The second target of the present study was to increase sialylation. To this end, SiaTs ST6GAL1 and ST3GAL6—known for their participation in *N*-glycan sialylation—were overexpressed by KI of the respective genes into the HEK 293-F cell line. Based on the publication by Sugimoto *et al.*, which suggests that soluble rather than membrane-bound ST6GAL1 might be more active in sialylating secreted proteins,<sup>150</sup> soluble versions of ST3GAL6 and ST6GAL1 were also overexpressed. Stable SiaT overexpressing pools were used for model protein expression and phenotype analysis. Later on, ST6GAL1 overexpressing pools were also compared to their clonal derivatives. In a different approach, some of the generated expression cell lines were cultured in medium supplemented with ManNAc and cytidine to test whether CMP-sialic acid is limiting in HEK 293-F cells.

Besides glyco-engineering as such, a main objective of this study was to validate whether the changes in *N*-glycosylation actually positively affect glycan-receptor-binding and PK properties of the model protein FVII-alb and whether this glyco-engineering approach was also applicable to other proteins like FVIII and FIX.



### 3 MATERIALS AND METHODS

#### 3.1 Materials

##### 3.1.1 Plasmids

| Plasmid Name                             | Plasmid ID | Description                                                                                                                                                                                                                                                      | Source/<br>Reference                  |
|------------------------------------------|------------|------------------------------------------------------------------------------------------------------------------------------------------------------------------------------------------------------------------------------------------------------------------|---------------------------------------|
| pAAVS1-SA-hygroR-EF1                     | pOcta127   | Donor plasmid backbone for CRISPR/Cas9-mediated KI with homology arms targeting the human AAVS1 integration site. Used for Gibson Assembly cloning of plasmids pAAVS1-SA-hygroR-EF1_ <i>ST6GAL1</i> / <i>ST3GAL6</i> / <i>ST6GAL1_sol</i> / <i>ST3GAL6_sol</i> . | BioCat, Heidelberg, Germany           |
| pcDNA3.1_ <i>ST6GAL1</i>                 | pOcta008   | pcDNA3.1 plasmid with coding sequence for insert <i>ST6GAL1</i> . Used as template for amplification of insert <i>ST6GAL1</i> .                                                                                                                                  | Laboratory inventory                  |
| pAAVS1-SA-hygroR-EF1_ <i>ST6GAL1</i>     | pOcta139   | pAAVS1-SA-hygroR-EF1 donor plasmid for CRISPR/Cas9-mediated KI with insert <i>ST6GAL1</i> . Used as template for amplification of <i>ST6GAL1</i> without signal peptide for insert <i>ST6GAL1_sol</i> .                                                          | This work                             |
| pEX-A258_ <i>ST3GAL6</i>                 | pOcta168   | Plasmid with coding sequence for insert <i>ST3GAL6</i> . Used for restriction digest to release insert <i>ST3GAL6</i> (codon optimized).                                                                                                                         | Eurofins Genomics, Ebersberg, Germany |
| pAAVS1-SA-hygroR-EF1_ <i>ST3GAL6</i>     | pOcta162   | pAAVS1-SA-hygroR-EF1 donor plasmid for CRISPR/Cas9-mediated KI with insert <i>ST3GAL6</i> . Used as template for amplification of <i>ST3GAL6</i> without signal peptide for insert <i>ST3GAL6_sol</i> .                                                          | This work                             |
| pEX-A128_cnInsSP- ( <i>ST6GAL1</i> )     | pOcta169   | pEX-A128 plasmid used for restriction digest to release the canine insulin precursor signal peptide DNA sequence <sup>150</sup> with overhangs to <i>ST6GAL1</i> (without signal peptide).                                                                       | Eurofins Genomics, Ebersberg, Germany |
| pEX-A128_cnInsSP- ( <i>ST3GAL6</i> )     | pOcta170   | pEX-A128 plasmid used for restriction digest to release the canine insulin precursor signal peptide DNA sequence <sup>150</sup> with overhangs to <i>ST3GAL6</i> (without signal peptide).                                                                       | Eurofins Genomics, Ebersberg, Germany |
| pAAVS1-SA-hygroR-EF1_ <i>ST6GAL1_sol</i> | pOcta166   | pAAVS1-SA-hygroR-EF1 donor plasmid for CRISPR/Cas9-mediated KI with insert <i>ST6GAL1_sol</i> .                                                                                                                                                                  | This work                             |
| pAAVS1-SA-hygroR-EF1_ <i>ST3GAL6_sol</i> | pOcta167   | pAAVS1-SA-hygroR-EF1 donor plasmid for CRISPR/Cas9-mediated KI with insert <i>ST3GAL6_sol</i> (codon optimized).                                                                                                                                                 | This work                             |

| <b>Plasmid Name</b>                       | <b>Plasmid ID</b> | <b>Description</b>                                                                                                                                                                  | <b>Source/<br/>Reference</b>          |
|-------------------------------------------|-------------------|-------------------------------------------------------------------------------------------------------------------------------------------------------------------------------------|---------------------------------------|
| <b>pUCOE Hu-P Ctrl</b>                    | pOcta016          | Backbone plasmid for mammalian protein expression.                                                                                                                                  | Merck KGaA, Darmstadt, Germany        |
| <b>pUCOE Hu-P Ctrl-IRES</b>               | pOcta035          | Modified version of pUCOE Hu-P Ctrl with SV40 polyA and mPGK promoter replaced by an IRES. Used for Gibson Assembly cloning of plasmid pUCOE Hu-P Ctrl-IRES_FVII-alb.               | Laboratory inventory                  |
| <b>pUCOE Hu-P Ctrl-IRES-WPRE</b>          | pOcta033          | Modified version of pUCOE Hu-P Ctrl with SV40 polyA and mPGK promoter replaced by an IRES and WPRE. Used for Gibson Assembly cloning of plasmid pUCOE Hu-P Ctrl-IRES-WPRE_FVII-alb. | Laboratory inventory                  |
| <b>pcDNA3.1_FVII</b>                      | pOcta006          | pcDNA3.1 plasmid with coding sequence for insert <i>FVII</i> . Used as template for amplification of insert <i>FVII</i> .                                                           | Laboratory inventory                  |
| <b>pUCOE Hu-P Ctrl-IRES_FVII</b>          | pOcta043          | pUCOE Hu-P Ctrl-IRES plasmid with insert <i>FVII</i> .                                                                                                                              | This work                             |
| <b>pHBG1C_FIX-PAPAP-Albumin</b>           | pOcta092          | pHBG1C plasmid with coding sequence for PAPAP-albumin. Used as template for amplification of PAPAP-albumin for insert <i>FVII-alb</i> .                                             | Laboratory inventory                  |
| <b>pHBG1C_FVII-alb</b>                    | pOcta063          | pHBG1C plasmid with coding sequence for <i>FVII</i> . Used as template for amplification of <i>FVII</i> for insert <i>FVII-alb</i> .                                                | Laboratory inventory                  |
| <b>pUCOE Hu-P Ctrl-IRES_FVII-alb</b>      | pOcta135          | pUCOE Hu-P Ctrl-IRES plasmid with insert <i>FVII-alb</i> .                                                                                                                          | This work                             |
| <b>pUCOE Hu-P Ctrl-IRES-WPRE_FVII-alb</b> | pOcta140          | pUCOE Hu-P Ctrl-IRES-WPRE plasmid with insert <i>FVII-alb</i> .                                                                                                                     | This work                             |
| <b>pcDNA3.1_FVIII-BDD</b>                 | pOcta142          | pcDNA3.1 plasmid with coding sequence for insert <i>FVIII-BDD</i> . Used as template for amplification of insert <i>FVIII-BDD</i> .                                                 | Laboratory inventory                  |
| <b>pUCOE Hu-P Ctrl-IRES_FVIII-BDD</b>     | pOcta154          | pUCOE Hu-P Ctrl-IRES plasmid with insert <i>FVIII-BDD</i> .                                                                                                                         | This work                             |
| <b>pEX-K4_FIX-PAPAP</b>                   | pOcta093          | pEX-K4 plasmid with coding sequence for insert <i>FIX</i> . Used as template for amplification of insert <i>FIX</i> .                                                               | Eurofins Genomics, Ebersberg, Germany |
| <b>pUCOE Hu-P Ctrl-IRES_FIX</b>           | pOcta144          | pUCOE Hu-P Ctrl-IRES plasmid with insert <i>FIX</i> .                                                                                                                               | This work                             |

### 3.1.2 Gene constructs

| Gene of interest          | Description                                                                                                                                                                                                                                                                                                                                                    | Source/Reference                                                                      |
|---------------------------|----------------------------------------------------------------------------------------------------------------------------------------------------------------------------------------------------------------------------------------------------------------------------------------------------------------------------------------------------------------|---------------------------------------------------------------------------------------|
| <b><i>ST6GAL1</i></b>     | Synthetic DNA construct coding for human <i>ST6GAL1</i> . Amplified from pcDNA3.1_ <i>ST6GAL1</i> .                                                                                                                                                                                                                                                            | NCBI Reference Sequence: NP_001340845.1                                               |
| <b><i>ST3GAL6</i></b>     | Synthetic DNA construct coding for a codon optimized version of human <i>ST3GAL6</i> isoform 1. Released from pEX-A258_ <i>ST3GAL6</i> .                                                                                                                                                                                                                       | NCBI Reference Sequence: NP_001258075.1                                               |
| <b><i>ST6GAL1_sol</i></b> | Synthetic DNA construct coding for human <i>ST6GAL1</i> with the signal peptide (AAs: 1-26) exchanged for that of the canine insulin precursor (AAs: 1-24). Canine insulin precursor released from pEX-A128_cnInsSP- ( <i>ST6GAL1</i> ) and <i>ST6GAL1</i> amplified from pAAVS1-SA-hygroR-EF1_ <i>ST6GAL1</i> .                                               | NCBI Reference Sequence: <i>ST6GAL1</i> : NP_001340845.1<br>Insulin: NP_001123565.1   |
| <b><i>ST3GAL6_sol</i></b> | Synthetic DNA construct coding for a codon optimized version of human <i>ST3GAL6</i> isoform 1 with the signal peptide (AAs: 1-25) exchanged for that of the canine insulin precursor (AAs: 1-24). Canine insulin precursor released from pEX-A128_cnInsSP- ( <i>ST3GAL6</i> ) and <i>ST3GAL6</i> amplified from pAAVS1-SA-hygroR-EF1_ <i>ST3GAL6</i> .        | NCBI Reference Sequence: <i>ST3GAL6</i> : NP_001258075.1<br>Insulin: NP_001123565.1   |
| <b><i>FVII</i></b>        | Synthetic DNA construct coding for the preproprotein of human coagulation factor VII. Amplified from pcDNA3.1_ <i>FVII</i> .                                                                                                                                                                                                                                   | NCBI Reference Sequence: NP_000122.1                                                  |
| <b><i>FVII-alb</i></b>    | Synthetic DNA construct coding for a fusion protein of the preproproteins of human coagulation factor VII and human serum albumin linked via a rigid linker consisting of 6 repeats of the AA sequence proline-alanine-proline-alanine-proline. <i>FVII</i> amplified from pHBG1C_ <i>FVII</i> -alb and PAPAP-Albumin amplified from pHBG1C_FIX-PAPAP-Albumin. | NCBI Reference Sequence: <i>FVII</i> : NP_062562.1<br>Alb: NP_000468.1                |
| <b><i>FVIII-BDD</i></b>   | Synthetic DNA construct coding for the preproprotein of a B domain-deleted human coagulation factor VIII. Amplified from pcDNA3.1_ <i>FVIII</i> -BDD.                                                                                                                                                                                                          | Modified version of GenBank accession: ABV90867.1 (AAs PPVLKR changed to SRHQAYRYRRG) |
| <b><i>FIX</i></b>         | Synthetic DNA construct coding for the preproprotein of human coagulation factor IX isoform 1. Amplified from pEX-K4_FIX-PAPAP.                                                                                                                                                                                                                                | NCBI Reference Sequence: NP_000124.1                                                  |

### 3.1.3 Oligonucleotides

#### 3.1.3.1 Primers

All primers were acquired from Sigma-Aldrich (Taufkirchen, Germany) and were diluted to 20 µM using water.

| Number | Purpose                                                                                                                                                                                                            | Sequence (5'-3')                                              |
|--------|--------------------------------------------------------------------------------------------------------------------------------------------------------------------------------------------------------------------|---------------------------------------------------------------|
| 1      | Sanger sequence confirmation of pUCOE Hu-P Ctrl-IRES_FVII-<br>alb insert sequence. GATC custom primer.                                                                                                             | CCAGTACATCGAGTG<br>GCTGC                                      |
| 2      | Sanger sequence confirmation of pUCOE Hu-P Ctrl-IRES_FVII-<br>alb insert sequence. GATC custom primer.                                                                                                             | CAAGGTCCACACCGA<br>GTGCTG                                     |
| 3      | Sanger sequence confirmation of pUCOE Hu-P Ctrl-IRES_FVII-<br>alb insert sequence. GATC custom primer.                                                                                                             | GCTTCGACAAGATCA<br>AGAACTGG                                   |
| 4      | Sanger sequence confirmation of pUCOE Hu-P Ctrl-IRES_FVII-<br>alb insert sequence. GATC custom primer.                                                                                                             | TCAACCAGCTCTGCGT<br>CCTCC                                     |
| 5      | Sanger sequence confirmation of pUCOE Hu-P Ctrl-IRES_FVII-<br>alb, pUCOE Hu-P Ctrl-IRES_FIX and pUCOE Hu-P Ctrl-<br>IRES_FVIII-BDD insert sequence. GATC custom primer.                                            | TGGTCCACGTACCCTA<br>TG                                        |
| 6      | Sanger sequence confirmation of pUCOE Hu-P Ctrl-IRES_FVIII-<br>BDD insert sequence. GATC custom primer.                                                                                                            | AGAGCGGAATTCGAG<br>CTC                                        |
| 22     | Sanger sequence confirmation of pUCOE Hu-P Ctrl-IRES_FVII-<br>alb insert sequence. GATC custom primer.                                                                                                             | GAGTGTCCATGGCAG<br>GTCCTG                                     |
| 23     | Gibson Assembly cloning forward primer for the amplification of<br>FVII. Used for cloning of pUCOE Hu-P Ctrl-IRES_FVII.                                                                                            | GTTAGTTAAGTTAACG<br>GCCGGCCGCTAGCAT<br>GGTCTCCAGGCCCTC<br>AG  |
| 23     | Sanger sequence confirmation of pAAVS1-SA-hygroR-<br>EF1_ST6GAL1, pAAVS1-SA-hygroR-EF1_ST3GAL6, pAAVS1-<br>SA-hygroR-EF1_ST6GAL1_sol and pAAVS1-SA-hygroR-<br>EF1_ST3GAL6_sol insert sequence. GATC custom primer. | CTGCTTGCTCAACTCT<br>ACG                                       |
| 24     | Gibson Assembly cloning reverse primer for the amplification of<br>FVII. Used for cloning of pUCOE Hu-P Ctrl-IRES_FVII.                                                                                            | TACGTAGTCGACTACG<br>TGGCCGCGCTAGCAA<br>ACGGGCCCTCTAGACT<br>CG |
| 25     | Sanger sequence confirmation of pAAVS1-SA-hygroR-<br>EF1_ST6GAL1 and pAAVS1-SA-hygroR-EF1_ST6GAL1_sol<br>insert sequence. GATC custom primer.                                                                      | ATCATGACGCAGTCCT<br>GAG                                       |
| 32     | Primer used for the Sanger sequencing of the AAVS1 integration<br>site.                                                                                                                                            | CCACCTCCTGTTAGGC<br>AGA                                       |
| 33     | Primer used for the Sanger sequencing of the AAVS1 integration<br>site.                                                                                                                                            | CATGTTTGCTGCCTCC<br>AGG                                       |
| 35     | Sanger sequence confirmation of pUCOE Hu-P Ctrl-IRES_FIX<br>insert sequence. GATC custom primer.                                                                                                                   | CAGAAGGCTATCGGTT<br>GGC                                       |
| 44     | Sanger sequence confirmation of pUCOE Hu-P Ctrl-IRES_FVIII-<br>BDD insert sequence. GATC custom primer.                                                                                                            | AGAAGGGAGTCTGGC<br>CAAGG                                      |
| 45     | Sanger sequence confirmation of pUCOE Hu-P Ctrl-IRES_FVIII-<br>BDD insert sequence. GATC custom primer.                                                                                                            | TTTGAACAATGGCCCT<br>CAGC                                      |

| <b>Number</b> | <b>Purpose</b>                                                                                                                                    | <b>Sequence (5'-3')</b>                                        |
|---------------|---------------------------------------------------------------------------------------------------------------------------------------------------|----------------------------------------------------------------|
| 46            | Sanger sequence confirmation of pUCOE Hu-P Ctrl-IRES_FVIII-BDD insert sequence. GATC custom primer.                                               | TTGGAGCACAGACTG<br>ACTTC                                       |
| 47            | Sanger sequence confirmation of pUCOE Hu-P Ctrl-IRES_FVIII-BDD insert sequence. GATC custom primer.                                               | TTCAGAAATCAGGCCT<br>CTCG                                       |
| 48            | Sanger sequence confirmation of pUCOE Hu-P Ctrl-IRES_FVIII-BDD insert sequence. GATC custom primer.                                               | CATCTACATGCTGGGA<br>TGAG                                       |
| 63            | Sanger sequence confirmation of pUCOE Hu-P Ctrl-IRES_FIX and pUCOE Hu-P Ctrl-IRES_FVIII-BDD insert sequence. GATC standard primer.                | TATAGACAAACGCAC<br>ACCG                                        |
| 128           | Forward primer for the amplification of the AAVS1 integration site for Sanger sequencing. Also used for sequencing of the AAVS1 integration site. | CAGGTCCTGCTTTCTC<br>TGACCTGCATTCTC                             |
| 128           | Primer for sequencing of the AAVS1 integration site in HEK 293-F cells                                                                            | CAGGTCCTGCTTTCTC<br>TGACCTGCATTCTC                             |
| 129           | Reverse primer for the amplification of the AAVS1 integration site for Sanger sequencing                                                          | GCTCAGTCTGAAGAG<br>CAGAGCCAGGAAC                               |
| 130           | Forward primer #1 for the PCR amplification of the AAVS1 integration site in HEK 293-F cells                                                      | GCCCTCATCTGGCGAT<br>TTCC                                       |
| 131           | Reverse primer #1 for the PCR amplification of the AAVS1 integration site in HEK 293-F cells                                                      | CACTAAGGCAATTGG<br>GGTGC                                       |
| 132           | Forward primer #2 for the PCR amplification of the AAVS1 integration site in HEK 293-F cells                                                      | GGA ACTCTGCCCTCTA<br>ACGC                                      |
| 133           | Reverse primer #2 for the PCR amplification of the AAVS1 integration site in HEK 293-F cells                                                      | TCTTGGCCACGTAACC<br>TGAG                                       |
| 134           | Gibson Assembly cloning forward primer for the amplification of FVII. Used for cloning of pUCOE Hu-P Ctrl-IRES_FVII-alb.                          | AGGGGCTGGAGCTGG<br>AGGAAATGGGGCTCT<br>CAGCAGCAC                |
| 134           | Primer for sequencing of the AAVS1 integration site in HEK 293-F cells                                                                            | CATGTTTGCTGCCTCC<br>AGG                                        |
| 135           | Primer for sequencing of the AAVS1 integration site in HEK 293-F cells                                                                            | CCACCTCCTGTTAGGC<br>AGA                                        |
| 136           | Gibson Assembly cloning forward primer for the amplification of FVII. Used for cloning of pUCOE Hu-P Ctrl-IRES_FVII-alb.                          | GTTAAGTTAACGGCCG<br>GCCGCTAGCATGGTGT<br>CCCAGGCCCTGAGACT<br>G  |
| 142           | Gibson Assembly cloning forward primer for the amplification of <i>ST6GALI</i> . Used for cloning of pAAVS1-SA-hygroR-EF1_ <i>ST6GALI</i> .       | ACCGGCGCCTACTCTA<br>GATGTACAACCGGTAT<br>CCGTCGCCACCATGAT<br>TC |
| 143           | Gibson Assembly cloning reverse primer for the amplification of <i>ST6GALI</i> . Used for cloning of pAAVS1-SA-hygroR-EF1_ <i>ST6GALI</i> .       | TTGTAATAACCGCGGA<br>ATACGCGTACCGGTTA<br>AACGGGCCCTCTAGA<br>CTC |

| <b>Number</b> | <b>Purpose</b>                                                                                                                                | <b>Sequence (5'-3')</b>                                                           |
|---------------|-----------------------------------------------------------------------------------------------------------------------------------------------|-----------------------------------------------------------------------------------|
| <b>151</b>    | Gibson Assembly cloning forward primer for the amplification of PAPAP-Albumin. Used for cloning of pUCOE Hu-P Ctrl-IRES_FVII-alb.             | CGTGCTGCTGAGAGCC<br>CCATTTCCCTCCAGCTC<br>CAGCCCCTCCTGC                            |
| <b>154</b>    | Gibson Assembly cloning reverse primer for the amplification of Albumin. Used for cloning of pUCOE Hu-P Ctrl-IRES_FVII-alb.                   | TAGTCGACTACGTGGC<br>CGCGCTAGCTCAGAG<br>GCCGAGGGCGGCC                              |
| <b>168</b>    | Gibson Assembly cloning forward primer for the amplification of <i>FLX</i> . Used for cloning of pUCOE Hu-P Ctrl-IRES_FIX.                    | GTTAGTTAAGTTAACG<br>GCCGCGCTAGCAT<br>GCAACGCGTGAACAT<br>GATTATGGCGGAAAG<br>TC     |
| <b>169</b>    | Gibson Assembly cloning reverse primer for the amplification of <i>FLX</i> . Used for cloning of pUCOE Hu-P Ctrl-IRES_FIX.                    | CTTACGTAGTCGACTA<br>CGTGGCCGCGCTAGCT<br>TAGGTCAGTTTGGTCT<br>TTTCTTTGATCCAGTT<br>G |
| <b>171</b>    | Primer for direct PCR exclusion of clones with undesired random plasmid integration. Reverse primer to detect RI at the left homology arm.    | TTCCTTGCGGTCCGAA<br>TG                                                            |
| <b>173</b>    | Primer for direct PCR screening of clones with successful plasmid KI. Reverse primer to detect correct integration at the left homology arm.  | ATCGGCGCAGCTATTT<br>ACC                                                           |
| <b>174</b>    | Primer for direct PCR screening of clones with successful plasmid KI. Forward primer to detect correct integration at the right homology arm. | CACAGGAACGAAGTC<br>CCTAAAG                                                        |
| <b>176</b>    | Primer for direct PCR exclusion of clones with undesired random plasmid integration. Forward primer to detect RI at the right homology arm.   | GTGTCTGCAGGCTCAA<br>AG                                                            |
| <b>180</b>    | Primer for direct PCR screening of clones with successful plasmid KI. Forward primer to detect correct integration at the left homology arm.  | CTCTAACGCTGCCGTC<br>TC                                                            |
| <b>181</b>    | Primer for direct PCR screening of clones with successful plasmid KI. Reverse primer to detect correct integration at the right homology arm. | GTCCAGGCCAAGTAG<br>GTG                                                            |
| <b>182</b>    | Primer for direct PCR exclusion of clones with undesired random plasmid integration. Forward primer to detect RI at the left homology arm.    | GTGCTGCAAGGCGATT<br>AAG                                                           |
| <b>185</b>    | Primer for direct PCR exclusion of clones with undesired random plasmid integration. Reverse primer to detect RI at the right homology arm.   | CAGGTTTCCCCGACTGG<br>AAAG                                                         |
| <b>194</b>    | Gibson Assembly cloning forward primer for the amplification of <i>FVIII-BDD</i> . Used for cloning of pUCOE Hu-P Ctrl-IRES_FVIII-BDD.        | GTTAGTTAAGTTAACG<br>GCCGCGCTAGCAT<br>GCAAATAGAGCTCTCC<br>ACCTGCTTC                |

| Number | Purpose                                                                                                                                                                                                  | Sequence (5'-3')                                                        |
|--------|----------------------------------------------------------------------------------------------------------------------------------------------------------------------------------------------------------|-------------------------------------------------------------------------|
| 195    | Gibson Assembly cloning reverse primer for the amplification of <i>FVIII-BDD</i> . Used for cloning of pUCOE Hu-P Ctrl-IRES_FVIII-BDD.                                                                   | CTTACGTAGTCGACTA<br>CGTGGCCGCGCTAGCT<br>CAGTAGAGGTCCTGTG<br>CCTCGCAGCCC |
| 256    | Gibson Assembly cloning forward primer for the amplification of the 3' part of <i>ST6GAL1</i> from pAAVS1-SA-hygroR-EF1_ <i>ST6GAL1</i> . Used for cloning of pAAVS1-SA-hygroR-EF1_ <i>ST6GAL1_sol</i> . | GTCTGATTCCCAGTCT<br>GTATCC                                              |
| 257    | Gibson Assembly cloning reverse primer for the amplification of the 3' part of <i>ST6GAL1</i> from pAAVS1-SA-hygroR-EF1_ <i>ST6GAL1</i> . Used for cloning of pAAVS1-SA-hygroR-EF1_ <i>ST6GAL1_sol</i> . | TTTGTAATAACCGCGG<br>AATACGCGTACCGGC<br>CGCTTAGCAGTGAATG<br>GTC          |
| 258    | Gibson Assembly cloning forward primer for the amplification of the 3' part of <i>ST3GAL6</i> from pAAVS1-SA-hygroR-EF1_ <i>ST3GAL6</i> . Used for cloning of pAAVS1-SA-hygroR-EF1_ <i>ST3GAL6_sol</i> . | ATTCAGCCCTGTCTGT<br>CTAAGC                                              |
| 259    | Gibson Assembly cloning reverse primer for the amplification of the 3' part of <i>ST3GAL6</i> from pAAVS1-SA-hygroR-EF1_ <i>ST3GAL6</i> . Used for cloning of pAAVS1-SA-hygroR-EF1_ <i>ST3GAL6_sol</i> . | TTTGTAATAACCGCGG<br>AATACGCGTACCGGG<br>CGTACCGGTTTATCAG<br>TCTTG        |

### 3.1.3.2 Primer/probe pairs for quantitative reverse transcription real-time PCR and digital PCR

All primer/probe pairs for quantitative reverse transcription real-time PCR (RT-qPCR) and digital PCR (dPCR) were acquired from Thermo Fisher Scientific (Applied Biosystems, Dreieich, Germany). The probes for the genes of interest were labelled with the fluorescent dye 6-carboxyfluorescein (FAM), while the probe of the reference gene *RNase P* was labelled with 2'-chloro-7'-phenyl-1,4-dichloro-6-carboxy-fluorescein (VIC). For off-the-shelf primer/probe pairs the Thermo Fisher Scientific assay ID and for self-designed primer/probe pairs the sequences are given in the following table.

| Number | Primer/<br>Probe Pair | Purpose                                                                                     | Sequence (5'-3')/Assay ID                                                                                               |
|--------|-----------------------|---------------------------------------------------------------------------------------------|-------------------------------------------------------------------------------------------------------------------------|
| 6      | AAVS1                 | Copy number determination of the adeno-associated virus integration site in HEK 293-F cells | Hs04027950_cn                                                                                                           |
| 1      | <i>RNase P</i>        | Housekeeper gene used as reference for RT-qPCR and dPCR                                     | 4403326                                                                                                                 |
| 34     | <i>HygR</i>           | Determination of number of donor plasmid copies that were integrated by KI                  | Forward primer:<br>AGGTCGCCAACATCTTCTCTG<br>Reverse Primer:<br>GATGCCTCCGCTCGAAGTAG<br>Probe:<br>TCTGCTGCTCCATACAAGCCAA |
| 25     | <i>ST6GAL1</i>        | Determination of <i>ST6GAL1</i> and <i>ST6GAL1_sol</i> expression                           | Hs00949382_m1                                                                                                           |

| Number | Primer/<br>Probe Pair | Purpose                                                                           | Sequence (5'-3')/Assay ID                                                                                                    |
|--------|-----------------------|-----------------------------------------------------------------------------------|------------------------------------------------------------------------------------------------------------------------------|
| 32     | <i>ST3GAL6</i>        | Determination of codon optimized <i>ST3GAL6</i> and <i>ST3GAL6_sol</i> expression | Forward primer:<br>GAGGAAGAGGTAGGCAGAAGGA<br>Reverse Primer:<br>TGAATCGGATCACTGAACACAGAT<br>T<br>Probe:<br>TTCGCCTGTTTTATCCC |

### 3.1.3.3 Guide RNA

| Number | gRNA  | Purpose                                                                                                     | Sequence (5'-3',<br>Reference                                |
|--------|-------|-------------------------------------------------------------------------------------------------------------|--------------------------------------------------------------|
| 6      | AAVS1 | Guide RNA for cleavage of the AAVS1 integration site by CRISPR/Cas9 for targeted integration <sup>209</sup> | GGGGCCACUAGGGAC<br>AGGAU, Synthego,<br>Redwood City, CA, USA |

## 3.1.4 Bacteria and cell lines

### 3.1.4.1 Bacteria

| Name                                                   | Description                                                         | Source/Reference                                      |
|--------------------------------------------------------|---------------------------------------------------------------------|-------------------------------------------------------|
| <b>NEB 5-alpha Competent E. coli (High Efficiency)</b> | Derivative of DH5 $\alpha$ . T1 phage resistant and endA deficient. | New England Biolabs,<br>Frankfurt am Main,<br>Germany |

### 3.1.4.2 Host cell lines

Host cell lines are cell lines that, upon transfection of a gene of interest, can be used for the expression of recombinant therapeutic proteins. The following table contains all host cell lines that were acquired from Thermo Fisher Scientific or Transposagen. Stable pools (SP) or clones (CL) selected for subsequent evaluation of *N*-glycosylation are underlined. An overview over all selected host cell lines and the corresponding expression cell lines is depicted in Figure 24.

| Name with stable pool (SP#) and clone numbers (CL#) | ID                                | Description                                                                                                             | Source/Reference                                    |
|-----------------------------------------------------|-----------------------------------|-------------------------------------------------------------------------------------------------------------------------|-----------------------------------------------------|
| <b>wt HEK 293-F</b>                                 | HEK 293-F                         | wt FreeStyle HEK 293-F cell line is derived from the HEK 293 cell line. It is adapted to serum-free suspension culture. | Thermo Fisher Scientific (Gibco), Dreieich, Germany |
| <b>NT3-KO</b>                                       | HEK 293-F<br>eclOcta01-01-2E6     | Clone of the HEK 293-F cell line with a functional KO of the gene <i>B4GALNT3</i> .                                     | Transposagen Biopharmaceuticals, Lexington, USA     |
| <b>NT4-KO</b>                                       | HEK 293-F<br>eclOcta02-01-2C8/2C2 | Clone of the HEK 293-F cell line with a functional KO of the gene <i>B4GALNT4</i> .                                     | Transposagen Biopharmaceuticals, Lexington, USA     |



| Name with stable pool (SP#) and clone numbers (CL#)                                                                                                                   | ID                                    | Description                                                                                                                                                                                        | Source/Reference                                       |
|-----------------------------------------------------------------------------------------------------------------------------------------------------------------------|---------------------------------------|----------------------------------------------------------------------------------------------------------------------------------------------------------------------------------------------------|--------------------------------------------------------|
| <b>NT3/4-KO-01</b>                                                                                                                                                    | HEK 293-F<br>eclOcta03-01-<br>2E6/1G2 | Clone of the HEK 293-F cell line with a functional KO of the genes <i>B4GALNT3</i> and <i>B4GALNT4</i> .                                                                                           | Transposagen<br>Biopharmaceuticals<br>, Lexington, USA |
| <b>NT3/4-KO-02</b>                                                                                                                                                    | HEK 293-F<br>eclOcta03-01-<br>2E6/1F7 | Clone of the HEK 293-F cell line with a functional KO of the genes <i>B4GALNT3</i> and <i>B4GALNT4</i> .                                                                                           | Transposagen<br>Biopharmaceuticals<br>, Lexington, USA |
| <b>wt+ST3GAL6_sol-KI-SP#</b><br>(SP# = <u>01</u> , <u>02</u> , <u>03</u> , <u>04</u> )                                                                                | eepOcta11-SP#                         | Stable pools of the wt HEK 293-F cell line overexpressing ST3GAL6_sol due to KI of donor plasmid pAAVS1-SA-hygroR-EF1_ST3GAL6_sol.                                                                 | This work                                              |
| <b>wt+ST6GAL1_sol-KI-SP#</b><br>(SP# = <u>01</u> , <u>02</u> , <u>03</u> , <u>04</u> )                                                                                | eepOcta09-SP#                         | Stable pools of the wt HEK 293-F cell line overexpressing ST6GAL1_sol due to KI of donor plasmid pAAVS1-SA-hygroR-EF1_ST6GAL1_sol.                                                                 | This work                                              |
| <b>wt+ST3GAL6-KI-SP#</b><br>(SP# = <u>07</u> , <u>09</u> , <u>10</u> )                                                                                                | eepOcta07-SP#                         | Stable pools of the wt HEK 293-F cell line overexpressing ST3GAL6 due to KI of donor plasmid pAAVS1-SA-hygroR-EF1_ST3GAL6.                                                                         | This work                                              |
| <b>wt+ST6GAL1-KI-SP#</b><br>(SP# = <u>03</u> , <u>06</u> , <u>07</u> , <u>08</u> , <u>09</u> )                                                                        | eepOcta05-SP#                         | Stable pools of the wt HEK 293-F cell line overexpressing ST6GAL1 due to KI of donor plasmid pAAVS1-SA-hygroR-EF1_ST6GAL1.                                                                         | This work                                              |
| <b>wt+ST6GAL1<br/>KI-SP#-CL#</b><br><br>(SP#-CL# = <u>03-091</u> , <u>03-101</u> , <u>06-131</u> , <u>06-157</u> , <u>06-167</u> )                                    | eclOcta05-<br>SP#-CL#                 | Clones of the wt HEK 293-F cell line overexpressing ST6GAL1 due to KI of donor plasmid pAAVS1-SA-hygroR-EF1_ST6GAL1. Single-cell cloned from the respective stable pools (NT3/4-KO+ST6GAL1-KI-SP). | This work                                              |
| <b>NT3/4-<br/>KO+ST3GAL6_sol-KI-<br/>SP#</b><br>(SP# = <u>05</u> , <u>06</u> , <u>07</u> , <u>08</u> , <u>09</u> ,<br><u>10</u> , <u>11</u> , <u>12</u> , <u>15</u> ) | eepOcta12-SP#                         | Stable pools of the NT3/4-KO-02 clone overexpressing ST3GAL6_sol due to KI of donor plasmid pAAVS1-SA-hygroR-EF1_ST3GAL6_sol.                                                                      | This work                                              |
| <b>NT3/4-<br/>KO+ST6GAL1_sol-KI-<br/>SP#</b><br>(SP# = <u>03</u> )                                                                                                    | eepOcta10-SP#                         | Stable pools of the NT3/4-KO-02 clone overexpressing ST6GAL1_sol due to KI of donor plasmid pAAVS1-SA-hygroR-EF1_ST6GAL1_sol.                                                                      | This work                                              |
| <b>NT3/4-KO+ST3GAL6-<br/>KI-SP#</b><br>(SP# = <u>07</u> , <u>08</u> , <u>09</u> , <u>10</u> )                                                                         | eepOcta08-SP#                         | Stable pools of the NT3/4-KO-02 clone overexpressing ST3GAL6 due to KI of donor plasmid pAAVS1-SA-hygroR-EF1_ST3GAL6.                                                                              | This work                                              |

| Name with stable pool (SP#) and clone numbers (CL#)                                                                                                                                                              | ID                | Description                                                                                                                                                                                          | Source/Reference |
|------------------------------------------------------------------------------------------------------------------------------------------------------------------------------------------------------------------|-------------------|------------------------------------------------------------------------------------------------------------------------------------------------------------------------------------------------------|------------------|
| <b>NT3/4-KO+ST6GAL1-KI-SP#</b><br>(SP# = <u>03</u> , <u>06</u> , <u>07</u> )                                                                                                                                     | ecpOcta06-SP#     | Stable pools of the NT3/4-KO-02 clone overexpressing <i>ST6GAL1</i> due to KI of donor plasmid pAAVS1-SA-hygroR-EF1_ST6GAL1.                                                                         | This work        |
| <b>NT3/4-KO+ST6GAL1-KI-SP#-CL#</b><br>(SP#-CL# = <u>06-085</u> , <u>06-098</u> , <u>06-103</u> , <u>06-127</u> , <u>06-145</u> , <u>06-154</u> , <u>06-156</u> , <u>06-158</u> , <u>06-160</u> , <u>06-192</u> ) | eclOcta06-SP#-CL# | Clones of the NT3/4-KO-02 clone overexpressing <i>ST6GAL1</i> due to KI of donor plasmid pAAVS1-SA-hygroR-EF1_ST6GAL1. Single-cell cloned from the respective stable pools (NT3/4-KO+ST6GAL1-KI-SP). | This work        |

### 3.1.4.3 Expression cell lines

To evaluate the phenotype of glyco-engineered host cell lines, the model protein FVII-alb—and in some also FVIII-BDD and FIX—was expressed. All expression cell lines that were evaluated for productivity are displayed in the following table. Expression cell lines selected for model protein expression and all subsequent *N*-glycosylation analysis are underlined. An overview over all host cell lines and the selected expression cell lines is depicted in Figure 24.

| Name with stable pool (SP#) and clone numbers (CL#)    | ID            | Description                                                                                                                         | Source/Reference     |
|--------------------------------------------------------|---------------|-------------------------------------------------------------------------------------------------------------------------------------|----------------------|
| <b>wt HEK 293-F_FVII-SP#</b><br>(SP# = <u>01</u> )     | cpOcta043-SP# | Stable pool expressing FVII. Derived from host cell line wt HEK 293-F by transfection of plasmid pUCOE Hu-P Ctrl-IRES_FVII.         | Laboratory inventory |
| <b>wt HEK 293-F_FVII-alb-SP#</b><br>(SP# = <u>01</u> ) | cpOcta135-SP# | Stable pool expressing FVII-alb. Derived from host cell line wt HEK 293-F by transfection of plasmid pUCOE Hu-P Ctrl-IRES_FVII-alb. | This work            |
| <b>NT3-KO_FVII-alb-SP#</b><br>(SP# = <u>15</u> )       | cpOcta135-SP# | Stable pool expressing FVI-Alb. Derived from host cell line NT3-KO by transfection of plasmid pUCOE Hu-P Ctrl-IRES_FVII-alb.        | This work            |
| <b>NT4-KO_FVII-alb-SP#</b><br>(SP# = <u>04</u> )       | cpOcta140-SP# | Stable pool expressing FVI-Alb. Derived from host cell line NT4-KO by transfection of plasmid pUCOE Hu-P Ctrl-IRES-WPRE_FVII-alb.   | This work            |
| <b>NT3/4-KO-01_FVII-alb-SP#</b><br>(SP# = <u>07</u> )  | cpOcta135-SP# | Stable pool expressing FVI-Alb. Derived from host cell line NT3/4-KO-01 by transfection of plasmid pUCOE Hu-P Ctrl-IRES_FVII-alb.   | This work            |
| <b>NT3/4-KO-02_FVII-alb-SP#</b><br>(SP# = <u>11</u> )  | cpOcta135-SP# | Stable pool expressing FVII-alb. Derived from host cell line NT3/4-KO-02 by                                                         | This work            |

| <b>Name with stable pool (SP#) and clone numbers (CL#)</b>                  | <b>ID</b>     | <b>Description</b>                                                                                                                                  | <b>Source/Reference</b> |
|-----------------------------------------------------------------------------|---------------|-----------------------------------------------------------------------------------------------------------------------------------------------------|-------------------------|
|                                                                             |               | transfection of plasmid pUCOE Hu-P Ctrl-IRES_FVII-alb.                                                                                              |                         |
| <b>wt+ST3GAL6_sol-KI-02_FVII-alb-SP# (SP# = <u>25</u>, <u>26</u>)</b>       | cpOcta135-SP# | Stable pool expressing FVII-alb. Derived from host cell line wt+ST3GAL6_sol-KI-02 by transfection of plasmid pUCOE Hu-P Ctrl-IRES_FVII-alb.         | This work               |
| <b>wt+ST6GAL1_sol-KI-01_FVII-alb-SP# (SP# = <u>31</u>, <u>32</u>)</b>       | cpOcta135-SP# | Stable pool expressing FVII-alb. Derived from host cell line wt+ST6GAL1_sol-KI-01 by transfection of plasmid pUCOE Hu-P Ctrl-IRES_FVII-alb.         | This work               |
| <b>wt+ST3GAL6-KI-07_FVII-alb-SP# (SP# = <u>21</u>, <u>22</u>)</b>           | cpOcta135-SP# | Stable pool expressing FVII-alb. Derived from host cell line wt+ST3GAL6-KI-07 by transfection of plasmid pUCOE Hu-P Ctrl-IRES_FVII-alb.             | This work               |
| <b>wt+ST6GAL1-KI-03_FVII-alb-SP# (SP# = <u>27</u>, <u>28</u>)</b>           | cpOcta135-SP# | Stable pool expressing FVII-alb. Derived from host cell line wt+ST6GAL1-KI-03 by transfection of plasmid pUCOE Hu-P Ctrl-IRES_FVII-alb.             | This work               |
| <b>wt+ST6GAL1-KI-06-131_FVII-alb-SP# (SP# = <u>35</u>, <u>36</u>)</b>       | cpOcta135-SP# | Stable pool expressing FVII-alb. Derived from clonal host cell line wt+ST6GAL1-KI-06-131 by transfection of plasmid pUCOE Hu-P Ctrl-IRES_FVII-alb.  | This work               |
| <b>wt+ST6GAL1-KI-06-167_FVII-alb-SP# (SP# = <u>33</u>, <u>34</u>)</b>       | cpOcta135-SP# | Stable pool expressing FVII-alb. Derived from clonal host cell line wt+ST6GAL1-KI-06-167 by transfection of plasmid pUCOE Hu-P Ctrl-IRES_FVII-alb.  | This work               |
| <b>NT3/4-KO+ST3GAL6_sol-KI-15_FVII-alb-SP# (SP# = <u>19</u>, <u>20</u>)</b> | cpOcta135-SP# | Stable pool expressing FVII-alb. Derived from host cell line NT3/4-KO +ST3GAL6_sol-KI-15 by transfection of plasmid pUCOE Hu-P Ctrl-IRES_FVII-alb.  | This work               |
| <b>NT3/4-KO+ST6GAL1_sol-KI-03_FVII-alb-SP# (SP# = <u>17</u>, <u>18</u>)</b> | cpOcta135-SP# | Stable pools expressing FVII-alb. Derived from host cell line NT3/4-KO +ST6GAL1_sol-KI-03 by transfection of plasmid pUCOE Hu-P Ctrl-IRES_FVII-alb. | This work               |
| <b>NT3/4-KO+ST3GAL6-KI-08_FVII-alb-SP# (SP# = <u>23</u>, <u>24</u>)</b>     | cpOcta135-SP# | Stable pool expressing FVII-alb. Derived from host cell line NT3/4-KO+ST3GAL6-KI-08 by transfection of plasmid pUCOE Hu-P Ctrl-IRES_FVII-alb.       | This work               |
| <b>NT3/4-KO+ST6GAL1-KI-03_FVII-alb-SP# (SP# = <u>29</u>, <u>30</u>)</b>     | cpOcta135-SP# | Stable pool expressing FVII-alb. Derived from host cell line NT3/4-KO+ST6GAL1-KI-03 by transfection of plasmid pUCOE Hu-P Ctrl-IRES_FVII-alb.       | This work               |

| <b>Name with stable pool (SP#) and clone numbers (CL#)</b>       | <b>ID</b>     | <b>Description</b>                                                                                                                                       | <b>Source/Reference</b> |
|------------------------------------------------------------------|---------------|----------------------------------------------------------------------------------------------------------------------------------------------------------|-------------------------|
| <b>NT3/4-KO+ST6GAL1-KI-03-154_FVII-alb-SP#</b><br>(SP# = 37, 38) | cpOcta135-SP# | Stable pool expressing FVII-alb. Derived from clonal host cell line NT3/4-KO+ST6GAL1-KI-03-154 by transfection of plasmid pUCOE Hu-P Ctrl-IRES_FVII-alb. | This work               |
| <b>NT3/4-KO+ST6GAL1-KI-06-160_FVII-alb-SP#</b><br>(SP# = 39, 40) | cpOcta135-SP# | Stable pool expressing FVII-alb. Derived from clonal host cell line NT3/4-KO+ST6GAL1-KI-06-160 by transfection of plasmid pUCOE Hu-P Ctrl-IRES_FVII-alb. | This work               |
| <b>wt HEK 293-F_FVIII-BDD-SP#</b><br>(SP# = 07, 08)              | cpOcta154-SP# | Stable pool expressing <i>FVIII-BDD</i> . Derived from host cell line wt HEK 293-F by transfection of plasmid pUCOE Hu-P Ctrl-IRES_FVIII-BDD.            | This work               |
| <b>NT3/4-KO-02_FVIII-BDD-SP#</b><br>(SP# = 13, 14)               | cpOcta154-SP# | Stable pool expressing <i>FVIII-BDD</i> . Derived from host cell line NT3/4-KO-02 by transfection of plasmid pUCOE Hu-P Ctrl-IRES_FVIII-BDD.             | This work               |
| <b>NT3/4-KO+ST6GAL1-KI-03_FVIII-BDD-SP#</b><br>(SP# = 15, 16)    | cpOcta154-SP# | Stable pool expressing <i>FVIII-BDD</i> . Derived from host cell line NT3/4-KO+ST6GAL1-KI-03 by transfection of plasmid pUCOE Hu-P Ctrl-IRES_FVIII-BDD.  | This work               |
| <b>wt HEK 293-F_FIX-SP#</b><br>(SP# = 02, 03)                    | cpOcta144-SP# | Stable pool expressing FIX. Derived from host cell line wt HEK 293-F by transfection of plasmid pUCOE Hu-P Ctrl-IRES_FIX.                                | This work               |
| <b>NT3/4-KO-02_FIX-SP#</b><br>(SP# = 14, 15)                     | cpOcta144-SP# | Stable pool expressing FIX. Derived from host cell line NT3/4-KO-02 by transfection of plasmid pUCOE Hu-P Ctrl-IRES_FIX.                                 | This work               |
| <b>NT3/4-KO+ST6GAL1-KI-03_FIX-SP#</b><br>(SP# = 16, 17)          | cpOcta144-SP# | Stable pool expressing FIX. Derived from host cell line NT3/4-KO+ST6GAL1-KI-03 by transfection of plasmid pUCOE Hu-P Ctrl-IRES_FIX.                      | This work               |

### 3.1.5 Laboratory animals

| <b>Name</b>                        | <b>Provider</b>                  |
|------------------------------------|----------------------------------|
| <b>CD (Sprague Dawley) IGS Rat</b> | Charles River, Sulzfeld, Germany |

### 3.1.6 Standards

| Name                                                                                | Fragment sizes                                                                                                                     | Source/Reference                                                |
|-------------------------------------------------------------------------------------|------------------------------------------------------------------------------------------------------------------------------------|-----------------------------------------------------------------|
| <b>GeneRuler DNA Ladder Mix</b>                                                     | 100, 200, 300, 400, 500, 600, 700, 800, 900, 1,000, 1,200, 1,500, 2,000, 2500, 3,000, 3,500, 4,000, 5,000, 6,000, 8,000, 10,000 bp | Thermo Fisher Scientific (Thermo Scientific), Dreieich, Germany |
| <b>Precision Plus Protein Unstained Protein Standards, Strep-tagged recombinant</b> | 10, 15, 20, 25, 37, 50, 75, 100, 150, 250 kDa                                                                                      | BioRad, Feldkirchen, Germany                                    |
| <b>GlycoWorks RapiFluor-MS Dextran Calibration Ladder</b>                           | 2-30 glucose units. GlycoWorks RapiFluor-MS N-Glycan Kit component                                                                 | Waters, Milford, USA                                            |

### 3.1.7 Enzymes and proteins

All restriction endonucleases were acquired from New England Biolabs (Frankfurt am Main, Germany).

| Name                                                                              | Description                                                                               | Source/Reference                                |
|-----------------------------------------------------------------------------------|-------------------------------------------------------------------------------------------|-------------------------------------------------|
| <b>Cas9 nuclease</b>                                                              | Recombinant Cas9 enzyme with two nuclear localization signals.                            | Synthego, Menlo Park, USA                       |
| <b>FVII-alb</b>                                                                   | Coagulation FVII-alb in-house standard produced in wt HEK 293-F cells.                    | Laboratory inventory                            |
| <b>Human coagulation factor VII concentrate BRP (batch 2.0, lot Y0000667-2EA)</b> | European Pharmacopoeia FVII reference standard                                            | Sigma Aldrich, Taufkirchen, Germany             |
| <b>Human serum albumin</b>                                                        | Plasma-derived; non-glycosylated                                                          | Pan Biotech, Aidenbach, Germany                 |
| <b>NovoSeven® (1 mg/mL, lot DS6J126)</b>                                          | Recombinant coagulation FVII produced in BHK cells.                                       | Novo Nordisk, Bagsværd, Denmark                 |
| <b>Nuwiq®</b>                                                                     | Recombinant FVIII-BDD produced in wt HEK 293-F cells; in-house standard.                  | Laboratory inventory                            |
| <b>Rapid PNGase F</b>                                                             | GlycoWorks RapiFluor-MS N-Glycan Kit component                                            | Waters, Milford, USA                            |
| <b>Recombinant human ASGR1</b>                                                    | ASGP-R subunit containing the C-type lectin domain.                                       | R&D Systems, Minneapolis, USA                   |
| <b>Recombinant human MMR/CD206</b>                                                | Recombinant mannose receptor                                                              | R&D Systems, Minneapolis, USA                   |
| <b>Shrimp alkaline phosphatase</b>                                                | DNA dephosphorylation                                                                     | New England Biolabs, Frankfurt am Main, Germany |
| <b>Sialidase A</b>                                                                | $\alpha$ 2-3,6,8,9 Neuraminidase A: Removal of sialic acids from N-glycans.               | New England Biolabs, Frankfurt am Main, Germany |
| <b>Sialidase S</b>                                                                | $\alpha$ 2-3 Neuraminidase S: Removal of $\alpha$ 2,3-linked sialic acids from N-glycans. | New England Biolabs, Frankfurt am Main, Germany |

### 3.1.8 Kits

| Name                                                             | Provider                                                         |
|------------------------------------------------------------------|------------------------------------------------------------------|
| <b>Amine Coupling kit</b>                                        | GE Healthcare, Freiburg, Germany                                 |
| <b>Asserachrom IX:Ag kit</b>                                     | Stago, Düsseldorf, Germany                                       |
| <b>Asserachrom VIII:Ag kit</b>                                   | Stago, Düsseldorf, Germany                                       |
| <b>DNeasy Blood &amp; Tissue Kit</b>                             | Qiagen, Hilden, Germany                                          |
| <b>FuGENE HD</b>                                                 | Promega, Mannheim, Germany                                       |
| <b>GlycoWorks RapiFluor-MS N-glycan kit</b>                      | Waters, Milford, USA                                             |
| <b>Lipofectamine CRISPRMAX Cas9 Transfection Reagent</b>         | Thermo Fisher Scientific (Invitrogen), Dreieich, Germany         |
| <b>LudgerTag 2 AA Monosaccharide Release and Labeling kit</b>    | Ludger, Oxfordshire, United Kingdom                              |
| <b>NEBuilder HiFi DNA Assembly Cloning kit</b>                   | New England Biolabs, Frankfurt am Main, Germany                  |
| <b>Phire Tissue Direct PCR Master mix</b>                        | Thermo Fisher Scientific (Thermo Scientific), Dreieich, Germany  |
| <b>Q5 High-Fidelity 2X Master mix</b>                            | New England Biolabs, Frankfurt am Main, Germany                  |
| <b>Q5 High-Fidelity DNA polymerase</b>                           | New England Biolabs, Frankfurt am Main, Germany                  |
| <b>QIAfilter EndoFree Plasmid Maxi kit</b>                       | Qiagen, Hilden, Germany                                          |
| <b>QIAprep Spin Miniprep kit</b>                                 | Qiagen, Hilden, Germany                                          |
| <b>QIAquick Gel Extraction kit</b>                               | Qiagen, Hilden, Germany                                          |
| <b>QIAquick PCR Purification kit</b>                             | Qiagen, Hilden, Germany                                          |
| <b>QuantStudio 3D Digital PCR 20K Chip kit v2 and Master mix</b> | Thermo Fisher Scientific (Applied Biosystems), Dreieich, Germany |
| <b>RNeasy Plus Mini kit</b>                                      | Qiagen, Hilden, Germany                                          |
| <b>SIGNAL DMB LABELING kit</b>                                   | ProZyme, Hayward, USA                                            |
| <b>SuperScript VILO cDNA Synthesis kit</b>                       | Thermo Fisher Scientific (Invitrogen), Dreieich, Germany         |
| <b>TaqMan Gene Expression Master mix</b>                         | Thermo Fisher Scientific (Applied Biosystems), Dreieich, Germany |
| <b>Vi-CELL XR Quad Pack Reagent kit</b>                          | Beckmann Coulter, Krefeld, Germany                               |
| <b>Zymutest Factor VII ELISA kit</b>                             | Hyphen BioMed, Neuville-sur-Oise, France                         |

### 3.1.9 Chemicals

If not stated otherwise, chemicals were of maximum purity and purchased from Sigma-Aldrich (Taufkirchen, Germany) or Carl Roth (Karlsruhe, Germany). Solvents were of liquid chromatography mass spectrometry (LC-MS) grade quality.

| Name                                      | Provider                                                        |
|-------------------------------------------|-----------------------------------------------------------------|
| <b>Acetonitrile</b>                       | Thermo Fisher Scientific (Thermo Scientific), Dreieich, Germany |
| <b>Agarose</b>                            | Sigma-Aldrich, Taufkirchen, Germany                             |
| <b>Ampicillin</b>                         | Sigma-Aldrich, Taufkirchen, Germany                             |
| <b>Butylamine</b>                         | Sigma Aldrich, Taufkirchen, Germany                             |
| <b>PageBlue Protein Staining Solution</b> | Thermo Fisher Scientific (Thermo Scientific), Dreieich, Germany |

| <b>Name</b>                               | <b>Provider</b>                                          |
|-------------------------------------------|----------------------------------------------------------|
| <b>Cytidine</b>                           | Sigma-Aldrich, Taufkirchen, Germany                      |
| <b>Deoxynucleotide Solutions, Mix</b>     | New England Biolabs, Frankfurt am Main, Germany          |
| <b>GeIRED</b>                             | GENEON, Ludwigshafen, Germany                            |
| <b>Gel Loading Dye, Purple (6x)</b>       | New England Biolabs, Frankfurt am Main, Germany          |
| <b>Hygromycin B</b>                       | Thermo Fisher Scientific (Gibco), Dreieich, Germany      |
| <b>IXSelect chromatography resin</b>      | GE Healthcare, Freiburg, Germany                         |
| <b>LDS sample buffer (4x)</b>             | NuPAGE                                                   |
| <b>N-acetylmannosamine</b>                | Dextra Laboratories, Reading, United Kingdom             |
| <b>Orthophosphoric acid</b>               | Carl Roth, Karlsruhe, Germany                            |
| <b>PageBlue Protein Staining Solution</b> | Thermo Scientific                                        |
| <b>Phenol Red, sodium salt</b>            | Sigma-Aldrich, Taufkirchen, Germany                      |
| <b>Polysorbate 80</b>                     | Merck KGaA, Darmstadt, Germany                           |
| <b>Puromycin</b>                          | Sigma-Aldrich, Taufkirchen, Germany                      |
| <b>Reducing agent (10x)</b>               | NuPAGE                                                   |
| <b>Tris(2-carboxyethyl)phosphin</b>       | Thermo Fisher Scientific (Invitrogen), Dreieich, Germany |
| <b>Tetrahydrofuran</b>                    | Sigma Aldrich, Taufkirchen, Germany                      |
| <b>Trifluoroacetic acid</b>               | Sigma Aldrich, Taufkirchen, Germany                      |
| <b>Tween20</b>                            | Carl Roth, Karlsruhe, Germany                            |
| <b>VIIISelect chromatography resin</b>    | GE Healthcare, Freiburg, Germany                         |
| <b>VIISelect chromatography resin</b>     | GE Healthcare, Freiburg, Germany                         |
| <b>Vitamin K</b>                          | Sigma-Aldrich, Taufkirchen, Germany                      |

### 3.1.10 Media and supplements

| <b>Name</b>                                                                            | <b>Provider</b>                                                 |
|----------------------------------------------------------------------------------------|-----------------------------------------------------------------|
| <b>Dulbecco's Modified Eagle's Medium, high glucose, GlutaMAX Supplement, pyruvate</b> | Thermo Fisher Scientific (Gibco), Dreieich, Germany             |
| <b>Fetal Bovine Serum (Australia, heat inactivated)</b>                                | Thermo Fisher Scientific (Life Technologies), Dreieich, Germany |
| <b>FreeStyle 293 Expression Medium</b>                                                 | Thermo Fisher Scientific (Gibco), Dreieich, Germany             |
| <b>Luria Broth Medium powder</b>                                                       | SERVA Electrophoresis, Heidelberg, Germany                      |
| <b>SF9-2 serum-free medium</b>                                                         | Thermo Fisher Scientific (Life Technologies), Dreieich, Germany |
| <b>SOC medium</b>                                                                      | New England Biolabs, Frankfurt am Main, Germany                 |

### 3.1.11 Buffers

| Name                                                                                                                             | Provider/Components                                                                                                                                              |
|----------------------------------------------------------------------------------------------------------------------------------|------------------------------------------------------------------------------------------------------------------------------------------------------------------|
| <b>ASGP-R running buffer</b>                                                                                                     | 20 mM 4-(2-hydroxyethyl)-1-piperazineethanesulfonic acid (HEPES)<br>150 mM NaCl<br>5 mM CaCl <sub>2</sub><br>0.005% Tween20 (v/v)<br>pH 7.4                      |
| <b>CutSmart buffer</b>                                                                                                           | New England Biolabs, Frankfurt am Main, Germany                                                                                                                  |
| <b>FVII activation buffer (final concentrations after mixing VIISelect elution buffer and Tris-CaCl<sub>2</sub> buffer 10:1)</b> | 90.9 mM Tris<br>90.9 μM ZnCl <sub>2</sub><br>45.5 mM glycine<br>10 mM CaCl <sub>2</sub><br>pH 8.0                                                                |
| <b>Glycan analysis buffer</b>                                                                                                    | 25 mM NaAc<br>pH 7.5                                                                                                                                             |
| <b>HEPES</b>                                                                                                                     | AppliChem, Darmstadt, Germany                                                                                                                                    |
| <b>IXSelect elution buffer</b>                                                                                                   | 0.02 M Tris<br>2 M MgCl <sub>2</sub><br>pH 7.4                                                                                                                   |
| <b>IXSelect equilibration buffer</b>                                                                                             | 0.02 M Tris<br>0.15 M NaCl<br>pH 7.4                                                                                                                             |
| <b>IXSelect wash buffer</b>                                                                                                      | 0.02 M Tris<br>0.5 M NaCl<br>0.01% Polysorbate 80 (v/v)<br>pH 7.4                                                                                                |
| <b>MOPS 20x buffer</b>                                                                                                           | Invitrogen                                                                                                                                                       |
| <b>MR running buffer</b>                                                                                                         | 10 mM (4-(2-hydroxyethyl)-1-piperazineethanesulfonic acid)<br>150 mM NaCl<br>1 mM MgCl <sub>2</sub><br>5 mM CaCl <sub>2</sub><br>0.005% Tween 20 (v/v)<br>pH 7.4 |
| <b>PAB Cleaning Solution</b>                                                                                                     | Merck KGaA, Darmstadt, Germany                                                                                                                                   |
| <b>Phosphate Buffered Saline</b>                                                                                                 | Thermo Fisher Scientific (Fisher Scientific), Dreieich, Germany                                                                                                  |
| <b>SPR regeneration buffer</b>                                                                                                   | 50 mM (4-(2-hydroxyethyl)-1-piperazineethanesulfonic acid)<br>100 mM ethylenediaminetetraacetic acid (EDTA)<br>pH 7.4                                            |
| <b>Tris-CaCl<sub>2</sub></b>                                                                                                     | 1 M Tris<br>110 mM CaCl <sub>2</sub><br>pH 8.0                                                                                                                   |



| <b>Name</b>                               | <b>Provider/Components</b>                                                                                                                     |
|-------------------------------------------|------------------------------------------------------------------------------------------------------------------------------------------------|
| <b>UltraPure tris-acetate buffer, 10X</b> | Thermo Fisher Scientific (Invitrogen), Dreieich, Germany                                                                                       |
| <b>VIIISelect elution buffer</b>          | 1.5 mol/kg NaCl<br>0.02 mol/kg CaCl <sub>2</sub><br>0.02 mol/kg histidine<br>0.02% Polysorbate 80 (v/v)<br>50% ethylene glycol (v/v)<br>pH 6.5 |
| <b>VIIISelect equilibration buffer</b>    | 0.3 mol/kg NaCl<br>0.02 mol/kg CaCl <sub>2</sub><br>0.02 mol/kg histidine<br>0.02% Polysorbate 80 (v/v)<br>pH 6.5                              |
| <b>VIIISelect wash buffer</b>             | 1 mol/kg NaCl<br>0.02 mol/kg CaCl <sub>2</sub><br>0.02 mol/kg histidine<br>0.02% Polysorbate 80 (v/v)<br>pH 6.5                                |
| <b>VIISelect elution buffer</b>           | 0.05 M glycine<br>pH 3                                                                                                                         |
| <b>VIISelect equilibration buffer</b>     | 0.05 M Tris<br>0.15 M NaCl<br>pH 7.5                                                                                                           |

### 3.1.12 Consumables

| <b>Material</b>                        | <b>Description</b>                    | <b>Provider</b>                                                 |
|----------------------------------------|---------------------------------------|-----------------------------------------------------------------|
| <b>Baffled/non-baffled shake flask</b> | E125, E250, E500, E1000, E2000, E3000 | Corning, Amsterdam, Netherlands                                 |
| <b>Centrifuge tubes</b>                | 15, 50, 250, 500 mL (Polypropylene)   | Corning, Amsterdam, Netherlands                                 |
| <b>Chromatography column</b>           | RoboColumns 200µl                     | Repligen, Ravensburg, Germany                                   |
| <b>Cryopreservation vials</b>          | 2 mL, inner thread                    | neoLab, Heidelberg, Germany                                     |
| <b>Desalting columns</b>               | HiPrep 26/10                          | GE Healthcare, Freiburg, Germany                                |
| <b>Eppendorf Protein LoBind tubes</b>  | 0.5, 1.5, 2.5 mL Protein LoBind       | Eppendorf, Wesseling, Germany                                   |
| <b>Glass inserts</b>                   | 8 mm; for HPLC and LC-MS              | Thermo Fisher Scientific (Thermo Scientific), Dreieich, Germany |
| <b>Glass screw thread vials</b>        | 8 mm; for HPLC and LC-MS              | Thermo Fisher Scientific (Thermo Scientific), Dreieich, Germany |

| <b>Material</b>                                            | <b>Description</b>                       | <b>Provider</b>                                                  |
|------------------------------------------------------------|------------------------------------------|------------------------------------------------------------------|
| <b>Glass screw thread vial caps</b>                        | 8 mm; for HPLC and LC-MS                 | Thermo Fisher Scientific (Thermo Scientific), Dreieich, Germany  |
| <b>Nunc multi-well plates</b>                              | 96-well, 24-well, 24-deep-well           | Thermo Fisher Scientific (Thermo Scientific), Dreieich, Germany  |
| <b>Optical adhesive film</b>                               | MicroAmp Optical Adhesive Film           | Thermo Fisher Scientific (Applied Biosystems), Dreieich, Germany |
| <b>PCR plates</b>                                          | MicroAmp Optical 96-Well Reaction Plate  | Thermo Fisher Scientific (Applied Biosystems), Dreieich, Germany |
| <b>PCR tubes</b>                                           | 0.2 mL 8 tube strips, 0.5 mL PCR clean   | Eppendorf, Wesseling, Germany                                    |
| <b>Precast agarose gels</b>                                | E-Gel with SYBR Safe DNA Gel Stain, 1.2% | Thermo Fisher Scientific (Invitrogen), Dreieich, Germany         |
| <b>Reagent reservoirs</b>                                  | 60 mL                                    | VWR, Darmstadt, Germany                                          |
| <b>Rebuffering columns</b>                                 | Miditrap G25 SpinTrap                    | GE Healthcare, Freiburg, Germany                                 |
| <b>Rebuffering columns</b>                                 | Sephadex G-25 in PD-10 Desalting Columns | GE Healthcare, Freiburg, Germany                                 |
| <b>SDS-PAGE gels</b>                                       | 4-12% Bis Tris gels                      | Thermo Fisher Scientific (Invitrogen), Dreieich, Germany         |
| <b>Single-Cell Printer cartridges</b>                      | SCP                                      | Cytexa, Freiburg, Germany                                        |
| <b>Single-use pipettes</b>                                 | 2, 5, 10, 25, 50, 100 mL                 | Corning, Amsterdam, Netherlands                                  |
| <b>SPR sensor chips</b>                                    | CM5                                      | GE Healthcare, Freiburg, Germany                                 |
| <b>Ultra-high performance liquid chromatography column</b> | XBridge BEH C18 XP                       | Waters Corporation, Milford, USA                                 |
| <b>Ultra-high performance liquid chromatography column</b> | ACQUITY UPLC Glycan BEH Amide column     | Waters, Milford, USA                                             |
| <b>Vented spin tubes</b>                                   | TPP TubeSpin, 50 mL                      | Faust Lab Science, Klettgau, Germany                             |

### 3.1.13 Devices

| <b>Name</b>                                  | <b>Type</b>                                                                               | <b>Provider</b>                                                  |
|----------------------------------------------|-------------------------------------------------------------------------------------------|------------------------------------------------------------------|
| <b>Agarose gel chamber</b>                   | Sub Cell GT / Sub Cell GT Mini                                                            | Bio-Rad Laboratories, Feldkirchen, Germany                       |
| <b>Bench centrifuge</b>                      | Biofuge pico II; Megafuge 40R, Multifuge 3SR+                                             | Thermo Fisher Scientific (Thermo Scientific), Dreieich, Germany  |
| <b>Benchtop incubator shaker</b>             | Innova 4000                                                                               | New Brunswick Scientific, Nürtingen, Germany                     |
| <b>Cell counter</b>                          | Vi-CELL XR                                                                                | Beckmann Coulter, Krefeld, Germany                               |
| <b>Chromatography column</b>                 | Tricorn 5/100, Tricorn 10/100                                                             | GE Healthcare, Freiburg, Germany                                 |
| <b>Chromatography system</b>                 | ÄKTA pure 150 M                                                                           | GE Healthcare, Freiburg, Germany                                 |
| <b>Densitometer</b>                          | GS-900 Calibrated Densitometer                                                            | Bio-Rad Laboratories, Feldkirchen, Germany                       |
| <b>Digital PCR chip loader</b>               | QuantStudio 3D                                                                            | Thermo Fisher Scientific (Applied Biosystems), Dreieich, Germany |
| <b>Digital PCR chip scanner</b>              | QuantStudio 3D                                                                            | Thermo Fisher Scientific (Applied Biosystems), Dreieich, Germany |
| <b>Freezer -80 °C</b>                        | DW 86L 626                                                                                | UniEquip, Planegg, Germany                                       |
| <b>Freezing container</b>                    | Mr. Frosty                                                                                | Thermo Fisher Scientific (Nalgene), Dreieich, Germany            |
| <b>Fume hood</b>                             | 2-453-DAND                                                                                | Köttermann, Uetze, Germany                                       |
| <b>Gel imaging system</b>                    | E-box UXS super bright                                                                    | Vilber Lourmat, Eberhardzell, Germany                            |
| <b>Heated plate reader</b>                   | BioTek ELx808                                                                             | BioTek, Bad Friedrichshall, Germany                              |
| <b>High-throughput chromatography system</b> | Freedom EVO 200                                                                           | Tecan, Wiesbaden, Germany                                        |
| <b>LC-MS system</b>                          | ACQUITY H-Class Bio equipped with fluorescence detector and coupled to a Xevo G2-XS Q-TOF | Waters, Milford, USA                                             |
| <b>Microtiter plate imaging system</b>       | Cell Metric                                                                               | Solentim, Wimborne Minster, United Kingdom                       |
| <b>Pipettes</b>                              | Transferpette 2 µL, 10 µL, 20 µL, 100 µL, 200 µL, 1,000 µL                                | BRAND, Wertheim, Germany                                         |
| <b>Power supply</b>                          | Power Pac 300                                                                             | Bio-Rad Laboratories, Feldkirchen, Germany                       |
| <b>Precast agarose gel system</b>            | E-Gel iBase Power System G64OOEU                                                          | Thermo Fisher Scientific (Invitrogen), Dreieich, Germany         |

| <b>Name</b>                                                | <b>Type</b>                                | <b>Provider</b>                                                  |
|------------------------------------------------------------|--------------------------------------------|------------------------------------------------------------------|
| <b>Quantitative real-time PCR system</b>                   | 7500 Fast Real-Time PCR system             | Thermo Fisher Scientific (Applied Biosystems), Dreieich, Germany |
| <b>Refrigerated vapor trap</b>                             | Savant RVT 5105                            | Thermo Fisher Scientific (Thermo Scientific), Dreieich, Germany  |
| <b>SDS-PAGE gel chamber</b>                                | PAGE equipment                             | Thermo Fisher Scientific (Invitrogen), Dreieich, Germany         |
| <b>Shaking incubator</b>                                   | Kuhner ISF1-X                              | Kuhner Shaker, Herzogenrath, Germany                             |
| <b>Single-Cell Printer</b>                                 | SCP                                        | Cytana, Freiburg, Germany                                        |
| <b>Surface Plasmon Resonance system</b>                    | Biacore T200 instrument                    | GE Healthcare, Freiburg, Germany                                 |
| <b>Thermocycler</b>                                        | Mastercycler gradient                      | Eppendorf, Wesseling, Germany                                    |
| <b>Digital PCR thermocycler</b>                            | ProFlex 2 x 96-well PCR System             | Thermo Fisher Scientific (Applied Biosystems), Dreieich, Germany |
| <b>Thermomixer</b>                                         | Thermomixer compact 5350                   | Eppendorf, Wesseling, Germany                                    |
| <b>Ultra-high performance liquid chromatography system</b> | UltiMate 3000, upgraded to an UHPLC system | Thermo Scientific, Waltham, USA                                  |
| <b>Ultra-deep freezer -196 °C</b>                          | MDF-C2156VAN-PE                            | Panasonic, Hamburg, Germany                                      |
| <b>UV table</b>                                            | ECX-F15.L                                  | Vilber Lourmat, Eberhardzell, Germany                            |
| <b>UV/Vis spectrophotometer</b>                            | NanoDrop 2000                              | Thermo Fisher Scientific (Thermo Scientific), Dreieich, Germany  |
| <b>Vacuum concentrator centrifuge</b>                      | Savant SPD131DDA SpeedVac Concentrator     | Thermo Fisher Scientific (Thermo Scientific), Dreieich, Germany  |
| <b>Vortex mixer</b>                                        | D-6012                                     | neoLab, Heidelberg, Germany                                      |
| <b>Water bath</b>                                          | VWB2                                       | VWR, Darmstadt, Germany                                          |
| <b>Water purification system</b>                           | OmniaPure                                  | Stakpure, Niederahr, Germany                                     |

### 3.1.14 Software

| Name                                   | Provider                                                         |
|----------------------------------------|------------------------------------------------------------------|
| Clone Manager Professional 9           | Scientific & Educational Software, Westminster, Colorado, USA    |
| QuantStudio 3D Analysis Suite          | Thermo Fisher Scientific (Applied Biosystems), Dreieich, Germany |
| Chromeleon 7.2 chromatography software | Thermo Scientific, Waltham, USA                                  |
| UNIFI 1.9 software                     | Waters, Milford, USA                                             |
| Biacore T200 Evaluation Software 3.0   | GE Healthcare, Freiburg, Germany                                 |
| SAS software version 9.4M5             | SAS Institute, Cary, USA                                         |
| Glyco Workbench                        | Damerell <i>et al.</i> <sup>210</sup>                            |

## 3.2 Methods

### 3.2.1 Microbiology and molecular biology methods

#### 3.2.1.1 Spectrophotometric DNA and RNA analysis

DNA or RNA concentration and purity were determined on a NanoDrop 2000 UV/Vis spectrophotometer. DNA or RNA concentrations were measured at a wavelength of 260 nm ( $A_{260}$ ). Protein contaminants were determined at a wavelength of 280 nm ( $A_{280}$ ) and salt and sugar contaminants were determined at 230 nm ( $A_{230}$ ). DNA or RNA samples with ratios of  $A_{260}/A_{280}$  greater than 1.8 and  $A_{260}/A_{230}$  greater than 2.0 were considered pure enough for subsequent steps.

#### 3.2.1.2 Restriction digest

##### Analytical digest

To verify the correctness of a newly assembled plasmid, analytical restriction digests were performed with suitable restriction enzymes. To this end, 0.5-2.0  $\mu$ g of plasmid DNA were digested with 10-20 U of the respective restriction enzymes in 1x CutSmart buffer for 0.5-2 h at 37 °C in a total volume of 20  $\mu$ L. Digested plasmid DNA was run on an agarose gel (3.2.1.4) and the band pattern was compared to the one expected from *in-silico* digest with the Clone Manager Professional 9 software.

##### Preparative digest

To prepare backbone plasmids for Gibson Assembly cloning (3.2.1.1), 5-10  $\mu$ g of plasmids pUCOE Hu-P Ctrl-IRES or pAAVS1-SA-hygroR-EF1 were linearized with 20-50 U *NheI-HF* or *AgeI* for 5-16 h at 37 °C in a total volume of 50  $\mu$ L 1x CutSmart buffer.

To release the insert sequences *ST3GAL6* and the canine insulin precursor signal peptides, 1.5  $\mu$ g of the synthetic DNA constructs were digested with 20 U *BsaI-HF* for 3 h at 37 °C in a total volume of 20  $\mu$ L 1x CutSmart buffer. To release the 5' part of insert sequences *ST6GAL1\_sol* and *ST3GAL6\_sol*, 0.4  $\mu$ g of the synthetic DNA constructs were digested with 5 U *BsaI-HF* for 15 min at 37 °C in a total volume of 10  $\mu$ L 1x CutSmart buffer. Insert sequences were dephosphorylated (3.2.1.3) and isolated from preparative agarose gels (3.2.1.5) prior to Gibson Assembly cloning (3.2.1.1).

##### Digest for digital PCR

Prior to digital PCR experiments (3.2.1.7), 1 ng of genomic DNA purified from HEK 293-F cells (3.2.1.6) was digested with 1 U of *NheI-HF* for 1 h at 37 °C in a total volume of 20  $\mu$ L 1x CutSmart buffer. Afterwards, *NheI-HF* was heat-inactivated at 80 °C for 5 min.

### **3.2.1.3 DNA dephosphorylation of linearized backbone plasmids**

To prevent re-ligation of linearized backbone plasmids and released insert sequences, they were dephosphorylated by incubating in a total volume of 20  $\mu$ L 1x CutSmart buffer with 5 U shrimp alkaline phosphatase (rSAP) at 37 °C for 1 h. Afterwards, restriction enzymes and rSAP were heat-inactivated at 80 °C for 5 min.

### **3.2.1.4 Agarose gel electrophoresis**

#### **Analytical agarose gels**

To evaluate analytical restriction digests or PCR reactions, analytical agarose gel electrophoresis was performed. Therefore, 0.5-2.0  $\mu$ g of plasmid DNA or 5  $\mu$ L of a PCR reaction were transferred to precast SYBR Safe DNA stained 1.2% agarose E-Gels. 5  $\mu$ L GeneRuler DNA Ladder Mix were used as size standard. Gels were run on an E-Gel iBase Power System for 26 min using the program for 0.8-2% agarose gels. Photographs of the gels were taken under UV light (260 nm) with an E-box UXS super bright gel imaging system.

#### **Preparative agarose gels**

To separate linearized and dephosphorylated backbone plasmids from non-linearized plasmid molecules and other DNA, preparative agarose gel electrophoresis was performed. Depending on the gel chamber size, 50 or 100 mL of 1% agarose in UltraPure TAE buffer (1x) were melted in a microwave, 1:10,000 GelRED DNA stain were added and the gel was cast. After polymerization of the gel, DNA samples were mixed with 6x loading dye and loaded on the solid agarose gel. 5  $\mu$ L GeneRuler DNA Ladder Mix were used as size standard. TAE buffer served as running buffer and running conditions were 5V/cm distance between the electrodes for 45-60 min at room temperature. Photographs of the gels were taken under UV light (260 nm) with an E-box UX5 super bright gel imaging system.

### **3.2.1.5 DNA isolation from preparative agarose gels**

After preparative agarose gel electrophoresis, linearized backbone plasmids were visualized on an UV table (365 nm) and excised using a scalpel. DNA was extracted from the gel using the QIAquick Gel Extraction Kit according to the protocol. In brief, three volumes of buffer QG were added to one volume of gel with a maximum of 400 mg gel per column. After 10 min incubation at 50 °C, one gel volume of isopropanol was added and the sample was applied to a QIAquick column. The column was washed with 500  $\mu$ L buffer QG and 750  $\mu$ L buffer PE and DNA was eluted by addition of 50  $\mu$ L buffer EB to the column, incubation for 1 min and centrifugation. Afterwards, DNA concentration and purity were determined (3.2.1.1) and isolated DNA was used for Gibson Assembly cloning (3.2.1.1).

### **3.2.1.6 Polymerase chain reaction from plasmid DNA**

Polymerase chain reaction (PCR) was performed to generate insert sequences with the required overhangs for Gibson Assembly cloning (3.2.1.1) or amplicons for Sanger sequencing (3.2.1.5). For a 50  $\mu$ L reaction, 10-50 ng DNA template and 0.5  $\mu$ M forward and reverse primer were diluted to 25  $\mu$ L with water and 25  $\mu$ L Q5 High-Fidelity 2X Master Mix were added. Thermocycler conditions are described in Table 1. Afterwards, success of the PCR was evaluated by agarose gel electrophoresis (3.2.1.4) and PCR products were purified (3.2.1.8).

Table 1: Thermocycler conditions used for PCR amplification from plasmid DNA

| Step                        | Temperature<br>[ °C] | Time<br>[s] | Number<br>of cycles |
|-----------------------------|----------------------|-------------|---------------------|
| <b>Initial denaturation</b> | 98                   | 30          | 1                   |
| <b>Denaturation</b>         | 98                   | 5           |                     |
| <b>Primer annealing</b>     | 50-72                | 20          | 32                  |
| <b>Extension</b>            | 72                   | 30 (per kb) |                     |
| <b>Final extension</b>      | 72                   | 120         | 1                   |

### 3.2.1.7 Polymerase chain reaction from genomic DNA

PCR was performed on purified genomic DNA (3.2.1.6) from HEK 293-F cells for subsequent analysis of the genomic sequence, e. g. following gene KI. For a 25  $\mu$ L reaction, 35 ng DNA template and 0.3  $\mu$ M forward and reverse primer were diluted to 19.25  $\mu$ L with water and 0.25  $\mu$ L Q5 High-Fidelity DNA polymerase and 0.5  $\mu$ L 10 mM dNTPs were added. Thermocycler conditions are described in Table 2. Afterwards, success of the PCR was evaluated by agarose gel electrophoresis (3.2.1.4) and PCR products were purified for Sanger sequencing (3.2.1.5) of the AAVS1 integration site.

Table 2: Thermocycler conditions used for PCR amplification from genomic DNA

| Step                        | Temperature<br>[ °C] | Time<br>[s] | Number of cycles |
|-----------------------------|----------------------|-------------|------------------|
| <b>Initial denaturation</b> | 98                   | 60          | 1                |
| <b>Denaturation</b>         | 98                   | 15          |                  |
| <b>Primer annealing</b>     | 67                   | 30          | 40               |
| <b>Extension</b>            | 72                   | 180         |                  |
| <b>Final extension</b>      | 72                   | 300         | 1                |

### 3.2.1.8 PCR product purification

Prior to Gibson Assembly cloning (3.2.1.1) or Sanger sequencing (3.2.1.5), PCR products were purified using the QIAquick PCR Purification Kit according to the kit protocol. Five volumes of buffer PB were mixed with one volume of PCR reaction, 10  $\mu$ L of 3 M sodium acetate pH 5.0 were added and the sample was applied to a QIAquick column and centrifuged at 17,900 xg for 1 min. The column was washed by adding 0.75 mL buffer PE and centrifuged again, whereafter any residual buffer PE was removed by another centrifugation step. DNA was eluted in a new 1.5 mL tube by addition of 50  $\mu$ L buffer EB to the center of the column, incubation for 1 min and centrifugation. Afterwards, DNA concentration and purity were determined (3.2.1.1).

#### 3.2.1.1 Gibson Assembly cloning

Gibson Assembly cloning was used for the assembly of linear DNA fragments to form a circular plasmid. Prerequisite of the method is that the DNA fragments to be assembled have overlapping homologous sequences of at least 15 bps to their neighboring fragments. During the reaction, an exonuclease chews back the 5' strand of the fragments, leading to single-stranded 3' overhangs. The 3' overhangs of fragments with sequence homology anneal, a DNA polymerase fills the gaps and a DNA ligase links the fragments.<sup>211</sup>

All mammalian expression and KI donor plasmids were cloned using Gibson Assembly. The plasmid backbones pUCOE Hu-P Ctrl-IRES and pAAVS1-SA-hygroR-EF1 were linearized by preparative restriction digest (3.2.1.2), dephosphorylated (3.2.1.3), separated on agarose gels (3.2.1.4) and purified from the gels (3.2.1.5). Insert sequences were PCR-amplified from synthetic DNA constructs using primers ending with the required overhangs for Gibson Assembly (3.2.1.6) and subsequently purified (3.2.1.8) or released from synthetic DNA constructs by restriction digest with *BsaI* (3.2.1.2). Gibson Assembly was performed using the NEBuilder HiFi DNA Assembly Cloning Kit. For each reaction, 0.05 pmol linearized plasmid and 0.15 pmol of insert sequence were filled up to 10  $\mu$ L with water, mixed with 10  $\mu$ L of master mix and incubated at 50 °C for 1 h.

### **3.2.1.2 Transformation of *E. coli***

After Gibson Assembly cloning, NEB 5-alpha Competent *E. coli* cells were transformed according to the supplier's high efficiency transformation protocol. 50  $\mu$ L of *E. coli* cells were thawed on ice, 2  $\mu$ L of the Gibson Assembly reaction were added, the mixture was incubated on ice for 30 minutes and heat shocked at 42 °C for 30 seconds. Afterwards the mixture was incubated on ice for 5 minutes, 500  $\mu$ L room temperature SOC medium were added and bacteria were incubated at 37 °C for 60 minutes while shaking at 250 rpm.

### **3.2.1.3 Cultivation of *E. coli***

For selection of successfully assembled plasmids NEB 5-alpha Competent *E. coli* cells were cultivated on Luria Broth agar plates containing 100  $\mu$ g/mL ampicillin at 37 °C overnight (14-16 hours).

For small-scale analytical plasmid preparations, single colonies of transformed NEB 5-alpha Competent *E. coli* cells were picked and transferred to 3 mL Luria Broth supplemented with 100  $\mu$ g/mL ampicillin in spin tubes and incubated at 37 °C and 250 rpm overnight.

For large-scale plasmid preparations, 0.5 mL of a 3 mL *E. coli* culture were used to inoculate 100-500 mL Luria Broth supplemented with 100  $\mu$ g/mL ampicillin in appropriate Erlenmeyer flasks and incubated at 37 °C and 250 rpm overnight.

### **3.2.1.4 Plasmid preparation from *E. coli***

#### **Small-scale plasmid preparation**

Small-scale plasmid preparations were performed for plasmid verification by analytical restriction digest (3.2.1.2) or Sanger sequencing (3.2.1.5). They were performed using the QIAprep Spin Miniprep Kit according to the kit protocol. In brief, 3 mL bacteria of a 3 mL overnight culture were pelleted by centrifugation at 8,000 xg for 3 min, resuspended in 250  $\mu$ L buffer P1 before adding 250  $\mu$ L buffer P2, mixed thoroughly and incubated for 1 min. Then, 350  $\mu$ L buffer N3 were added, the tube was mixed thoroughly, centrifuged at 17,900 xg and the supernatant was applied to a QIAprep spin column. The column was centrifuged at 17,900 xg for 30 sec and afterwards washed two times with 0.5 mL buffer PB and 0.75 mL buffer PE. Residual wash buffer was removed by centrifugation and plasmid DNA was eluted into a new tube by addition of 50  $\mu$ L buffer EB, incubation for 1 min and centrifugation.

#### **Large-scale, endotoxin-free plasmid preparation**

Plasmid preparations were performed using the QIAfilter EndoFree Plasmid Maxi Kit according to the kit protocol. In brief, bacteria of a 250 mL overnight culture were pelleted by centrifugation at 8,000 xg for 15 min, resuspended in 10 mL buffer P1 before adding 10 mL buffer P2, mixed thoroughly and incubated for 5 min. Then, 10 mL chilled buffer P3 were added, the mixture was shaken vigorously, the lysate was transferred to the QIAfilter cartridge and incubated for 10 min. The cell lysate was filtered,



2.5 mL buffer ER were added, mixed and incubated on ice for 30 min. Afterwards, the mixture was applied to an equilibrated QIAGEN-tip 500 column, the resin was washed twice with 30 mL buffer QC and DNA was eluted with 15 mL buffer QN. Finally, DNA was precipitated by adding 10.5 mL isopropanol, pelleted by centrifugation at 17,900 xg for 10 min and the supernatant was decanted carefully. The DNA pellet was washed with 5 mL endotoxin-free 70% ethanol, air-dried and dissolved in 500 µL endotoxin-free buffer TE. DNA concentration was determined (3.2.1.1), the DNA was diluted to 1 µg/µL and stored at -80 °C until CRISPR/Cas9 KI (3.2.2.2) or transfection (3.2.2.3).

#### **3.2.1.5 DNA sequencing and sequence verification**

To verify the correct assembly of newly cloned plasmids (3.2.1.1), inserts were Sanger sequenced at GATC Biotech (Konstanz, Germany) with primers listed in 3.1.3. In addition, Sanger sequencing was performed to characterize the AAVS1 integration site. For sequencing, 20 µL of DNA sample with concentrations between 10-100 ng/µL were sent to GATC Biotech. Sequencing results were compared to the *in silico* designed or genomic sequences using Clone Manager.

#### **3.2.1.6 Genomic DNA preparation from HEK 293-F cells**

Genomic DNA was prepared from HEK 293-F cells prior to sequencing of genomic DNA (3.2.1.5), determination of donor plasmid copy number (3.2.1.7) and direct PCR clone screening (3.2.1.8). Genomic DNA was isolated from HEK 293-F-derived cells using the DNeasy Blood & Tissue Kit using the spin column protocol for purification of total DNA from animal blood or cells. From a cell culture flask  $1 \times 10^6$  cells were pelleted by centrifugation at 140 xg for 5 min, the pellet was resuspended in 200 µL PBS and 20 µL proteinase K and 200 µL buffer AL were added. After 10 min incubation at 56 °C, 200 µL ethanol were added, the mixture was applied to a DNeasy Mini spin column and centrifuged at 17,900 xg for 1 min. Columns were washed with 500 µL buffer AW1 and 500 µL AW2. Then, columns were placed into a new tube, 200 µL buffer AE were added, they were incubated for 1 min and DNA was eluted by centrifugation. Afterwards, DNA concentration was determined (3.2.1.1).

#### **3.2.1.7 Donor plasmid copy number determination by digital PCR**

Digital PCR (dPCR) is used for the absolute quantification of DNA molecules. For amplification and detection, sequence-specific primers and a probe carrying a fluorescent reporter and a non-fluorescent quencher are used. Upon binding of the primers and probe to the single-stranded DNA during the PCR reaction, the second strand is formed by the polymerase and due to its 5' to 3' exonuclease activity, the probe is digested. This releases the fluorescent reporter from the quencher and the fluorescence can be detected. The total volume of a PCR reaction is partitioned in thousands of small reactions, for example in wells of a micro-scale chip. When the PCR reaction—containing an unknown number of DNA template molecules—is distributed into the partitions, each partition either contains a template DNA molecule or not. In partitions containing a template DNA molecule, the PCR reaction can take place, leading to fluorescence, while in partitions containing no template DNA molecule no fluorescence is generated. In contrast to RT-qPCR, the amount of fluorescence signal is not considered and the partitions are only classified as positive or negative. Since the fluorescence signal intensity is not considered, dPCR is much more robust towards PCR inhibitors<sup>212</sup>, or primer/probe pairs with low amplification efficiencies<sup>213</sup>. Also, the partitioning in dPCR leads to higher sensitivity compared to qPCR.<sup>214</sup>

With the number of positive partitions and the used sample volume, the number of template DNA molecules per volume can be determined. However, if a partition contains multiple copies of the template DNA, it will not change the result—the partition will be positive. Therefore, it does not affect the determined number of template DNA molecules per volume, leading to false results. To correct for this problem, Poisson's law of small numbers is applied to calculate the probability that one partition

contains more than one template DNA molecule. This probability is proportional to the number of positive wells, since with an increasing number of DNA template molecules, the probability that multiple molecules end up in one partition increases. After applying Poisson's law, the readout of a digital PCR is DNA template copies per microliter. To determine the gene copy number per cell, two primer/probe pairs labelled with different fluorophores were used in the same reaction. By comparing the DNA template concentration of the gene of interest (GOI) with that of a housekeeper gene (where the number of copies per cell is known), GOI copies per cell can be assessed (Formula 1). Due to the pseudotriploidy of the used HEK 293-F cell line,<sup>130,215</sup> the counts of most chromosomes vary from one to four within individual cells. *RNase P* was selected as housekeeper in this study, which is either found in two or three copies per cell. Therefore, GOI copy numbers per cell were always calculated once assuming two *RNase P* copies and once assuming three *RNase P* copies.

Digital PCR was used to determine the number of AAVS1 integration site copies in HEK 293-F cells and the number of integrated donor plasmid copies after gene KI in single-cell clones. Prior to dPCR, genomic DNA was restriction digested (3.2.1.2) in order to separate multiple copies of the same gene from one another. Then, 50-150 ng of digested genomic DNA were mixed with 2x QuantStudio 3D digital PCR Master Mix v2, 20x GOI primer/probe pair, 20x *RNase P* primer/probe pair and filled up to 14.5  $\mu\text{L}$  with water. Then, the mixture was loaded on a 20K dPCR chip using the QuantStudio 3D digital PCR chip loader and run on a ProFlex 2 x 96-well PCR System using the thermocycler conditions outlined in Table 3. After PCR, the chip was read on a QuantStudio 3D digital PCR chip scanner and data was analyzed in the QuantStudio 3D Analysis Suite.

Formula 1: Calculation of GOI copies per cell

$$GOI \text{ copies per cell} = \frac{\frac{\text{copies}}{\mu\text{L}} (GOI)}{\frac{\text{copies}}{\mu\text{L}} (\text{housekeeper})} * \text{copies per cell (housekeeper)}$$

Table 3: Thermocycler conditions used for digital PCR

| Step                                  | Temperature<br>[ °C] | Time<br>[s] | Number of cycles |
|---------------------------------------|----------------------|-------------|------------------|
| <b>Initial denaturation</b>           | 96                   | 600         | 1                |
| <b>Denaturation</b>                   | 98                   | 30          | 39               |
| <b>Primer annealing and extension</b> | 60                   | 120         |                  |
| <b>Final extension</b>                | 60                   | 120         |                  |

### 3.2.1.8 Direct PCR for characterization of clones with successful *ST6GALI* KI

For characterization of *ST6GALI* overexpressing clones (see 3.2.2.4) direct PCR was performed. In a direct PCR approach, the PCR is performed on lysates of the respective clones, making genomic DNA preparation not necessary. Direct PCR was performed using the Phire Tissue Direct PCR Master Mix. Therefore, 1  $\mu\text{L}$  cell suspension was sampled into PCR plates and diluted with 10  $\mu\text{L}$  dilution buffer and 0.25  $\mu\text{L}$  DNA Release additive. This mixture was incubated at 98 °C for 2 min. For PCR, 1  $\mu\text{L}$  thereof was mixed with 0.5  $\mu\text{L}$  forward and reverse primer, 7.5  $\mu\text{L}$  water and 9.5  $\mu\text{L}$  Phire Tissue Direct PCR Master Mix. In every PCR experiment, two negative controls were performed using 1  $\mu\text{L}$  genomic DNA released from wt HEK 293-F cells and the respective primers. In addition, two no template controls were

performed with 1  $\mu$ L of water instead of DNA using kit control primers amplifying a highly conserved fragment of mammalian genomic DNA. Positive controls were performed with 1  $\mu$ L genomic DNA released from wt HEK 293-F cells and the kit control primers. Thermocycler conditions are described in Table 4. PCR products were analyzed by agarose gel electrophoresis for the presence of the expected fragment (3.2.1.4).

Table 4: Thermocycler conditions used for direct PCR clone characterization

| Step                        | Temperature<br>[ °C] | Time<br>[s] | Number of<br>cycles |
|-----------------------------|----------------------|-------------|---------------------|
| <b>Initial denaturation</b> | 98                   | 300         | 1                   |
| <b>Denaturation</b>         | 98                   | 5           |                     |
| <b>Primer annealing</b>     | 65                   | 5           | 40                  |
| <b>Extension</b>            | 72                   | 40          |                     |
| <b>Final extension</b>      | 72                   | 60          | 1                   |

Four primer pairs were designed such that different combinations thereof could be used to analyze the outcome of a gene KI in a clone (Table 3). The interpretation of the results of the direct PCR characterization is described in the following sections.

Table 5: Primer pairs used for direct PCR clone characterization

| Primer pair    | Primer numbers | Type of integration                                  | Amplification of homology arm | PCR fragment size<br>[bp] |
|----------------|----------------|------------------------------------------------------|-------------------------------|---------------------------|
| <b>KI HA-L</b> | 180+173        | Single or multiple KI in one AAVS1 site              | Left                          | 1,270                     |
| <b>KI HA-R</b> | 174+181        |                                                      | Right                         | 1,337                     |
| <b>RI HA-L</b> | 182+171        | Random integrations or multiple KI in one AAVS1 site | Left                          | 1,516                     |
| <b>RI HA-R</b> | 176+185        |                                                      | Right                         | 1,297                     |

In the wt AAVS1 integration site, the sequences used for homologous recombination with the donor plasmid are separated by an 18 bp gRNA recognition sequence, where CRISPR/Cas9-mediated double-strand breaks are induced (Figure 3). In a clone with only wt AAVS1 integration sites and no random integrations, none of the primer pairs will result in a PCR product.

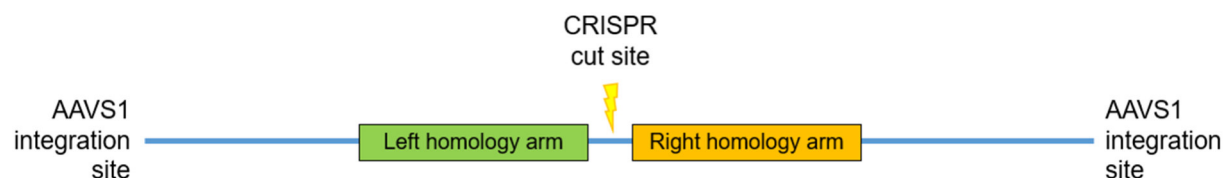


Figure 3: Wild-type AAVS1 integration site with left and right homology arm, separated by the CRISPR/Cas9 cut site (indicated by a yellow flash).

### 1. Integration of a single donor plasmid copy per AAVS1 integration site (S-KI)

When integration of a single donor plasmid copy takes place (S-KI), the sequences of the AAVS1 integration sites that are homologous to the donor plasmid homology arms provide homology for HDR (Figure 5A). After successful S-KI by HDR, the gRNA recognition sequence is replaced by the KI sequence of the donor plasmid, which contains the hygromycin B resistance gene and the *ST6GAL1* gene (Figure 4). To detect AAVS1 integration sites with an S-KI, the primer pairs “KI HA-L” and “KI HA-R” were designed. One of the primers of each pair binds inside the KI sequence and the other primer binds in the genome left or right of the homology arms, respectively. If only S-KIs take place in a clone, both primer pairs KI HA-L and KI HA-R can anneal, leading to PCR amplification, while the primer pairs RI HA-L and RI HA-R cannot anneal, leading to no PCR amplification. This was the desired integration event.

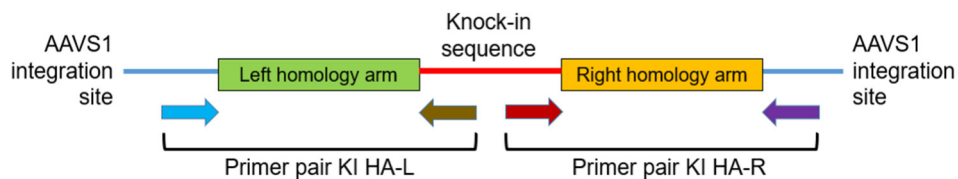


Figure 4: AAVS1 integration site after a successful KI. Arrows indicate primer pairs leading to PCR amplicons at the left (HA-L) and right (HA-R) homology arms, indicating an S-KI.

### 2. Integration of multiple donor plasmid copies per AAVS1 integration site (M-KI)

Integration of multiple donor plasmid copies in a single AAVS1 integration site (M-KI) can occur, since during HDR the backbone of a donor plasmid copy can provide homology for the next one (Figure 5B). If a clone contains a M-KI, all primer pairs will result in PCR products (Figure 6). In this case, it is not possible to tell whether the clone contains a M-KI, an S-KI plus a RI or all three events.

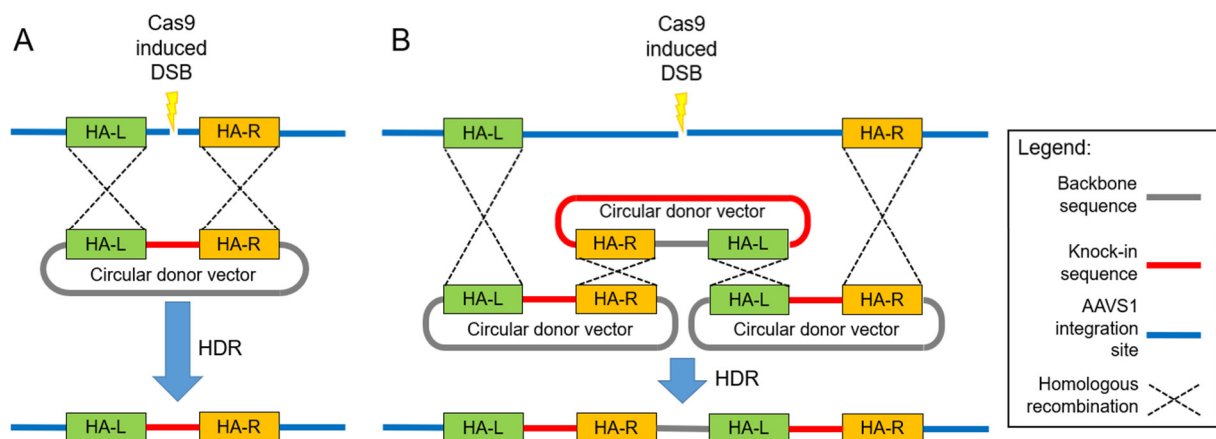


Figure 5: Schematic of homology-directed repair (HDR) integration of (A) an S-KI and (B) a M-KI with two copies integrated via the left (HA-L) and right (HA-R) homology arms. The site of the Cas9-induced double strand break (DSB) is indicated by a yellow flash. The same way, more than two donor plasmid copies can integrate in a single AAVS1 site.

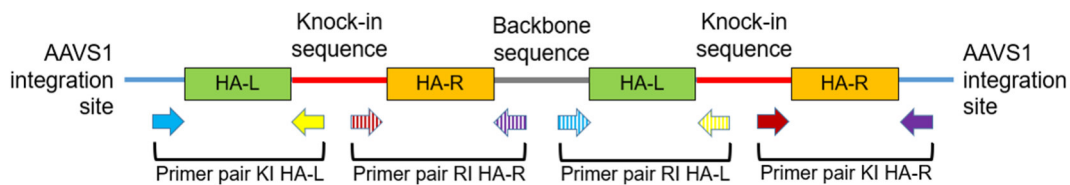


Figure 6: AAVS1 integration site after a M-KI. The indicated PCR amplicons detect supposed correct (KI) and random (RI) integrations at the left (HA-L) and right (HA-R) homology arms.

### 3. Random donor plasmid integration (RI)

Random donor plasmid integration is not a targeted process, which makes detection by PCR more difficult. Since integration occurs at random sites, the genome sequences left and right of the integration are unknown and thus the donor backbone sequences adjacent to the homology arms have to be used for detection. If a donor plasmid randomly integrates into the genome, three situations are possible.

#### 3.1. Donor plasmid backbone sequences left **and** right are present

If the donor plasmid backbone sequences directly adjacent to both the left **and** right homology arms have integrated into the genome, both primer pairs RI HA-L and RI HA-R will result in a PCR product (Figure 7).

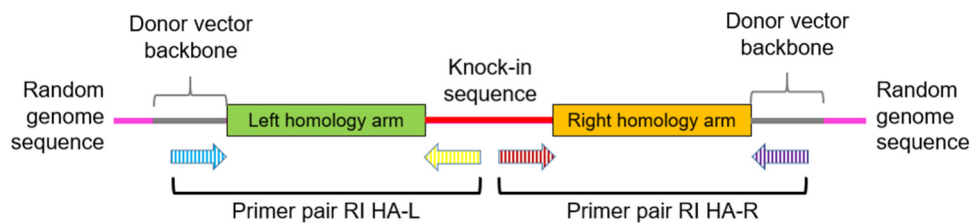


Figure 7: Genome locus with a randomly integrated donor plasmid copy with PCR amplicons able to detect random integrations (RI) at the left (HA-L) and right (HA-R) homology arms.

#### 3.2. Donor plasmid backbone sequences left **or** right are present

If the donor plasmid backbone sequences directly adjacent to the left homology arm **or** to the right of the right homology arm have integrated into the genome, only the respective primer pairs RI HA-L **or** RI HA-R will result in a PCR product (Figure 8).

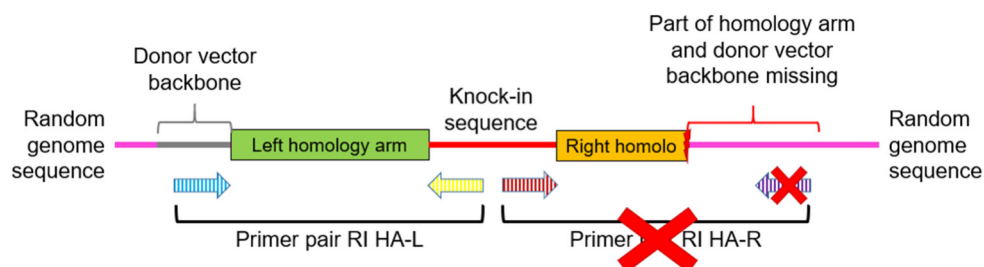


Figure 8: Genome locus with a randomly integrated donor plasmid copy with PCR amplicons able to detect random integrations (RI) at the left (HA-L) but not at the right (HA-R) homology arm.

### 3.3. Donor plasmid backbone sequences left and right are not present

If **neither** the donor plasmid backbone sequences directly adjacent to the left homology arm **nor** those to the right of the right homology arm have integrated into the genome, none of the primer pairs RI HA-L or RI HA-R will result in a PCR product (Figure 9). This event can therefore not be detected by the direct PCR design.

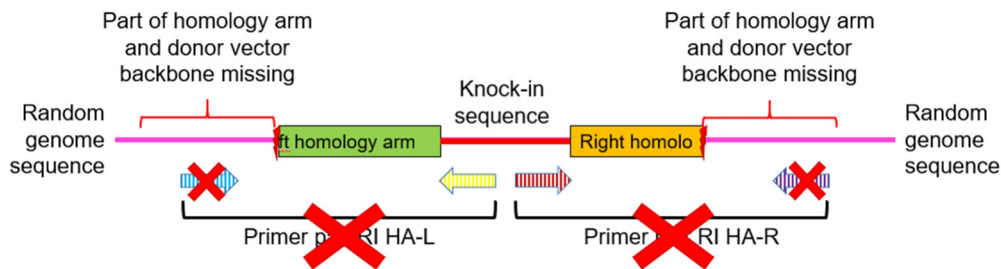


Figure 9: Genome locus with a randomly integrated donor plasmid copy with no PCR amplicon able to detect random integrations (RI) at the left (HA-L) but not at the right (HA-R) homology arm.

#### 3.2.1.9 Preparation of total RNA from HEK 293-F cells

Total RNA was isolated from HEK 293-F cells prior to gene expression analysis (3.2.1.11) using the RNeasy Plus Mini Kit with the protocol for purification of total RNA from animal cells. From a cell culture flask  $1 \times 10^6$  cells were pelleted by centrifugation at 140 xg for 5 min, the supernatant was discarded, and cells were lysed by adding 350  $\mu$ L buffer RLT plus and 30 s of vortexing. The lysate was added to a genomic DNA eliminator spin column, the column was centrifuged at 17,900 xg for 1 min and the flow-through was diluted with 350  $\mu$ L of 70% ethanol. The mixture was pipetted into a RNeasy spin column and centrifuged at 17,900 xg for 1 min. The column was washed by addition of 700  $\mu$ L buffer RW1 and 500  $\mu$ L buffer RPE. The column was placed in a new tube, 500  $\mu$ L buffer RPE were added and the column was centrifuged at 17,900 xg for 2 min. Total RNA was eluted in a new tube by addition of 50  $\mu$ L water, incubation for 1 min and elution by centrifugation at 17,900 xg for 1 min. Afterwards, RNA concentration was determined (3.2.1.1) and samples were stored at -80 °C until reverse transcription (3.2.1.10).

#### 3.2.1.10 Reverse transcription of total RNA

Reverse transcription of total RNA to complementary DNA (cDNA) was performed using the SuperScript VILO cDNA Synthesis Kit. In a 0.2 mL tube, 2,000 ng total RNA, 4  $\mu$ L 5x VILO Reaction Mix and 2  $\mu$ L 10x SuperScript Enzyme Mix were combined and water was added to achieve a total volume of 20  $\mu$ L. The mixture was incubated at 25 °C for 10 min, then at 42 °C for 60 min and then at 85 °C for 5 min. Samples were stored at -80 °C until gene expression analysis (3.2.1.11). A cDNA control with water instead of RNA was performed.

#### 3.2.1.11 Relative gene expression analysis by RT-qPCR

For the selection of cell pools and clones overexpressing *ST6GAL1*, *ST3GAL6* and their soluble versions, the expression of the respective SiaTs was determined by RT-qPCR. Therefore, the GOI and the housekeeper gene *RNase P* were amplified from reverse transcribed cDNA with sequence-specific FAM- and VIC-labelled primer/probe sets.

For reaction setup, a master mix was prepared from the two 20x primer/probe pairs, the 2x TaqMan Gene Expression Master Mix and water. For each reaction, 2  $\mu$ L of reverse transcribed cDNA were added to 18  $\mu$ L of the master mix and the mixture was pipetted into a PCR plate. The PCR plate was

sealed with optical adhesive film and run on a 7500 Fast real-time PCR system according to the thermocycler protocol in Table 6. A cDNA sample from wt HEK 293-F cells, the cDNA control from the reverse transcription and a no-template control (NTC) using water instead of sample were analyzed as zero point for quantification and to control for contaminations in the reagents, respectively. All samples and no-template controls were measured in triplicates.

Table 6: Thermocycler conditions used for gene expression analysis

| Step                           | Temperature<br>[ °C] | Time<br>[s] | Number<br>of cycles |
|--------------------------------|----------------------|-------------|---------------------|
| Incubation                     | 50                   | 120         | 1                   |
| Initial denaturation           | 95                   | 600         | 1                   |
| Denaturation                   | 95                   | 15          | 40                  |
| Primer annealing and extension | 60                   | 60          |                     |

For each sample and reference sample, the cycle threshold (Ct) is determined. For data evaluation, first the delta Ct (dCt) values were calculated from the Ct values of the GOI and those of *RNase P* for each sample (Formula 2) and the reference (Formula 3). Under the assumption of comparable expression of *RNase P* in all cells, this step controls for slightly differing numbers of cells used.

Formula 2: Calculation of delta Ct for samples

$$dCt(\text{sample } X) = Ct(\text{GOI}, \text{sample } X) - Ct(\text{RNase } P, \text{sample } X)$$

Formula 3: Calculation of delta Ct for the reference sample

$$dCt(\text{reference}) = Ct(\text{GOI}, \text{reference}) - Ct(\text{RNase } P, \text{reference})$$

Then, the dCt value of the reference was subtracted from the dCt value of each sample, yielding delta delta Ct (ddCt) values (Formula 4). The ddCt values were then transformed to fold-change (FC) expression values (Formula 5). The FC describes the expression level of the GOI in a sample relative to that in the reference sample. For example, a FC of 1.0 means that the expression level of the GOI in the sample is identical to that in the reference sample, a FC of 2.0 means that the expression level of the GOI in the sample is twice as high as that in the reference sample. The FC was used to rank stably expressing cell pools or clones according to their GOI expression level.

Formula 4: Calculation of delta delta Ct for samples

$$ddCt(\text{sample } X) = dCt(\text{sample } X) - dCt(\text{reference})$$

Formula 5: Calculation of fold-change expression values for samples

$$FC \text{ expression } (\text{sample } X \text{ vs. reference}) = 2^{-ddCt}$$

## 3.2.2 Mammalian cell culture methods

### 3.2.2.1 Determination of viable cell density and viability

Viable cell density and viability were determined using the Vi-CELL XR cell viability analyzer with the analysis parameters described in Table 7. To this end, 600  $\mu\text{L}$  of cell suspension were taken from a cell culture, transferred to a Vi-CELL sample cup and placed into the sample carousel of the Vi-CELL for measurement.

Table 7: Vi-CELL parameters for HEK 293-F cells

| Parameter                                          | Setpoint |
|----------------------------------------------------|----------|
| <b>Minimum diameter [<math>\mu\text{m}</math>]</b> | 12       |
| <b>Maximum diameter [<math>\mu\text{m}</math>]</b> | 50       |
| <b>Number of images</b>                            | 100      |
| <b>Aspirate cycles</b>                             | 2        |
| <b>Trypan blue mixing cycles</b>                   | 2        |
| <b>Cell brightness [%]</b>                         | 85       |
| <b>Cell sharpness</b>                              | 100      |
| <b>Viable cell spot brightness [%]</b>             | 80       |
| <b>Viable cell spot area [%]</b>                   | 5        |
| <b>Minimum circularity</b>                         | 0        |
| <b>Decluster degree</b>                            | Medium   |

### 3.2.2.2 Cultivation of HEK 293-F cells

If not stated otherwise, HEK 293-F cells and derivatives were cultivated in baffled Erlenmeyer flasks in shaking incubators (37 °C, 8% CO<sub>2</sub>, humid atmosphere, 25 mm shaking diameter and 150 rpm) using the proprietary serum-free culture medium SF9-2, which is based on the FreeStyle 293 Expression Medium. FVII/FVII-alb and FIX expressing cells were cultured in medium containing 11  $\mu\text{g}/\text{mL}$  vit K to achieve adequate  $\gamma$ -carboxylation. On Mondays, Wednesdays and Fridays viable cell density was determined (3.2.2.1). Then, in order to achieve constant logarithmic growth, cell suspension was removed and fresh medium was added so that a concentration of  $5 \times 10^5$  cells/mL (Monday and Wednesday) or  $3 \times 10^5$  cells/mL (Friday) was obtained.

### 3.2.2.3 Cryopreservation of HEK 293-F cells

For cryopreservation of cells for long-term storage, a cell suspension containing  $1 \times 10^7$  cells was centrifuged at 200 xg for 5 min, the cell pellet was resuspended in 1 mL of 4-8 °C cold culture medium with 10% DMSO and the cell suspension was transferred to 2 mL cryopreservation vials. The vials were placed into a Mr. Frosty freezing container, which was transferred to -80 °C for at least one day to ensure a cooling rate of 1 °C/min. For final storage vials were transferred into an ultra-deep freezer at -150 °C.

### 3.2.2.1 Revitalization of HEK 293-F cells

For revitalization, cryopreserved cells were thawed in a water bath at 37 °C until no ice crystals were visible. Then, they were transferred to a shake flask filled with 17 mL culture medium that was pre-warmed in a shaking incubator. Fifteen minutes after revitalization, viable cell density and viability were determined (3.2.2.1) and cells were cultured as described in 3.2.2.2.



### 3.2.2.2 CRISPR/Cas9-mediated SiaT KI in HEK 293-F cells

To generate host cell lines overexpressing different SiaTs (ST6GAL1, ST3GAL6, ST6GAL1\_sol and ST3GAL6\_sol), the plasmid pAAVS1-SA-hygroR-EF1 with the respective GOI was knocked into the wt HEK 293-F and the NT3/4-KO-02 cell lines. KIs were performed using ribonucleoprotein particles (RNP; a complex of recombinant Cas9 and synthetic guide RNAs [gRNA]) due to higher editing efficiencies observed compared to plasmid-based setups.<sup>216</sup>

One day before the gene KI, the respective host cell lines (wt HEK 293-F or NT3/4-KO-02) were seeded in 3.6 mL FreeStyle culture medium in spin tubes at a viable cell density of  $6 \times 10^5$  c/mL, in order to achieve a target cell density of  $1 \times 10^6$  c/mL on the day of KI. For KI the Lipofectamine CRISPRMAX Cas9 Transfection Reagent kit was used. To prepare the RNP complex, Cas9 and gRNA as well as 25  $\mu$ L Lipofectamine Cas9 Plus Reagent were added to 500  $\mu$ L of FreeStyle medium and incubated for 10 min at RT. In a separate tube, 500  $\mu$ L of FreeStyle medium were mixed with the donor plasmid and 37.5  $\mu$ L Lipofectamine CRISPRMAX Transfection Reagent and the mixture was directly added to the RNP complex. The final mixture was incubated at RT for 10 min and slowly added to the cells. After KI, pools were cultivated for two days before starting stable pool selection (3.2.2.3). Multiple KI experiments using different amounts of Cas9 (between 15 and 150 pmol), gRNA (between 45 and 450 pmol) and donor plasmid (between 1 and 30  $\mu$ g) were performed for each host cell line and SiaT combination.

### 3.2.2.3 Generation of pools stably overexpressing SiaTs

The donor plasmid pAAVS1-SA-hygroR-EF1 contains a resistance gene for the antibiotic hygromycin B (*HygR*), in order to select for cells with a stable integration of the donor plasmid after CRISPR/Cas9 KI.

Two days after the KI, the FreeStyle culture medium was replaced by centrifugation at 200 xg for 5 min, removal of the supernatant and resuspension of the cell pellet in fresh FreeStyle medium containing 12.5  $\mu$ g/mL hygromycin B. During stable pool selection, cells were seeded to  $1 \times 10^6$  c/mL two to three times a week, while expanding the cultures when the cell numbers increased and medium was replaced once a week to guarantee sufficient hygromycin B selection pressure. Once the stable pools reached 90% viability, selection pressure was removed, a cell pellet containing  $1 \times 10^6$  cells was taken for relative gene expression analysis by RT-qPCR (3.2.1.11), pools were cryopreserved for storage (3.2.2.3) and subsequently cultivated according to standard conditions (3.2.2.2).

### 3.2.2.4 Single-cell clone generation from stable *ST6GAL1* overexpressing pools

In order to isolate genotypically homogenous clones from heterogeneous stable KI pools, single-cell cloning was performed for the KI pools wt+ST6GAL1-KI-03, wt+ST6GAL1-KI-06, NT3/4-KO+ST6GAL1-KI-03 and NT3/4-KO+ST6GAL1-KI-06 using the Single-Cell Pinter. To prepare for single-cell isolation, a cell suspension containing  $1 \times 10^6$  cells was centrifuged at 200 xg for 5 min and the resulting pellet was washed with 5 mL SF9-2 medium. The cells were again washed, centrifuged and finally resuspended in 1 mL SF9-2 medium. From this cell suspension, 50  $\mu$ L were transferred to a Single-Cell Printer cartridge, which was attached to the Single-Cell Pinter. Single-cell isolation was performed with the recognition criteria of 13  $\mu$ m minimal cell size, 35  $\mu$ m maximal cell size and a minimal roundness of 0.5. The Single-Cell Printer deposited single cells that met those criteria into the wells of a 96-well plate (96-wp), which was prefilled with 200  $\mu$ L of DMEM medium supplemented with 10% fetal bovine serum. For each pool, two 96-wps with single cell clones were prepared.

### **3.2.2.5 Expansion of *ST6GAL1* overexpressing clones**

The clones were incubated in 96-wps at 37 °C, 8% CO<sub>2</sub>, humid atmosphere without shaking for two to three weeks. During that time, confluency was monitored with the Cell Metric microtiter plate imaging system and cells were resuspended twice a week by pipetting to break apart cell clumps. Upon reaching more than 95% confluency, clones were transferred to 24-well plates (24-wps) and incubated in 1 mL SF9-2 medium containing 1x phenol red at 37 °C, 8% CO<sub>2</sub>. Clones transferred to 24-wps were initially shaken at 100 rpm. Due to the attachment and subsequent death of most cells at the well wall, shaking speed was reduced to 50 rpm. After four weeks of culturing in 24-wps, growing clones—identified by visible turbidity and medium turning yellow—were expanded to 2 mL in 24-deep-well plates (24-dwps) with shaking at 150 rpm. Growing clones were further expanded to shake flask, a cell pellet containing 1x10<sup>6</sup> cells was taken for relative gene expression analysis by RT-qPCR (3.2.1.11) and clones were cryopreserved for storage (3.2.2.3) and subsequently cultivated according to standard conditions (3.2.2.2).

### **3.2.2.6 Transfection of plasmids coding for model proteins**

To generate cell lines expressing the model proteins FVII-alb, FVIII-BDD and FIX as well as the FVII control, the respective host cell lines were transfected with plasmids coding for the model proteins. One day prior to transfection, 6x10<sup>5</sup> c/mL of the respective host cell lines (underlined in 3.1.4.2) were seeded in 28.5 mL SF9-2 culture medium in baffled shake flasks. On the day of transfection, 35 µg of endotoxin-free plasmid DNA (3.2.1.4) were added to 1.5 mL culture medium before adding 70 µL FuGENE HD transfection reagent. This mixture was incubated for 20 min at RT before it was slowly added to the cell suspension under soft shaking. After transfection, pools were cultivated for two days before starting stable pool selection (3.2.2.3). All transfections were performed in duplicates.

### **3.2.2.7 Generation of stable pools expressing model proteins**

The expression plasmids pUCOE Hu-P Ctrl-IRES and pUCOE Hu-P Ctrl-IRES-WPRE contain a resistance gene for the antibiotic puromycin, to select for cells with a stable integration of the plasmid in the genome. Two days after transfection, the SF9-2 culture medium was replaced by centrifugation of the cells at 200 xg for 5 min, removal of the supernatant and resuspension of the cell pellet in fresh medium containing 2.5 µg/mL puromycin. During stable pool selection, cells were seeded to 1x10<sup>6</sup> c/mL two to three times a week, while expanding the cultures when the cell numbers increased and medium was replaced completely once a week to guarantee sufficient selection pressure. Once the stable pools reached 90% viability, selection pressure was removed, a part of each pool was cryopreserved for storage (3.2.2.3) and they were subsequently cultivated according to standard conditions (3.2.2.2).

### **3.2.2.8 Cell-specific productivity assay for characterization of expression cell lines**

The pools stably expressing FVII, FVII-alb, FVIII-BDD or FIX were analyzed for cell growth and protein expression by performing a cell-specific productivity (CSP) assay. Therefore, 3x10<sup>5</sup> c/mL of each pool were seeded in 30 mL of fresh SF9-2 medium in baffled shake flasks and cultured for three days. After three days, viable cell density was determined (3.2.2.1) and 500 µL of sample was taken for the determination of model protein concentration by enzyme-linked immunosorbent assay (ELISA) (3.2.3.6, 3.2.3.7, 3.2.3.8). The CSP and division rate were calculated according to Formula 6 and Formula 7 and best expressing and growing cell lines were selected for subsequent model protein production.

Formula 6: Cell-specific productivity calculation

$$CSP \left[ \frac{pg}{c * d} \right] = \frac{\text{protein concentration on day 3} \left[ \frac{\mu g}{mL} \right] * \text{culture volume} [mL]}{\frac{(\text{cell number on day 3} [c] - \text{cell number on day 0} [c]) * \text{number of days} [d]}{\ln \frac{\text{cell number on day 3} [c]}{\text{cell number on day 0} [c]}}}$$

Formula 7: Division rate calculation

$$\text{Division rate} \left[ \frac{div.}{d} \right] = \frac{\text{viable cell density on day 3} \left[ \frac{c}{mL} \right] - \text{viable cell density on day 0} \left[ \frac{c}{mL} \right]}{\ln 2 * \text{number of days} [d]}$$

### 3.2.2.9 Model protein expression in batch cultures

To produce sufficient model proteins for all downstream analyses, selected expression cell lines were cultivated in batch mode. Therefore,  $5 \times 10^5$  cells/mL were seeded in the desired volume (between 0.5 L and 1 L) in baffled Erlenmeyer flasks and cultivated in shaking incubators (37 °C, 8% CO<sub>2</sub>, humid atmosphere, 25 mm shaking diameter and 150 rpm) in SF9-2 medium. On Mondays, Wednesdays and Fridays, viable cell density was determined and cell culture supernatant was harvested after 5 to 7 days by centrifugation at 2,000 xg for 20 minutes. Protein content was determined by ELISA (3.2.3.6, 3.2.3.7, 3.2.3.8).

To evaluate feeding the sialic acid precursors *N*-acetylmannosamine (ManNAc) and cytidine on sialylation levels, expression cell lines derived from wt HEK 293-F, NT3/4-KO-02, NT3/4-KO+ST3GAL6\_sol-KI, NT3/4-KO+ST6GAL1\_sol-KI, NT3/4-KO+ST3GAL6-KI and NT3/4-KO+ST6GAL1-KI cells were additionally cultivated in medium supplemented with 20 mM ManNAc and 5 mM cytidine. Furthermore, the NT3/4-KO-02-derived expression cell line was cultured in either ManNAc or cytidine alone. To control for potential changes caused by the required sterile filtering, the expression cell lines derived from wt HEK 293-F and NT3/4-KO-02 cells were cultured in sterile filtered SF9-2 medium.

## 3.2.3 Protein biochemistry methods

### 3.2.3.1 Purification of FVII and FVII-alb on a Tecan system

FVII and FVII-alb were purified on a Tecan high throughput chromatography system. RoboColumns containing 200 μL VIISelect resin were equilibrated with 5 column volumes (CV) of VIISelect equilibration buffer. Then, 50 mL of cell culture supernatant were applied to the column, it was washed with 10 CV equilibration buffer and FVII or FVII-alb were eluted with 10 CV VIISelect elution buffer. Equilibration was performed with a flow rate of 300 cm/h and sample loading, wash and elution were performed at 100 cm/h.

The fractions containing FVII/FVII-alb were pooled, rebuffed in water using Miditrap G25 SpinTraps and FVII/FVII-alb concentration was determined by FVII ELISA (3.2.3.6).

### 3.2.3.2 Purification of FVII and FVII-alb on an ÄKTA system

For the PK rat experiments, FVII and FVII-alb were purified on an ÄKTA chromatography system, which was cleaned with 1 M NaOH for 2 h prior to purification to remove endotoxins. Then, Tricorn 10/100 columns containing 4.7 mL VIISelect resin were equilibrated with 5 CV of VIISelect equilibration buffer. Afterwards, 1.4 L of cell culture supernatant were applied to the column, it was

washed with 10 CV equilibration buffer and FVII or FVII-alb were eluted with 10 CV VIISelect elution buffer. Equilibration, sample loading and wash were performed with a flow rate of 300 cm/h and elution was performed at 100 cm/h.

The fractions containing FVII/FVII-alb were pooled, rebuffered in 25 mM NaAc using Sephadex G-25 in PD-10 Desalting Columns and FVII/FVII-alb concentration was determined by FVII ELISA.

#### **3.2.3.3 Purification of Factor VIII on an ÄKTA system**

FVIII-BDD was purified on an ÄKTA pure system. Tricorn 10/100 columns containing 7.9 mL VIISelect resin were equilibrated with 7 CV of VIISelect equilibration buffer. Then, 2.5 L of cell culture supernatant were applied to the column, it was washed with 10 CV VIISelect wash buffer and FVIII-BDD was eluted with 10 CV VIISelect elution buffer. Equilibration, sample loading and wash were performed with a flow rate of 300 cm/h and elution was performed at 90 cm/h.

The fractions containing FVIII-BDD were pooled, rebuffered in water using HiPrep 26/10 Desalting Columns and FVIII-BDD concentration was determined by FVIII ELISA (3.2.3.7).

#### **3.2.3.4 Purification of Factor IX on an ÄKTA system**

FIX was purified on an ÄKTA pure system. Tricorn 10/100 columns containing 3.9 mL IXSelect resin were equilibrated with 6 CV of IXSelect equilibration buffer. Then, 1 L of cell culture supernatant was applied to the column, it was washed with 10 CV IXSelect wash buffer and FIX was eluted with 10 CV IXSelect elution buffer. All steps were performed with a flow rate of 300 cm/h.

The fractions containing FIX were pooled, rebuffered in water using Sephadex G-25 in PD-10 Desalting Columns and FIX concentration was determined by FIX ELISA (3.2.3.8).

#### **3.2.3.5 Evaluation of FVII-alb, FVII, FVIII-BDD and FIX purity by SDS-PAGE**

For sodium dodecyl sulfate polyacrylamide gel electrophoresis (SDS-PAGE), 13 µL of diluted protein sample were mixed with 2 µL 10x reducing agent and 5 µL LDS sample buffer and denatured at 70 °C for 10 min. Afterwards, the gels were placed in the gel chamber, the gel chamber was filled with MOPS buffer and samples as well as 4 µL Precision Plus Unstained protein ladder were loaded on the gel. For 12 lane gels 20 µL of sample and for 15 lane gels 15 µL sample were loaded per lane. The gels were run at 200 V for 45 min, stained with PageBlue Protein Staining Solution overnight, destained in water and imaged.

#### **3.2.3.6 Determination of FVII concentration by enzyme-linked immunosorbent assay**

FVII and FVII-alb were quantified by enzyme-linked immunosorbent assay (ELISA) using the ZYMUTEST Faktor VII Antigen kit as described in the kit protocol. Calibration curves were generated using the Human Coagulation Factor VII Concentrate BRP batch 2 and an in-house FVII-alb standard. NovoSeven® was used as a control sample.

Quantification of FVII and FVII-alb samples from the animal study was performed at Octapharma Biopharmaceuticals.

#### **3.2.3.7 Determination of FVIII-BDD concentration by ELISA**

FVIII-BDD was quantified by ELISA using the Asserachrom VIII:Ag kit as described in the kit protocol. Calibration curves were generated using an in-house FVIII-BDD standard and compared to an in-house control sample, both based on diluted Nuwiq® (recombinant coagulation FVIII-BDD).

### 3.2.3.8 Determination of FIX concentration by ELISA

FIX was quantified by ELISA using the Asserachrom IX:Ag kit as described in the kit protocol. Calibration curves were generated using the kit calibrator sample and compared to a kit control sample.

### 3.2.3.1 Activation of FVII and FVII-alb for the PK rat experiment

Auto-activation of FVII and FVII-alb samples for the animal study was performed at Octapharma Biopharmaceuticals.

FVII in VIISelect buffer was mixed with 1/10 volume of Tris-CaCl<sub>2</sub> buffer pH 8.0, generating the final activation buffer. For activation, FVII samples were incubated at 4 °C and samples were taken at different time points (63 h, 86 h, 110 h) for reducing SDS-PAGE analysis (3.2.3.5). The activation reaction was stopped by rebuffering in a proprietary FVII formulation buffer which is based on the NovoSeven® formulation buffer. The percentage of activated FVII was determined using a GS-900 Calibrated Densitometer.

### 3.2.3.2 Monosaccharide analysis

Monosaccharide analysis was performed for FVII and FVII-alb samples using the LudgerTag 2-aminobenzoic acid Monosaccharide Release and Labeling Kit according to the kit instructions with minor modifications. 75 µg FVII-alb or FVII were freeze-dried in an SpeedVac vacuum concentrator centrifuge and monosaccharides (galactose, GalNAc, mannose, glucose, GlcNAc, fucose, xylose) were released by incubating in 200 µL 4 M trifluoroacetic acid for 3 h at 100 °C. Samples were frozen, freeze-dried, dissolved in 10 µL sodium acetate and mixed with 10 µL 2-aminobenzoic acid dye and 10 µL sodium cyanoborohydride. Labelling was performed at 80 °C for 45 min. 2 µL were mixed with 178 µL Solvent A (0.2% (v/v) butylamine, 0.5% (v/v) orthophosphoric acid, 1% (v/v) tetrahydrofuran in ddH<sub>2</sub>O). Of the diluted samples, 1 µL were separated by ultra-high performance liquid chromatography (UHPLC) on an UltiMate 3000 system equipped with a fluorescence detector FLD-3100 using an XBridge BEH C18 XP column, using the gradient described in the kit protocol. Fluorescence signals were detected at 425 nm and peak areas were determined according to pre-defined parameters using the Chromeleon 7.2 chromatography software. For quantification, peak areas were compared to monosaccharide standard curves (0.16 to 10 nmol of the respective monosaccharide per injection). Input protein amounts were normalized by calculating monosaccharide levels relative to mannose, assuming three core mannoses per FVII *N*-glycan. This is a valid assumption since existence of high-mannose type or hybrid type *N*-glycans is negligible for FVII molecules expressed in HEK 293-F cells. During the sample preparation, GlcNAc is converted to glucosamine and approximately 4% of the glucosamine is converted to mannosamine by epimerization. The mannosamine co-elutes with the galactosamine generated from GalNAc. To achieve reliable results for GalNAc, 4% of the glucosamine signal—corresponding to the generated mannosamine—was subtracted from the galactosamine signal. NovoSeven® was injected twice and all other FVII samples were injected three times and mean as well as standard deviation were calculated. To ensure reproducibility of the complete workflow, three batches of FVII-alb produced individually in a pool derived from the wt HEK 293 F cell line, were analyzed and compared.

In this thesis, monosaccharide symbols follow the symbol nomenclature of the Consortium of Functional Glycomics.<sup>217</sup> Mannose: green circle; galactose: yellow circle; GlcNAc: blue square; fucose: red triangle; Neu5Ac: purple diamond (facing up/right: α2,3 linked; facing down/left: α2,6 linked; straight: undetermined). All *N*-glycan structures were drawn using GlycoWorkbench.<sup>210</sup>

### 3.2.3.3 Sialic acid analysis

Sialic acid analysis was performed using the SIGNAL DMB LABELING kit. Therefore, 40 µg FVII and FVII-alb samples were freeze-dried and sialic acids were released with acetic acid via mild acid hydrolysis. After a second step of freeze-drying, samples were dissolved in 5 µL water and labelled by reductive amination with 20 µL 1,2-diamino-4,5-methylenedioxybenzene (DMB) dissolved in sodium dithionite, acetic acid and β-mercaptoethanol. Labelled samples were freeze-dried and dissolved in 525 µL water. For subsequent UHPLC analysis on an UltiMate 3000 system equipped with a fluorescence detector FLD-3100 using a XBridge BEH C18 XP column, 1.5 µL sample were used. Fluorescence signals were detected at 448 nm and peak areas were determined automatically according to pre-defined parameters using the Chromeleon 7.2 chromatography software. For quantification, peak areas were compared to Neu5Ac and Neu5Gc standard curves (0.27 to 17.14 pmol per injection). Each sample was injected 3 times and mean as well as standard deviation were calculated. To ensure reproducibility of the complete workflow, three batches of FVII-alb produced individually in a pool derived from the wt HEK 293 F cell line, were analyzed and compared.

### 3.2.3.4 N-glycan profiling and quantification

N-glycan profiling and quantification was performed using the GlycoWorks *RapiFluor*-MS N-glycan kit according to the deglycosylation workflow for challenging glycoproteins.

#### Preparation of released N-glycans

For denaturation, 15 µg lyophilized protein were reconstituted in 22.8 µL of water, mixed with 6 µL of *RapiGest* SF including 20 mM tris(2-carboxyethyl)phosphine and incubated for 3 min at 90 °C. After cooling, 1.2 µL Rapid PNGase F was added and incubated for 5 min at 50 °C. Successful enzymatic N-glycan release was shown by molecular mass shift via SDS-PAGE. For labelling, 12 µL *RapiFluor*-MS Reagent was added to the cooled deglycosylation reactions and incubated at RT for 5 min. To stop the labelling reactions, 358 µL acetonitrile were added. For vacuum-driven clean-up, samples were applied to the conditioned wells (200 µL of 15:85 water/acetonitrile) of a GlycoWorks HILIC µElution plate, washed two times with 600 µL of 1:9:90 formic acid/water/acetonitrile and eluted with three time 30 µL of GlycoWorks SPE elution buffer. After lyophilization, samples were reconstituted in 4.5 µL water and diluted with 15.5 µL GlycoWorks Sample Diluent-dimethylformamide/acetonitrile. The *RapiFluor*-MS Intact mAB Standard was used as control.

#### Sialic acid removal by Sialidase A and Sialidase S

For Sialidase A and Sialidase S digestion, samples were lyophilized after vacuum-driven clean-up with the GlycoWorks HILIC µElution plate, resuspended in 32 µL Sialidase A or 34 µL Sialidase S buffer and split in two fractions. To both fractions, 2 µL Glycobuffer 1 and to one of the fractions 2 µL Sialidase A or 1 µL Sialidase S were added, while the same amount of water was added to the undigested reference fraction. Samples were incubated at 37 °C for 3 h, followed by addition of 10 µL water, 12 µL dimethylformamide and 358 µL acetonitrile and vacuum-driven clean-up was performed with the GlycoWorks HILIC µElution plate as described above. After lyophilization, samples were reconstituted in 4.5 µL water and diluted with 15.5 µL GlycoWorks Sample Diluent-dimethylformamide/acetonitrile. The *RapiFluor*-MS Intact mAB Standard was used as control.

#### N-glycan profiling

N-glycans from 3 µL sample were separated on an ACQUITY H-Class Bio liquid chromatography system, equipped with fluorescence detector and piloted by the UNIFI 1.9 software, using an ACQUITY

UPLC Glycan BEH Amide column with hydrophobic interaction liquid chromatography (HILIC) retention mechanism, according to the GlycoWorks *RapiFluor* MS *N*-glycan kit universal *N*-glycan profiling method. The coupled Xevo G2-XS Q-TOF mass spectrometer was operated in MS<sup>E</sup> mode by electrospray ionization with a measuring range of 100-2,000 *m/z*, a capillary voltage of 2.75 kV, a sample cone of 80 V, a source temperature of 120 °C, a desolvation temperature of 500 °C and a high energy ramp of 20-30 eV. The GlycoWorks *RapiFluor*-MS Dextran Calibration Ladder was run as a reference for peak identification.

### Identification and quantification

*N*-glycan peaks were identified by dextran ladder calibration (expressed in glucose units [GU]; based on fluorescence signal), Sialidase A and Sialidase S digestion, *m/z* signals as well as MS/MS fragmentation with peak annotation in GlycoWorkbench.<sup>218</sup> From all peaks identified, a scientific *N*-glycan library was built as a tool within the UNIFI 1.9 software. All fluorescence peaks with more than 0.5% of the total peak area were used for relative quantification. For peaks containing multiple co-eluting structures, relative proportions of each individual structure were determined using the mass signal (charge variants 2H<sup>+</sup> and/or 3H<sup>+</sup>). From the relative abundance of the detected *N*-glycans, the average amount of each monosaccharide per protein molecule was calculated. This calculation was based on the assumption that all *N*-glycosylation sites of the protein are fully occupied, which in turn is based on reports where only fully *N*-glycosylated FVII<sup>49,197-199</sup> and FIX<sup>48,207</sup> were detected. Two of the six putative *N*-glycosylation sites present in FVII-BDD are unoccupied,<sup>50,125,205,206</sup> and therefore only the four remaining sites were used for average monosaccharide amount calculation. Since three of the four sites are fully occupied and the last one is occupied to more than 85%,<sup>206</sup> calculations were performed idealistically assuming full occupancy of the four sites of FVIII-BDD. To ensure reproducibility of the complete workflow, three batches of FVII-alb produced individually in a pool derived from the wt HEK 293-F cell line, were analyzed and compared.

#### 3.2.3.5 Determination of ASGP-R and MR binding by SPR

Binding studies were performed using a Biacore T200 instrument equipped with CM5 sensor chips and equilibrated with ASGP-R running buffer at 25 °C. Recombinant human ASGR1 (ASGP-R subunit containing the C-type lectin domain) and recombinant human MR were diluted to 10 µg/mL with 10 mM NaAc buffer pH 4.0 and pH 5.5, respectively and immobilized using the Amine Coupling kit according to the kit protocol. Immobilization levels were between 2,500 and 4,000 RU for ASGR1 and between 6,300 and 9,500 RU for MR. In the negative control flow cell immobilization was performed only with running buffer for 2 min and was used as reference to correct for background noise and instrument drift. SPR measurements were performed with a flow of 30 µL/min and 600 nM of the analytes. FVII, FVII-alb, and human serum albumin were injected for 180 s followed by a 200 s dissociation phase with running buffer. After each injection, the surface was regenerated with regeneration buffer for 5-15 s. Every fourth cycle, only running buffer was injected for blank subtraction. All samples were measured in triplicates and each receptor was immobilized three times at different flow cell positions. Biacore T200 Evaluation Software 3.0 was used to analyze the SPR data. After double reference subtraction and molecular weight adjustment, the report points for binding (5 s before sample injection stop) were used as read out and were normalized to NovoSeven®. Reproducibility was assessed by analyzing three biologic FVII alb replicates produced individually in the wt HEK 293-F cell line.

#### 3.2.4 Pharmacokinetic rat experiment

The PK rat experiment was planned by Octapharma Biopharmaceuticals and conducted by LPT Laboratory of Pharmacology and Toxicology. The study was performed based on Good Laboratory

Practice Regulations of the EC enacted in Germany in the 'Chemikaliengesetz' [Chemicals Act] and "OECD Principles of Good Laboratory Practice" Document nos. 1, 8 and 13 ENV/MC/CHEM (98) 17, ENV/JM/MONO (99) 24, ENV/JM/MONO (2002) 9, respectively. Furthermore, all animal activities were approved by the Animal Protection Authority in Hamburg (Germany) "Behörde für Gesundheit und Verbraucherschutz, Amt für Verbraucherschutz, Lebensmittelsicherheit und Veterinärwesen" (GZ: V 1305-591-00.33) and performed in accordance with the "Guide on the Care and Use of Laboratory Animals". Data analysis and interpretation were performed within the scope of this work.

At the start of the study, equimolar amounts of activated FVII (270 µg/kg rat body weight of FVIIa and 650 µg/kg rat body weight of FVIIa-Alb constructs) were injected into the tail vein of 16 male CD (Sprague Dawley) International Genetic Standardization rats (mean body weight 276 g). Blood was sampled at different time points (0 min, 5 min, 15 min, 1 h, 3 h, 6 h, 12 h, 18 h, 24 h, 30 h, 36 h, 42 h, 48 h, 54 h, 60 h, 66 h and 72 h) after injection from 4 animals per time point. Sampling was performed from the retrobulbar venous plexus under isoflurane anesthesia. Samples were immediately cooled, centrifuged and sodium citrate stabilized plasma was stored at -80 °C. Quantification of FVIIa and FVIIa-alb in the rat plasma by ELISA was performed at Octapharma Biopharmaceuticals.

Area under the curve (AUC) was determined using non-compartmental analysis in the SAS software version 9.4M5 and calculation was based on the trapezoidal rule. Early half-life and terminal half-life were determined using non-compartmental analysis in the SAS software version 9.4M5. For terminal half-life calculation, the terminal data points with the best fit to the exponential decay curve were used for calculation (at least 5 data points). For early half-life calculation, only the data points up to 360 min and 1,440 min were considered for FVII and FVII-alb, respectively. Recovery 5 min after administration was calculated with Excel 2013 according to Formula 8, assuming a plasma volume of 11.3 mL per rat.<sup>219</sup>

Formula 8: Recovery 5 min after injection

$$\text{Recovery} = \frac{\text{Plasma concentration 5 min after injection}}{\text{Theoretical plasma concentration after injection}}$$



## 4 RESULTS

### 4.1 Generation of host cell lines overexpressing different sialyltransferases

#### 4.1.1 Characterization of the AAVS1 integration site

To abolish *N*-glycan GalNAc on FVII-alb, HEK 293-F cells with knock-outs of *B4GALNT3*, *B4GALNT4* and *B4GALNT3* as well as *B4GALNT4* were generated by Transposagen Biopharmaceuticals. Subsequently, to increase the sialylation of FVII-alb from wt HEK 293-F cells and the *B4GALNT3* and *B4GALNT4* double-KO clone NT3/4-KO-02, SiaTs were knocked-in to the AAVS1 integration site. The AAVS1 locus is well-suited for gene KI, since it allows for long-term, high-level expression of proteins<sup>158–161</sup>. Due to the pseudotriploidy of the HEK 293 cell line,<sup>130,215</sup> the resulting clonal variation between different HEK 293 lines,<sup>130</sup> and the genomic instability of immortalized cell lines in general,<sup>131,132,220,221</sup> the AAVS1 integration site was characterized before performing KIs.

##### 4.1.1.1 AAVS1 integration site sequencing

The donor plasmid for CRISPR/Cas9 KI contains two 800 bp sequences that are homologous to the AAVS1 integration site in the human reference genome. To ensure that the AAVS1 integration site was not mutated in HEK 293-F cells, these homologous region was sequenced. For sequencing, genomic DNA was extracted from wt HEK 293-F cells and the AAVS1 locus was PCR-amplified using the primer pairs indicated in (Figure 10). The amplicons generated with primers 132 and 133 were without unspecific bands and was thus used for Sanger sequencing. Sequencing revealed that the homology region in the AAVS1 integration site of HEK 293-F cells was identical to the human reference sequence (Figure 11). Therefore, the CRISPR donor plasmid was suitable for SiaT KI.

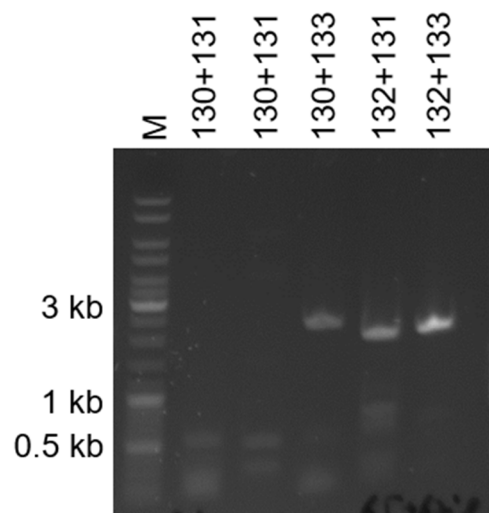


Figure 10: 1.2% SYBR Safe pre-stained agarose E-Gel with PCR amplicons of the AAVS1 integration site generated with the indicated primer pairs. The desired amplicon is around 2 kb in size. M: DNA ladder; kb: kilo base pairs.

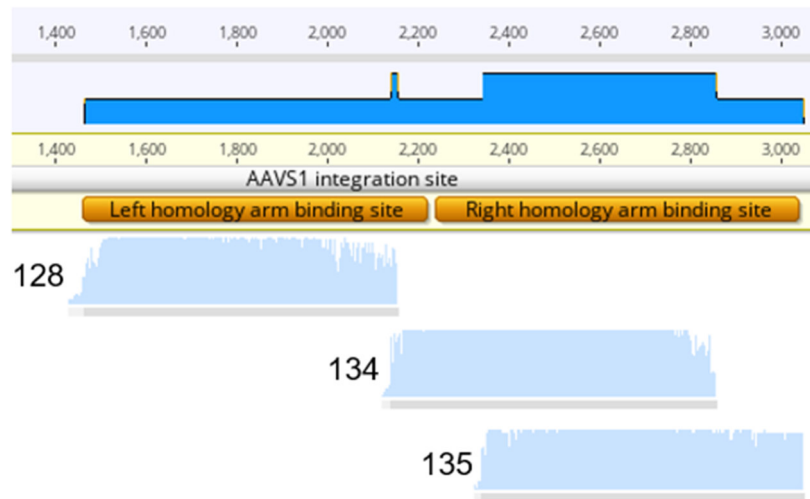


Figure 11: Sequence alignment of the Sanger sequencing results of the PCR-amplified AAVS1 locus in wt HEK 293-F cells. Sequencing results generated with primers 128, 134 and 135 are mapped to the human AAVS1 integration site reference sequence.

#### 4.1.1.2 Determination of the number of AAVS1 integration site alleles

The number of AAVS1 integration site alleles in the wt HEK 293-F and GalNAcT KO clones was analyzed by dPCR (Figure 12) in order to determine how many gene copies of SiaTs can potentially be knocked-in to the AAVS1 locus. Due to the pseudotriploidy of the HEK 293-F cell line,<sup>130,215</sup> the *RNase P* reference gene is present in either two or three alleles per cell and hence AAVS1 allele numbers were calculated for both cases. Depending on the number of *RNase P* alleles assumed, all tested clones had between one and three copies of the AAVS1 integration site, making them suitable for the planned gene KI experiments.

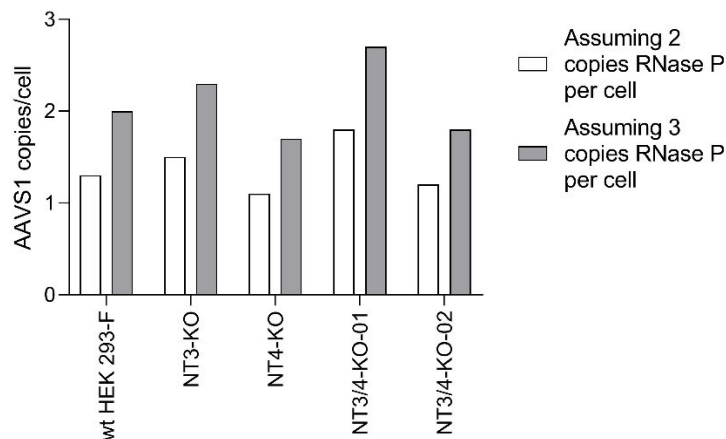


Figure 12: Copy number of AAVS1 locus in the wt HEK 293-F cell line and GalNAcT KO clones as determined with digital PCR (N=1).

#### 4.1.2 Generation of pools stably overexpressing sialyltransferases

For generating cell pools overexpressing SiaTs, CRISPR/Cas9 KIs of *ST6GAL1*, *ST3GAL6* and soluble versions *ST6GAL1\_sol* and *ST3GAL6\_sol* into the host cell lines wt HEK 293-F and NT3/4-KO-02 were performed. Afterwards, cells with a stable integration of the donor plasmids were enriched by selection with hygromycin B. Between four and sixteen individual KIs were performed for each host cell line and SiaT combination, to generate at least one stable pool per combination. The numbers of KIs performed

and the numbers of pools that survived stable pool selection are depicted in Table 8. Growth and viability curves of pools that survived selection are shown in Figure 13 and Figure 14. KI pools derived from wt HEK 293-F remained more viable during selection, recovered faster from it, and generally survived better than pools derived from the NT3/4-KO-02 cell line. This was most likely caused by the faster division rate of the wt HEK 293-F cell line (between 0.8 to 1.1 divisions/d) compared to the NT3/4-KO-02 cell line (between 0.6 and 0.9 divisions/d).

Table 8: Number of performed KI, number of pools that survived stable pool selection and survival rate for each host cell line and sialyltransferase combination.

| Host cell line | Sialyltransferase | Number of KI | Number of stable pools | Survival rate [%] |
|----------------|-------------------|--------------|------------------------|-------------------|
| wt HEK 293-F   | ST6GAL1           | 10           | 5                      | 50                |
| NT3/4-KO-02    | ST6GAL1           | 10           | 3                      | 30                |
| wt HEK 293-F   | ST3GAL6           | 10           | 3                      | 30                |
| NT3/4-KO-02    | ST3GAL6           | 10           | 4                      | 40                |
| wt HEK 293-F   | ST6GAL1_sol       | 4            | 4                      | 100               |
| NT3/4-KO-02    | ST6GAL1_sol       | 4            | 1                      | 25                |
| wt HEK 293-F   | ST3GAL6_sol       | 4            | 4                      | 100               |
| NT3/4-KO-02    | ST3GAL6_sol       | 16           | 9                      | 56                |

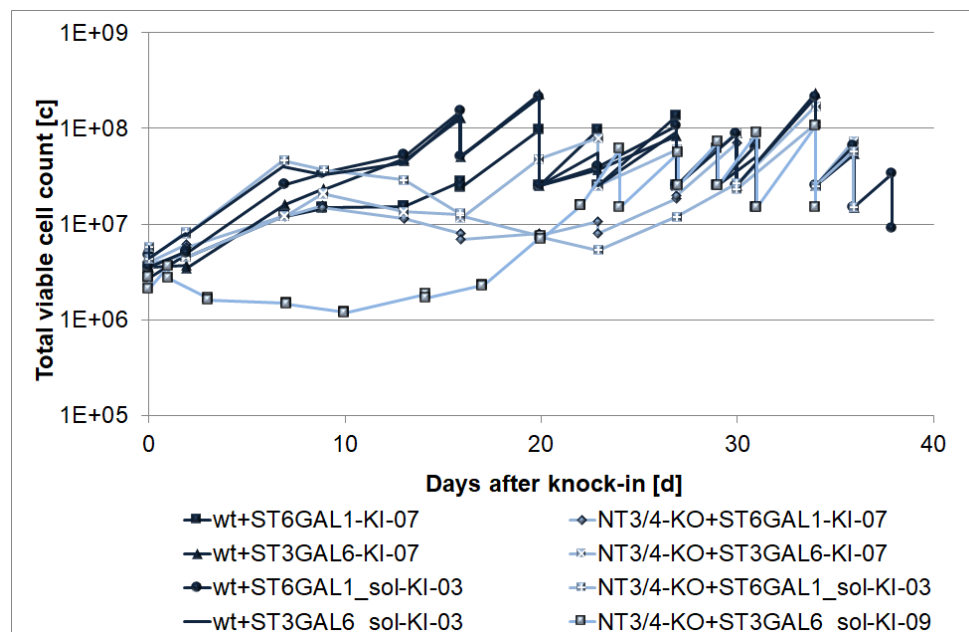


Figure 13: Total viable cell count of wt HEK 293-F and NT3/4-KO-02 cells during stable pool selection after CRISPR/Cas9 KI of SiaTs. Only pools that survived selection are shown.

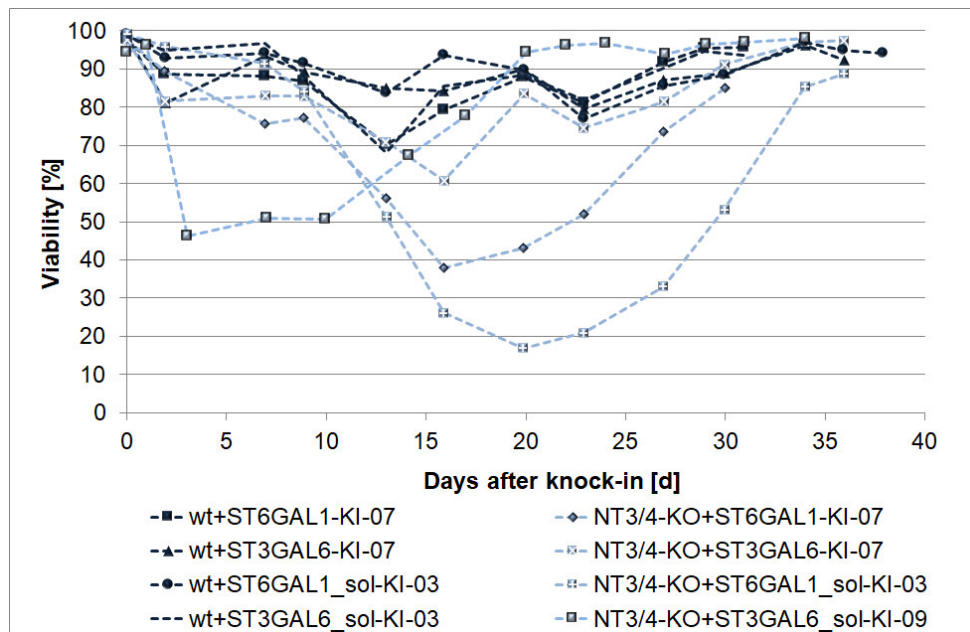


Figure 14: Viability of exemplary pools during selection of pools stably overexpressing SiaTs. Only pools that survived selection are shown.

### 4.1.3 Characterization of pools stably overexpressing sialyltransferases

For each host cell line–SiaT combination, the pools with the highest levels of SiaT mRNA were selected for characterization. Therefore, relative mRNA levels of the SiaTs were determined by RT-qPCR.

#### 4.1.3.1 *ST6GAL1* and *ST6GAL1\_sol* overexpressing pools

The NT3/4-KO-02 line expressed similar levels of *ST6GAL1* as the wt HEK 293-F. The endogenous *ST6GAL1* mRNA levels in wt HEK 293-F and NT3/4-KO-02 were only 0.006-fold and 0.002-fold that of *RNase P* (Figure 15), respectively, which demonstrates the low expression levels expected for endogenous glycosyltransferases.<sup>222,223</sup> In comparison, *ST6GAL1* and *ST6GAL1\_sol* expression in the stable pools was 0.4-fold to 1.1-fold relative to *RNase P* and between 59-fold to 180-fold compared to the wt HEK 293-F cell line. Thus, all pools overexpressed *ST6GAL1* or *ST6GAL1\_sol* and the KIs were successful.

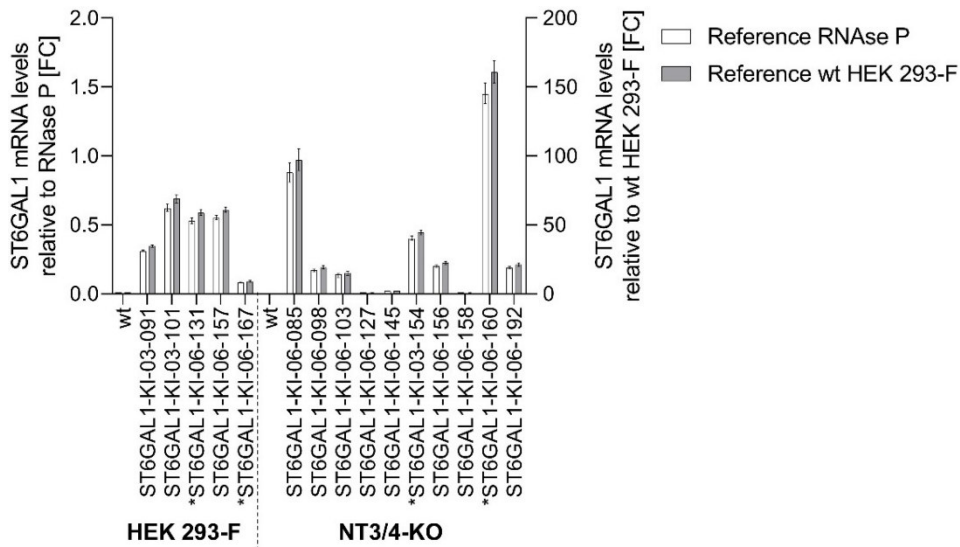


Figure 15: *ST6GAL1* and *ST6GAL1\_sol* mRNA levels of stable pools relative to *RNase P* and to the wt HEK 293-F cell line. All measurements were performed in triplicates and bars represent the mean with confidence intervals ( $\alpha=0.05$ ). FC: fold-change.

#### 4.1.3.1 *ST3GAL6* and *ST3GAL6\_sol* overexpressing pools

*ST3GAL6* and *ST3GAL6\_sol* expression in the respective stable pools was 0.55-fold to 1.74-fold relative to *RNase P* and between  $1.7 \times 10^6$ -fold to  $5.7 \times 10^6$ -fold compared to the wt HEK 293-F cell line (Figure 16). The reason for the high difference between the stable pools and the wt HEK 293-F cell line is the codon optimization of the knocked-in *ST3GAL6* gene. The used primer/probe pair can detect codon-optimized but not endogenous *ST3GAL6* mRNA molecules. All pools overexpressed *ST3GAL6* or *ST3GAL6\_sol*—also to a similar extent than the *ST6GAL1* and *ST6GAL1\_sol* pools overexpressed *ST6GAL1* and *ST6GAL1\_sol*—and the KIs were considered successful.

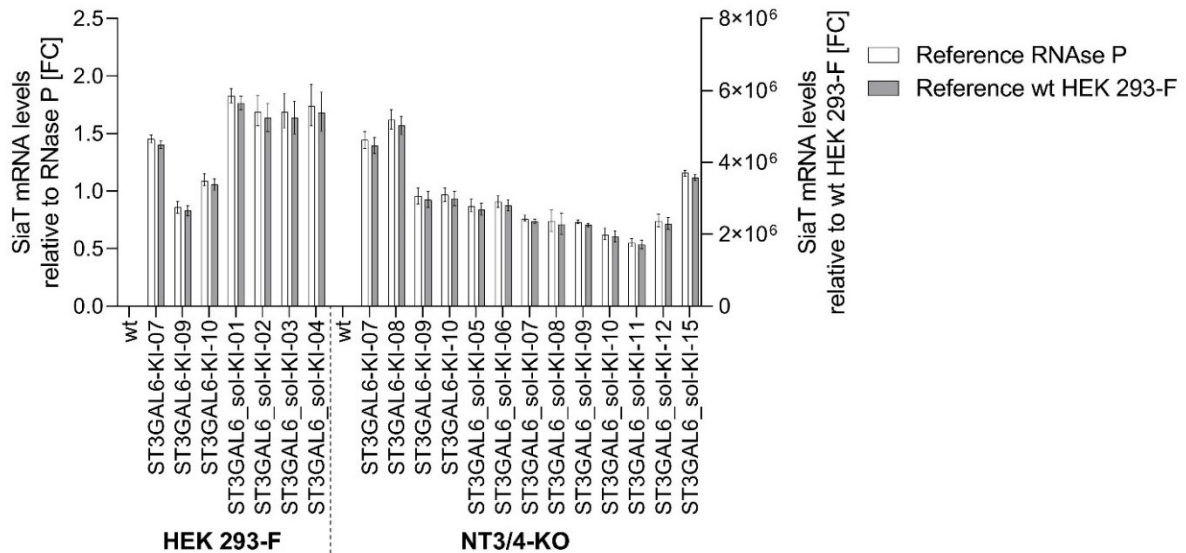


Figure 16: *ST3GAL6* and *ST3GAL6\_sol* mRNA levels of stable pools relative to *RNase P* and to the wt HEK 293-F cell line. All measurements were performed in triplicates and bars represent the mean with confidence intervals ( $\alpha=0.05$ ). FC: fold-change.

#### 4.1.3.1 Selection of stable pools overexpressing sialyltransferases as host cell lines

The stable pools with the highest SiaT overexpression were selected as new host cell lines for the expression of FVII-alb (Table 9). An overview over all selected host cell lines is shown in Figure 24.

Table 9: Stable KI pools selected as new host cell lines.

| Host cell line | Sialyltransferase | Stable KI pool             |
|----------------|-------------------|----------------------------|
| wt HEK 293-F   | ST6GAL1           | wt+ST6GAL1-KI-03           |
|                | ST3GAL6           | wt+ST3GAL6-KI-07           |
|                | ST6GAL1_sol       | wt+ST6GAL1_sol-KI-01       |
|                | ST3GAL6_sol       | wt+ST3GAL6_sol-KI-02       |
| NT3/4-KO-02    | ST6GAL1           | NT3/4-KO+ST6GAL1-KI-03     |
|                | ST3GAL6           | NT3/4-KO+ST3GAL6-KI-08     |
|                | ST6GAL1_sol       | NT3/4-KO+ST6GAL1_sol-KI-03 |
|                | ST3GAL6_sol       | NT3/4-KO+ST3GAL6_sol-KI-15 |

#### 4.1.4 Generation of clones from *ST6GAL1* overexpressing pools

Due to the heterogeneous SiaT expression levels of individual cells in a stable pool, stable pools are well suited to give an impression of the glyco-engineering effects over the whole cell population generated by a KI. However, clonal isolates are better suited for the generation of production cell lines for therapeutic proteins since the glycosylation pattern in all derived production clones is similar. Therefore, potential differences in *N*-glycosylation were assessed for individual cell clones. In this regard, the two main questions were whether the sialylation of FVII-alb depends on the *ST6GAL1* mRNA level and whether clones show other *N*-glycosylation differences. To this end, clones were isolated from *ST6GAL1* overexpressing pools of the wt HEK 293-F and the NT3/4-KO-02 backgrounds.

From the 768 clones that were isolated, 227 grew to colonies and were expanded to 24-wp. Fast growing clones were expanded to 24-wp and shaken at 100 rpm. This shake speed led to attachment on the well walls and subsequent cell death and thus, none of the clones could be further expanded to 24-hdwp. The clones that were expanded later—slower growing clones—were shaken at only 50 rpm. Of those, 44 grew in 24-wp and were expanded to 24-dwp. Of those expanded to 24-hdwp, 15 grew and were further expanded to shake flask and were then cryopreserved (Table 10).

Table 10: ST6GAL1 overexpressing clones that survived expansion to shake flask.

| Host cell line | Clone                      |
|----------------|----------------------------|
| wt HEK 293-F   | wt+ST6GAL1-KI-03-091       |
|                | wt+ST6GAL1-KI-03-101       |
|                | wt+ST6GAL1-KI-06-131       |
|                | wt+ST6GAL1-KI-06-157       |
|                | wt+ST6GAL1-KI-06-167       |
| NT3/4-KO-02    | NT3/4-KO+ST6GAL1-KI-06-085 |
|                | NT3/4-KO+ST6GAL1-KI-06-098 |
|                | NT3/4-KO+ST6GAL1-KI-06-103 |
|                | NT3/4-KO+ST6GAL1-KI-06-127 |
|                | NT3/4-KO+ST6GAL1-KI-06-145 |
|                | NT3/4-KO+ST6GAL1-KI-06-154 |
|                | NT3/4-KO+ST6GAL1-KI-06-156 |
|                | NT3/4-KO+ST6GAL1-KI-06-158 |
|                | NT3/4-KO+ST6GAL1-KI-06-160 |
|                | NT3/4-KO+ST6GAL1-KI-06-192 |

#### 4.1.5 Characterization of clones overexpressing *ST6GAL1*

The clones that survived expansion to shake flask were characterized to select the best ones for FVII-alb production.

##### 4.1.5.1 *ST6Gall* copy number determination

Digital PCR was used to determine the number of *ST6Gall* copies knocked into the genome of each clone.

In all tested clones between one and up to thirty-one *ST6Gall* copies were successfully integrated (Figure 17), even though it was expected, that the number of integrated donor plasmid copies in a clone would range between one and the number of AAVS1 integration site alleles in the respective cell line (see Figure 12). This expectation was based on the assumptions that (1) a clone without an integration will not survive antibiotic selection, (2) that only a single donor plasmid copy can integrate in each AAVS1 integration site and (3) that random integrations (RI) happen with a frequency much lower than targeted HDR integration. In contrast to those assumptions, the number of integrated *ST6Gall* copies was higher than the number of AAVS1 integration site alleles in most clones. Thus, it was discovered that not only one, but multiple donor plasmid copies can integrate in a single AAVS1 integration site allele. To evaluate whether multiple donor plasmid copies in a single AAVS1 integration site caused the unexpectedly high *ST6Gall* copy numbers, a direct PCR clone characterization was performed.

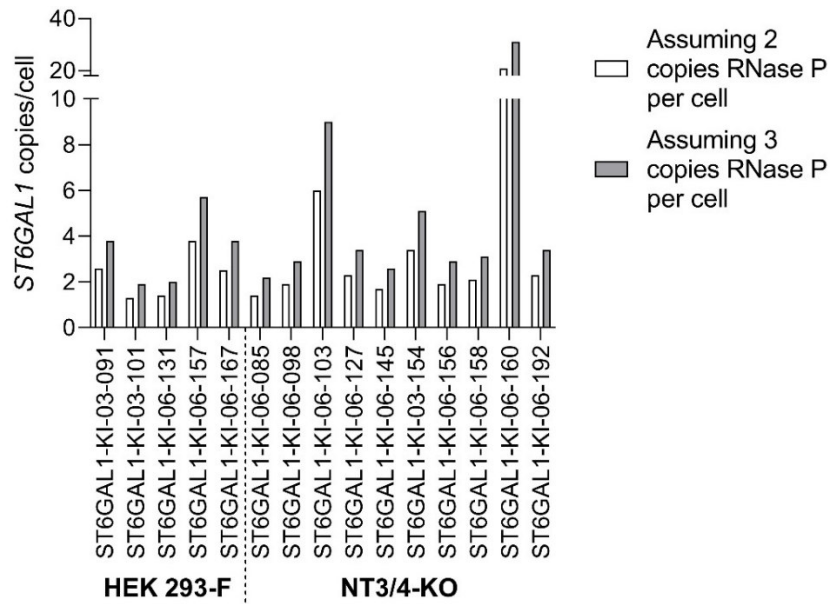


Figure 17: Copy number of *ST6GAL1* in wt HEK 293-F- and NT3/4-KO-derived clones as determined with digital PCR (N=1).

#### 4.1.5.1 Identification of successful knock-in and random integration events

For direct PCR clone evaluation, primer pairs that can distinguish between the different possible integration events were designed (see 3.2.1.8) and all *ST6GAL1* overexpressing clones were characterized using all four primer pairs in duplicates. An exemplary gel picture is shown for primer pair RI HA-L in Figure 18. The results of all direct PCR experiments are summarized in Table 11 and compared to the other clone characterization results in 4.1.5.2.

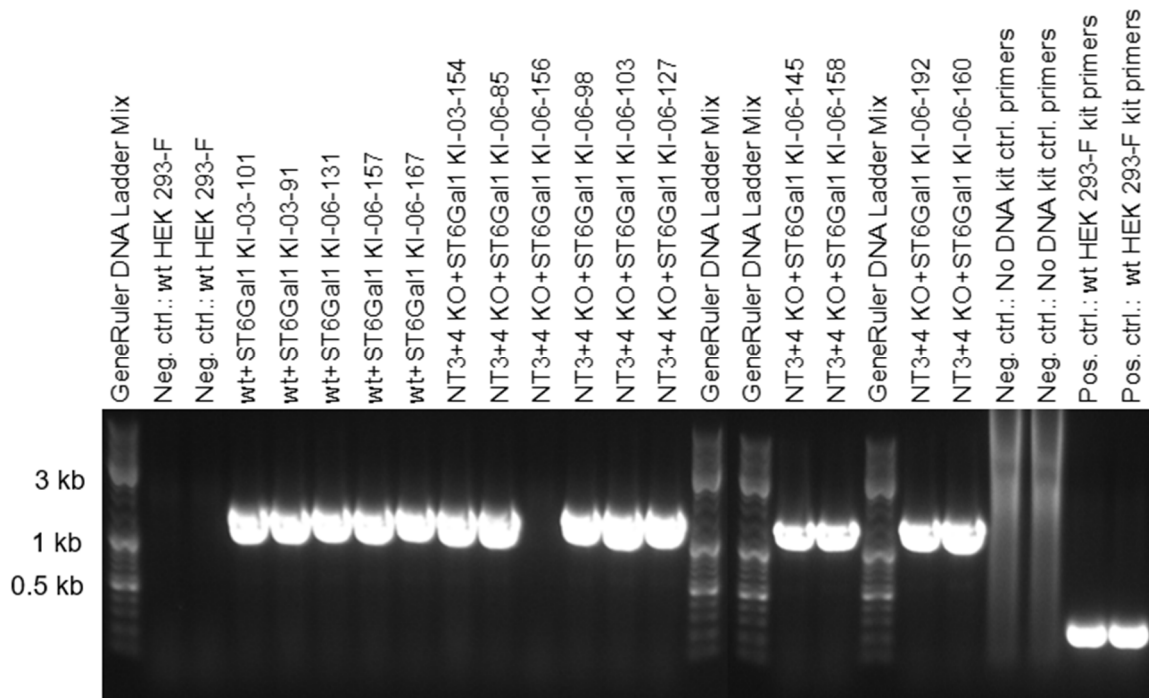


Figure 18: 1% GelRED-stained agarose gel of direct PCR amplicons from primer pair RI HA-L. A band at 1,516 bp indicates the presence of a donor plasmid backbone sequence next to the left homology arm. All clones except NT3/4-KO+ST6GAL1-KI-06-156 were positive for that sequence. All positive and negative controls showed the expected band pattern. Kb: kilo base pairs.



Table 11: Direct PCR results for all primer sets for *ST6GAL1* overexpressing clones. “+” denotes the detection of a DNA band at the expected size and “-” denotes no detection of a DNA band at the expected size (N=2). KI: knock-in; RI: random integration; HA-L: left homology arm; HA-R: right homology arm.

| Clone                      | Primer pair<br>KI HA-L | Primer pair<br>KI HA-R | Primer pair<br>RI HA-L | Primer pair<br>RI HA-R |
|----------------------------|------------------------|------------------------|------------------------|------------------------|
| wt+ST6GAL1-KI-03-091       | -                      | -                      | +                      | +                      |
| wt+ST6GAL1-KI-03-101       | +                      | +                      | +                      | +                      |
| wt+ST6GAL1-KI-06-131       | +                      | +                      | +                      | +                      |
| wt+ST6GAL1-KI-06-157       | +                      | +                      | +                      | +                      |
| wt+ST6GAL1-KI-06-167       | +                      | -                      | +                      | -                      |
| NT3/4-KO+ST6GAL1-KI-06-085 | +                      | +                      | +                      | +                      |
| NT3/4-KO+ST6GAL1-KI-06-098 | +                      | +                      | +                      | -                      |
| NT3/4-KO+ST6GAL1-KI-06-103 | +                      | +                      | +                      | +                      |
| NT3/4-KO+ST6GAL1-KI-06-127 | -                      | -                      | +                      | -                      |
| NT3/4-KO+ST6GAL1-KI-06-145 | +                      | +                      | +                      | +                      |
| NT3/4-KO+ST6GAL1-KI-03-154 | -                      | -                      | +                      | +                      |
| NT3/4-KO+ST6GAL1-KI-06-156 | +                      | +                      | -                      | -                      |
| NT3/4-KO+ST6GAL1-KI-06-158 | +                      | -                      | +                      | -                      |
| NT3/4-KO+ST6GAL1-KI-06-160 | +                      | +                      | +                      | +                      |
| NT3/4-KO+ST6GAL1-KI-06-192 | +                      | +                      | +                      | -                      |

#### 4.1.5.2 Evaluation of number and type of integration events in single cell clones

To assess whether the unexpectedly high *ST6Gall* copy numbers result from M-KIs or RIs, the number of AAVS1 integration site alleles in the host cell line (wt HEK 293-F or NT3/4-KO-02; Figure 12), the *ST6Gall* copy number (Figure 17) and the direct PCR results (Table 11) of each clone were compared.

- Only clone NT3/4-KO+ST6GAL1-KI-06-156 carried S-KIs exclusively.
- Two clones (NT3/4-KO+ST6GAL1-KI-06-098 and NT3/4-KO+ST6GAL1-KI-06-192) carried and S-KIs and a RI where the donor plasmid backbone sequence right of the right homology arm is not present.
- Seven clones (wt+ST6GAL1-KI-03-101, wt+ST6GAL1-KI-06-131, wt+ST6GAL1-KI-06-157, NT3/4-KO+ST6GAL1-KI-06-085, NT3/4-KO+ST6GAL1-KI-06-103, NT3/4-KO+ST6GAL1-KI-06-145 and NT3/4-KO+ST6GAL1-KI-06-160) could carry any combination of S-KIs, M-KIs and RIs.
- Two clones (wt+ST6GAL1-KI-06-167 and NT3/4-KO+ST6GAL1-KI-06-158) led to PCR amplicons with the primer pairs KI HA-L and RI HA-L but not for KI HA-R and RI HA-R. The positive RI HA-L in absence of RI HA-R can be explained by RIs where the donor plasmid backbone sequence right of the right homology arm is not present. However, for a positive KI HA-L signal one would also expect a positive KI HA-R signal since both originate from a single HDR event. A potential explanation could be a combination of an S-KI and a RI event.
- One clone (NT3/4-KO+ST6GAL1-KI-06-127) only carried RIs where the donor plasmid backbone sequence right of the right homology arm is not present.
- Two clones (wt+ST6GAL1-KI-03-091 and NT3/4-KO+ST6GAL1-KI-03-154) only carried RIs.

Overall, the direct PCR experiments revealed RI and M-KI events in most clones, explaining the unexpectedly high donor plasmid copies in some clones. Furthermore, solely a single clone showed only S-KI events. Since linearization of the donor plasmid can prevent M-KI events, plasmids will be linearized in future experiments.

Since the main reason for single-cell cloning was to generate clones with different *ST6GAL1* overexpression levels, the clones were deemed suitable for downstream analyses despite the unexpected RI and M-KI events.

#### 4.1.5.3 *ST6GAL1* gene expression analysis

Clones were chosen as host cell lines for FVII-alb expression based on *ST6GAL1* overexpression.

Not all cells in a stable pool necessarily overexpress the GOI, which is shown by the fact that *ST6GAL1* expression in two of the clones (NT3/4-KO+*ST6GAL1*-KI-06-127 and NT3/4-KO+*ST6GAL1*-KI-06-158) was similar to that of the wt HEK 293-F and NT3/4-KO-02 host cell lines (Figure 19). These clones only carried integrations where the sequences adjacent to the right homology arm were most likely lost during RI. This could indicate incomplete integration of the plasmid in these clones and explain the missing *ST6GAL1* overexpression. *ST6GAL1* expression in the other clones was between 10- to 160-fold over that of the wt HEK 293-F cell line. The clones wt+*ST6GAL1*-KI-06-131, wt+*ST6GAL1*-KI-06-167, NT3/4-KO+*ST6GAL1*-KI-03-154 and NT3/4-KO+*ST6GAL1*-KI-06-160 (highlighted by asterisk in Figure 19) were selected as new host cell lines for the expression of the model protein FVII-alb in order to cover different *ST6GAL1* expression levels. An overview over all selected host cell lines is shown in Figure 24.

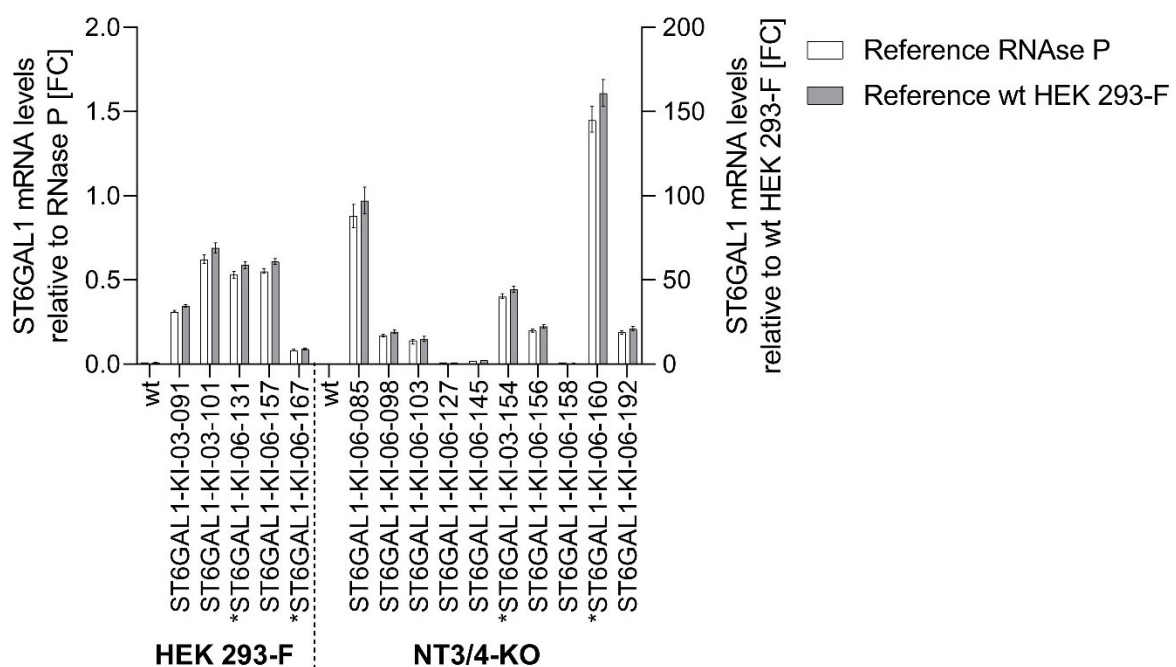


Figure 19: *ST6GAL1* mRNA levels relative to *RNase P* and to wt HEK 293-F cells. Clones selected for model protein expression are marked with an asterisk. All measurements were performed in triplicates and bars represent the mean with confidence intervals ( $\alpha=0.05$ ). FC: fold-change.

## 4.2 Generation and evaluation of cell lines expressing model proteins

To evaluate whether the KO of GalNAcTs or KI of SiaTs exhibit the desired effect on *N*-glycosylation, FVII-alb was expressed in the generated set of host cell lines (overview in Figure 24). FVIII-BDD and FIX were additionally expressed in a selection of host cell lines (wt HEK 293-F, NT3/4-KO-02, NT3/4-KO-ST6GAL1-KI-03).

### 4.2.1 Generation of cell lines expressing model proteins

Expression plasmids coding for FVII-alb, FVIII-BDD and FIX were transfected into the host cell lines and stable expression cell lines were generated by puromycin selection. A wt HEK 293-F cell line expressing FVII which was genera was already available.

Transfection and stable pool selection were performed in duplicates for each host cell line. Exemplary growth and viability curves during stable pool selection are shown in Figure 20 and Figure 21. All pools survived selection.

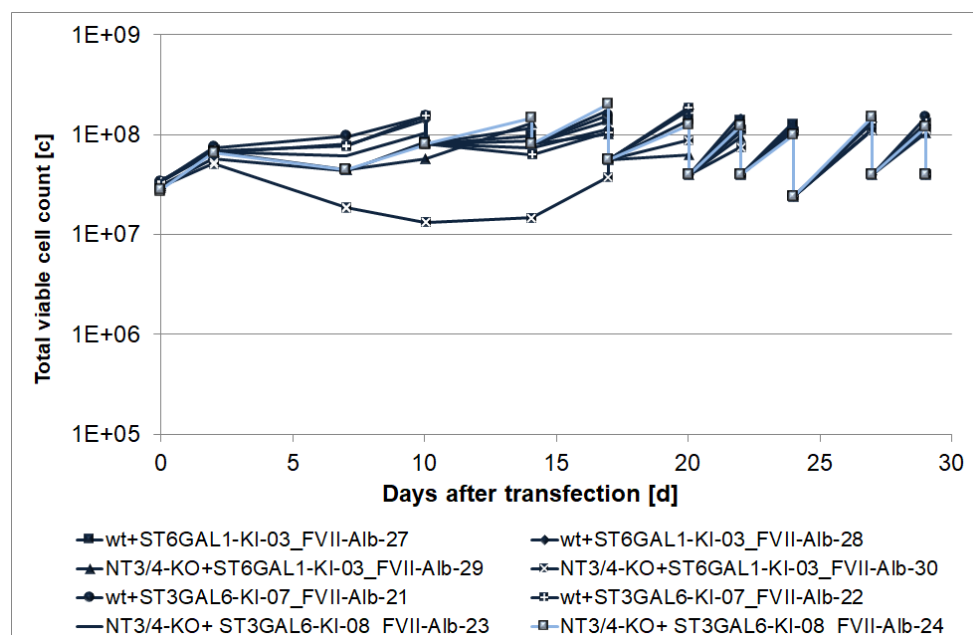


Figure 20: Total viable cell count of two ST6GAL1 and two ST3GAL6 overexpressing pools derived from wt HEK 293-F and NT3/4-KO cells during stable pool selection.

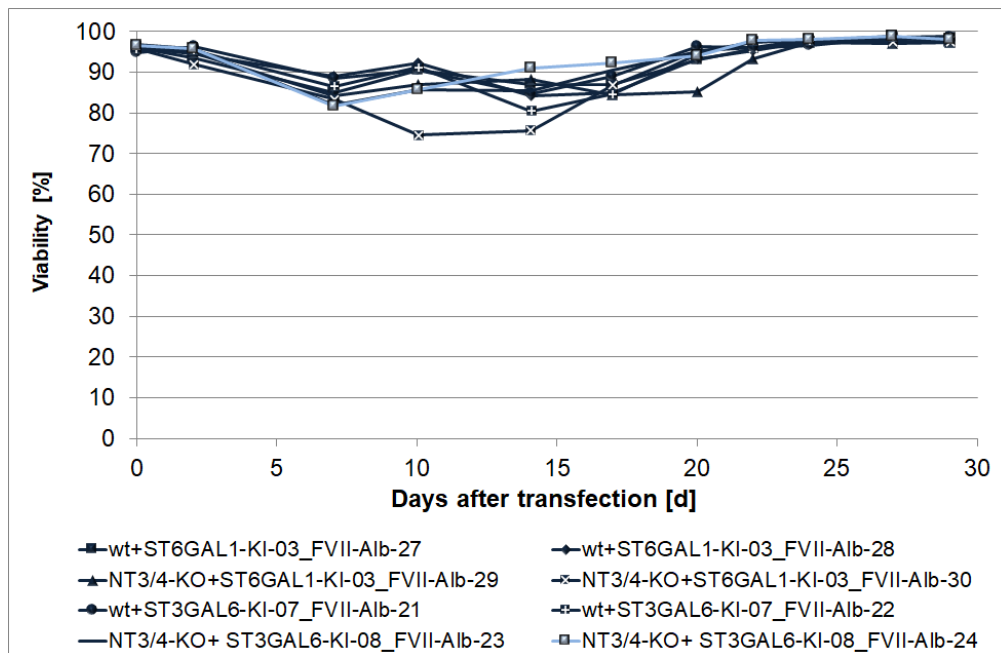


Figure 21: Viability of two ST6GAL1 and two ST3GAL6 overexpressing pools derived from wt HEK 293-F and NT3/4-KO cells during stable pool selection.

#### 4.2.2 Characterization of cell lines expressing model proteins

Potential expression cell lines were analyzed for growth and cell-specific productivity (CSP).

Division rate and CSP were comparable between FVII-alb expression cell lines derived from SiaT overexpressing pools (Figure 22). However, division rates of FVII-alb expression cell lines derived from clonal host cell lines were lower than those derived from the originating pools, which is a result of the too high initial shaking speed during clone expansion, which killed the fast growing clones (see 4.1.4). Division rates of FVIII-BDD expressing pools from host cell lines NT3/4-KO-02 and NT3/4-KO-02+ST6GAL1-KI\_03 were lower than those from the wt HEK 293-F cell line (Figure 23) because for those, the CSP was measured shortly after the pools recovered from antibiotic selection.

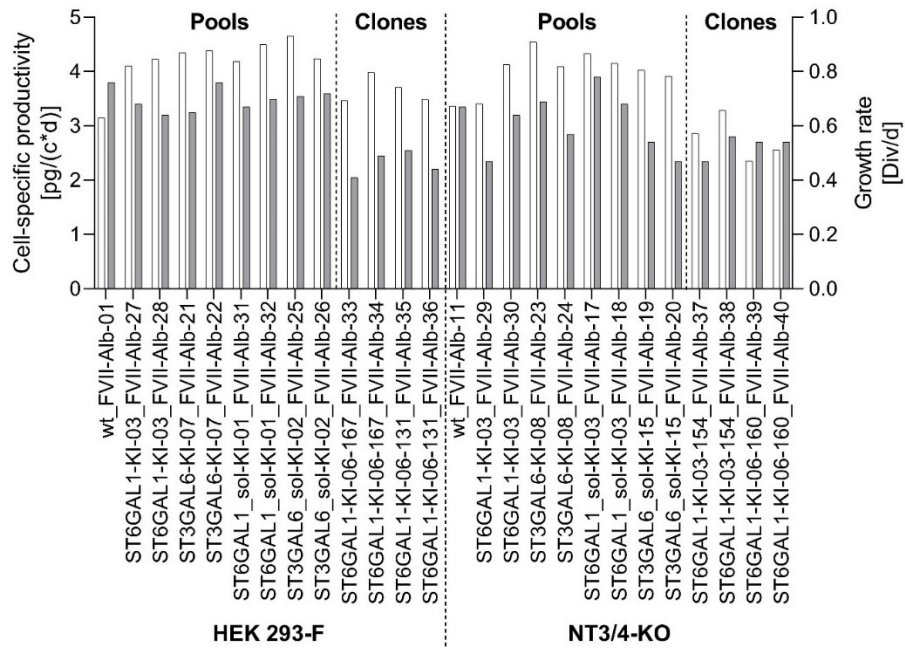


Figure 22: Cell-specific productivity (white bars) and division rate (grey bars) of expression cell lines generated from stable sialyltransferase overexpressing pools and clones (N=1). Div: divisions.

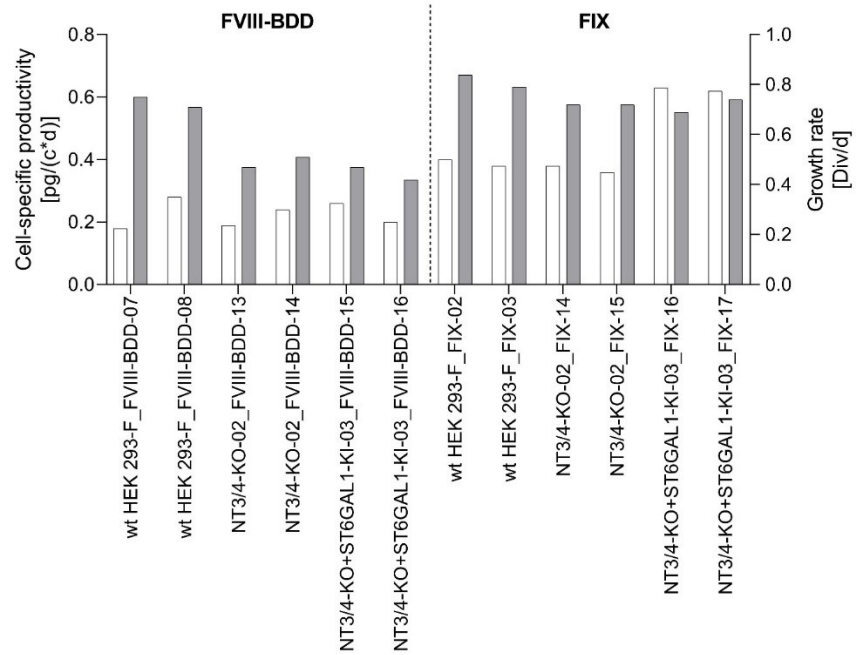


Figure 23: Cell-specific productivity (white bars) and division rate (grey bars) of FVIII-BDD and FIX expression cell lines (N=1). Div: divisions.

### 4.2.3 Selection of cell lines for protein expression

The stable pools with the highest CSPs were selected for subsequent model protein expression and purification. An overview over all selected expression cell lines is shown in Figure 24.

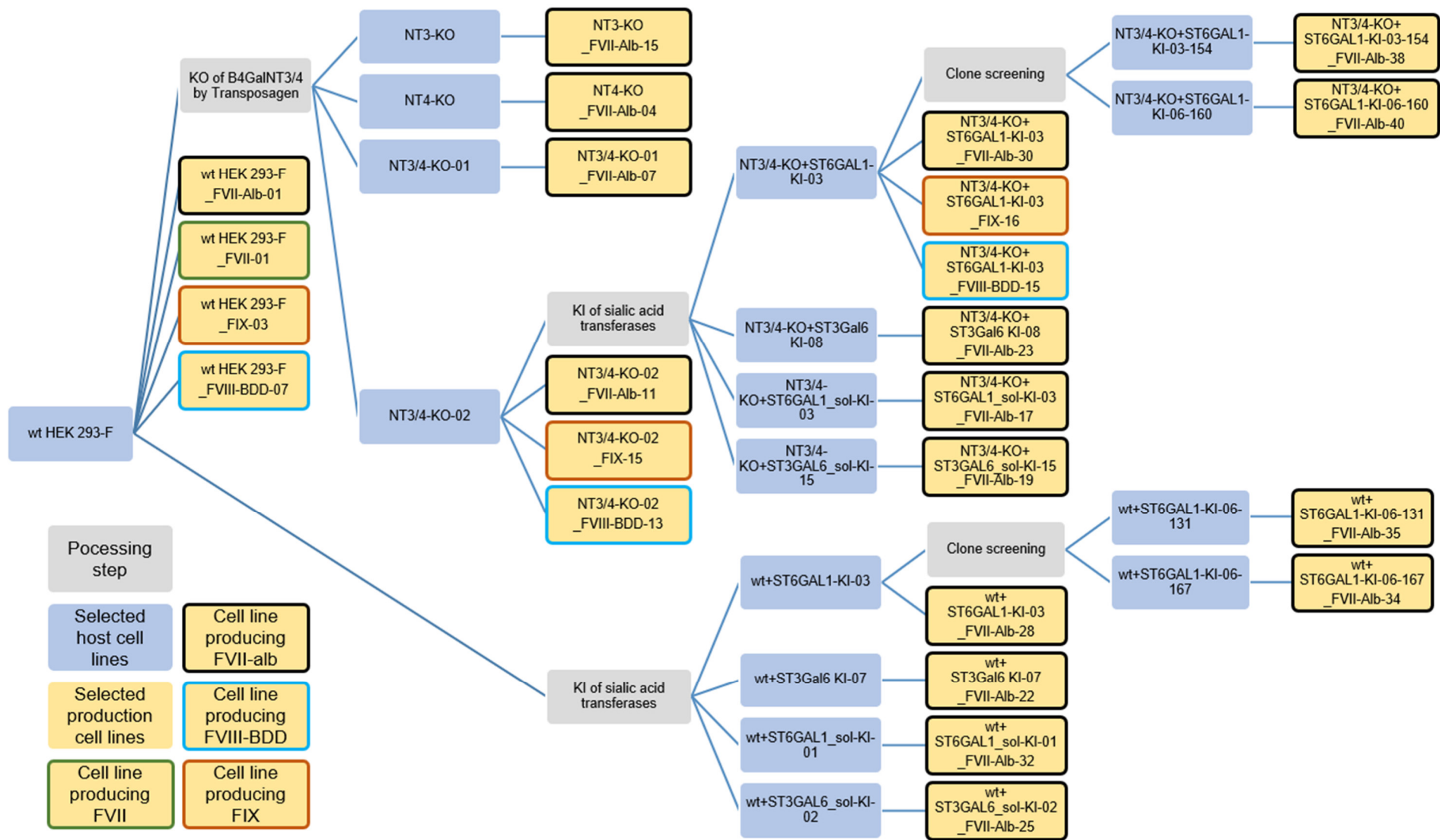


Figure 24: Overview of selected host cell lines, expression cell lines and the most important processing steps.

## 4.3 Production and purification of model proteins

### 4.3.1 Production of model proteins

FVII, FVII-alb, FVIII-BDD and FIX were produced in different host cell lines in order to analyze the glyco-engineering-induced changes in *N*-glycosylation. Furthermore, sialic acid metabolism precursors ManNAc (20 mM) and cytidine (5 mM) were added to the culture medium for some selected host cell lines expressing FVII-alb.

Model proteins were produced in batch culture. After five to seven days, culture supernatant was harvested and protein concentration was determined by protein-specific ELISA. Harvest concentrations were between 15.0 and 35.0 µg/mL for FVII-alb, between 0.8 to 1.0 µg/mL for FVIII-BDD, and between 2.0 to 6.0 µg/mL for FIX and at least 2 mg of protein were produced in each host cell line.

### 4.3.2 Purification of model proteins

For animal experiments, culture supernatants containing FVII or FVII-alb were purified by VIISelect affinity chromatography on an ÄKTA Pure system, rebuffered, and analyzed by SDS-PAGE (Figure 25). For *N*-glycan analysis, culture supernatants containing FVIII-BDD or FIX were purified by VIISelect or IXSelect affinity chromatography on an ÄKTA Pure system, rebuffered, and analyzed by SDS-PAGE (Figure 26). No contaminating host cell proteins were detected in the eluates and purity was deemed adequate for downstream analyses.

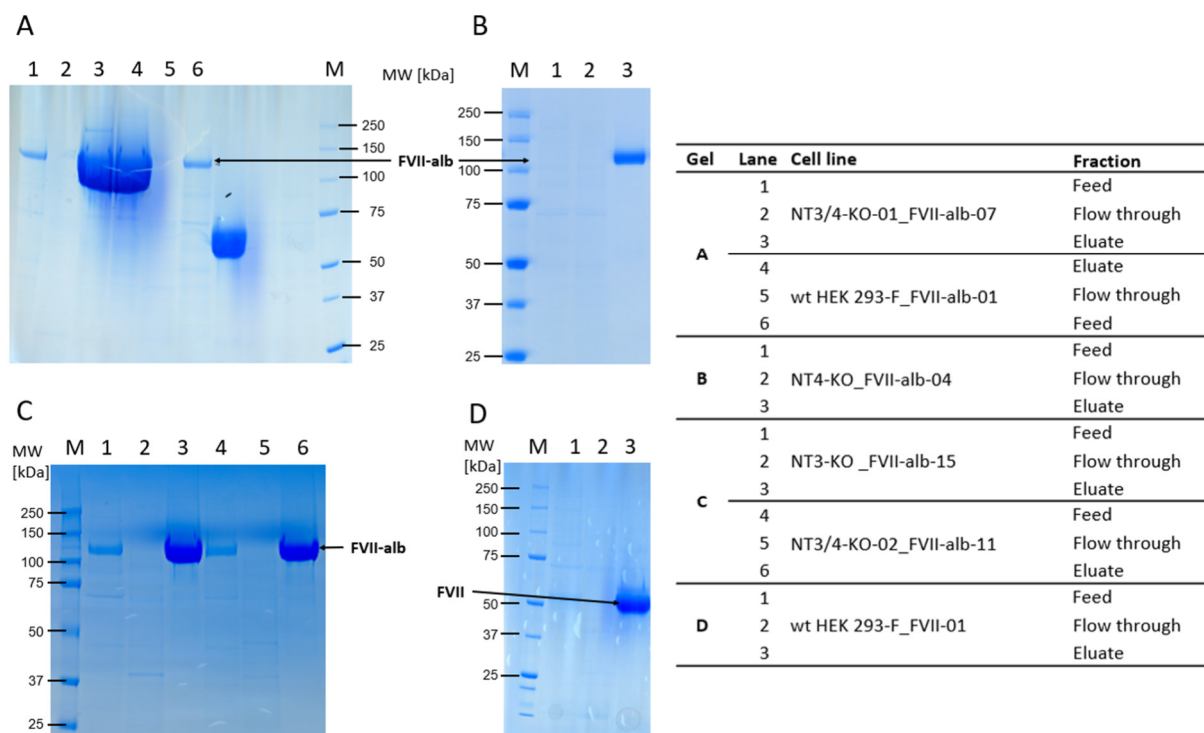


Figure 25: Reducing SDS-PAGE of feed, flow through and eluate fractions of ÄKTA-purified FVII-alb (A-C) and FVII (D). Feed and flow through were applied undiluted. Eluates were diluted 1:5 (FVII-alb NT4-KO: 2 µg/lane, all other conditions: 5 µg/lane). M: protein ladder; MW: molecular weight; Da: Dalton.

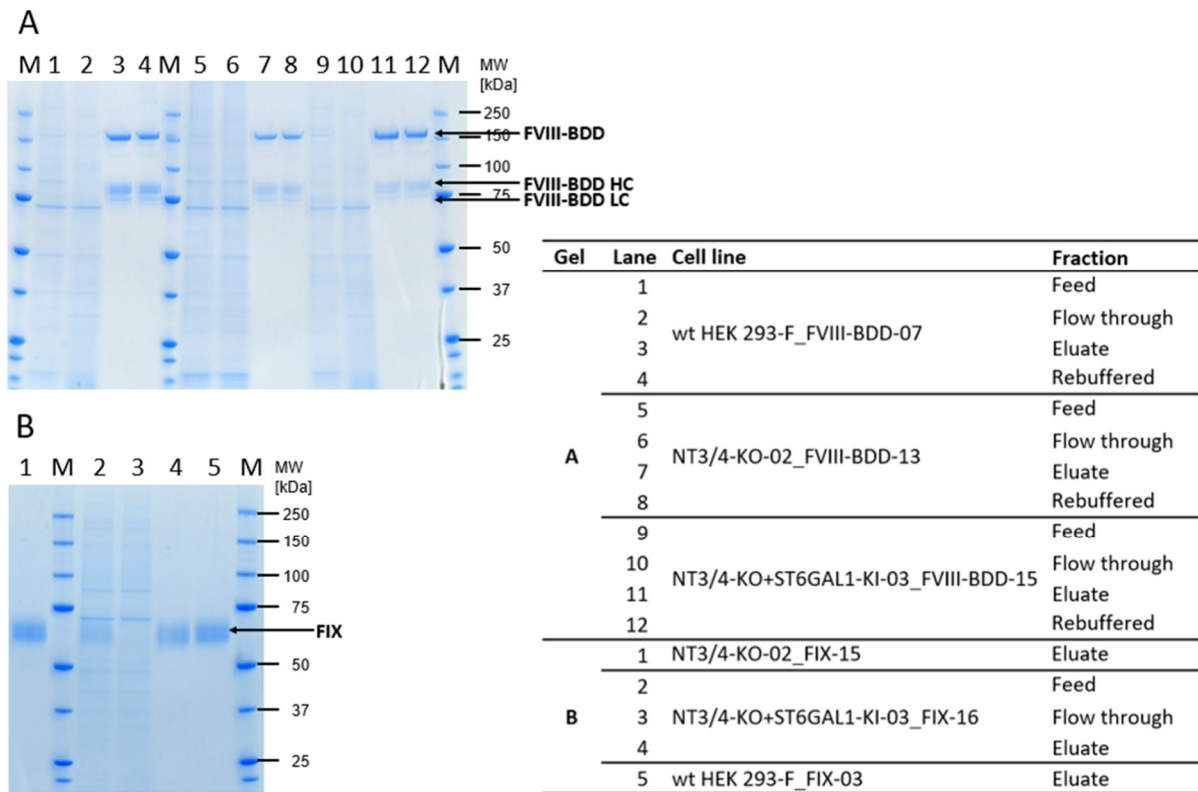


Figure 26: Reducing SDS-PAGE of feed, flow through and eluate of ÄKTA purified FVIII-BDD (A) and FIX (B). Feed and flow through were applied undiluted. Eluates and rebuffered samples were diluted to 33  $\mu\text{g}/\text{mL}$  for FVIII-BDD and 50  $\text{mg}/\text{mL}$  for FIX (FVIII-BDD: 0.6  $\mu\text{g}/\text{lane}$ , FIX: 0.75  $\mu\text{g}/\text{lane}$ ). M: protein ladder; MW: molecular weight; Da: Dalton; HC, heavy chain; LC, light chain.

For *N*-glycan analysis and binding studies, FVII- or FVIII-alb-containing culture supernatants were purified by VIISelect affinity chromatography on a Tecan system, rebuffered, and analyzed by SDS-PAGE (Figure 27). The Tecan system is an automated downscale model of the ÄKTA system and allowed high throughput purification of FVII-alb samples. To ensure maximum comparability between the ÄKTA and Tecan purified samples, both methods were performed with the same flow rates and volumes with respect to their scale. FVII-alb from wt HEK 293-F cells purified on the Tecan and ÄKTA systems showed identical *N*-glycosylation but a difference in receptor binding (Figure 66). Therefore, apart from one exception (see 4.7.2), all samples used for binding experiments were purified on the Tecan system. No contaminating host cell proteins were detected in the eluates and purity was deemed adequate for downstream analyses.



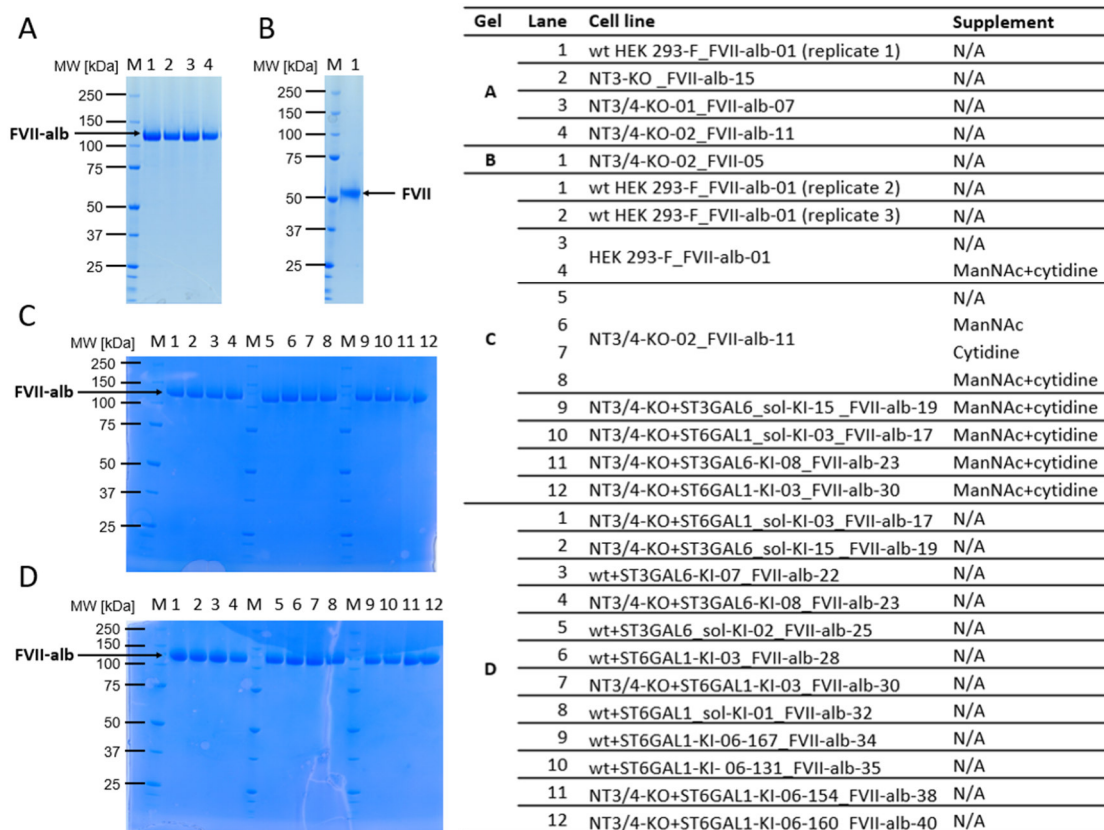


Figure 27: Reducing SDS-PAGE of Tecan purified FVII-alb (A, C, D) and /FVII (B) eluate (1.5 µg/lane). M: protein ladder; MW: molecular weight; Da: Dalton.

### 4.3.3 Activation of FVII and FVII-alb for the pharmacokinetic rat experiment

Since the commercially available reference FVII product NovoSeven® is administered to patients in its activated form, the other FVII and FVII-alb molecules for the PK experiment were also activated *in vitro*.

FVII and FVII-alb were activated by incubating in FVII activation buffer. Activation was stopped after different incubation times to achieve a comparable activation between the samples. More than 90% of the FVII and FVII-alb was activated by cleavage into HC and LC, while a small amount of the HC was further cleaved in an N-terminal and C-terminal part (Figure 28). The activation profiles were comparable to that of NovoSeven®.

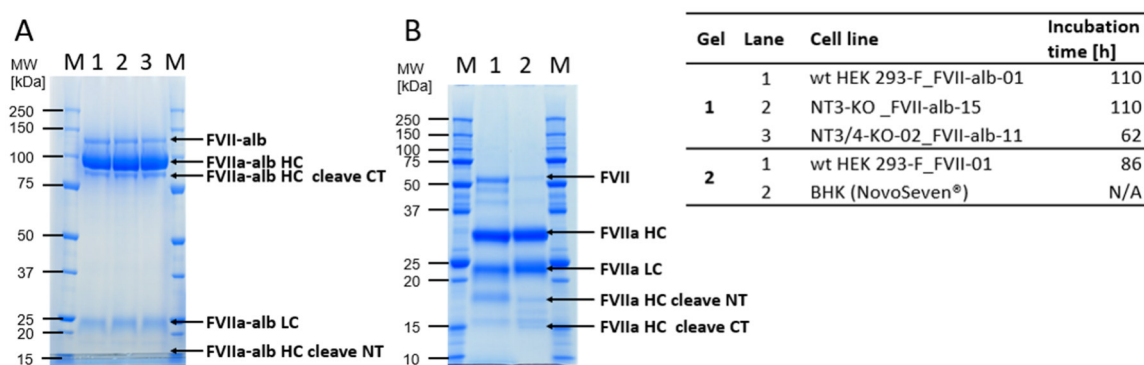


Figure 28: Reducing SDS-PAGE of activated FVII-alb (A) and FVII (B) samples. (FVII-alb: 5 µg/lane, FVII and NovoSeven®: 20 µg/lane). M: protein ladder; MW: molecular weight; Da: Dalton; NT: N-terminal; CT: C-terminal; HC, heavy chain; LC, light chain.

## 4.4 Establishment of the glycosylation analysis methods

### 4.4.1 Identification of released monosaccharides

Released and labelled monosaccharides were separated by reversed-phase chromatography in the monosaccharide (Figure 29A; 3.2.3.2) and sialic acid analysis (Figure 30A; 3.2.3.3) and subsequently identified by comparison of the retention time to reference samples (Figure 29B and Figure 30B and C). For quantification, the peak areas of a sample were compared to a standard curved of the reference samples.

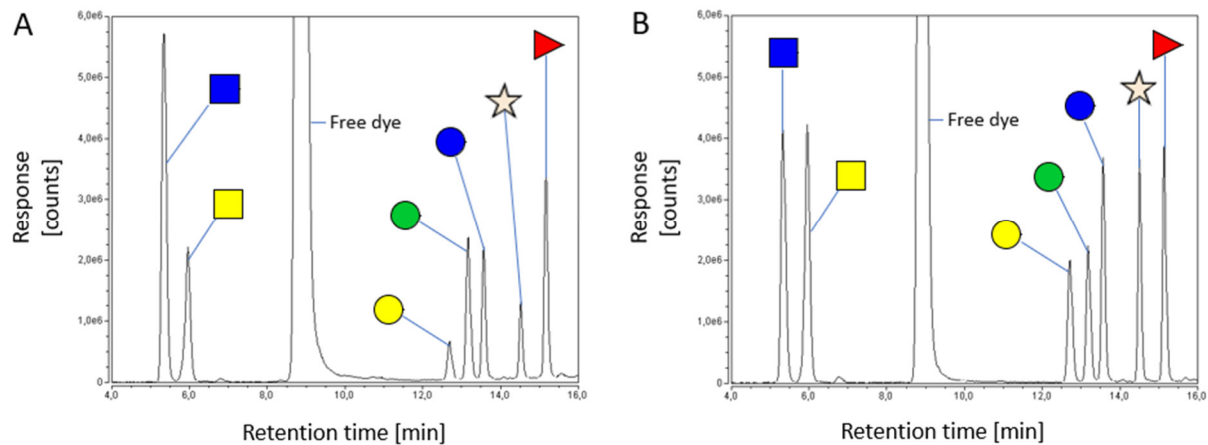


Figure 29: (A) Fluorescence peak spectra of 2-aminobenzoic acid-labelled monosaccharides released from FVII-alb from wt HEK 293-F cells and (B) 2-aminobenzoic acid-labelled monosaccharide reference panel (625 pmol per monosaccharide), separated by reversed-phase chromatography. Mannose: green circle; glucose: blue circle; galactose: yellow circle; GlcNAc: blue square; GalNAc: yellow square; fucose: red triangle; xylose: light brown star.

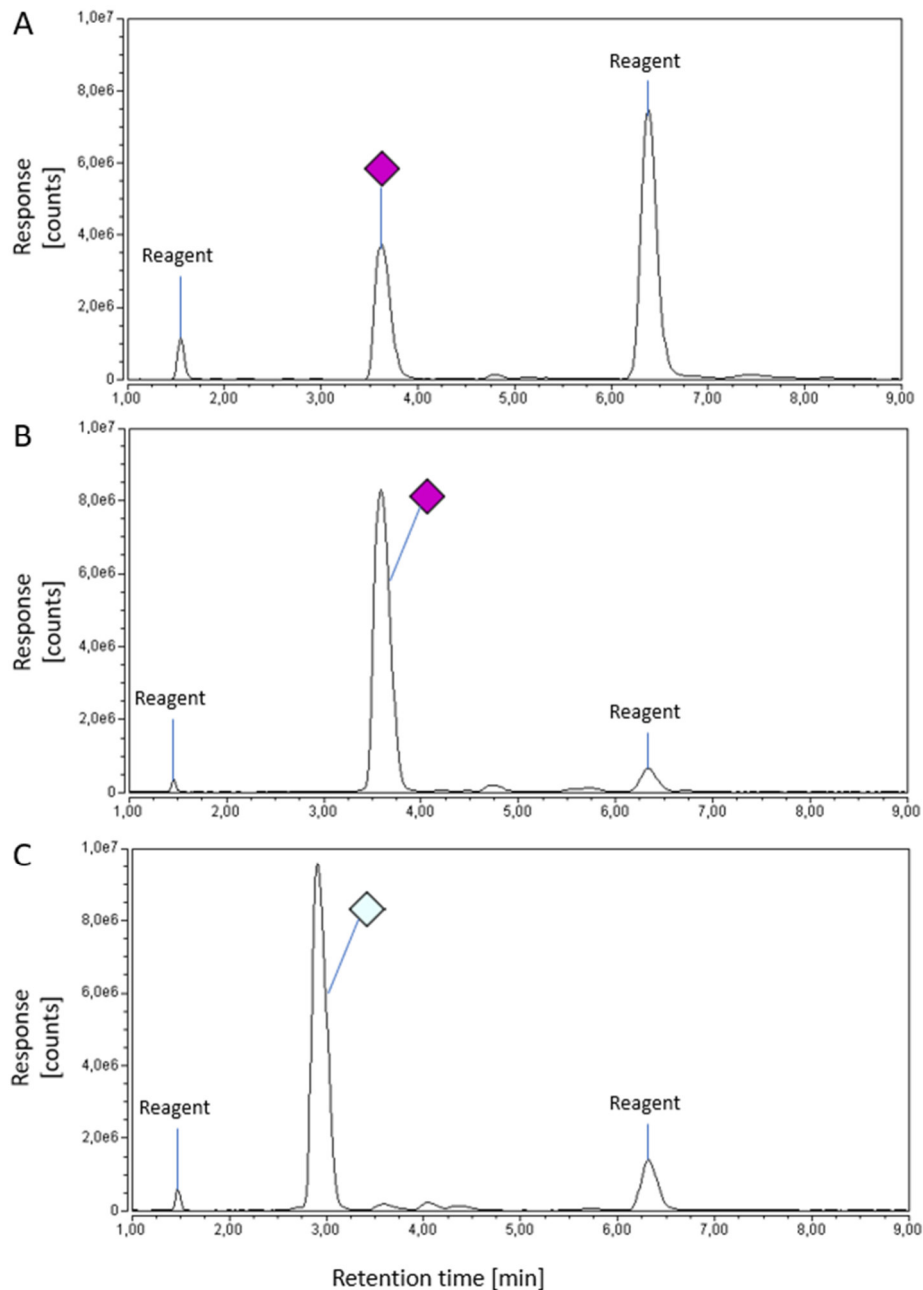


Figure 30: (A) Fluorescence peak spectra of DMB-labelled sialic acids released from FVII-alb from wt HEK 293-F cells and (B) DMB-labelled Neu5Ac standard (250 pmol) and (C) DMB-labelled Neu5Gc standard (250 pmol), separated by reversed-phase chromatography. Neu5Ac: purple diamond; Neu5Gc: white diamond.

#### 4.4.2 Identification of *N*-glycans in *N*-glycan profiles

The main challenge in *N*-glycan profiling is to dissect the *N*-glycan microheterogeneity on proteins. On the FVII, FVIII-BDD and FIX proteins analyzed in this study, for example, as many as 98, 50 and 87 different *N*-glycan species were found, respectively (only considering those with more than 0.5% of the total fluorescence signal). Individual FVII, FVIII-BDD and FIX samples contained up to 41 (NT3-KO), 35 (NT3/4-KO) and 48 (wt HEK 293-F) different *N*-glycan species. With the high number of different species, coelution of multiple species was the most challenging aspect in the identification of the different *N*-glycans. This required multiple approaches which are described in the following sections.

#### 4.4.2.1 Identification by retention time

For *N*-glycan profiling, *N*-glycans were separated with a HILIC retention mechanism. In simple profiles (e.g. Figure 37A or E), *N*-glycans can be identified based on retention time (expressed in glucose units). However, for profiles as complex as most of those in this study (e.g. Figure 37B to D), where peaks are not well separated and where multiple *N*-glycans elute at the same time, other means for identification are required.

#### 4.4.2.2 Identification by Sialidase digest

Sialidase A is an enzyme that cleaves  $\alpha$ 2-3,6,8,9-linked sialic acids from *N*-glycans. Sialidase A digests of FVII-alb *N*-glycans resulted in a shift of the peak spectrum, with peaks of sialylated *N*-glycans disappearing and peaks of many non-sialylated *N*-glycans increasing in peak area (exemplarily shown in Figure 31). This was used to distinguish sialylated from neutral *N*-glycans.

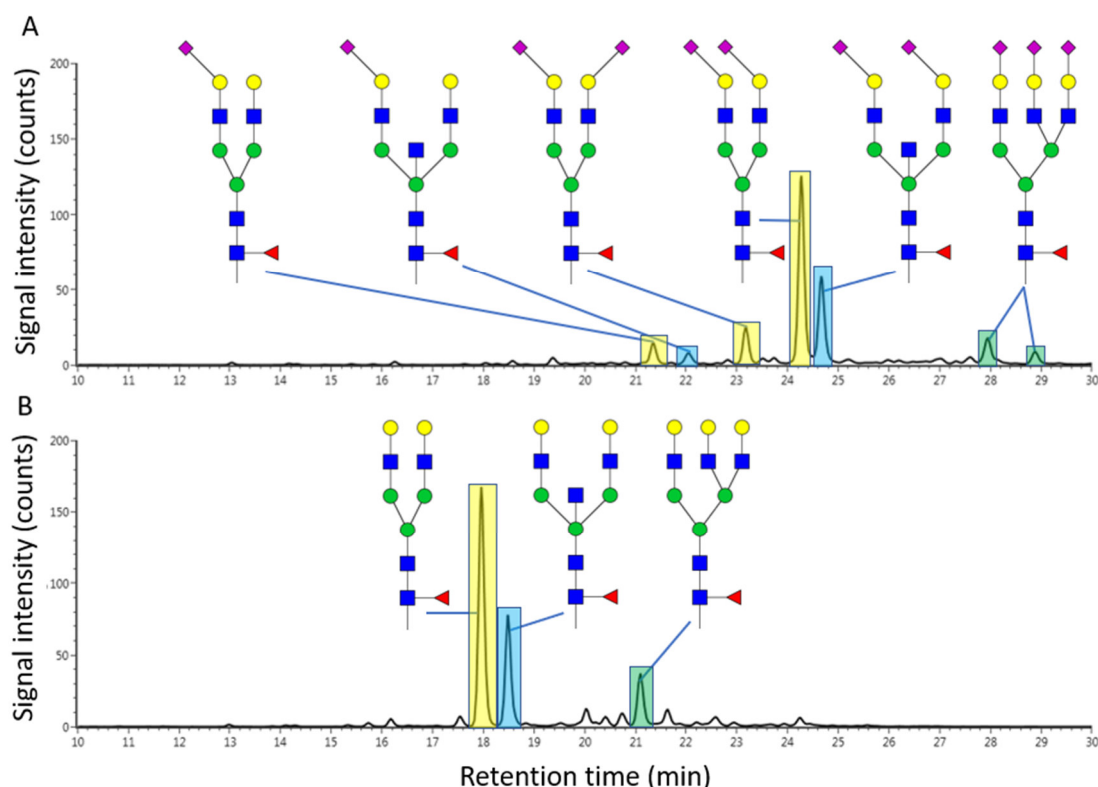


Figure 31: Fluorescence peak spectra of HILIC-separated *N*-glycans of FVII-alb from cell line NT3/4-KO+ST6GAL1-KI-03 (A) and the same *N*-glycans digested with Sialidase A (B): Sialic acids of the biantennary (yellow highlight), bisected (blue highlight) and triantennary (green highlight) *N*-glycans in (A) were removed by Sialidase A, which resulted in a shift of the peaks to the respective non-sialylated/neutral form (B; same colors). Mannose: green circle; galactose: yellow circle; GlcNAc: blue square; GalNAc: yellow square; fucose: red triangle; Neu5Ac: purple diamond (facing left,  $\alpha$ 2,6-linked; facing right,  $\alpha$ 2,3-linked; facing up: undetermined).

*N*-glycan isomers only differing in sialic acid linkage type are distinguishable by retention time on the used HILIC column, with  $\alpha$ 2,3-sialylated ones eluting earlier than  $\alpha$ 2,6-sialylated ones. For confirmation of the linkage, some samples were additionally digested with Sialidase S, an enzyme that only cleaves  $\alpha$ 2,3-linked sialic acids. For triantennary *N*-glycans the two approaches were not sufficient to clearly differentiate between  $\alpha$ 2,3 and  $\alpha$ 2,6-linked sialic acids. Therefore, in all following data concerning sialic acid linkages, only biantennary *N*-glycans were considered.

#### 4.4.2.3 Identification by m/z values in MS mode

The LC-MS methodology allows to record m/z values for the eluting *N*-glycans in MS mode. Using GlycoWorkbench, *N*-glycans were constructed *in silico* and their theoretical m/z values were compared with the detected ones. Due to the high mass precision of the Xevo G2-XS Q-TOF mass spectrometer, *N*-glycans with mass differences as small as 1 Da could be clearly differentiated (Figure 32). This allowed to define the overall composition of the *N*-glycan.

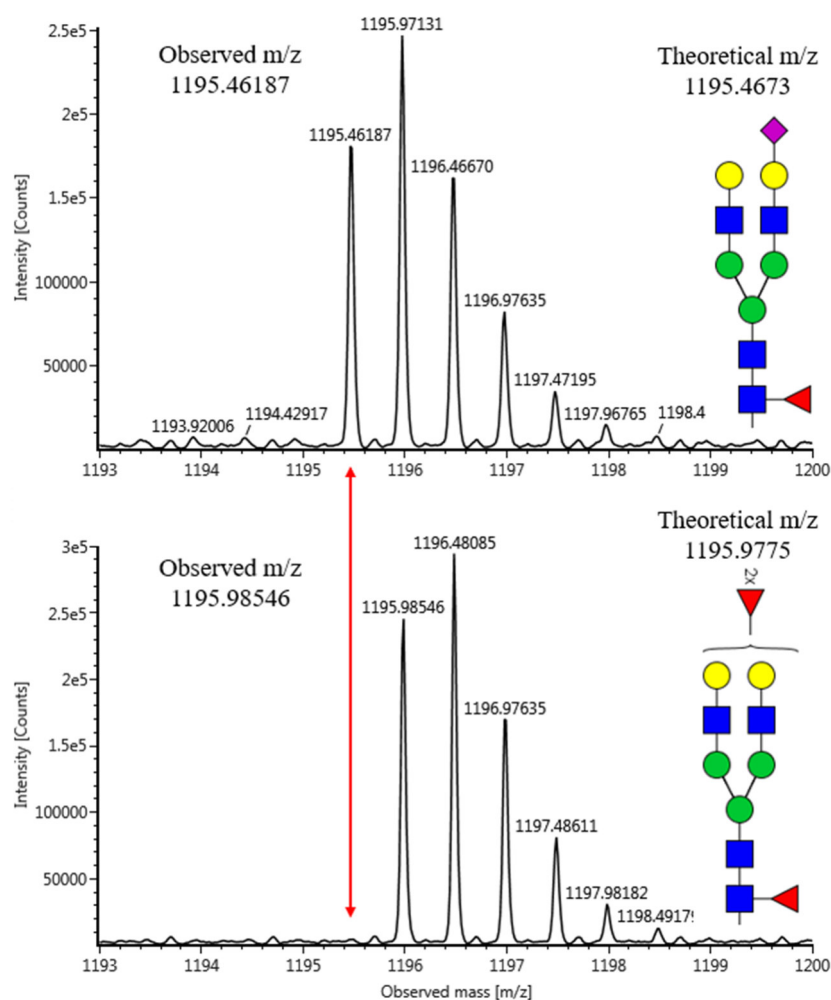


Figure 32: Observed and theoretical mass per charge (m/z) values for two *RapiFluor*-MS-labelled *N*-glycans with a mass difference of 1.0 Da (charge variants:  $2xH^+$ ). The red arrow indicates the mass difference between the two *N*-glycans. Mannose: green circle; GlcNAc: blue square; galactose: yellow circle; fucose: red triangle; Neu5Ac, purple diamond.

#### 4.4.2.4 Identification by fragmentation in MS/MS mode

However, for more specific questions—like the differentiation between monosaccharides with the same mass (e.g. mannose and galactose, GlcNAc and GalNAc), or the discrimination between core- and antenna-linked fucoses—knowledge of the monosaccharide composition alone was not sufficient. For these questions, fragmentation of the *N*-glycans in MS/MS mode was required.

Core and antennary fucoses were differentiated by confirming the presence of a core fucose-specific fragment (Figure 34). Similarly, bis-GlcNAc was determined via a bis-GlcNAc-specific fragment (Figure 34). Furthermore, GalNAc-containing *N*-glycans were differentiated from those with an identical mass but with an additional GlcNAc instead of a GalNAc residue by a typical fragment of GalNAc-containing *N*-glycans (Figure 35).

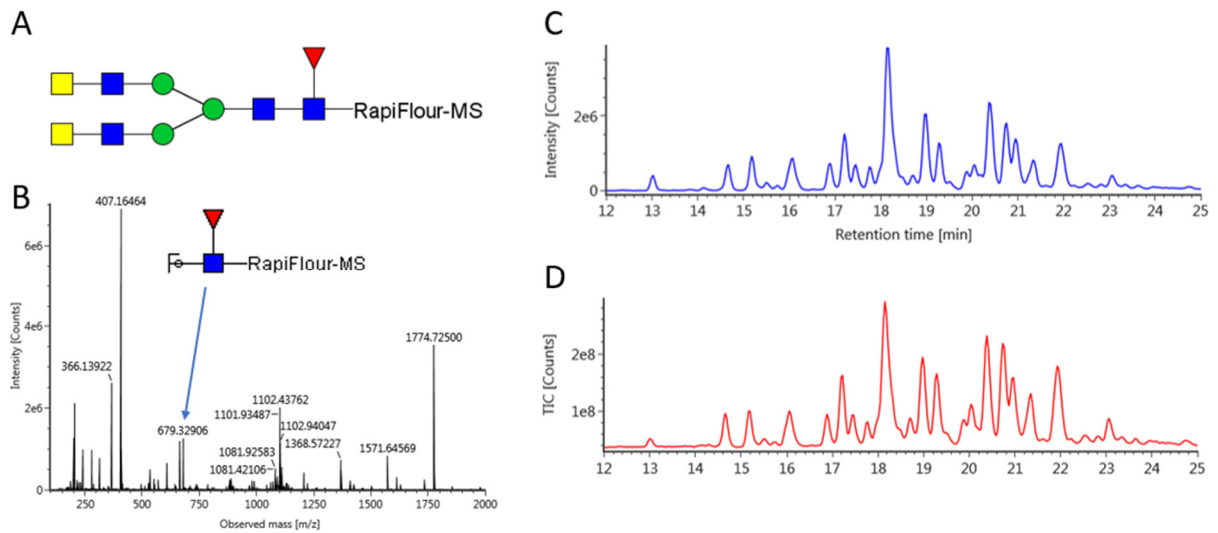


Figure 33: A core fucose-containing biantennary *N*-glycan (A; theoretical  $m/z$  of charge variant  $2xH^+$ : 1,090.9462) and the MS/MS spectrum of the respective parent peak of FVII-alb from wt HEK 293-F cells (B). The fragment at 607.32906  $m/z$  is specific for core-fucosylated *N*-glycans. An extracted ion chromatogram for this fragment (C), shows a superimposable peak pattern than the total ion chromatogram of the same sample (D), indicating that all *N*-glycans of that sample are core-fucosylated. Mannose: green circle; GlcNAc: blue square; GalNAc: yellow square; fucose: red triangle;  $m/z$ : mass per charge; TIC: total ion count.

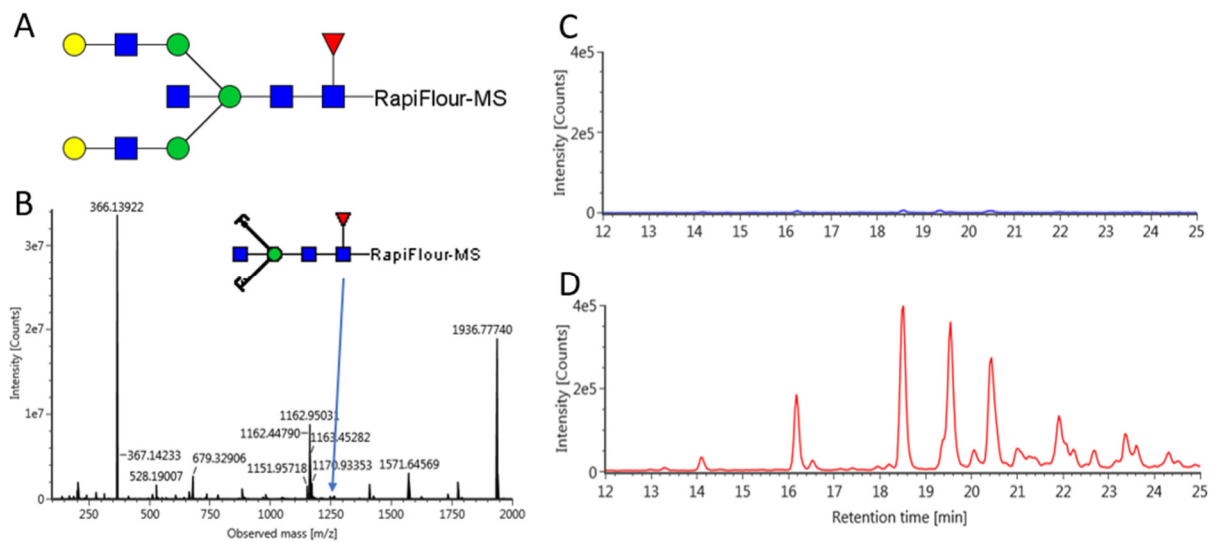


Figure 34: A bis-GlcNAc-containing biantennary *N*-glycan (A; theoretical  $m/z$  of charge variant  $2xH^+$ : 1,151.4593) and the MS/MS spectrum of the respective parent peak of FVII-alb from NT3/4-KO cells (B). The fragment at 1,247.54336  $m/z$  is specific for bisected *N*-glycans. Using extracted ion chromatograms of this fragment, the absence of bisected *N*-glycans on FVII-alb from the wt HEK 293-F cell line (C) and the presence of considerable amounts of bisected *N*-glycans on FVII-alb from the NT3/4-KO cell line was confirmed (D). Mannose: green circle; GlcNAc: blue square; galactose: yellow circle; fucose: red triangle;  $m/z$ : mass per charge.

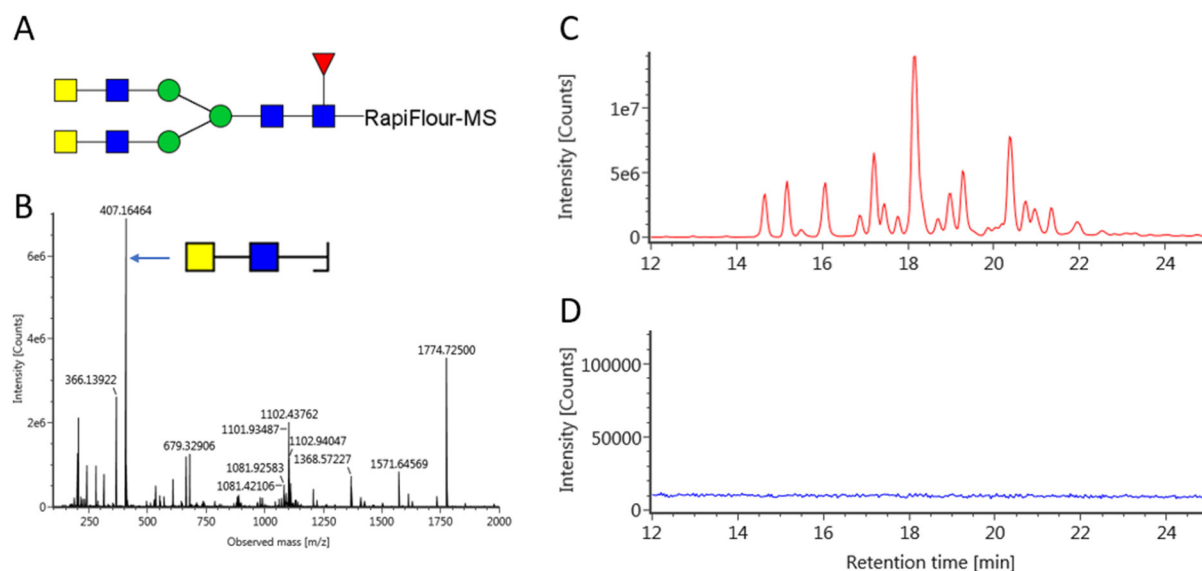


Figure 35: A GalNAc-containing biantennary *N*-glycan (A; theoretical  $m/z$  of charge variant  $2xH^+$ : 1,090.9462) and the MS/MS spectrum of the respective parent peak from FVII-alb from wt HEK 293-F cells (B). The dominant fragment at 407.16464  $m/z$  is GalNAc $\beta$ 4GlcNAc, which is specific for GalNAc-containing *N*-glycans. Using extracted ion chromatograms of this fragment, GalNAc-containing peaks were identified on FVII-alb from the wt HEK 293-F cell line (C), while the absence of GalNAc on FVII-alb from the NT3/4-KO cell line was confirmed (D). Mannose: green circle; GlcNAc: blue square; GalNAc: yellow square; fucose: red triangle;  $m/z$ : mass per charge.

#### 4.4.2.5 Evidence for sulfated GalNAc on FVII-alb *N*-glycans

Due to very similar masses of the sulfated GalNAc $\beta$ 4GlcNAc disaccharide (486.1155 Da) and three hexoses (486.1584 Da), with a theoretical difference of less than 0.05 Da, a clear differentiation between *N*-glycans carrying the one or the other was not possible with only the  $m/z$  values. One example is shown in Figure 36A. For this *N*-glycan, the MS spectrum of the corresponding peak already hinted at a sulfated structure due to characteristic in-source fragments (-1S and -2S in Figure 36B). Furthermore, MS/MS peak spectra were compared to the fragments computed in GlycoWorkbench for the rival sulfated and high-mannose *N*-glycans. The peak coverage was double for the sulfated *N*-glycan compared to the high-mannose *N*-glycan (43 vs. 19 matching fragments, accuracy: 5 ppm), with seven assigned sulfate-specific fragments.

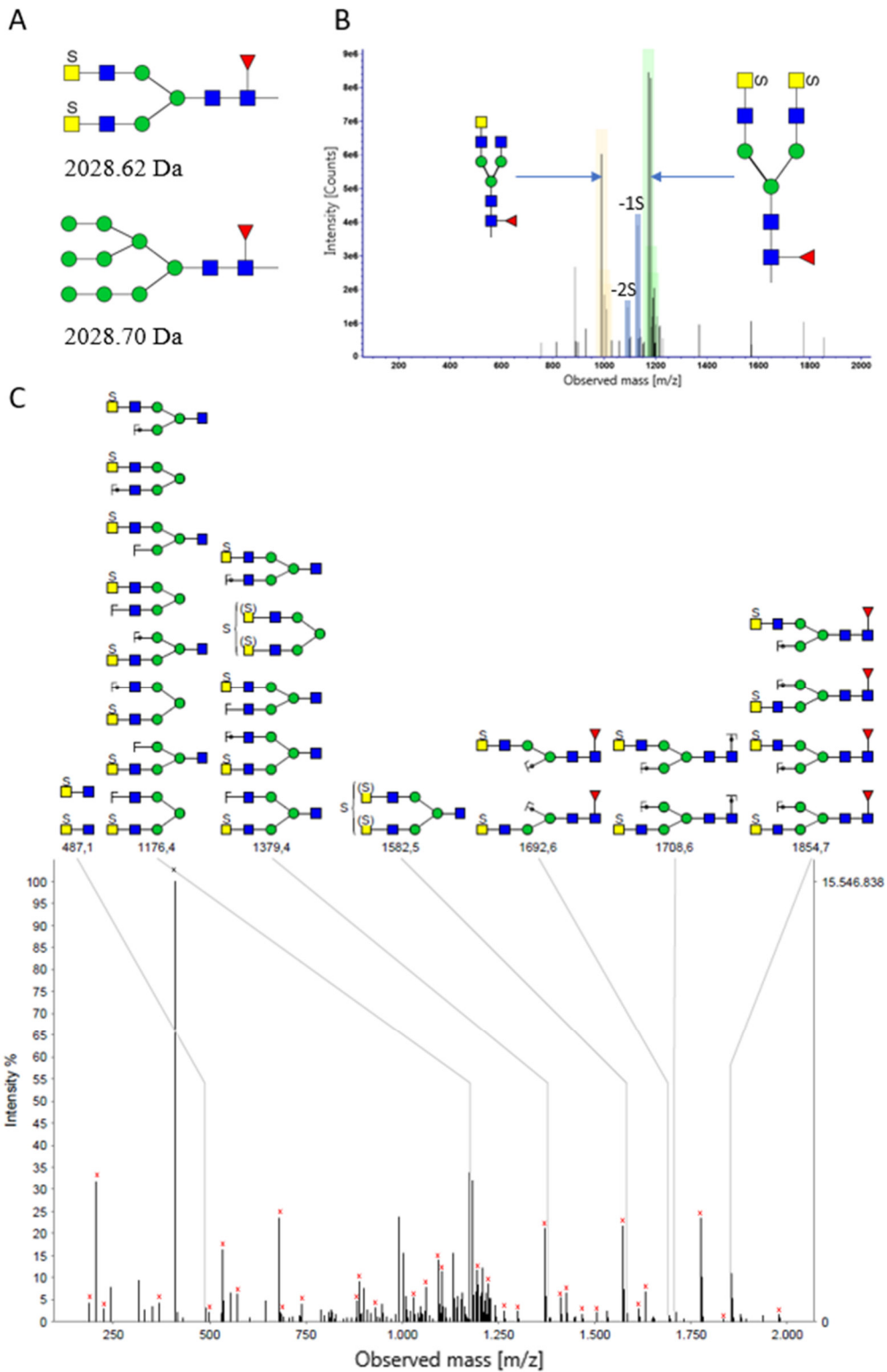


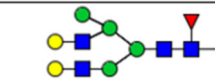
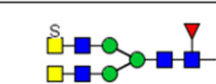
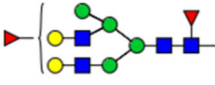
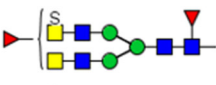
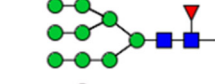
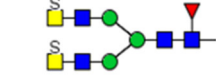

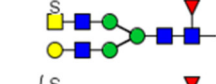


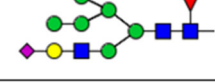

Figure 36: (A) Double-sulfated and high-mannose *N*-glycans with highly similar masses. (B) MS spectrum for the asterisk-labeled peak in Figure 37, presumably consisting of a core-fucosylated biantennary *N*-glycan with two sulfated GalNAc residues (green shaded), in-source fragments lacking one and two of the sulfate residues (blue shaded) and a co-eluting *N*-glycan (yellow shaded). Due to the low energy required to fragment the bond between GalNAc and sulfate, it is already destroyed in the ion source. (C) The correspondent MS/MS peak spectrum annotated with the seven fragments indicating a sulfated GalNAc structure (while non-sulfate relative annotations (red x) are not shown via glycan pictogram for better lucidity). Mannose: green circle; GlcNAc: blue square; GalNAc: yellow square; fucose: red triangle; Sulfate, S; m/z: mass per charge. Adapted from Uhler *et al.*<sup>224</sup>



For further evidence supporting the assignment of sulfated *N*-glycans, the sulfated *N*-glycans (Table 12 column 2) were compared to the respective hybrid and high-mannose *N*-glycans with similar masses, which were assigned in a study by Böhm *et al.* (Table 12 column 1).<sup>49</sup>

Four of the differently assigned *N*-glycans were on average 72% less abundant on FVII-alb from NT3-KO compared to wt HEK 293-F cells and were completely absent from the NT3/4-KO (Table 12). For sulfated GalNAc structures this decrease would result simply collateral to the overall decrease of GalNAc after NT3-KO (74%) and NT3/4-KO (100%). Yet, how GalNAcT KO would translate to a complete loss of hybrid and high-mannose structures seems less obvious.

Table 12: Hybrid and high-mannose *N*-glycans assigned by Böhm *et al.*<sup>49</sup> and sulfated GalNAc ones assigned in this study and their relative proportion on FVII-alb from wt HEK 293-F, NT3-KO and NT3/4-KO cell lines. Mannose: green circle; galactose: yellow circle; GlcNAc: blue square; GalNAc: yellow square; fucose: red triangle; Neu5Ac, purple diamond; Sulfate, S. From Uhler *et al.*<sup>224</sup>

| <i>N</i> -glycans assigned by Böhm <i>et al.</i>                                    | <i>N</i> -glycans assigned in this study                                            | Relative proportion of the <i>N</i> -glycan in question on FVII-alb from wt HEK 293-F [% of all <i>N</i> -glycans] | Relative proportion of the <i>N</i> -glycan in question on FVII-alb from NT3-KO [% of all <i>N</i> -glycans] | Relative proportion of the <i>N</i> -glycan in question on FVII-alb from NT3/4-KO [% of all <i>N</i> -glycans] |
|-------------------------------------------------------------------------------------|-------------------------------------------------------------------------------------|--------------------------------------------------------------------------------------------------------------------|--------------------------------------------------------------------------------------------------------------|----------------------------------------------------------------------------------------------------------------|
|    |    | 2.2                                                                                                                | 0.7                                                                                                          | 0.0                                                                                                            |
|  |  | 7.3                                                                                                                | 1.7                                                                                                          | 0.0                                                                                                            |
|  |  | 0.8                                                                                                                | 0.3                                                                                                          | 0.0                                                                                                            |
|  |  | 0.8                                                                                                                | 0.5                                                                                                          | 0.0                                                                                                            |
|  |  | 0.0                                                                                                                | 0.0                                                                                                          | 0.0                                                                                                            |
|  |  | 0.0                                                                                                                | 0.0                                                                                                          | 0.0                                                                                                            |

HILIC elution times of the six structures differently assigned between the two studies, fit better to sulfated GalNAc-containing *N*-glycans than hybrid or high-mannose *N*-glycans. This becomes clear when comparing the elution time of the differently assigned *N*-glycans (Table 13 columns 2 and 5) to *N*-glycans being one or two monosaccharides smaller but with similar structure (columns 3 and 6). The observed elution times of the *N*-glycans in question (column 1) are in all six cases closer to those from the sulfated GalNAc (column 7) than to those of the hybrid and high-mannose *N*-glycans (column 4). Furthermore, the six structures had a characteristic shift in retention time of 0.25 GU per sulfate group compared to the respective non-sulfated *N*-glycans, which is similar to the characteristic shift described for sulfated *N*-glycans by Wang *et al.*<sup>225</sup>

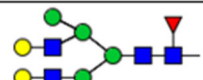
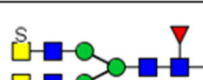
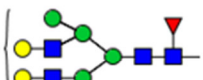

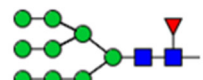
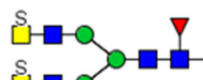






Table 13: Comparison of HILIC elution times in glucose units (GU) of *N*-glycans in question and smaller *N*-glycans with comparable structure. Mannose: green circle; galactose: yellow circle; GlcNAc: blue square; GalNAc: yellow square; fucose: red triangle; Neu5Ac, purple diamond; Sulfate, S. From Uhler *et al.*<sup>224</sup>

| Elution time of <i>N</i> -glycans in question [GU] | <i>N</i> -glycan assigned by Böhm <i>et al.</i> | <i>N</i> -glycan with similar structure and smaller size than the <i>N</i> -glycan assigned by Böhm <i>et al.</i> | Elution time of <i>N</i> -glycan similar to the one assigned by Böhm <i>et al.</i> [GU] | <i>N</i> -glycan assigned in this study | <i>N</i> -glycan with similar structure and smaller size than the <i>N</i> -glycan assigned in this study | Elution time of <i>N</i> -glycan similar to the one assigned in this study [GU] |
|----------------------------------------------------|-------------------------------------------------|-------------------------------------------------------------------------------------------------------------------|-----------------------------------------------------------------------------------------|-----------------------------------------|-----------------------------------------------------------------------------------------------------------|---------------------------------------------------------------------------------|
| 6.45                                               |                                                 |                                                                                                                   | 7.34                                                                                    |                                         |                                                                                                           | 6.28                                                                            |
| 7.09                                               |                                                 |                                                                                                                   | 8.11                                                                                    |                                         |                                                                                                           | 7.07                                                                            |
| 6.29                                               |                                                 |                                                                                                                   | 9.65                                                                                    |                                         |                                                                                                           | 6.28                                                                            |
| 6.81                                               |                                                 |                                                                                                                   | 7.34                                                                                    |                                         |                                                                                                           | 6.51                                                                            |
| 7.37                                               |                                                 |                                                                                                                   | 7.53                                                                                    |                                         |                                                                                                           | 7.28                                                                            |
| 7.42                                               |                                                 |                                                                                                                   | 8.54                                                                                    |                                         |                                                                                                           | 7.88                                                                            |

In addition, the mass differences between the *N*-glycans proposed by Böhm *et al.* and this study (Table 14 column 3) is smaller than Böhm *et al.*'s standard deviations of the observed masses (column 6).<sup>49</sup> Therefore, the differentiation between the hybrid and high-mannose and sulfated *N*-glycans was not possible with their data (column 4 and 5). In this study, the standard deviations of the observed masses were minute (column 9) and in all cases the detected masses matched better to sulfated GalNAc than hybrid and high-mannose *N*-glycans (column 7 and 8).

In summary, there are multiple pieces of evidence for the assignment of sulfated rather than hybrid or high-mannose *N*-glycans to the mass signals in question.

Table 14: Hybrid and high-mannose *N*-glycans assigned by Böhm *et al.*<sup>49</sup> and sulfated GalNAc ones assigned in this study with the theoretical molecular masses and mass difference (columns 1-3). Mass differences between the theoretical masses and the observed masses and standard deviations of observed masses for hybrid and high-mannose (columns 4-6) and sulfated *N*-glycans (columns 7-9). Mannose: green circle; galactose: yellow circle; GlcNAc: blue square; GalNAc: yellow square; fucose: red triangle; Neu5Ac, purple diamond; Sulfate, S. From Uhler *et al.*<sup>224</sup>

| <i>N</i> -glycans assigned by Böhm <i>et al.</i> with theoretical mass<br>[Da]<br><br>(In the Böhm study the <i>N</i> -glycans are attached to the T16 peptide with a mass of ~838.433 Da) | <i>N</i> -glycans assigned in this study with theoretical mass<br>[Da]                       | Mass difference between the <i>N</i> -glycans [Da] | Böhm <i>et al.</i> 's results (N=4)                   |                  |                                                                      | Results from this study (N=4)                         |                  |                                                                      |
|--------------------------------------------------------------------------------------------------------------------------------------------------------------------------------------------|----------------------------------------------------------------------------------------------|----------------------------------------------------|-------------------------------------------------------|------------------|----------------------------------------------------------------------|-------------------------------------------------------|------------------|----------------------------------------------------------------------|
|                                                                                                                                                                                            |                                                                                              |                                                    | Mean difference: theoretical minus observed mass [Da] |                  | Standard deviation of masses observed for this <i>N</i> -glycan [Da] | Mean difference: theoretical minus observed mass [Da] |                  | Standard deviation of masses observed for this <i>N</i> -glycan [Da] |
|                                                                                                                                                                                            |                                                                                              |                                                    | to Böhm <i>et al.</i> 's assignment                   | to my assignment |                                                                      | to Böhm <i>et al.</i> 's assignment                   | to my assignment |                                                                      |
|  1948.703                                                                                                 |  1948.660   | 0.043                                              | 0.176                                                 | 0.133            | 0.415                                                                | 0.033                                                 | -0.010           | 0.000                                                                |
|  2094.761                                                                                                 |  2094.718   | 0.043                                              | -0.099                                                | -0.142           | 0.273                                                                | 0.045                                                 | 0.002            | 0.000                                                                |
|  2028.703                                                                                                 |  2028.617   | 0.086                                              | 0.203                                                 | 0.118            | 0.298                                                                | 0.095                                                 | 0.009            | 0.000                                                                |
|  1907.676                                                                                                |  1907.633  | 0.043                                              | 0.284                                                 | 0.241            | 0.230                                                                | 0.025                                                 | 0.004            | 0.000                                                                |
|  2053.734                                                                                               |  2053.691 | 0.043                                              | 0.137                                                 | 0.095            | 0.275                                                                | 0.050                                                 | 0.007            | 0.000                                                                |
|  2198.772                                                                                               |  2198.729 | 0.043                                              | -0.038                                                | -0.081           | 0.436                                                                | 0.018                                                 | -0.003           | 0.000                                                                |

#### 4.4.3 Matching identified *N*-glycans to HILIC fluorescence chromatogram peaks

Using the presented approaches, all detected *N*-glycans were identified and a custom-made *N*-glycan library was built within the UNIFI 1.9 software. The identified *N*-glycans were subsequently matched to the HILIC fluorescence chromatogram peaks of each sample to enable elucidation of each individual glycan pattern and to calculate the relative proportions of individual monosaccharides as well as characteristic glycan features (e.g. antennarity, core fucosylation or sialic acid linkages).

Exemplary HILIC fluorescence chromatograms with annotated peaks of (i) NovoSeven®; (ii) FVII from the wt HEK 293-F cell line; and (iii) FVII-alb from the wt HEK 293-F, the NT3/4-KO-02 and the NT3/4-KO+ST6GAL1-KI-03 cell lines are depicted in Figure 37. The *N*-glycans making up the peaks and their proportion in the sample are shown in Table 15 to Table 19.

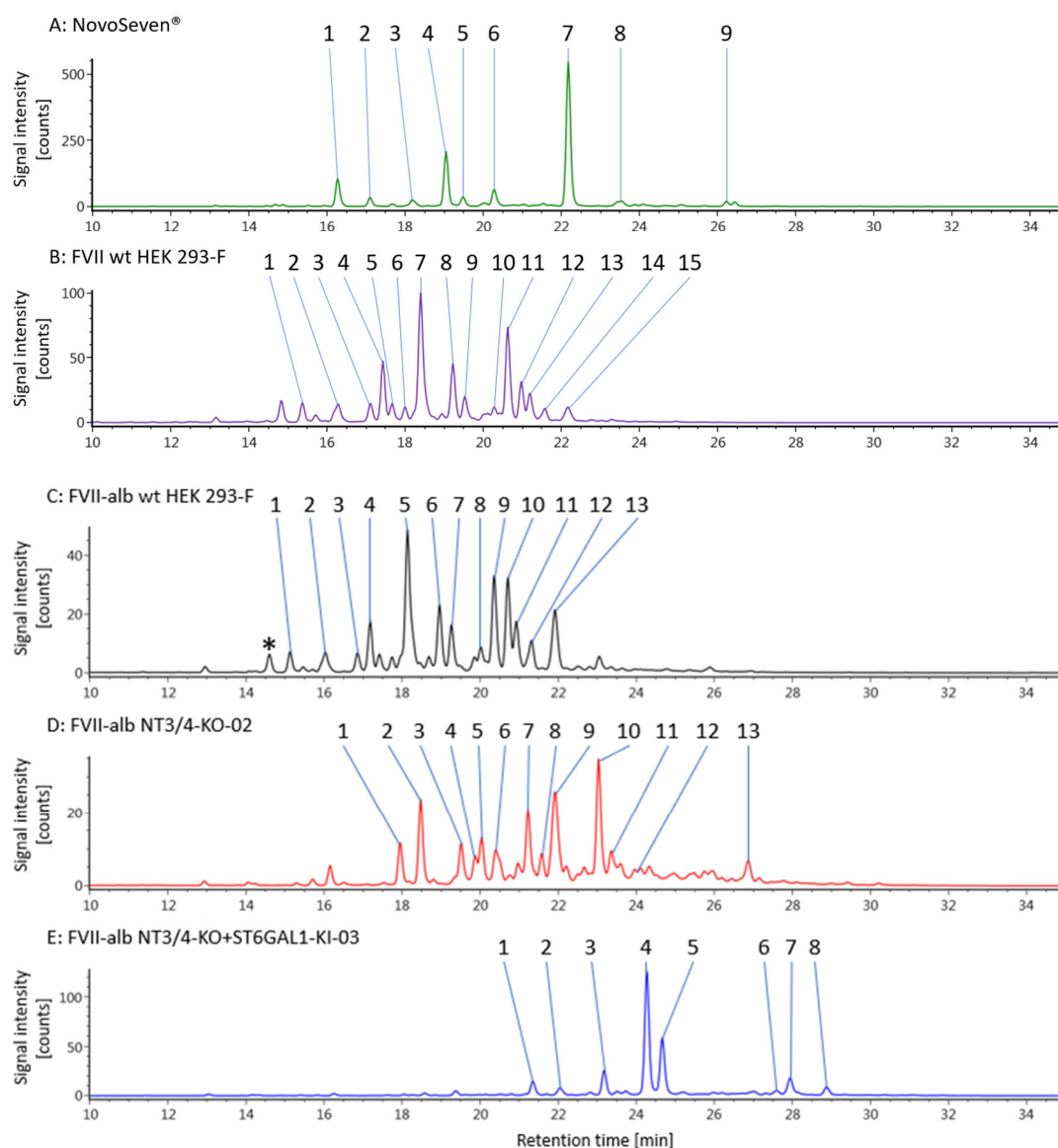


Figure 37: Exemplary HILIC fluorescence chromatograms of enzymatically released and *RapiFluor*-MS labeled *N*-glycans of NovoSeven® (A), FVII from the wt HEK 293-F cell line (B), FVII-alb from the wt HEK 293-F (C), the NT3/4-KO-02 (D) and the NT3/4-KO+ST6GAL1-KI-03 (E) cell lines with labeled peaks. For better lucidity only peaks >2% of the total fluorescence signal are labeled (while all structures >0.5% of the total fluorescence were considered for quantification purposes). *N*-glycan identifications are depicted in Table 15 to Table 19. The double sulfated *N*-glycan from Figure 36 is depicted with an asterisk but is below the 2% threshold. Adapted from Uhler *et al.*<sup>224</sup>

Table 15: Assignment of *N*-glycans to peaks labeled in Figure 37A for NovoSeven<sup>®</sup>, with relative proportions of the *N*-glycans (N=1). For peaks containing multiple co-eluting structures, they are displayed next to each other. Relative proportions of the different structures in one peak were quantified according to the ratio of their mass signals. Mannose: green circle; galactose: yellow circle; GlcNAc: blue square; GalNAc: yellow square; fucose: red triangle; Neu5Ac: purple diamond (facing up:  $\alpha$ 2,3-linked; straight: undetermined); Neu5Gc: white diamond (facing up:  $\alpha$ 2,3-linked). Adapted from Uhler *et al.*<sup>224</sup>

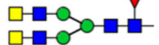

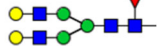



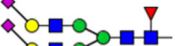

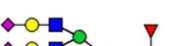
| Peak number | NovoSeven <sup>®</sup> <i>N</i> -glycans                                            | Relative proportion [% of all <i>N</i> -glycans] |
|-------------|-------------------------------------------------------------------------------------|--------------------------------------------------|
| 1           |    | 9.1                                              |
| 2           |    | 3.0                                              |
| 3           |    | 3.0                                              |
| 4           |    | 18.1                                             |
| 5           |    | 3.3                                              |
| 6           |    | 7.5                                              |
| 7           |    | 47.3                                             |
| 8           |   | 3.3                                              |
| 9           |  | 3.3                                              |

Table 16: Assignment of *N*-glycans to peaks labeled in Figure 37B for FVII from the wt HEK 293-F cell line, with relative proportions of the *N*-glycans (N=1). For peaks containing multiple co-eluting structures, they are displayed next to each other. Relative proportions of the different structures in one peak were quantified according to the ratio of their mass signals. Mannose: green circle; galactose: yellow circle; GlcNAc: blue square; GalNAc: yellow square; fucose: red triangle; Neu5Ac: purple diamond (facing up:  $\alpha$ 2,3 linked; facing down:  $\alpha$ 2,6 linked); Sulfate, S. Adapted from Uhler *et al.*<sup>224</sup>

| Peak number | wt HEK 293-F FVII <i>N</i> -glycans | Relative proportion [% of all <i>N</i> -glycans] |
|-------------|-------------------------------------|--------------------------------------------------|
| 1           |                                     | 2.7                                              |
| 2           |                                     | 2.5                                              |
| 3           |                                     | 1.9/0.8                                          |
| 4           |                                     | 8.1                                              |
| 5           |                                     | 2.8                                              |
| 6           |                                     | 2.1                                              |
| 7           |                                     | 21.5                                             |
| 8           |                                     | 8.8                                              |
| 9           |                                     | 4.6                                              |
| 10          |                                     | 3.1                                              |
| 11          |                                     | 14.0                                             |
| 12          |                                     | 6.2                                              |
| 13          |                                     | 7.1                                              |
| 14          |                                     | 3.3                                              |
| 15          |                                     | 1.5/1.9                                          |

Table 17: Assignment of *N*-glycans to peaks labeled in Figure 37C for FVII-alb from the wt HEK 293-F cell line, with relative proportions of the *N*-glycans (N=1). For peaks containing multiple co-eluting structures, they are displayed next to each other. Relative proportions of the different structures in one peak were quantified according to the ratio of their mass signals. Mannose: green circle; galactose: yellow circle; GlcNAc: blue square; GalNAc: yellow square; fucose: red triangle; Neu5Ac: purple diamond (facing up:  $\alpha$ 2,3 linked; facing down:  $\alpha$ 2,6 linked); Sulfate, S. Adapted from Uhler *et al.*<sup>224</sup>

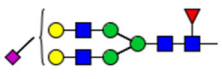
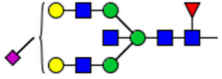
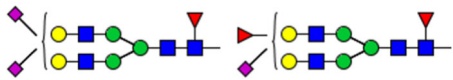
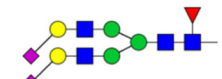
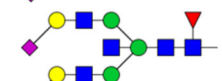
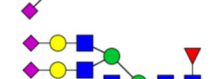
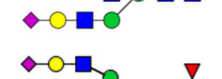
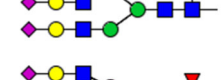
| Peak number | wt HEK 293-F FVII-alb <i>N</i> -glycans | Relative proportion [% of all <i>N</i> -glycans] |
|-------------|-----------------------------------------|--------------------------------------------------|
| 1           |                                         | 2.2                                              |
| 2           |                                         | 2.3                                              |
| 3           |                                         | 1.6/0.5                                          |
| 4           |                                         | 5.3                                              |
| 5           |                                         | 18.9                                             |
| 6           |                                         | 7.6                                              |
| 7           |                                         | 5.2                                              |
| 8           |                                         | 2.7                                              |
| 9           |                                         | 10.8                                             |
| 10          |                                         | 8.6                                              |
| 11          |                                         | 5.3                                              |
| 12          |                                         | 4.6                                              |
| 13          |                                         | 3.2/5.0                                          |



Table 18: Assignment of *N*-glycans to peaks labeled in Figure 37D for FVII-alb from the NT3/4-KO-02 cell line, with relative proportions of the *N*-glycans (N=1). For peaks containing multiple co-eluting structures, they are displayed next to each other. Relative proportions of the different structures in one peak were quantified according to the ratio of their mass signals. Mannose: green circle; galactose: yellow circle; GlcNAc: blue square; fucose: red triangle; Neu5Ac: purple diamond (facing up:  $\alpha$ 2,3 linked; facing down:  $\alpha$ 2,6 linked; straight: undetermined). Adapted from Uhler *et al.*<sup>224</sup>

| Peak number | NT3/4-KO-02 FVII-alb <i>N</i> -glycans | Relative proportion [% of all <i>N</i> -glycans] |
|-------------|----------------------------------------|--------------------------------------------------|
| 1           |                                        | 4.3                                              |
| 2           |                                        | 8.0                                              |
| 3           |                                        | 3.6                                              |
| 4           |                                        | 3.6                                              |
| 5           |                                        | 3.0/4.1                                          |
| 6           |                                        | 2.3/1.3                                          |
| 7           |                                        | 7.8                                              |
| 8           |                                        | 3.2                                              |
| 9           |                                        | 5.5/3.9/3.7                                      |
| 10          |                                        | 8.3/3.7                                          |
| 11          |                                        | 3.4                                              |
| 12          |                                        | 3.4                                              |
| 13          |                                        | 3.5                                              |

Table 19: Assignment of *N*-glycans to peaks labeled in Figure 37E for FVII-alb from the NT3/4-KO-02+ST6GAL1-KI-03 cell line, with relative proportions of the *N*-glycans (N=1). For peaks containing multiple co-eluting structures, they are displayed next to each other. Relative proportions of the different structures in one peak were quantified according to the ratio of their mass signals. Mannose: green circle; galactose: yellow circle; GlcNAc: blue square; fucose: red triangle; Neu5Ac: purple diamond (facing up:  $\alpha$ 2,3 linked; facing down:  $\alpha$ 2,6 linked; straight: undetermined).

| Peak number | NT3/4-KO-02+ST6GAL1-KI-03 FVII-alb <i>N</i> -glycans                                | Relative proportion [% of all <i>N</i> -glycans] |
|-------------|-------------------------------------------------------------------------------------|--------------------------------------------------|
| 1           |    | 4.1                                              |
| 2           |    | 2.8                                              |
| 3           |    | 3.7/3.5                                          |
| 4           |    | 36.6                                             |
| 5           |    | 17.8                                             |
| 6           |   | 2.3                                              |
| 7           |  | 4.5                                              |
| 8           |  | 2.2                                              |

#### 4.4.4 Reproducibility and comparability of glycosylation analysis methods

To determine the reproducibility and comparability of the *N*-glycan profiling (3.2.3.4), monosaccharide analysis (3.2.3.2) and sialic acid analysis (3.2.3.3) methods, three biologic replicates of FVII-alb from the wt HEK 293-F cell line were produced, purified and analyzed independently.

Standard deviations for all monosaccharides were below 2% in the *N*-glycan profiling (calculated from identified *N*-glycans), below 4% in the monosaccharide analysis (GlcNAc, GalNAc, galactose, and fucose) and below 5% in the sialic acid analysis (Figure 38). The low standard deviations show the reproducibility of the used methods. Since the results for the three biologic replicates of FVII-alb from the wt HEK 293-F cell line are basically identical, only the results for one replicate are shown in the following.

The *N*-glycan profiling results were comparable to those of the orthogonal monosaccharide and sialic acid analysis for GlcNAc, GalNAc, galactose, and sialic acid (Figure 38). However, fucose content determined by *N*-glycan profiling and monosaccharide analysis differed by approximately one. This is caused by the single *O*-linked fucose found on Ser<sub>60</sub> of FVII<sup>196,197</sup> that is not covered by the *N*-glycan

profiling method but by the monosaccharide approach. Therefore, *N*-glycan profiling results are consistent with the orthogonal monosaccharide and sialic acid analysis.

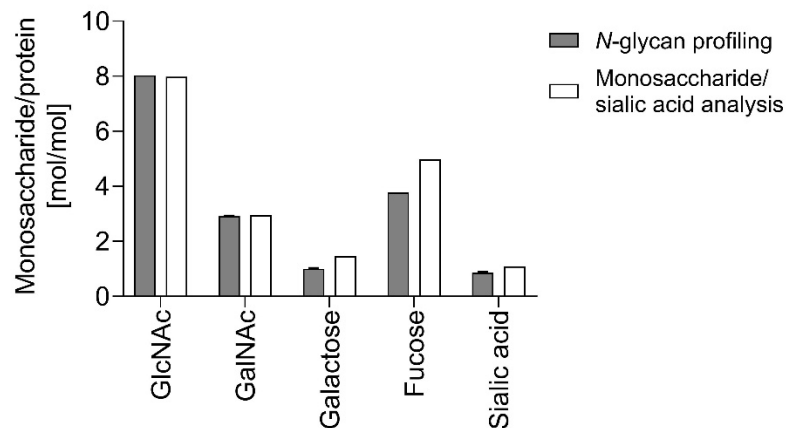


Figure 38: Mean and standard deviation of the monosaccharide content of three biologic replicates of FVII-alb expressed in the wt HEK 293-F cell line compared between *N*-glycan profiling and the monosaccharide and sialic acid analysis.

#### 4.5 *N*-glycosylation analysis of glyco-engineered FVII-alb

The *N*-glycosylation of FVII-alb expressed in different host cell lines was studied by *N*-glycan profiling, monosaccharide analysis and sialic acid analysis and compared to that of FVII from the wt HEK 293-F cell line and to NovoSeven®, an activated FVII produced in BHK cells.

In the following, the host cell line names will be displayed without stable pool numbers. The original and abbreviated host cell line names are summarized in Table 20.

Table 20: Abbreviated host cell line names.

| Full host cell line name   | Abbreviated host cell line name |
|----------------------------|---------------------------------|
| wt HEK 293-F               | wt HEK 293-F                    |
| NT3-KO                     | NT3-KO                          |
| NT4-KO                     | NT4-KO                          |
| NT3/4-KO-01                | NT3/4-KO-01                     |
| NT3/4-KO-02                | NT3/4-KO-02                     |
| wt+ST3GAL6_sol-KI-02       | wt+ST3GAL6_sol-KI               |
| wt+ST6GAL1_sol-KI-01       | wt+ST6GAL1_sol-KI               |
| wt+ST3GAL6-KI-07           | wt+ST3GAL6-KI                   |
| wt+ST6GAL1-KI-03           | wt+ST6GAL1-KI                   |
| wt+ST6GAL1-KI-06-131       | wt+ST6GAL1-KI-131               |
| wt+ST6GAL1-KI-06-167       | wt+ST6GAL1-KI-167               |
| NT3/4-KO+ST3GAL6_sol-KI-15 | NT3/4-KO+ST3GAL6_sol-KI         |
| NT3/4-KO+ST6GAL1_sol-KI-03 | NT3/4-KO+ST6GAL1_sol-KI         |
| NT3/4-KO+ST3GAL6-KI-08     | NT3/4-KO+ST3GAL6-KI             |
| NT3/4-KO+ST6GAL1-KI-03     | NT3/4-KO+ST6GAL1-KI             |
| NT3/4-KO+ST6GAL1-KI-06-154 | NT3/4-KO+ST6GAL1-KI-154         |
| NT3/4-KO+ST6GAL1-KI-06-160 | NT3/4-KO+ST6GAL1-KI-160         |

#### 4.5.1 Evaluation of GalNAc-transferase knock-out

B4GALNT3 and B4GALNT4 transfer GalNAc to *N*-glycans in mammalian cells.<sup>40–42</sup> To abolish *N*-glycan GalNAc, the two GalNAcTs were knocked-out by CRISPR/Cas9. Subsequently, the influence on the *N*-glycosylation of FVII-alb was determined for a *B4GALNT3* and a *B4GALNT4* KO clone and for two *B4GALNT3* plus *B4GALNT4* double KO clones.

The levels of GalNAc on FVII and FVII-alb expressed in the wt HEK 293-F cell line were comparable, while KO of *B4GALNT4* slightly decreased it (Figure 39A). KO of *B4GALNT3* further decreased it to a level similar to that on NovoSeven®, and in both NT3/4-KO clones GalNAc was completely absent. Similarly, galactose levels increased proportionally to the decline of GalNAc levels (Figure 39B), which suggests a complete replacement of GalNAc with galactose.

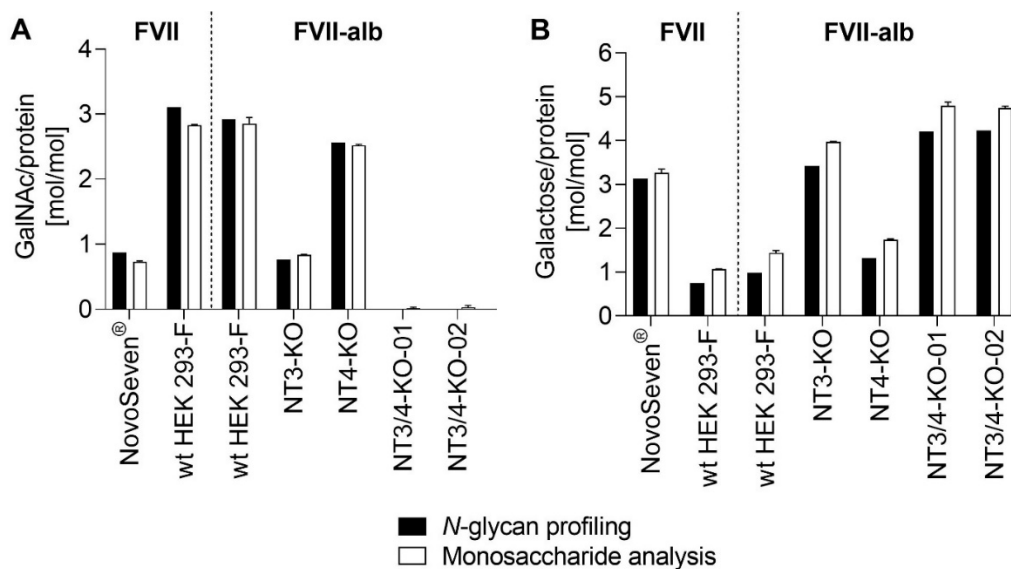


Figure 39: Evaluation of GalNAcT KO clones: *N*-linked GalNAc (A) and galactose (B) units per molecule of FVII and FVII-alb. For *N*-glycan profiling N=1. For monosaccharide analysis, all groups N=3 technical replicates, except NovoSeven® N=2.

With increasing levels of galactose, sialylation also increased by ~2.5 fold in the NT3-KO and NT3/4-KO cell lines, while the NT4-KO—where galactose levels did not change considerably—did not alter sialylation of FVII-alb (Figure 40A). All sialic acids found on HEK 293-F-derived proteins were Neu5Ac, while 2.7% non-human Neu5Gc was detected on NovoSeven®. Simultaneous KO of *B4GALNT3* and *B4GALNT4* also shifted the balance towards  $\alpha$ 2,3-linked and away from  $\alpha$ 2,6-linked sialic acids (from 35% to 48%  $\alpha$ 2,3-linked), while NovoSeven® with its BHK origin only carried  $\alpha$ 2,3-linked sialic acids (Figure 40B).

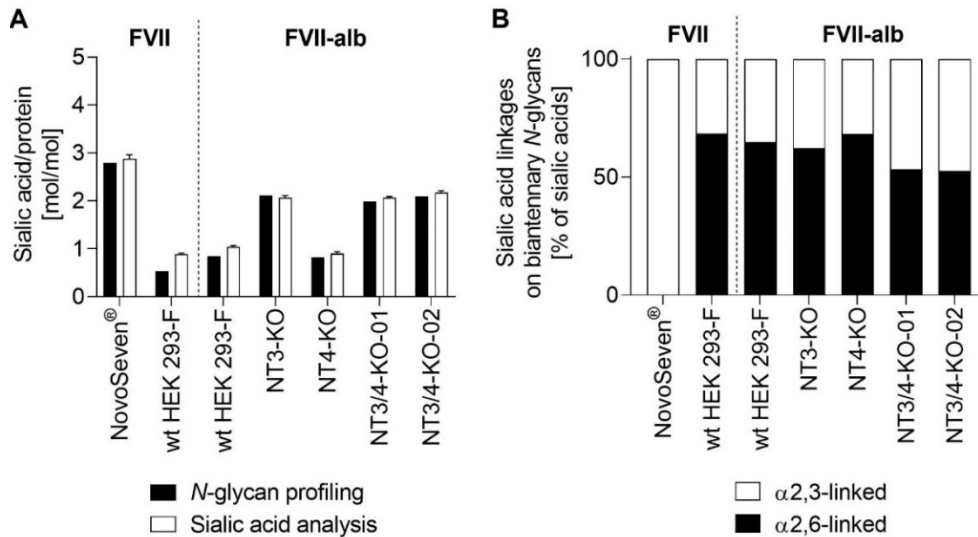


Figure 40: Evaluation of GalNAcT KO clones: Sialic acid units per molecule FVII and FVII-alb (A) and percentage of  $\alpha$ 2,3- and  $\alpha$ 2,6-linked sialic acids on biantennary *N*-glycans in the *N*-glycan profiling. For *N*-glycan profiling N=1. For sialic acid analysis, all groups N=3 technical replicates.

On FVII-alb expressed in the wt HEK 293-F cell line, 12% and 9% of GalNAc were sialylated and sulfated, respectively (Figure 41A). In the NT4-KO clone, the level of sulfated GalNAc decreased to ~4%. The absence of GalNAc in the NT3/4-KO clones precluded both sialylation and sulfation of GalNAc. GalNAc on NovoSeven® was neither sialylated nor sulfated.

All *N*-glycans on FVII and FVII-alb were core-fucosylated. Furthermore, FVII and FVII-alb produced in wt HEK 293-F cells additionally carried, on average, nearly two fucoses on the antennae (Figure 41B). The *B4GALNT3* KO and double-KO decreased antenna fucosylation to approximately one per FVII-alb molecule in both clones.

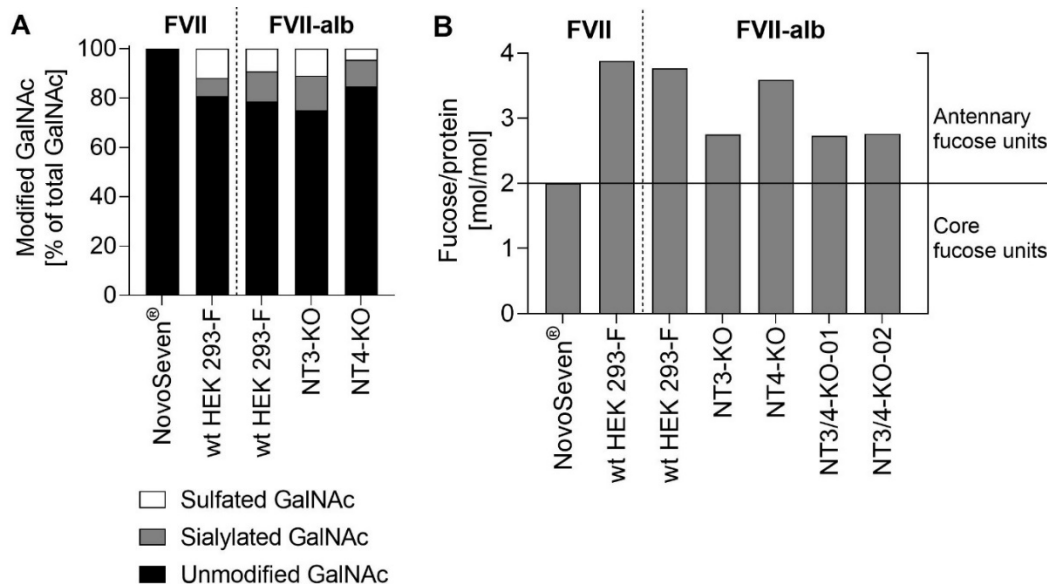


Figure 41: Evaluation of GalNAcT KO clones: Percentage of GalNAc modified with  $\alpha$ 2,6-linked sialic acid or 4-linked sulfate (A; only FVII-alb variants carrying GalNAc) and *N*-linked fucose units per molecule of FVII and FVII-alb (B) in the *N*-glycan profiling (N=1). Fucose units located on the *N*-glycan core and on the antennae are indicated.

Bisected (Figure 42A) and triantennary *N*-glycans (Figure 42B) were basically absent on FVII and FVII-alb from wt HEK 293-F and NT4-KO cells. In the B4GALNT3 KO and double-KOs, bis-GlcNAc and the proportion of triantennary *N*-glycans surged to 26% and 38% and 10% and 16%, respectively. This indicates that GalNAc might play a role in *N*-glycan bisection and branching. Approximately 3% of the *N*-glycans of NovoSeven® carried three antenna.

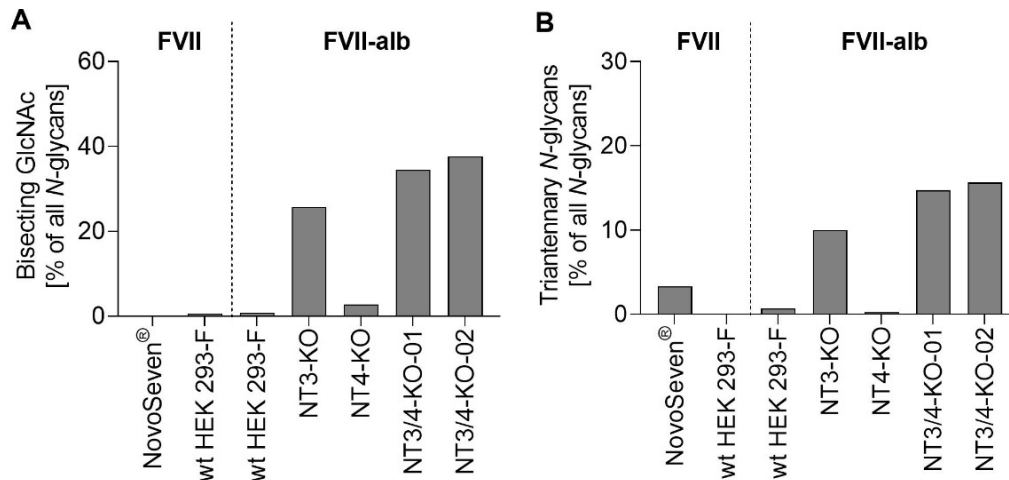


Figure 42: Evaluation of GalNAcT KO clones: Percentage of bis-GlcNAc-containing (A) and triantennary (B) *N*-glycans in the *N*-glycan profiling (N=1).

In summary, FVII and FVII-alb *N*-glycans were substantially identical, which confirms that albumin fusion does not considerably alter *N*-glycosylation of FVII. Furthermore, GalNAc was completely absent on FVII-alb *N*-glycans after KO of both *B4GALNT3* and *B4GALNT4*, while it was only reduced after individual KO of *B4GALNT3* or *B4GALNT4*. This shows that both GalNAcTs play a role in the addition of GalNAc to *N*-glycans in HEK 293-F cells. KO of both GalNAcTs changed also changed other *N*-glycan features that may reduce binding to clearance receptors. Specifically, the increased sialylation and the change in sialic acid linkage type distribution might reduce ASGP-R binding. Similarly, reduced antenna fucosylation and GalNAc sulfation might reduce MR binding. Since *N*-glycosylation was comparable between the two NT3/4-KO clones, only clone NT3/4-KO-02 was selected for all further experiments. While the level of GalNAc on FVII-alb from the NT3/4-KO clones was now lower than on NovoSeven®, the sialylation was still higher on the latter. Therefore, only considering *N*-glycosylation, NovoSeven® was still expected to bind less efficiently to the ASGP-R than FVII-alb from the NT3/4-KO clones. To further increase sialylation of FVII-alb, SiaT KIs and sialic acid metabolism precursor feeding were tested.

#### 4.5.2 Evaluation of sialyltransferase overexpression

The cause for the low levels of sialic acids on wt HEK 293-F-derived proteins was so far unknown. If SiaT activity is rate limiting in sialylation, then overexpression of SiaTs might improve it. Therefore, different SiaTs were knocked into the wt HEK 293-F cell line and into the NT3/4-KO-02 clone. ST3GAL6 and ST6GAL1 were selected since they are known to be responsible for *N*-glycan sialylation in  $\alpha$ 2,3 and  $\alpha$ 2,6-linkage, respectively.<sup>39</sup> Furthermore, soluble variants of both enzymes were included too based on the publication by Sugimoto *et al.*, which showed that they might exhibit stronger activity towards secreted proteins.<sup>150</sup> Wt HEK 293-F and NT3/4-KO-02-derived pools stably overexpressing SiaTs ST3GAL6, ST6GAL1 and the soluble versions ST3GAL6\_sol and ST6GAL1\_sol were analyzed for the *N*-glycosylation of expressed FVII-alb and compared to FVII-alb expressed in the parental cell lines.

None of the SiaT KIs had a clear effect on the level of GalNAc (Figure 43A) or galactose (Figure 43B). However, a slight decrease in GalNAc and a slight increase in galactose levels was detected for FVII-alb from the wt+ST6GAL1-KI pool.

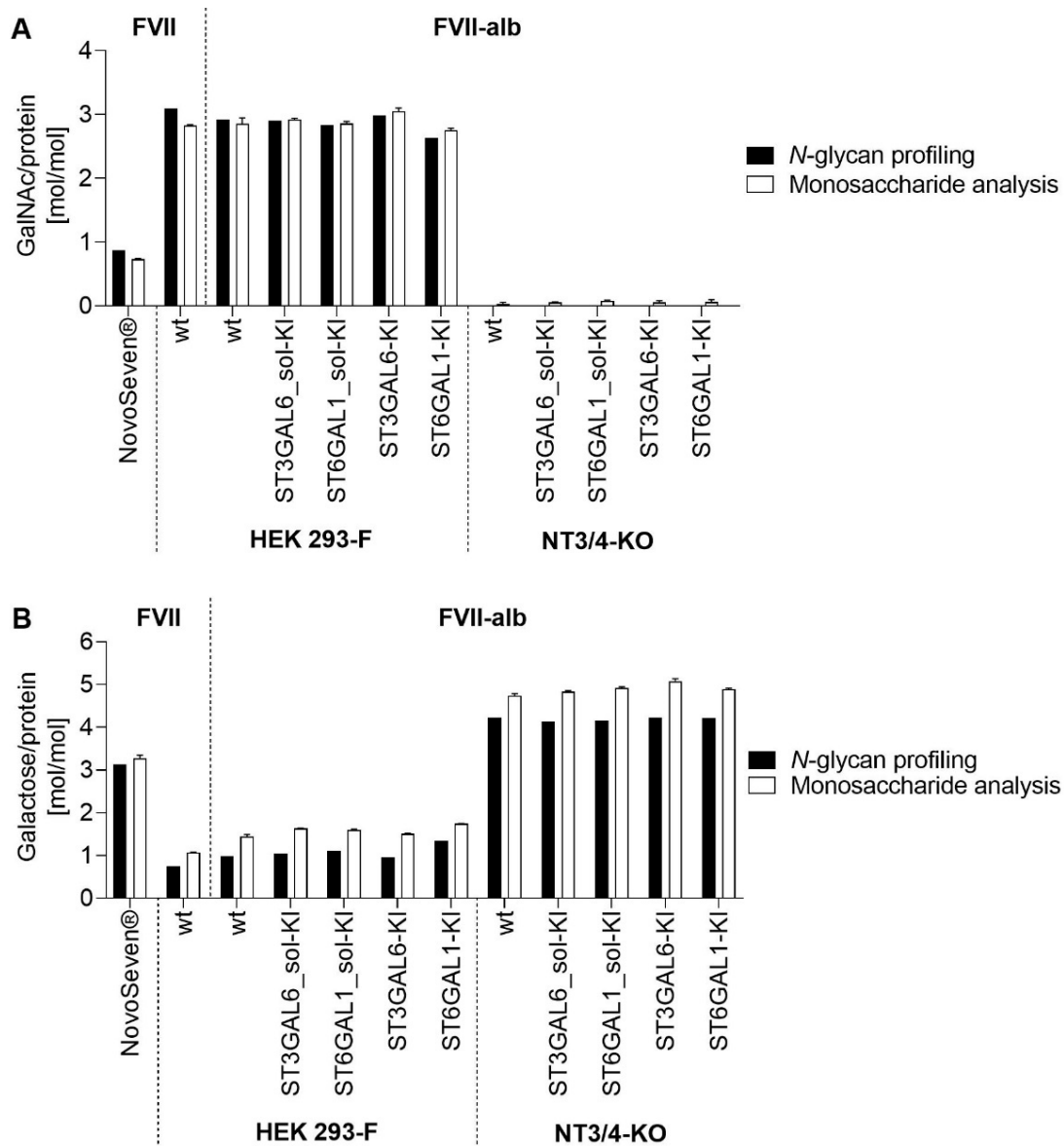


Figure 43: Evaluation of SiaT KI pools: N-linked GalNAc (A) and galactose (B) units per molecule of FVII and FVII-alb. For N-glycan profiling N=1. For monosaccharide analysis, all groups N=3 technical replicates, except NovoSeven® N=2.

While *ST6GAL1* improved FVII-alb sialylation in both backgrounds, *ST6GAL1\_sol* worked on the wildtype, and *ST3GAL1* worked on the NT3/4-KO (Figure 44A). The soluble SiaT versions were outperformed by the membraned-bound ones. *ST6GAL1* KI resulted in the highest increase in sialylation in both backgrounds. In the NT3/4-KO background the *ST6GAL1* KI also resulted in the highest overall sialylation in the study, 36% higher than that of NovoSeven®. The ~3.8 mol/mol sialic acids from the NT3/4-KO+*ST6GAL1*-KI pool translated into 91% sialylated antenna—resulting in a close to completely sialylated FVII-alb molecule— while the ~2.8 mol/mol of NovoSeven® translated into only 70% sialylated antenna. As expected, *ST6GAL1\_sol* and *ST6GAL1* KIs promoted  $\alpha$ 2,6-sialylation while *ST3GAL6* KI promoted  $\alpha$ 2,3-sialylation (Figure 44B). After KI of *ST6GAL1*, nearly all sialic acids were  $\alpha$ 2,6-linked. However, *ST3GAL6\_sol* KI promoted  $\alpha$ 2,3-sialylation only on the wt HEK 293-F background but not on the NT3/4-KO background.

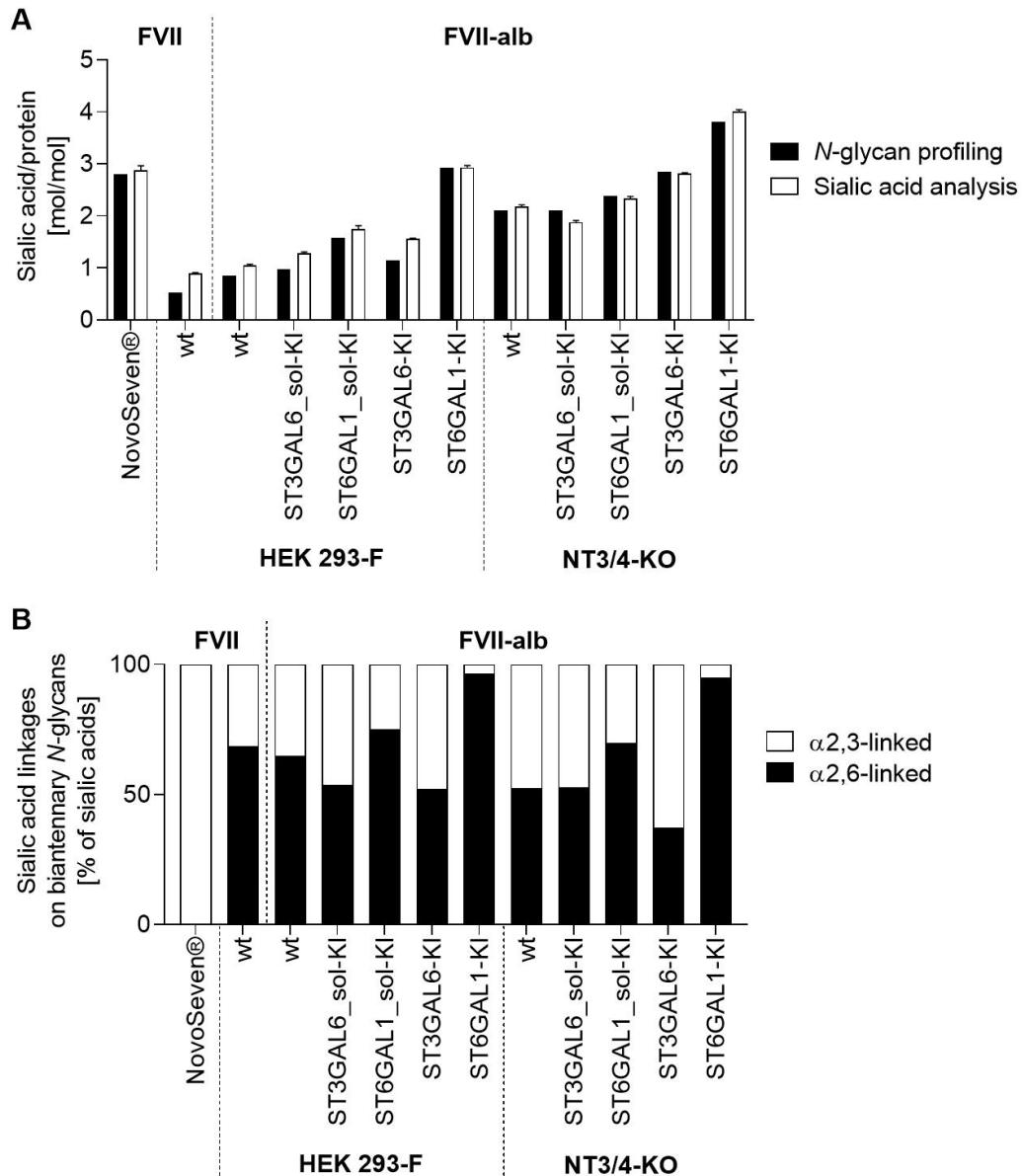


Figure 44: Evaluation of SiaT KI pools: Sialic acid units per molecule FVII and FVII-alb (A) and percentage of  $\alpha$ 2,3- and  $\alpha$ 2,6-linked sialic acids on biantennary *N*-glycans in the *N*-glycan profiling. For *N*-glycan profiling N=1. For sialic acid analysis, all groups N=3 technical replicates.

In the *ST6GAL1\_sol* and *ST6GAL1* KI pools GalNAc sialylation was increased and GalNAc sulfation was reduced (Figure 45A). Antenna fucosylation was considerably reduced by *ST6GAL1* KIs on both backgrounds, while *ST6GAL1\_sol* and *ST3GAL6* reduced it only on the wt HEK 293-F and NT3/4-KO backgrounds, respectively (Figure 45B). On FVII-alb from the NT3/4-KO+*ST6GAL1*-KI pool, antenna fucosylation was basically absent.



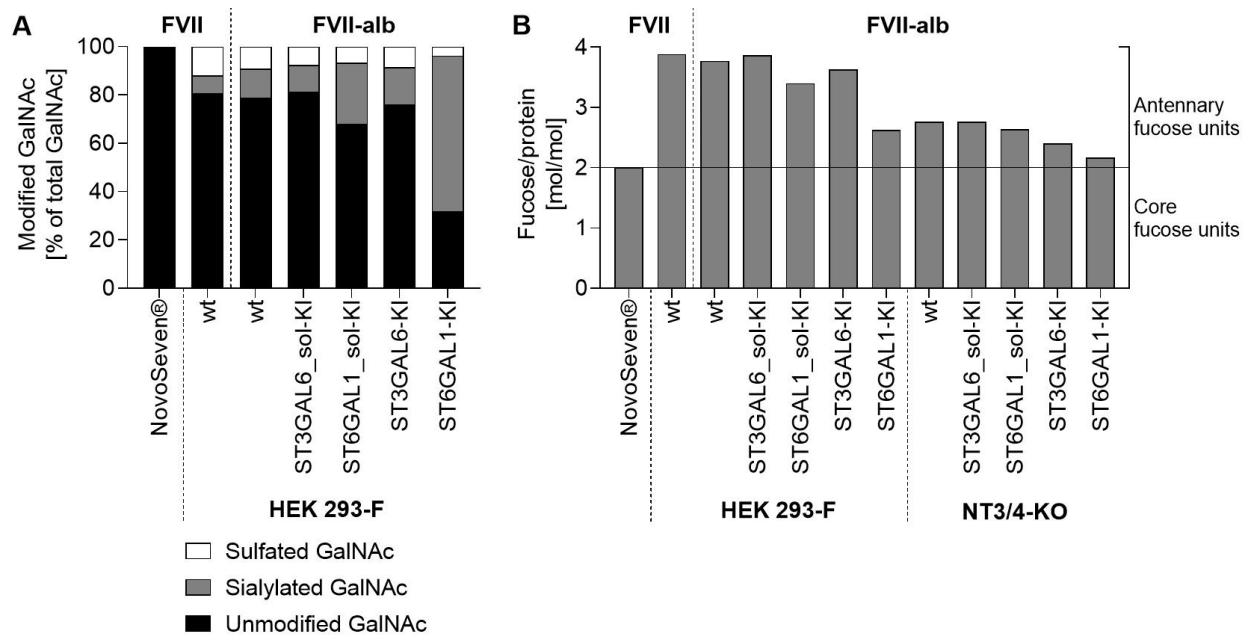


Figure 45: Evaluation of SiaT KI pools: Percentage of GalNAc modified with  $\alpha$ 2,6-linked sialic acid or 4-linked sulfate (A; only FVII-alb variants carrying GalNAc) and *N*-linked fucose units per molecule of FVII and FVII-alb (B) in the *N*-glycan profiling (N=1). Fucose units located on the *N*-glycan core and on the antennae are indicated.

SiaT KIs in the wt HEK 293-F background did not affect levels of bis-GlcNAc or triantennary glycans (Figure 46). However, in the NT3/4-KO background, KI of *ST6GAL1* slightly reduced the level of bis-GlcNAc, while the other SiaTs increased it. The proportion of triantennary glycans slightly changed upon SiaT KIs.

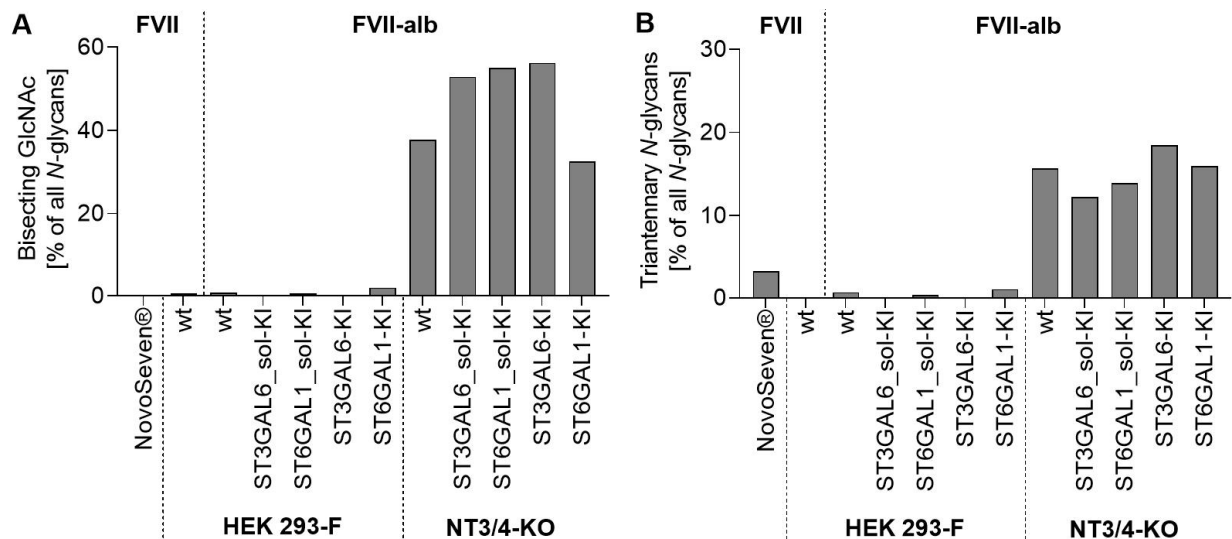


Figure 46: Evaluation of SiaT KI pools: Percentage of bis-GlcNAc-containing (A) and triantennary (B) *N*-glycans in the *N*-glycan profiling (N=1).

Overexpression of *ST3GAL6\_sol* and *ST6GAL1\_sol* at best moderately altered *N*-glycosylation of FVII-alb, while *ST3GAL6* increased  $\alpha$ 2,3-sialylation levels and antenna fucosylation in the NT3/4-KO background. *ST6GAL1* KI in both backgrounds heavily increased  $\alpha$ 2,6-sialylation levels and antenna fucosylation. Moreover, the almost complete sialylation of FVII-alb from the NT3/4-KO+*ST6GAL1*-KI pool was the desired outcome of the glyco-engineering approach. From these results, distinct ASGP-R

and MR binding reduction was anticipated for the *ST6GAL1* KI in the wt and for the *ST6GAL1* KI and *ST3GAL6* KI in the NT3/4-KO backgrounds. Therefore, the engineered host cell lines were suitable to produce FVII-alb with desirable *N*-glycan patterns.

Furthermore, the complexity of the HILIC peak spectrum and thus of the *N*-glycan pattern was substantially decreased between FVII-alb from wt HEK 293-F and NT3/4-KO+*ST6GAL1*-KI cells (Figure 37), due to the abolished *N*-glycan GalNAc as well as sulfated GalNAc and due to the reduced antenna fucosylation as well as  $\alpha$ 2,3-sialylation. This greatly reduced the heterogeneity between the FVII-alb molecules to a level comparable to NovoSeven®.

### 4.5.3 Comparison of *ST6GAL1* knock-in pools and clones

In recombinant cell pools GOI expression levels are usually quite heterogeneous between cells. Accordingly, different clones express the GOI to different extents. If the GOI is a SiaT, different expression levels will result in diverse sialic acid transfer capabilities. And if the transfer rate is limiting for sialylation, then target molecules such as FVII-alb will carry varying levels of sialylation and of other *N*-glycan features that are influenced by sialylation (described in 4.5.2). Hence, FVII-alb from different clones will also be differently glycosylated. Besides the GOI, endogenous genes relevant for *N*-glycosylation can also be differently expressed—for example because of different chromosome counts and hence different gene copy numbers<sup>130,215</sup>—and the variation across pools will again lead to variation between clones. To get a first impression of the extent of such clonal variation, the differences in FVII-alb *N*-glycosylation between selected clones was assessed. Based on its substantial impact on FVII-alb *N*-glycosylation, *ST6GAL1* overexpressing clones were selected for this study (see chapter 4.1.4 and 4.1.5).

To assess the influence of the *ST6GAL1* mRNA level on FVII-alb *N*-glycosylation two clones from the wt+*ST6GAL1*-KI and two of the NT3/4-KO-*ST6GAL1*-KI pools—covering a wide range of *ST6GAL1* mRNA levels (Figure 47)—were selected.

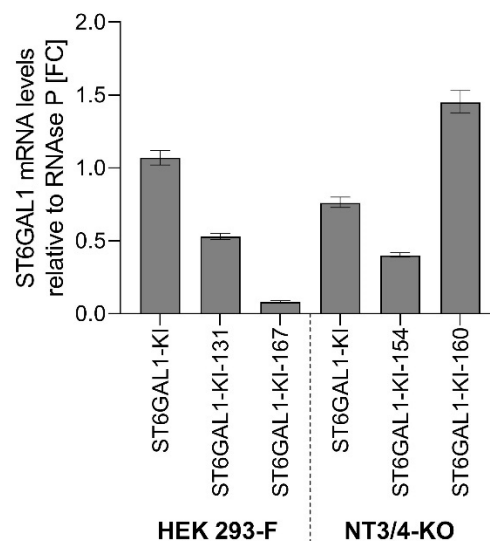


Figure 47: *ST6GAL1* mRNA levels of pools and clones relative to *RNase P* (white bars) and relative to the wt HEK 293-F cell line (grey bars). All measurements were performed in triplicates and bars represent the mean with confidence intervals ( $\alpha=0.05$ ).

For the wt HEK 293-F cell-derived pool and clones, differences in *ST6GAL1* mRNA levels were consistent with the changes in sialylation and the other *N*-glycosylation attributes that were affected by sialylation (4.5.2). Specifically, total sialylation,  $\alpha$ 2,6-linked sialylation, and GalNAc sialylation were

more pronounced with higher *ST6GAL1* mRNA levels (Figure 48 and Figure 49A), while antenna fucosylation was less pronounced (Figure 49B). This indicates that *ST6GAL1* mRNA levels correlate with changes in *N*-glycosylation.

However, for the NT3/4-KO-derived pools and clones, the picture was different. While clone 160 had the highest *ST6GAL1* mRNA levels, its effect on total sialylation,  $\alpha$ 2,6-linked sialylation, GalNAc sialylation, and antenna fucosylation was the lowest (Figure 48 and Figure 49). And while clone 154 had only half the *ST6GAL1* mRNA level than the pool it was isolated from, *N*-glycosylation between the two was largely comparable. Therefore, for the NT3/4-KO-derived pool and clones, differences in *ST6GAL1* mRNA levels were not consistent with the changes in sialylation and the other *N*-glycosylation attributes.

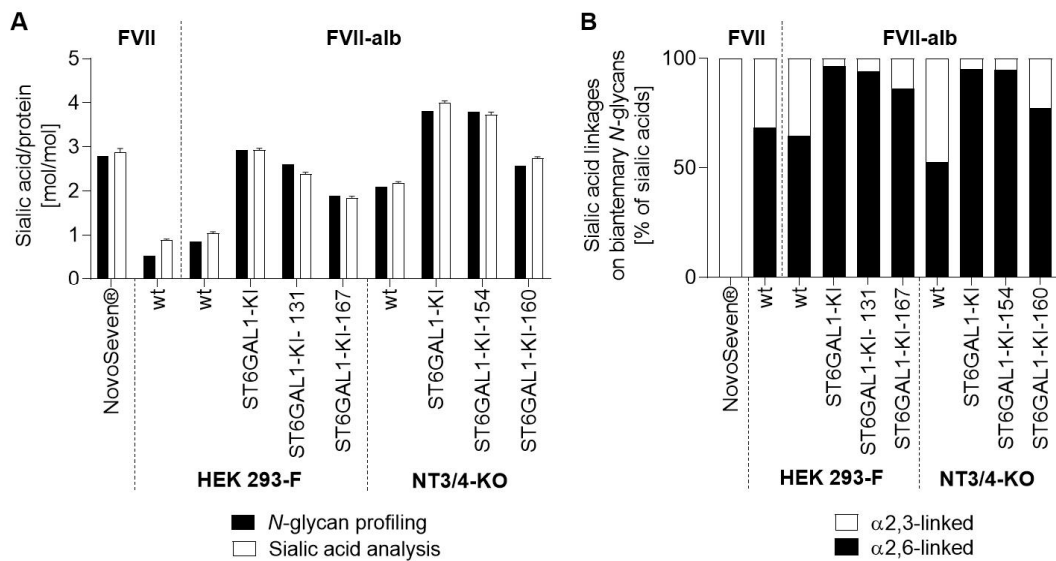


Figure 48: Evaluation of *ST6GAL1* overexpressing clones compared to pools: Sialic acid units per molecule FVII and FVII-alb (A) and percentage of  $\alpha$ 2,3- and  $\alpha$ 2,6-linked sialic acids on biantennary *N*-glycans in the *N*-glycan profiling. For *N*-glycan profiling N=1. For sialic acid analysis, all groups N=3 technical replicates.

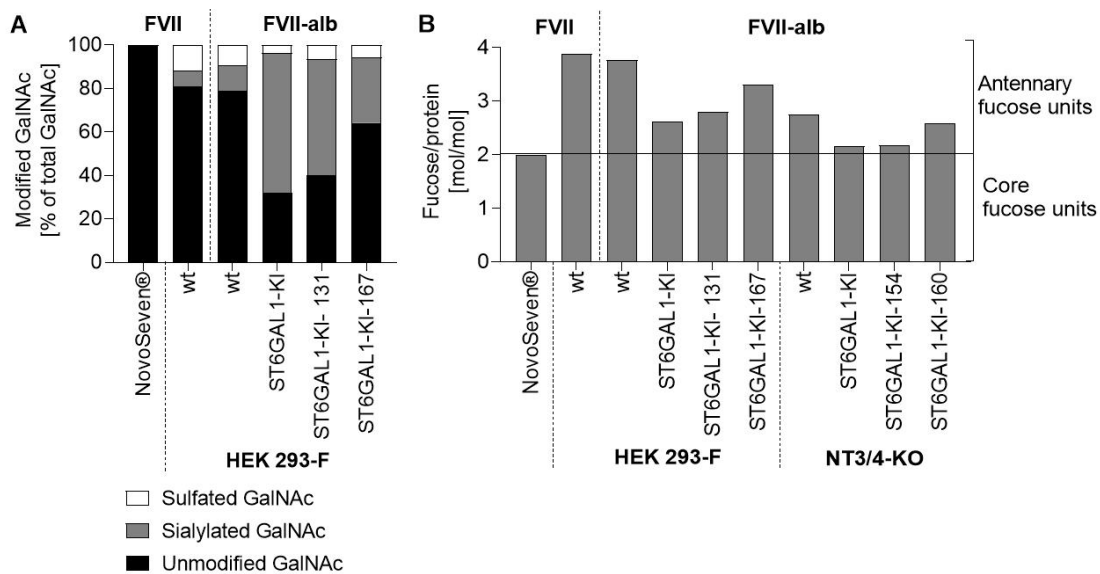


Figure 49: Evaluation of *ST6GAL1* overexpressing clones compared to pools: Percentage of GalNAc modified with  $\alpha$ 2,6-linked sialic acid or 4-linked sulfate (A; only FVII-alb variants carrying GalNAc) and *N*-linked fucose units per molecule of FVII and FVII-alb (B) in the *N*-glycan profiling (N=1). Fucose units located on the *N*-glycan core and on the antennae are indicated.

The *N*-glycosylation of the four clones was additionally assessed for differences that might be caused by differential expression of endogenous genes. In that respect, no changes in the levels of GalNAc (Figure 50A), galactose (Figure 50B) and bis-GlcNAc (Figure 51A) were detected. However, while the proportion of triantennary *N*-glycans was comparable between FVII-alb from the NT3/4-KO and that from the NT3/4-KO+ST6GAL1-KI pools, it was decreased in clone 154 and even more so in clone 160 (Figure 51B). In absence of other differences in *N*-glycosylation between the NT3/4-KO+ST6GAL1-KI pool and clone 154 and with the differences to clone 160 most likely being induced by the differences in sialylation itself (see previous passage), differential expression of the enzymes responsible for *N*-glycan branching (MGAT4 and MGAT5) in the clones might cause the reduced antennarity.

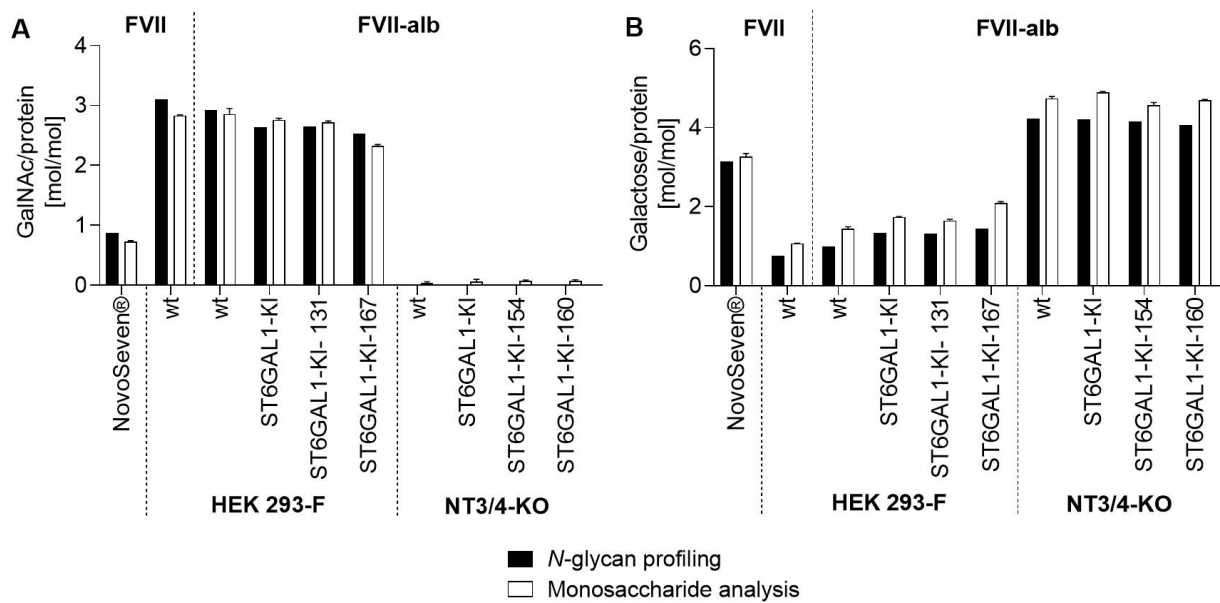


Figure 50: Evaluation of *ST6GAL1* overexpressing clones compared to pools: *N*-linked GalNAc (A) and galactose (B) units per molecule of FVII and FVII-alb. For *N*-glycan profiling N=1. For monosaccharide analysis, all groups N=3 technical replicates, except NovoSeven® N=2.

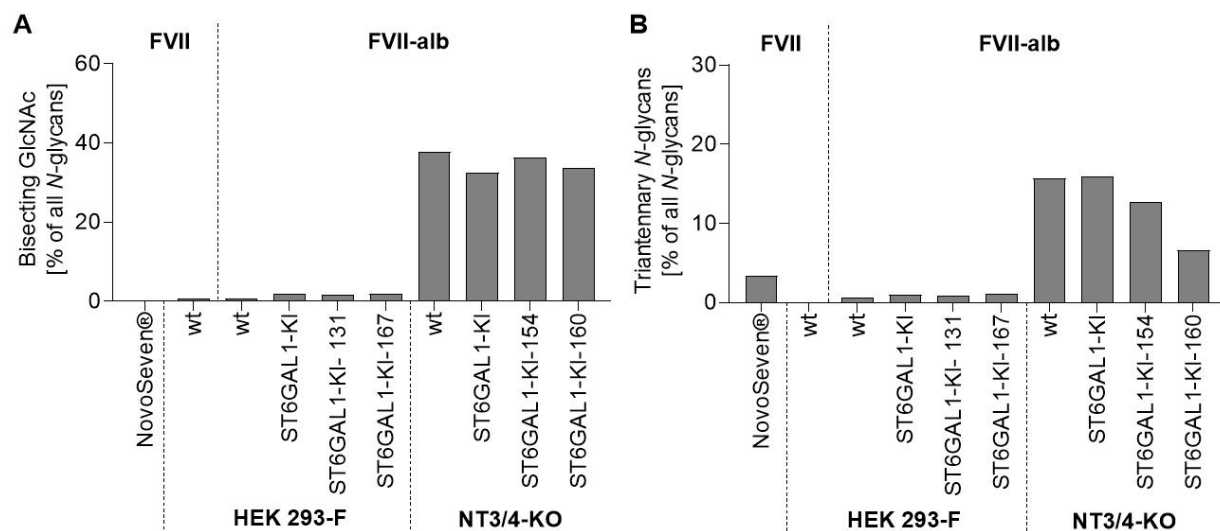


Figure 51: Evaluation of *ST6GAL1* overexpressing clones compared to pools: Percentage of bis-GlcNAc-containing (A) and triantennary (B) *N*-glycans in the *N*-glycan profiling (N=1).

#### 4.5.4 Evaluation of sialic acid metabolism precursor supplementation

The cause for the low levels of sialic acids on wt HEK 293-F-derived proteins is so far unknown. If the availability of CMP-sialic acid, the substrate for SiaTs, is rate limiting, supplementation of the culture medium with the precursors ManNAc or cytidine could lead to higher levels of sialylation.<sup>167-170</sup> Therefore, the wt HEK 293-F, NT3/4-KO-02, NT3/4-KO+ST3GAL6\_sol-KI, NT3/4-KO+ST6GAL1\_sol-KI, NT3/4-KO+ST3GAL6-KI, and NT3/4-KO+ST6GAL1-KI cell lines were cultured in medium supplemented with ManNAc and cytidine and the NT3/4-KO-02 cell line was cultured in either ManNAc or cytidine alone. After addition of the non-sterile ManNAc and cytidine powders to the culture medium it had to be sterile filtered. To control for potential changes in medium composition caused by the required sterile filtering, the wt HEK 293-F and NT3/4-KO-02 cell lines were cultured in sterile filtered SF9-2 medium.

Growth rates and in some cases CSPs were lower for the cells cultured in medium supplemented with ManNAc and cytidine compared to the cells without supplements (Figure 52). However, the difference was considered acceptable to continue with *N*-glycan analysis.

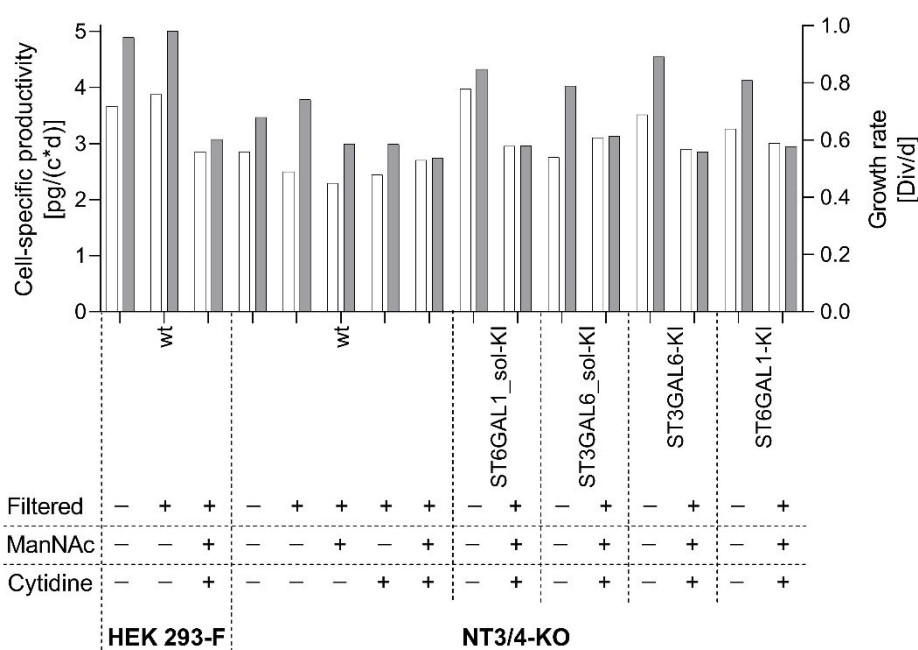


Figure 52: Cell-specific productivity (white bars) and growth rate (grey bars) of expression cell lines with and without supplementation of ManNAc and cytidine. Medium filtration and ManNAc as well as cytidine supplementation are indicated by a plus. Straight lines separate the different expression cell lines (N=1). Div: divisions; c: cell.

Neither medium filtration nor supplementation with ManNAc or cytidine influenced the level of the individual monosaccharides, or altered sialylation linkage types, GalNAc sialylation or sulfation on FVII-alb (Figure 53, Figure 54 and Figure 55).

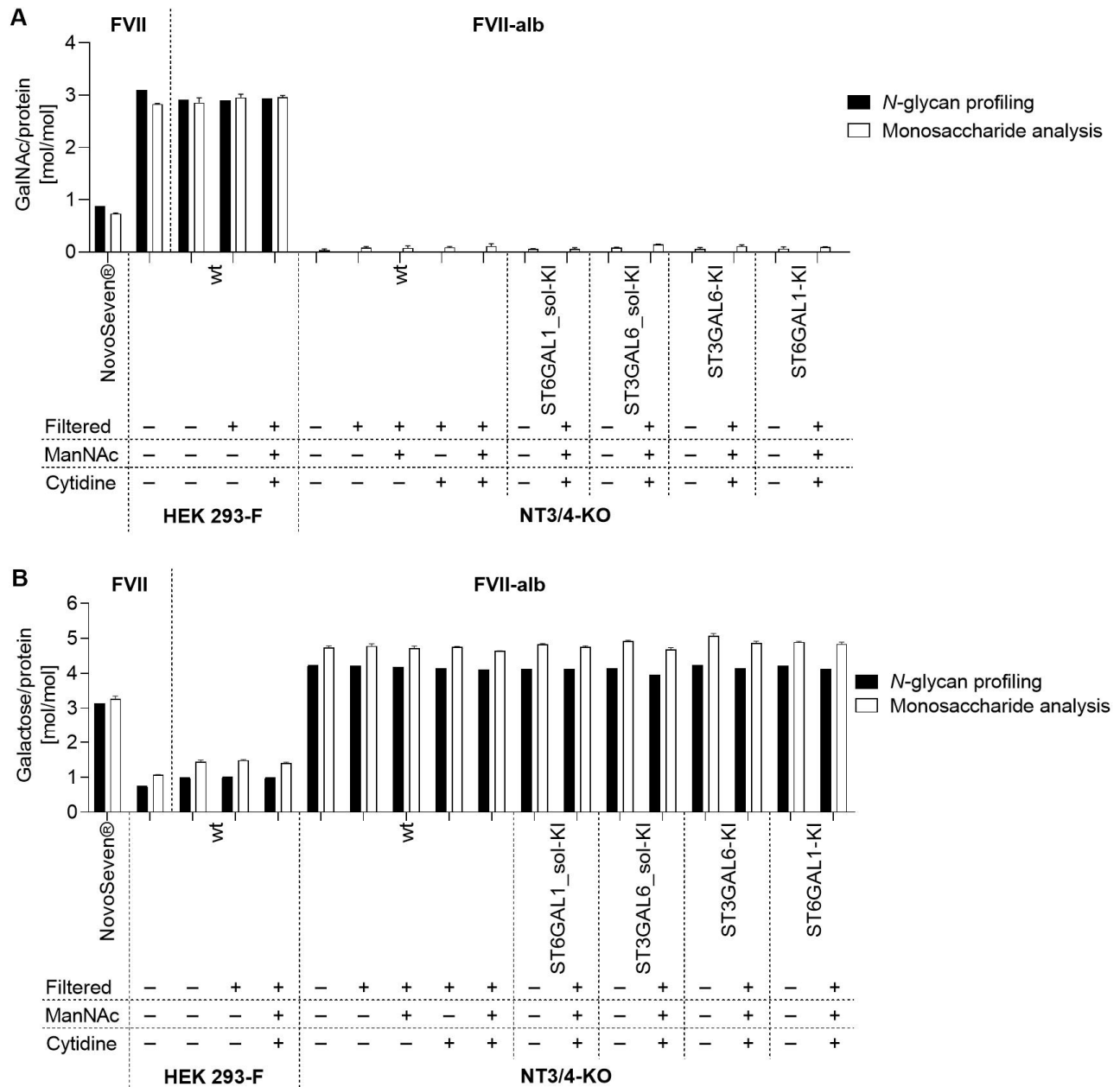


Figure 53: Evaluation of sialic acid precursor feed: *N*-linked GalNAc (A) and galactose (B) units per molecule of FVII and FVII-alb. Medium filtration and ManNAc as well as cytidine supplementation are indicated by a plus. For *N*-glycan profiling *N*=1. For monosaccharide analysis, all groups *N*=3 technical replicates, except NovoSeven® *N*=2.

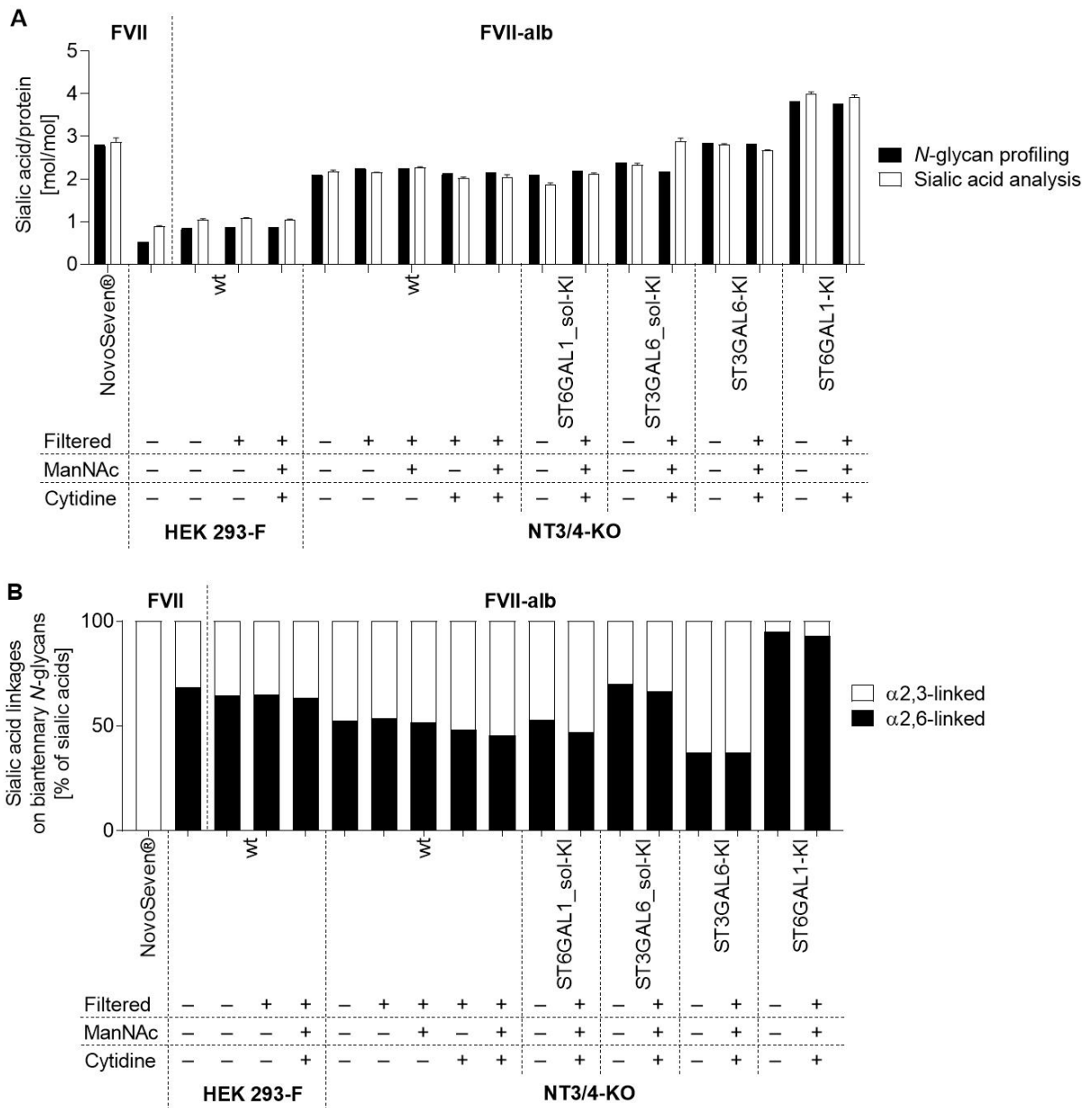


Figure 54: Evaluation of sialic acid precursor feed: Sialic acid units per molecule FVII and FVII-alb (A) and percentage of  $\alpha$ 2,3- and  $\alpha$ 2,6-linked sialic acids on biantennary *N*-glycans in the *N*-glycan profiling. Medium filtration and ManNAc as well as cytidine supplementation are indicated by a plus. For *N*-glycan profiling N=1. For sialic acid analysis, all groups N=3 technical replicates.

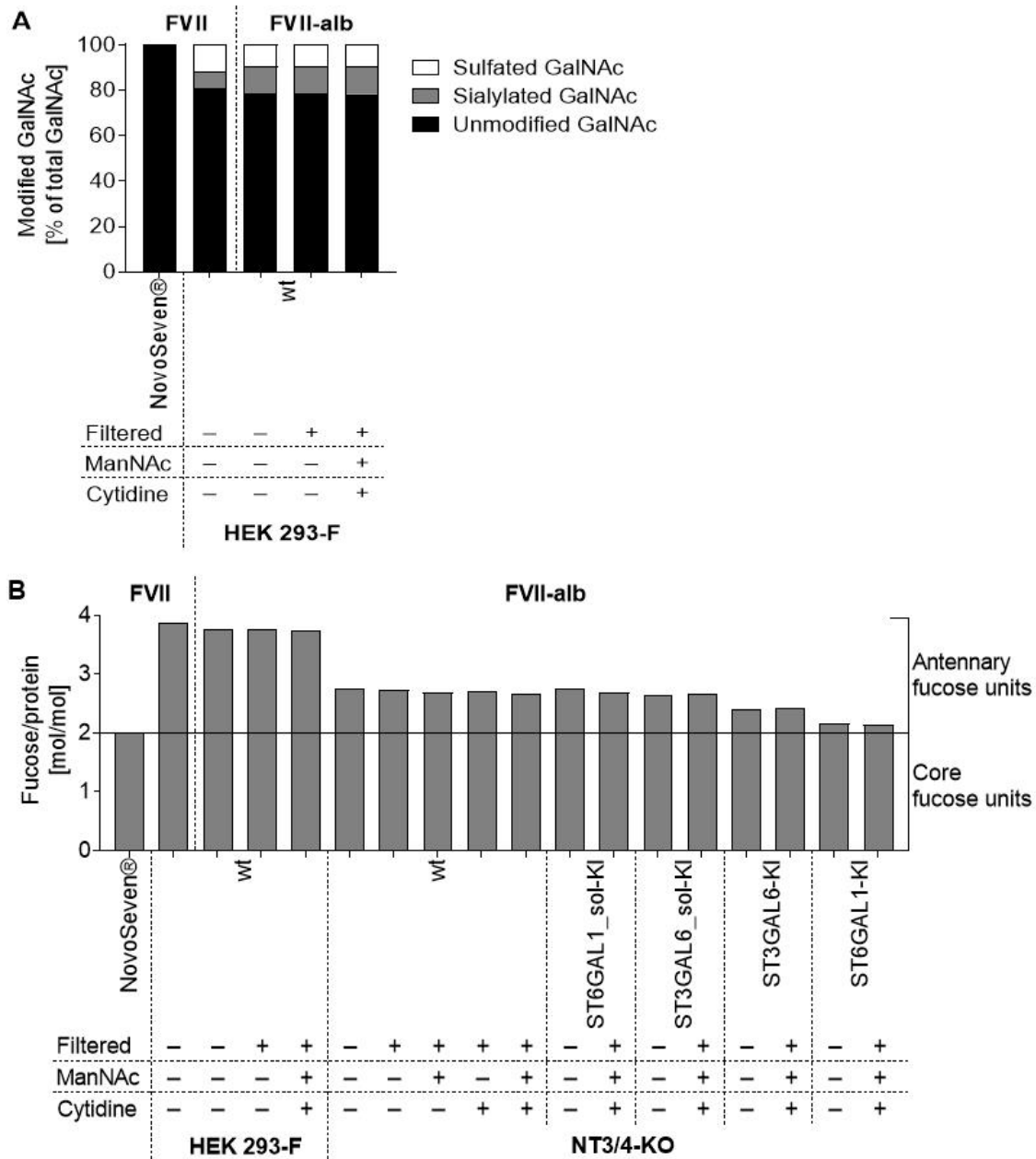


Figure 55: Evaluation of sialic acid precursor feed: Percentage of GalNAc modified with  $\alpha$ 2,6-linked sialic acid or 4-linked sulfate (A; only FVII-alb variants carrying GalNAc) and *N*-linked fucose units per molecule of FVII and FVII-alb (B) in the *N*-glycan profiling (N=1). Fucose units located on the *N*-glycan core and on the antennae are indicated. Medium filtration and ManNAc as well as cytidine supplementation are indicated by a plus.

The percentage of bis-GlcNAc-containing and triantennary glycans varied by up to 10% and 3%, respectively, between FVII-alb produced in medium supplemented or not with ManNAc and cytidine (Figure 56). The only considerable difference was detected in the percentage of triantennary glycans from FVII-alb expressed in the NT3/4-KO+ST6GAL1\_sol-KI cell line with and without supplementation.



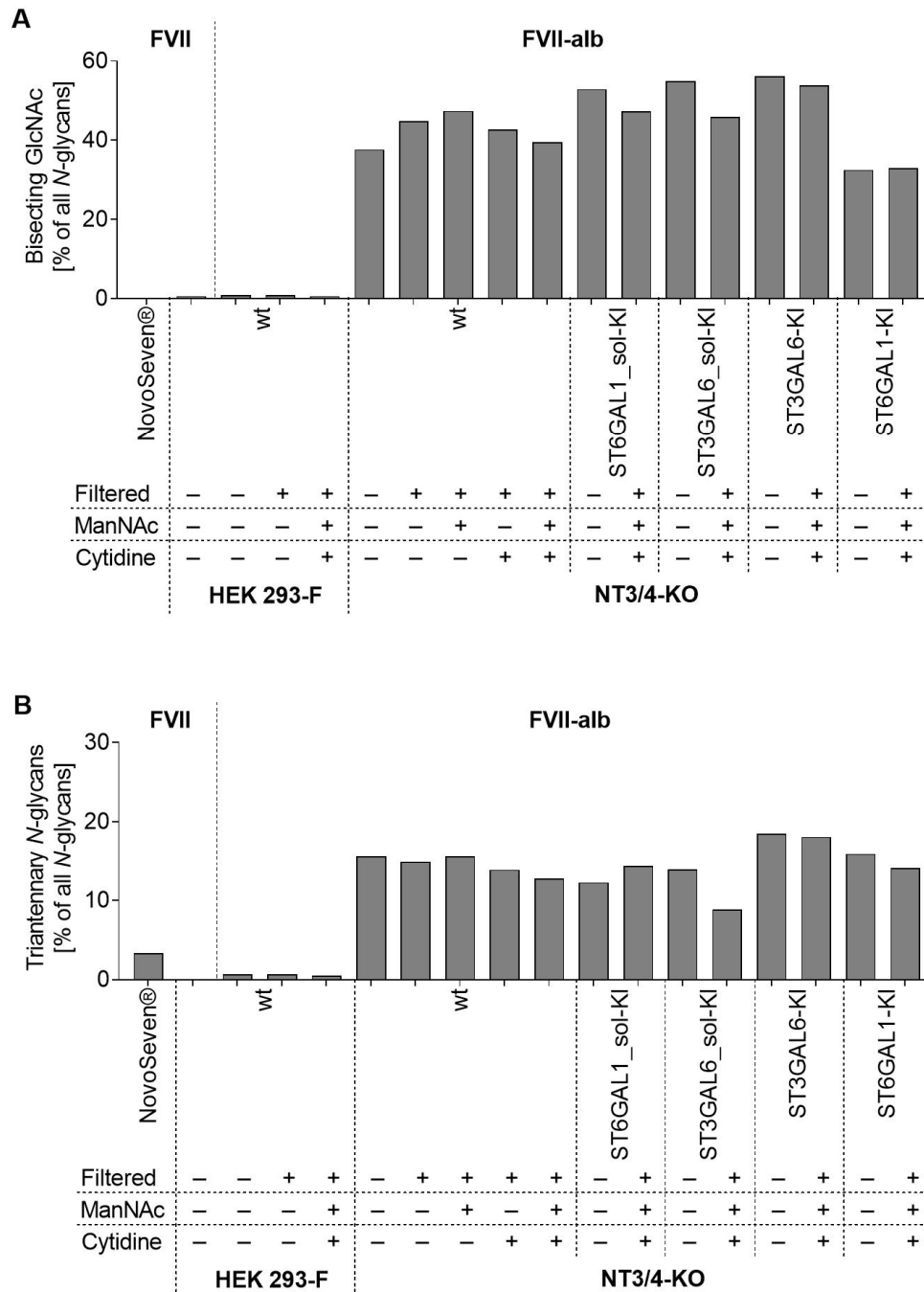


Figure 56: Evaluation of sialic acid precursor feed: Percentage of bis-GlcNAc-containing (A) and triantennary (B) *N*-glycans in the *N*-glycan profiling (N=1). Medium filtration and ManNAc as well as cytidine supplementation are indicated by a plus.

Overall, supplementation with ManNAc and cytidine did not increase sialylation and therefore, substrate limitation is not a likely cause for the low levels of sialylation in the HEK 293-F cell line.

#### 4.6 Comparison of FVII-alb, FVIII-BDD and FIX *N*-glycans

To evaluate whether the glyco-engineering approach is also applicable to other proteins of therapeutical relevance, FVIII-BDD and FIX were produced in the wt HEK 293-F, the NT3/4-KO and the NT3/4-KO+ST6GAL1-KI cell lines and analyzed by *N*-glycan profiling.

The HILIC fluorescence profiles of the three proteins were different even when expressed in the same cell lines under comparable cultivation conditions, which indicates that *N*-glycosylation is protein-specific. The used HILIC retention mechanism separates *N*-glycans based on their hydrophobicity, which in case of *N*-glycans results in separation mainly by mass and charge. Therefore, longer or more branched *N*-glycans generally elute later. When produced in the wt HEK 293-F cell line, the complex biantennary *N*-glycans of FVII-alb mainly elute between 17 and 22 min (Figure 57), while the complex biantennary, hybrid and high-mannose *N*-glycans of FVIII-BDD spread out between 15 and 24 min (Figure 58). The bulk of the complex tri- and tetraantennary *N*-glycans of FIX from wt HEK 293-F cells elute later between 22 and 32 min (Figure 59). After NT3/4-KO, the peaks of FVII-alb and FIX shift to later elution times, while the FVIII-BDD peaks remain largely constant. After KI of *ST6GAL1*, the peaks of all three proteins shift further to the right, which indicates larger and more sialylated *N*-glycans. These observations are consistent with the specific glyco-engineering-induced changes in *N*-glycosylation of the three proteins, which are detailed in the following paragraphs.

Similar to those of FVII-alb, the peak spectra of both FVIII-BDD and FIX were less complex and thus the heterogeneity of all three proteins was decreased when produced in the NT3/4-KO+ST6GAL1-KI cell line.

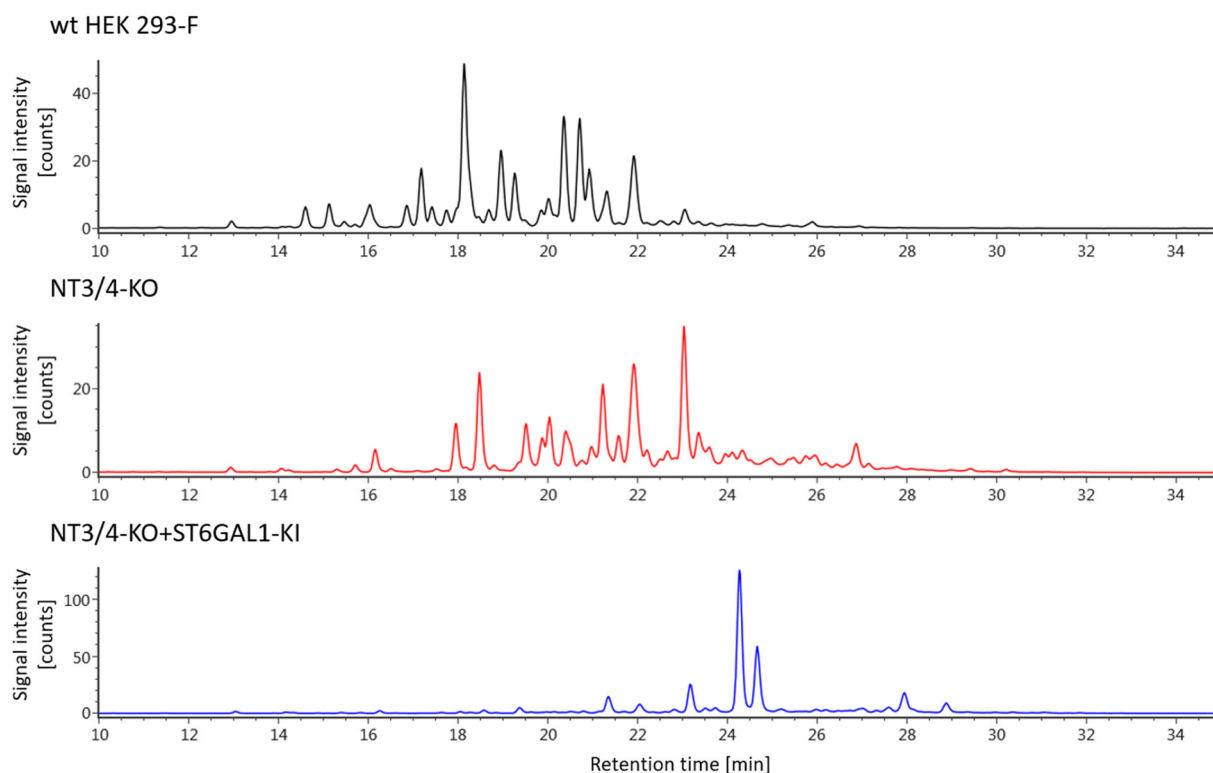


Figure 57: HILIC fluorescence chromatograms of enzymatically released and *RapiFluor*-MS labelled *N*-glycans of FVII-alb from the wt HEK 293-F, the NT3/4-KO-02 and the NT3/4-KO+ST6GAL1-KI cell lines.

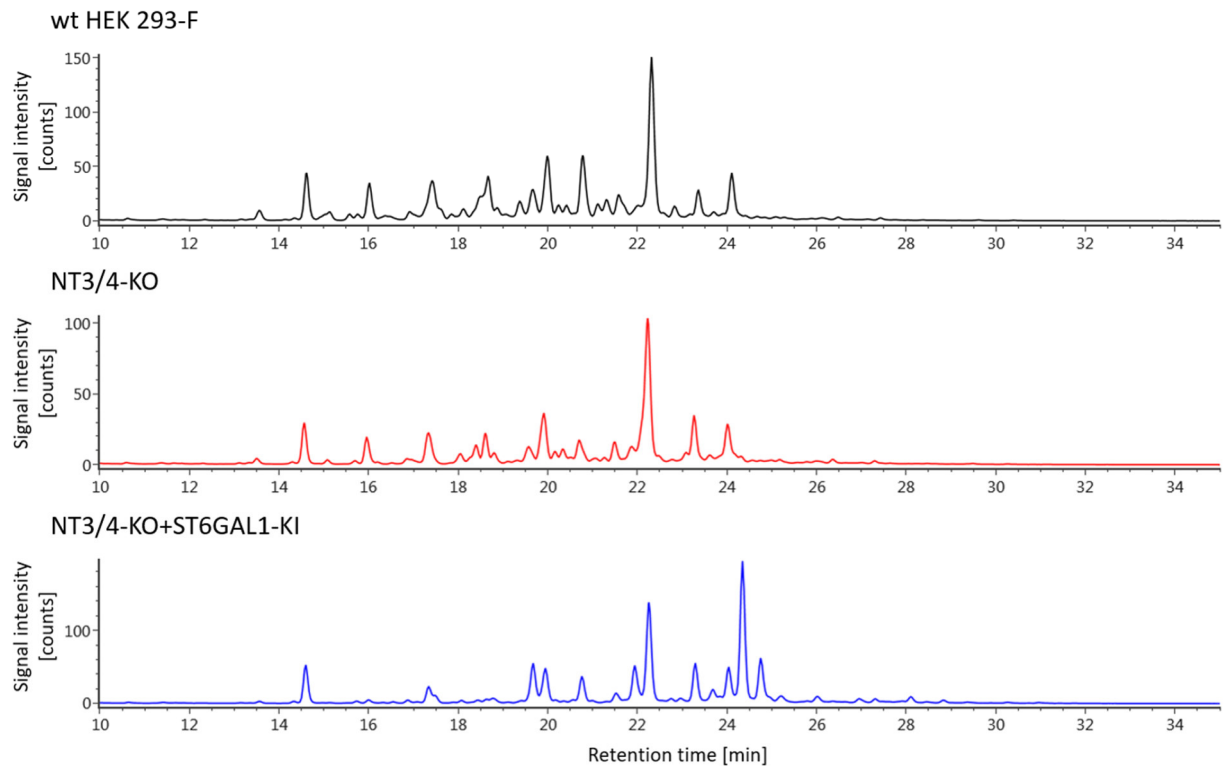


Figure 58: HILIC fluorescence chromatograms of enzymatically released and *RapiFluor*-MS labelled *N*-glycans of FVIII-BDD from the wt HEK 293-F, the NT3/4-KO-02 and the NT3/4-KO+ST6GAL1-KI cell lines.

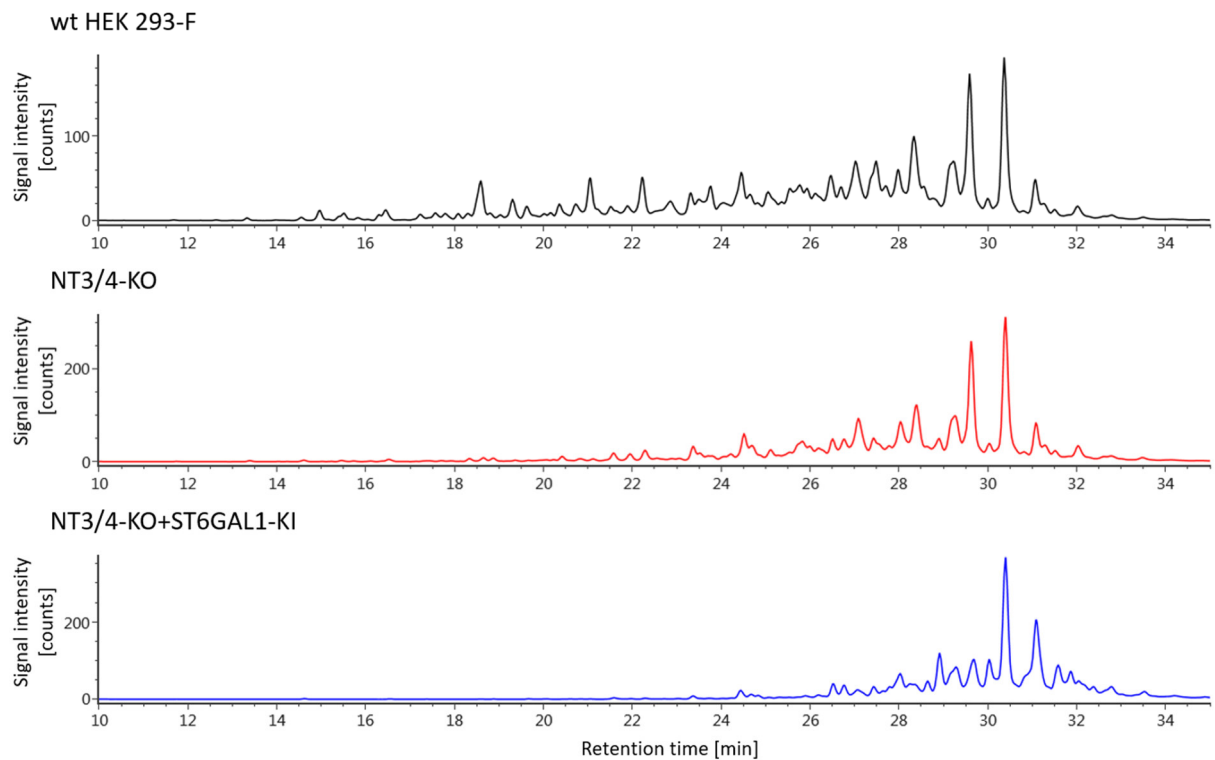


Figure 59: HILIC fluorescence chromatograms of enzymatically released and *RapiFluor*-MS labelled *N*-glycans of FIX from the wt HEK 293-F, the NT3/4-KO-02 and the NT3/4-KO+ST6GAL1-KI cell lines.

Since the three proteins carry different numbers of *N*-glycans (two on FVII-alb and FIX<sup>48,207</sup>, four on FVIII-BDD<sup>50,125,205,206</sup>), mean numbers of monosaccharides were calculated per *N*-glycan rather than per protein molecule.

The number of GalNAc units per *N*-glycan was approximately five times lower in FVIII-BDD and FIX compared to FVII-alb when produced in the wt HEK 293-F cell line (Figure 60A). After KO of *B4GALNT3* and *B4GALNT4*, GalNAc was completely replaced by galactose in all proteins (Figure 60B), which confirms the results for FVII-alb.

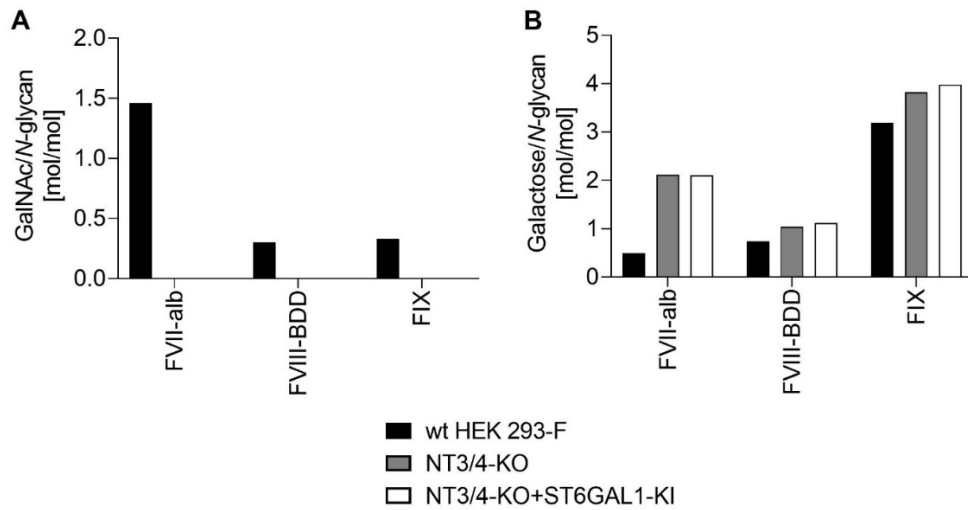


Figure 60: Evaluation of FVII-alb, FVIII-BDD and FIX *N*-glycosylation: GalNAc (A) and galactose (B) units per *N*-glycan (N=1).

The sum of GalNAc and galactose residues differs between the three proteins (FVII-alb: ~2; FVIII-BDD: ~1; FIX: ~4) because of the following differences in their *N*-glycan profiles. FVIII-BDD contained approximately 40% high-mannose and 15% hybrid *N*-glycans (Figure 61A), which resulted in ~50% fewer complex antennae (Figure 61B) and since only complex antennae carry GalNAc or galactose, this reduced the sum of GalNAc and galactose residues also by ~50%. FIX *N*-glycans on the other hand, carried on average 3.5 to 3.9 complex antennae per *N*-glycan (wt HEK 293-F and NT3/4-KO+ST6GAL1-KI, respectively), approximately twice as many as FVII-alb, resulting the double amount of GalNAc plus galactose residues.

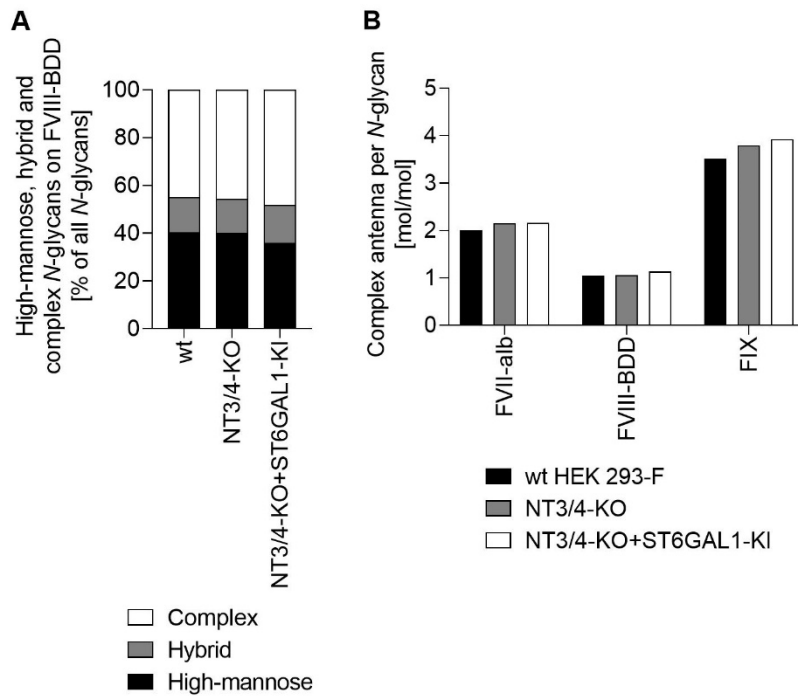


Figure 61: Evaluation of FVII-alb, FVIII-BDD and FIX *N*-glycosylation: High-mannose, hybrid and complex *N*-glycans on FVIII-BDD (A; FIX and FVII-alb carried no high-mannose or hybrid *N*-glycans above the quantification limit) and complex antennae per *N*-glycan of FVII-alb, FVIII-BDD and FIX (B) (N=1).

Only complex antennae carry galactose or GalNAc and only they can be sialylated. Therefore, the differences in the number of complex antennae on FVII-alb, FVIII-BDD and FIX also result in differences in the number of sialic acids (Figure 62A). As observed for FVII-alb, also FVIII-BDD and FIX produced in the NT3/4-KO and NT3/4-KO+ST6GAL1-KI cell lines carried more sialic acids than the proteins produced in the wt HEK 293-F cell line and the proportions of  $\alpha$ 2,3 and  $\alpha$ 2,6-linkage were similarly altered (Figure 62B).

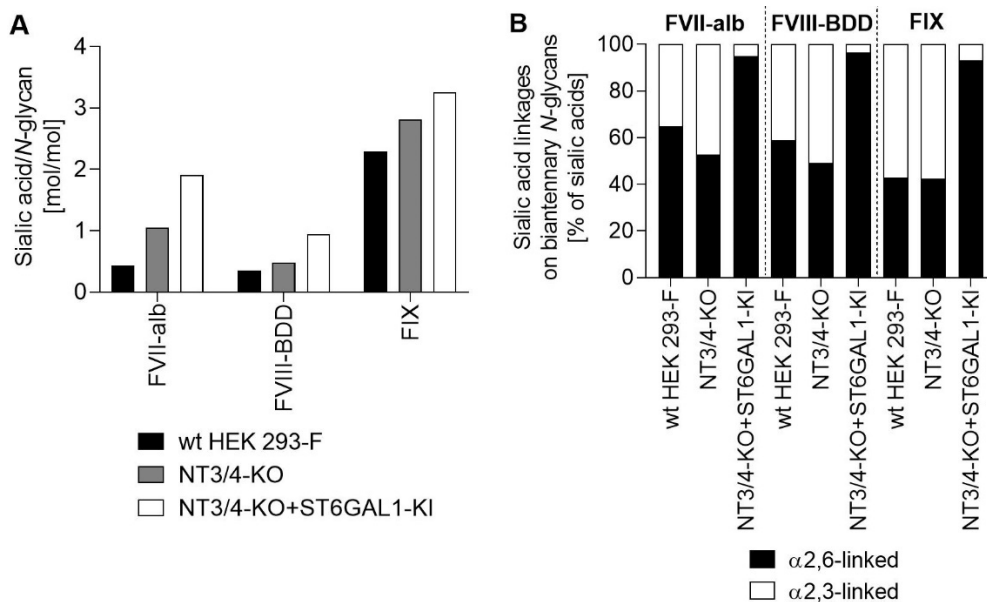


Figure 62: Evaluation of FVII-alb, FVIII-BDD and FIX *N*-glycosylation: Sialic acid units per *N*-glycan (A) and percentage of  $\alpha$ 2,3- and  $\alpha$ 2,6-linked sialic acids on biantennary *N*-glycans (B) (N=1).

Similar to FVII-alb *N*-glycans, all *N*-glycans on FIX were core-fucosylated (Figure 63A). Minimal antenna fucosylation was detected on FIX *N*-glycans when produced in the wt HEK 293-F cell line and it was almost absent after *B4GALNT3* and *B4GALNT4* double-KO, which precluded additional reduction by *ST6GAL1* KI. On FVIII-BDD, not all *N*-glycans were core-fucosylated and a clear differentiation between core and antennary fucoses was not possible. Fucosylation was not decreased by GalNAcT KO, but it was decreased after KI of *ST6GAL1*.

In contrast to FVII-alb, bis-GlcNAc did not increase on FVIII-BDD and FIX after GalNAcT KO (Figure 63B), potentially because there was little GalNAc on FVIII-BDD and FIX from the beginning. However, the reduction of bis-GlcNAc on both molecules was also observed after *ST6GAL1* KI.

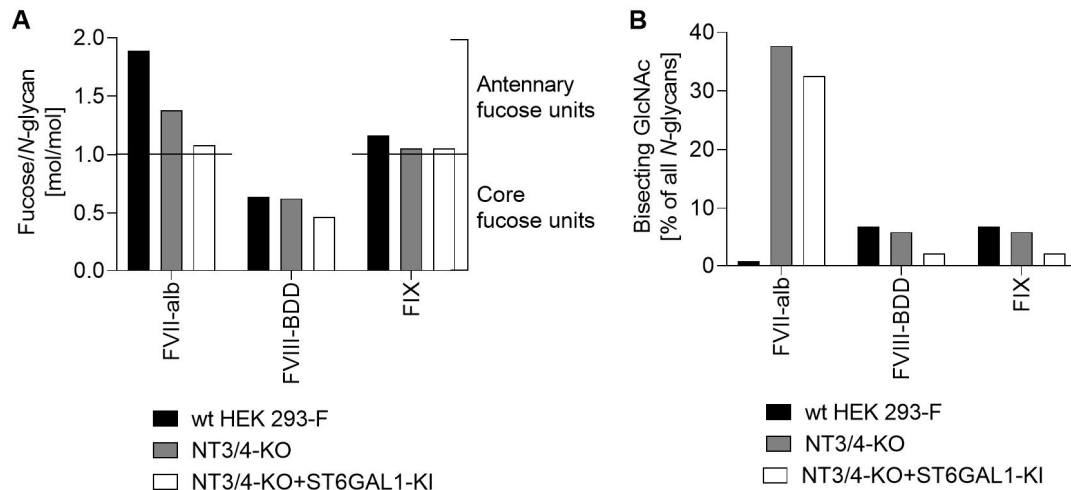


Figure 63: Evaluation of FVII-alb, FVIII-BDD and FIX *N*-glycosylation: Fucose units per *N*-glycan (A) and percentage of bis-GlcNAc-containing *N*-glycans (B) (N=1).

In summary, while the *N*-glycosylation of the three proteins produced in the wt HEK 293-F cell line differed markedly in some respects—specifically high GalNAc levels on FVII-alb, hybrid and high-mannose *N*-glycans on FVIII-BDD and high antennarity on FIX—the GalNAcT KOs and *ST6GAL1* KI affected FVII-alb, FVIII-BDD and FIX in a similar fashion. GalNAc was completely abolished and replaced by galactose, while total sialylation (particularly  $\alpha$ 2,6 sialylation) increased and antenna fucosylation decreased. This shows that the used glyco-engineering approach is also applicable to other proteins.

## 4.7 Analysis of ASGP-R and MR binding of glyco-engineered FVII-alb

With the glyco-engineering approach, the *N*-glycosylation of FVII-alb was modified such that reduced glycan-receptor-binding was anticipated. To confirm this hypothesis, binding of FVII-alb variants to the ASGP-R and the MR was analyzed by SPR.

### 4.7.1 Reproducibility of glycan-receptor-binding experiments

To determine the reproducibility of the glycan-receptor-binding experiments, triplicates of FVII-alb from wt HEK 293-F cells were produced, purified, and analyzed independently.

The standard deviation for the three replicates was fairly low with 3% and 9% for ASGP-R and MR binding, respectively (Figure 64), which confirmed the reproducibility of the methods.

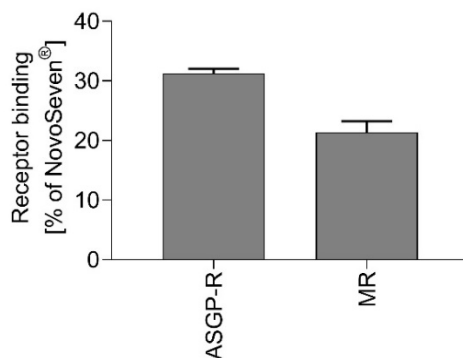


Figure 64: Binding of FVII-alb expressed in wt HEK 293-F cells to the ASGP-R and MR, relative to NovoSeven®. Mean and standard deviation of three biologic replicates is shown. From Uhler *et al.*<sup>224</sup>

#### 4.7.2 Evaluation of GalNAc-transferase knock-out

Binding to ASGP-R and MR were compared for FVII-alb from different GalNAcT KO clones.

The non-glycosylated human serum albumin (HSA) control did not bind either receptor. FVII from wt HEK 293-F cells bound stronger to both ASGP-R and MR compared to NovoSeven® (Figure 65), which was expected based on its *N*-glycosylation (4.5.1). Unexpectedly, the albumin fusion itself dramatically reduced FVII binding to both receptors, although *N*-glycosylation was not altered. KO of *B4GALNT3* further reduced binding to both receptors, while the combined KO of *B4GALNT3* and *B4GALNT4*—in line with the glycosylation data—had no additional effect.

Even though their *N*-glycosylation was comparable (Figure 39 to Figure 42), FVII-alb from the NT4-KO cell line bound stronger to ASGP-R and MR compared to FVII-alb from the wt HEK 293-F cell line (Figure 65). However, it must be noted that due to the unavailability of material in the later stages of the project, FVII-alb from the NT4-KO cell line was purified on the ÄKTA system, rebuffered into 25 mM NaAc, and subsequently rebuffered into water, while all other proteins for the binding experiments were purified on the Tecan system and directly rebuffered into water. To evaluate the potential influence on *N*-glycosylation and receptor binding, FVII-alb from wt HEK 293-F cells purified with the two purification protocols was compared to FVII-alb from NT4-KO cells. Independent of the purification protocol, FVII-alb from wt HEK 293-F and NT4-KO cells showed comparable *N*-glycosylation (Figure 66A). Furthermore, when purified with the ÄKTA protocol NT4-KO- and wt HEK 293-F cell-derived FVII-alb showed similar binding to ASGP-R and MR. However, when purified with the ÄKTA protocol, FVII-alb from wt HEK 293-F cells showed a stronger binding to ASGP-R and MR compared to when purified with the Tecan protocol (Figure 66B). In combination, these three observations indicate that if NT4-KO cell-derived FVII-alb had been purified with the Tecan protocol, it might have shown weaker receptor binding than it did when purified with the ÄKTA protocol. Since the purification setpoints (e.g. flow rates, wash and elution volume) were identical with respect to the scale of the purification system and since the used SPR method is susceptible to changes in buffer composition, the difference in ASGP-R and MR binding between FVII-alb from wt HEK 293-F (Tecan protocol) and NT4-KO cells (ÄKTA protocol) is more likely attributed to the minor changes in buffer composition that were caused by the additional rebuffering step in 25 mM NaAc. In any case, the KO of *B4GALNT4* did not have the desired effect on the *N*-glycosylation of FVII-alb (4.5.1) and no interpretations were made based on the NT4-KO receptor binding data.

Due to the encouraging binding data, an *in vivo* experiment was performed with a subset of those molecules to analyze the PK profile (see section 4.8).

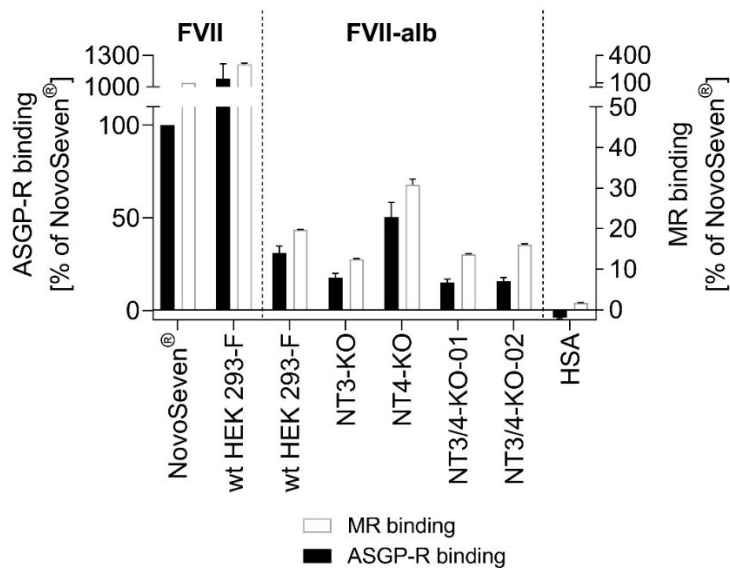


Figure 65: Evaluation of GalNAcT KO clones: Binding of FVII and FVII-alb to the ASGP-R (A) and MR (B) relative to NovoSeven® (determined by SPR). All groups N=3 technical replicates measured on three independent immobilizations. The non-glycosylated human serum albumin (HSA) negative control did not bind the receptor.

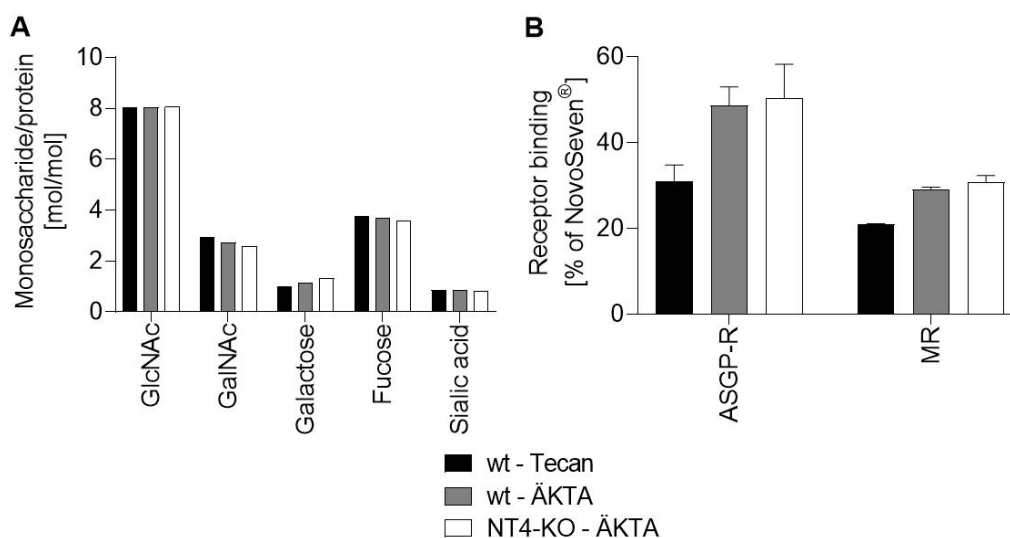


Figure 66: Comparison of N-glycan profiling results (A; N=1) and ASGP-R as well as MR binding (B; N=3 technical replicates) of FVII-alb from wt HEK 293-F cells purified on the Tecan and on the ÄKTA system and from NT4-KO purified on the ÄKTA system. Adapted from Uhler *et al.*<sup>224</sup>

### 4.7.3 Evaluation of sialyltransferase overexpression

Binding to ASGP-R and MR was compared for FVII-alb from different SiaT KI pools.

In the wt HEK 293-F background, only the *ST6GAL1* KI considerably improved sialylation (4.5.2) and consequently only the *ST6GAL1* KI reduced ASGP-R binding (Figure 67A). In the NT3/4-KO background, the *ST6GAL1\_sol* KI and *ST3GAL6\_sol* KI reduced ASGP-R binding, while the other two SiaTs abolished it.

MR binding was generally less affected by the SiaT KIs, but *ST6GAL1\_sol*, *ST3GAL6* and *ST6GAL1* KIs in the NT3/4-KO background all slightly reduced binding (Figure 67B).



In summary, both the albumin fusion and the glyco-engineering reduced ASGP-R and MR binding, which might improve PK properties of a therapeutic FVII-alb produced in a glyco-engineered cell line.

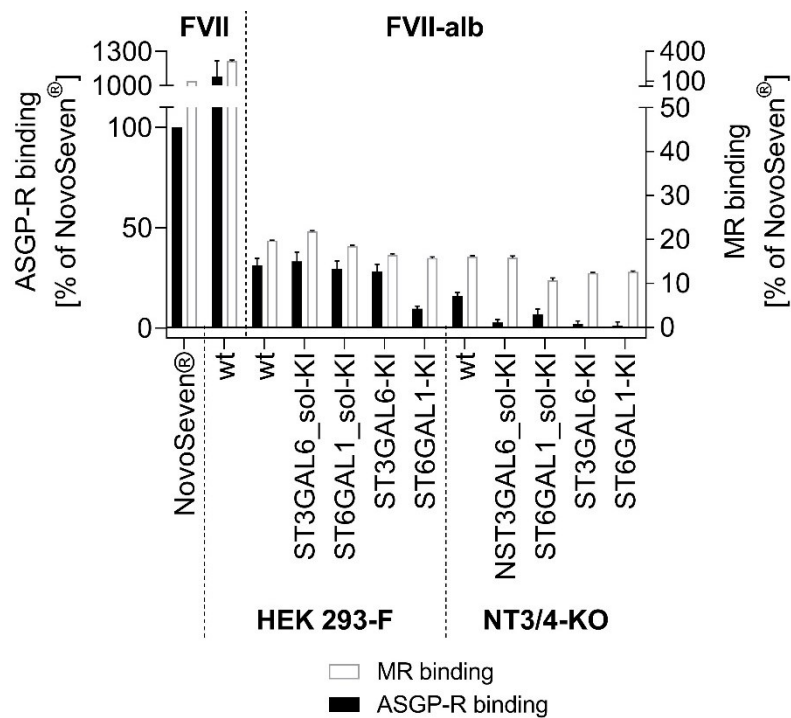


Figure 67: Evaluation of SiaT KI pools: Binding of FVII and FVII-alb to the ASGP-R (A) and MR (B) relative to NovoSeven® (determined by SPR). All groups N=3 technical replicates measured on three independent immobilizations.

#### 4.8 Evaluation of pharmacokinetic properties of glyco-engineered FVII-alb

In the PK rat experiment, NovoSeven®, FVIIa from wt HEK 293-F cells and FVIIa-alb from the NT3-KO, NT4-KO and NT3/4-KO cell lines were compared regarding the PK properties recovery, terminal half-life and AUC, in order to determine the *in vivo* effect of the glyco-engineering approach. From the FVIIa and FVIIa-alb concentration curves (Figure 68), the PK properties were calculated.

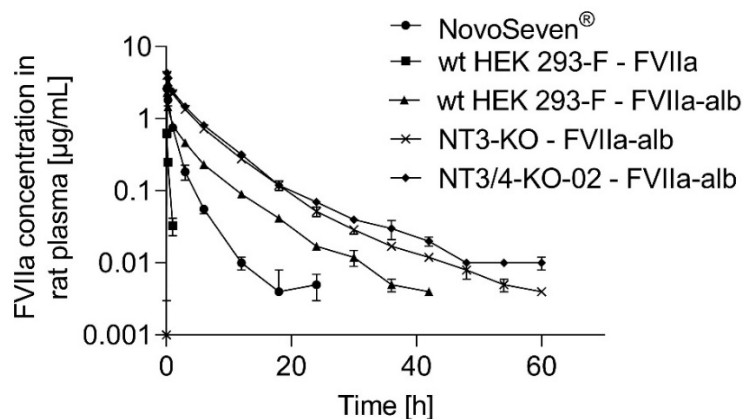


Figure 68: FVIIa/FVIIa-alb concentrations over time in rat plasma (four animals sampled per time point; logarithmic scale). For better comparability to NovoSeven® and FVIIa from wt HEK 293-F cells, only the pharmacologically active FVIIa fraction of FVIIa-alb samples was used for the concentration calculation. Only data points above the limit of quantification were plotted. From Uhler *et al.*<sup>224</sup>

### 4.8.1 Recovery

With only 10%, plasma recovery 5 min after injection was very poor for FVIIa from wt HEK 293-F cells, while 40% of NovoSeven®—with its higher sialic acid and lower GalNAc content—was recovered (Figure 69). Albumin fusion alone improved the recovery by 365% to 35%—a level comparable to NovoSeven®—while KO of *B4GALNT3* as well as the double-KO both further improved it to 61% and 66%, respectively. These results are consistent with the reduction in *in vitro* ASGP-R and MR binding (Figure 65).

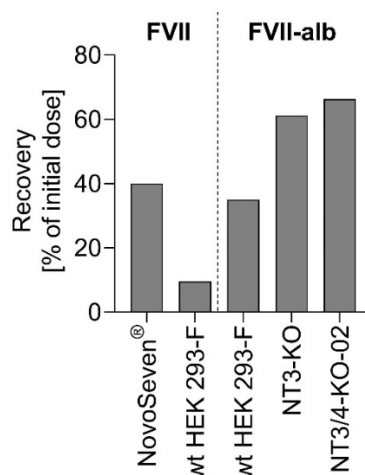


Figure 69: Recovery of FVIIa/FVIIa-alb variants. From Uhler *et al.*<sup>224</sup>

### 4.8.2 Half-life

The observed time interval and which datapoints are used for half-life calculation play a crucial role for the resulting half-life and comparing results between studies thus requires them to be comparable. In the present study, terminal half-life was calculated for the terminal points of the FVIIa and FVIIa-alb concentration curves (Table 21 column 2). In contrast, early datapoints were used for half-life calculation in comparable studies and the observed time intervals in those studies were shorter (Table 21 column 3).<sup>55,226–228</sup> To be able to compare the results between the studies, half-life was additionally calculated for those shorter intervals with earlier datapoints. Since the shorter intervals encompass the earliest points of the concentration curves, the calculated half-life will be referred to as early half-life.

Table 21: Half-life calculated for the terminal phase and for time intervals similar to other publications.<sup>55,226–228</sup> From Uhler *et al.*<sup>224</sup>

| Construct             | Terminal phase      |             | Time intervals similar to other publications |             | Literature values   |           |
|-----------------------|---------------------|-------------|----------------------------------------------|-------------|---------------------|-----------|
|                       | Time interval [min] | Data points | Time interval [min]                          | Data points | Time interval [min] | Reference |
| NovoSeven®            | 180-1,080           | 5           | 5-360                                        | 5           | 5-240               | [226]     |
|                       |                     |             |                                              |             | 5-300               | [227]     |
|                       |                     |             |                                              |             | 5-480               | [55]      |
|                       |                     |             |                                              |             | 5-240               | [228]     |
| FVII-alb wt HEK 293-F | 360-2,520           | 7           | 5-1,440                                      | 8           | 5-1,440             | [226]     |
| FVII-alb NT3-KO       | 2,160-3,600         | 5           | 5-1,440                                      | 8           | 5-1,440             | [228]     |
| FVII-alb NT3/4-KO     | 1,440-3,960         | 8           | 5-1,440                                      | 8           |                     |           |

While poor recovery of FVIIa from wt HEK 293-F cells precluded meaningful half-life analysis, NovoSeven® had early and terminal half-lives of 66 min and 167 min (Figure 70). The half-life of FVIIa-alb from the wt HEK 293-F cell line was triple and double that, respectively, again showing the benefit of albumin fusion. The KO of GalNacTs did not improve the early half-life of FVIIa-alb (NT3-KO: 238 min; NT3/4-KO-02: 242 min), while it strongly improved its terminal half-life (NT3-KO: 668 min; NT3/4-KO-02: 654 min).

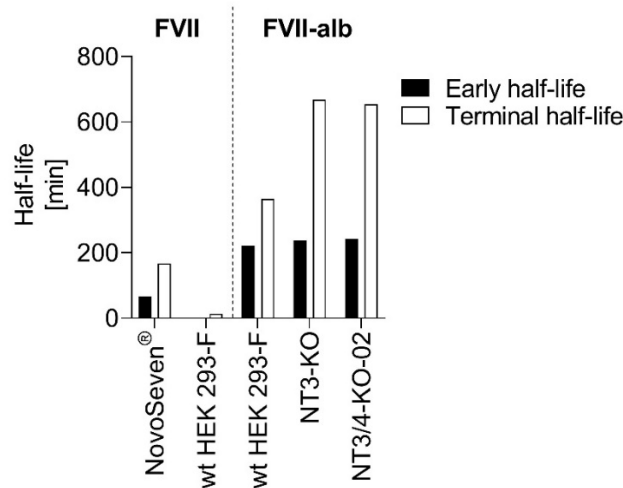


Figure 70: Initial and terminal half-life of FVIIa/FVIIa-alb variants. Adapted from Uhler *et al.*<sup>224</sup>

### 4.8.3 Area under the curve

Increasing the recovery and half-life of a drug leads to higher plasma levels over time and thereby improves the area under the curve (AUC; Figure 71). This was the case for FVIIa-alb from the wt HEK 293-F, the NT3-KO and the NT3/4-KO cell lines, demonstrating ~1.8-fold, ~4.9-fold and ~5.4-fold increased AUC compared to NovoSeven®.

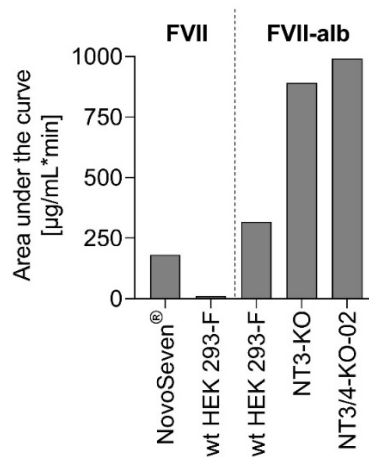


Figure 71: AUC of FVIIa/FVIIa-alb variants. From Uhler *et al.*<sup>224</sup>

Taken together, these data are in line with the *in vitro* binding results and show that albumin fusion and glyco-engineering improve the PK properties of FVII-alb.

## 5 DISCUSSION

### 5.1 Evidence for sulfated GalNAc on FVII-alb *N*-glycans

*N*-glycan profiling results for NovoSeven® were highly consistent with the results by Montacir *et al.* regarding the detected *N*-glycans and their proportion (Table 15).<sup>199</sup> Similarly, the antenna-fucosylated, high-GalNAc, biantennary *N*-glycans with little sialylation on FVII from the wt HEK 293-F cell line were in accordance with those reported by Böhm *et al.* (Table 16).<sup>49</sup> However, for some of the detected *N*-glycan signals, Böhm *et al.* assigned hybrid and high-mannose structures, since they interpreted a part of their mass as three hexoses (486.1584 Da), while the same *N*-glycan signals were interpreted to carry a sulfated GalNAc $\beta$ 4GlcNAc disaccharide with a close to identical mass (486.1155 Da) in this study (Table 12 columns 1 and 2). While experimental evidence for sulfated *N*-glycans was already presented in chapter 4.4.2.5, the following section will discuss two more arguments for the assignment of sulfated GalNAc over hybrid and high-mannose structures.

Hybrid and high-mannose *N*-glycans are a result of incomplete processing, which is usually caused by inaccessibility of those *N*-glycans to processing by mannosidases.<sup>36–38</sup> Since plasma-derived FVII and FVII produced in cell lines such as CHO or BHK only feature complex *N*-glycans,<sup>48</sup> it might be assumed that the *N*-glycans of FVII are accessible for processing and hence should be of the complex type in HEK 293-F cells as well. Furthermore, two structures proposed by Böhm *et al.*<sup>49</sup> (Table 12 lines 1 and 2) are inconsistent with the current understanding of the *N*-glycosylation pathway, which holds that mannosidase II must remove both the  $\alpha$ 1,3 and  $\alpha$ 1,6-linked mannose moieties from the  $\alpha$ 1,6-linked core mannose before any complex-type *N*-glycosylation can be initiated.<sup>34</sup> If true, one antenna cannot carry both a mannose and a Gal $\beta$ 4GlcNAc disaccharide.

Based on multiple pieces of evidence, the presence of sulfated GalNAc rather than hybrid and high-mannose *N*-glycans on FVII-alb seems likely. However, since choice of cell line and culture conditions affect *N*-glycosylation, it cannot be excluded that there is an actual difference to the results of Böhm *et al.*<sup>49</sup> (and not just a differing interpretation), which could originate from the suspension adaption or the serum-free culture of the HEK 293-F cell line compared to the serum-containing adherent culture of HEK 293 cells.<sup>51,229–235</sup>

### 5.2 The desired *N*-glycosylation of FVII-alb can be achieved by glyco-engineering

#### 5.2.1 Knock-out of *B4GALNT3* and *B4GALNT4* abolishes *N*-glycan GalNAc

*N*-glycan GalNAc itself is an efficient ligand for the ASGP-R,<sup>61,62</sup> and on top is an inferior substrate for sialylation compared to galactose,<sup>39,63</sup> which renders proteins carrying GalNAc prone to fast clearance from the bloodstream.<sup>30,63</sup> Therefore, the first aim of this study was to abolish GalNAc by KO of GalNAcTs.

B4GALNT3 and B4GALNT4 play a role in GalNAc transfer to FVII-alb, indicated by the need to knock-out both transferases in order to completely abolish GalNAc, which confirms previous reports by Gotoh *et al.* and Sato *et al.*<sup>236,237</sup> However, the fact that *B4GALNT4* KO does not considerably alter GalNAc levels shows that B4GALNT3 can replace B4GALNT4 activity completely and therefore is the predominant GalNAcT in HEK 293-F cells.

Diminishing GalNAcT activity increased galactose incorporation because GalNAcT KO increases the availability of substrate protein for GalTs. While it is known that a peptide recognition sequence motif on the protein is required for B4GALNT3 and B4GALNT4 to transfer GalNAc to *N*-glycans,<sup>40–42</sup> it is currently unknown how GalNAcTs preclude galactosylation on those proteins. Conceivably, in the presence of both GalTs and GalNAcTs, higher levels of ambient activity of the latter could cause

predominant GalNAc capping. And alternatively, sequential access to the target protein through differential localization in the secretory pathway might be responsible—or any combination of the two factors. In line with this notion, GalTs mostly reside in the *trans*-Golgi and *trans*-Golgi network and therefore generally have late access to the substrate *N*-glycan.<sup>238–241</sup> However, in one study, B4GALNT3 was detected in the *trans*-Golgi network as well and therefore both GalTs and GalNAcTs should have simultaneous access the substrate *N*-glycan.<sup>242</sup> In the absence of GalNAcTs, however, basically all antennae of FVII-alb, FVIII-BDD and FIX were galactosylated, so it can be ruled out that GalT activity itself limits galactosylation in HEK 293-F cells.

Sialylation increased with decreasing levels of GalNAc and increasing levels of galactose, most likely because  $\alpha$ 2,3-SiaTs like ST3GAL6 can sialylate galactose but not GalNAc.<sup>39,63</sup> In a similar fashion, the replacement of the exclusive ST6GAL1 substrate GalNAc with the ST6GAL1 and ST3GAL6 substrate galactose shifted the enzymatic flux towards more  $\alpha$ 2,3-linked sialic acids.

No bis-GlcNAc-containing or triantennary *N*-glycans were detected on FVII-alb from wt HEK 293-F cells. However, after KO of *B4GALNT3* or double-KO of *B4GALNT3* and *B4GALNT4*, levels of both *N*-glycan types increased substantially. Furthermore, on FVII-alb from the NT3-KO cell line—featuring GalNAc and bis-GlcNAc-containing as well as triantennary *N*-glycans—*N*-glycans that carried GalNAc never also carried bis-GlcNAc or a third antenna. In previous studies with proteins containing high levels of GalNAc, *N*-glycans were also predominantly biantennary and nonbisected.<sup>44,243–246</sup> These findings imply that GalNAc incorporation might impair the activity of enzymes responsible for bis-GlcNAc (MGAT3) and tri-/tetraantennarity (MGAT4/5) towards the *N*-glycan. However, for GalNAc to impact bisection and branching, it would require GalNAcTs to act on the *N*-glycan before the MGAT enzymes. This is contradicted by the findings that MGAT enzymes are mainly localized in the earlier Golgi compartments,<sup>247,248</sup> and GalNAcTs are localized in the *trans*-Golgi in HeLa cells<sup>242</sup>. However, the localization of glycosyltransferases is presumed to be cell type-specific,<sup>249</sup> and GalNAcTs might be localized in earlier Golgi compartments in HEK 293 cells. This might also explain why FVII-alb predominantly carries GalNAc in the presence of GalTs.

In contrast to plasma-derived FVII, *N*-glycans on FVII and FVII-alb produced in HEK 293-F cells were completely core-fucosylated and carried high levels of antennary fucoses.<sup>49</sup> However, antenna fucosylation decreased in the absence of B4GALNT3 and even more so in the absence of both GalNAcTs. The surge of bis-GlcNAc after KO of GalNAcTs might be partially responsible for this decrease, since it can impede the addition of successive monosaccharides.<sup>250–252</sup> Furthermore, the decrease in antenna fucosylation might be a result of the increased sialylation, since it was shown that the most abundant FucTs in HEK 293 cells (FUT4, FUT10, and FUT11)<sup>253</sup> all prefer nonsialylated over 2,3-sialylated antennae,<sup>254–257</sup> and that  $\alpha$ 2,6-sialylation and antenna fucosylation are mutually exclusive.<sup>258</sup>

## 5.2.2 Knock-in of sialyltransferases improves sialylation

Sialylation of *N*-glycans reduces ASGP-R mediated clearance and thereby improves PK properties of glycoproteins.<sup>30,63,64</sup> Therefore, high levels of sialic acids are desired on circulating therapeutic proteins. Since the KO of GalNAcTs did not result in complete sialylation of FVII-alb, additional overexpression of SiaTs was evaluated.

Sialylation was most improved by KI of *ST6GAL1* in both the wt and the NT3/4-KO background. The improvement in wt HEK 293 cells agrees with previous studies by Zhang *et al.* and Dekkers *et al.*<sup>151,154</sup> In the NT3/4-KO background, the KI of *ST6GAL1* resulted in almost full sialylation of FVII-alb, a level similar to plasma-derived FVII and beyond that of BHK, CHO or HEK cell-derived FVII.<sup>49</sup>

Additionally, in contrast to NovoSeven®, no nonhuman, potentially immunogenic Neu5Gc<sup>7,92,109</sup> was detected on HEK 293 cell-derived FVII or FVII-alb in this study.

ST3GAL6 overexpression did not improve sialylation of FVII-alb in the wt background, similar to the report for erythropoietin by Zhang *et al.*<sup>154</sup> However, the reasons seem to differ between the two studies. In the present study, ST3GAL6 did not improve sialylation due to the predominance of GalNAc on FVII-alb from the wt background and its inability to sialylate this substrate.<sup>39,63</sup> In the study by Zhang *et al.*, erythropoietin contained ample galactose for ST3GAL6 to sialylate and thus the reason why ST3GAL6 did not sialylate erythropoietin must be different.<sup>137</sup> After all, in the NT3/4-KO background, where GalNAc was completely replaced by galactose, *ST3GAL6* KI promoted sialylation.

The presence of bis-GlcNAc, which impairs  $\alpha$ 2,3- but not  $\alpha$ 2,6-sialylation,<sup>251,252</sup> might be the reason why ST6GAL1 was more efficient than ST3GAL6 in the NT3/4-KO background. Bisected *N*-glycans were two to three times less likely to be sialylated than the non-bisected counterparts. Furthermore, in the absence of differences in *ST6GAL1* and *ST3GAL6* mRNA abundance in the generated pools, the distinct phenotypes might be attributed to different specific activities of the two enzymes. Creating cell pools with an even higher *ST3GAL6* expression to make up for a potentially lower specific activity, might help understand the underlying mechanism.

In general, the soluble versions of ST6GAL1 and ST3GAL6 were outperformed by their respective membrane-bound counterparts, which contradicts the results by Sugimoto *et al.*<sup>150</sup> This discrepancy might result from the use of different cell lines and proteins since, judging from multiple previous studies,<sup>140,146,150–156</sup> both factors seem to impact the success of increasing sialylation via SiaT overexpression. Alternatively, a lower ambient activity of soluble SiaTs might explain this difference because, after all, soluble SiaTs are secreted and therefore do not accumulate in the Golgi like membrane-bound SiaTs do.

Overexpression of ST3GAL6 and ST6Gal1 promoted  $\alpha$ 2,3- and  $\alpha$ 2,6-sialylation, respectively, as expected. However, ST6GAL1 more efficiently promoted  $\alpha$ 2,6-sialylation than ST3GAL6 promoted  $\alpha$ 2,3-sialylation. The inability of ST3GAL6 to sialylate GalNAc and the resulting lack of a sialyltransferase competing with ST6GAL1, was most likely responsible for the residual  $\alpha$ 2,6-linked sialic acids after *ST3GAL6* KI in the wt background. In the NT3/4-KO background, the KI of *ST3GAL6* did not result in full sialylation and there was substrate left for ST6GAL1 to sialylate.

KI of *ST6GAL1* most likely reduced GalNAc sulfation and antenna fucosylation due to the mutual exclusivity of sialylation and these structures.<sup>44,59,258</sup> And as discussed for the NT3/4-KO cell line in the last passage of 5.2.1, the low availability of FucTs that act on  $\alpha$ 2,3-sialylated *N*-glycans in HEK 293 cells might be responsible for the reduction of antenna fucosylation in the NT3/4-KO+ST3GAL6-KI cell line.<sup>254–257</sup> Mechanistically, this may result from elevated SiaT levels that outcompete FucTs and sulfotransferases at a shared physical location in the secretory pathway, or from a spill of the SiaTs to earlier secretory pathway compartments<sup>259</sup> where they can sialylate nascent *N*-glycans before FucTs or sulfotransferases can access them. That overexpressed SiaTs are located throughout the Golgi—instead of only in the *trans*-Golgi<sup>240</sup>—was indeed confirmed by Lucocq *et al.*<sup>259</sup>

### 5.2.3 The choice of clone can impact the *N*-glycosylation of the therapeutic protein

ST6GAL1 overexpressing clones were generated to assess whether the level of sialylation on FVII-alb depends on the *ST6GAL1* mRNA level and whether individual clones differ from the respective pool in other *N*-glycosylation features.

For the ST6GAL1 overexpressing clones derived from the wt HEK 293-F cell line, the changes in *N*-glycosylation were consistent with the detected *ST6GAL1* mRNA levels—e.g. high *ST6GAL1* mRNA levels resulted in a high sialylation. However, for the clones derived from the NT3/4-KO cell line, sialylation was the least affected in the one with the highest mRNA levels. A potential explanation is that the mRNA levels do not necessarily correlate with protein levels of the encoded transferase (reviewed in reference<sup>260</sup>). Especially in the clone with 20 to 30 copies of *ST6GAL1*, genomic rearrangements that lead to detectable mRNA molecules but not to functional protein are possible. Also, the genotype and phenotype of clones from a heterogeneous cell pool can vary markedly,<sup>162,164–166</sup> which may affect its ability to sialylate proteins in various ways including through availability of the ST6GAL1 substrate CMP-sialic acid, through mRNA and protein turnover rates, or through translation efficiency. Furthermore, the capability for post-translational modifications can differ between clones and this can impact protein stability, expression or specific activity.<sup>20–24,120</sup> The latter was shown for ST6GAL1 without core fucosylation.<sup>261</sup> An example for such a difference in post-translational modification capability of different clones might be observable in clone NT3/4-KO+ST6GAL1-KI-160, which produced only few triantennary *N*-glycans, possibly as a result of low MGAT4 and MGAT5 expression.

In summary, *ST6GAL1* mRNA levels correlated with the changes in *N*-glycosylation in a subset of clones. Furthermore, different clones of a pool can differ in the expression of other *N*-glycosylation pathway enzymes and these differences might influence *N*-glycosylation independent of the performed glyco-engineering. While the small number of analyzed clones does not allow for a detailed analysis of the clonal variation in the respective pools, differential *N*-glycosylation of FVII-alb produced by the clones was observed nonetheless. This shows that the choice of host cell line clone can be important for the glycosylation-dependent properties of a therapeutic protein product.

### 5.2.4 Sialic acid metabolism precursor supplementation does not improve sialylation

As an alternative to the overexpression of SiaTs to increase sialylation, FVII-alb was produced in cells cultured in medium supplemented with ManNAc and cytidine. However, supplementation with ManNAc and cytidine did not improve sialylation of FVII-alb. It might be that ManNAc and cytidine did not enter the cells in sufficient amounts to improve sialylation due to the lack of a specific uptake mechanism.<sup>263,264</sup> The used concentrations were in the ranges of those described in previous reports<sup>167,169,262</sup>—where an increase in intracellular CMP-sialic acid<sup>167,169,262</sup> and protein sialylation was reported<sup>167,169</sup>—but they were not determined experimentally. In a follow-up experiment, different ManNAc and cytidine concentrations could be tested to determine the optimal concentration. Furthermore, strategies to improve the cellular uptake of ManNAc—for example peracetylation<sup>262</sup>—could be evaluated. However, since ST6GAL1 overexpression in the NT3/4-KO background resulted in a close to full sialylation, it seems more likely that CMP-sialic acid is not limiting for sialylation in HEK 293-F cells—at least not at the low expression levels of highly complex coagulation factors like FVII-alb—and therefore supplementation did not improve it.

As previously shown for other cell systems, the growth of HEK 293-F cells was reduced by medium supplementation with ManNAc and cytidine.<sup>169,262,265</sup> This results from the high concentrations of ManNAc and cytidine required due to the lack of a specific uptake mechanism.<sup>263,264</sup>

### 5.3 The used glyco-engineering approach is applicable to other proteins

To check whether the glyco-engineering approach is applicable to other proteins, model proteins FVIII-BDD and FIX were produced in the wt HEK 293-F, the NT3/4-KO and the NT3/4-KO+ST6GAL1-KI cell lines and analyzed by *N*-glycan profiling.

The *N*-glycosylation of FVIII-BDD from wt HEK 293-F cells was consistent with that reported by Kannicht *et al.* and Canis *et al.*, carrying approximately 40% high-mannose, 15% hybrid and 45% complex, almost exclusively biantennary *N*-glycans.<sup>50,125</sup> Furthermore, around 35% and 60% of the complex antennae were sialylated and fucosylated, respectively.<sup>50,125</sup> *N*-glycosylation data of FIX produced in HEK 293 cells is not available to date. However, the detected tri- and tetraantennary *N*-glycans with little fucosylation are consistent with those on plasma- and CHO-cell derived FIX.<sup>48,208</sup> In addition, the approximately two sialic acid residues per *N*-glycan—compared to around three and four for CHO cell- and plasma-derived FIX<sup>48,208</sup>—are in accordance with the generally lower sialylation of HEK 293 cell-derived proteins.

As expected from the literature, the *N*-glycosylation of FVII-alb, FVIII-BDD and FIX was distinctly different,<sup>48–50,125,208</sup> even when expressed in the same cell lines under comparable cultivation conditions, showcasing the protein-specificity of *N*-glycosylation. Nonetheless, the glyco-engineering affected the three proteins in a similar fashion. GalNAc was completely replaced by galactose upon GalNAcT KOs. Sialylation was increased by GalNAcT KOs and *ST6GAL1* KI and shifted to more  $\alpha$ 2,6-linked sialic acids after *ST6GAL1* KI. And if assuming a close to complete core fucosylation of the complex *N*-glycans of FVIII-BDD from HEK cells, which was reported by Kannicht *et al.* and Canis *et al.*,<sup>50,125</sup> antenna fucosylation was basically absent on FVIII-BDD and on FIX from the NT3/4-KO+ST6GAL1-KI cell line.

Therefore, the glyco-engineering seems to be applicable to different proteins and the new cell lines might therefore be suitable expression systems for the production of therapeutic proteins with improved PK properties and fully human PTMs.

### 5.4 Sialyltransferase activity is the limiting factor for sialylation in HEK 293 cells

Previous attempts to improve the sialylation of proteins expressed in various mammalian cell lines revealed that in most cases either SiaT activity or CMP-sialic acid availability was limiting. In these studies, the former was solved by overexpression of sialyltransferases and the latter by either overexpression of proteins involved in sialic acid metabolism and transport or by medium supplementation with sialic acid metabolism precursors.<sup>140,146,150–156</sup> In the other cases, the sialylation could not be improved and the cause for the incomplete sialylation remained unclear.<sup>150,151,154,168</sup> Considering all these studies, it seems to depend on the cell line, the protein itself and the expression level of the protein whether SiaT overexpression or elevation of CMP-sialic acid levels improve sialylation.

In two studies with HEK 293-F cells expressing an IgG and erythropoietin, sialylation was increased by overexpression of SiaTs.<sup>151,154</sup> However, in both studies, sialylation was not complete and therefore there might have been other limiting factors. Furthermore, no data are available regarding the impact of modulated CMP-sialic acid levels in HEK 293 cells. Therefore, the question remains what limits sialylation in HEK 293 cells.

Due to the increase in sialylation after GalNAcT KO, GalNAc certainly is one factor. But, even in the absence of GalNAc, supplementation of the culture medium with ManNAc and cytidine did not alter the sialylation of FVII-alb from various host cell lines, indicating that CMP-sialic acid was not limiting.



On the other hand, overexpression of ST6GAL1 and ST3GAL6 improved sialylation of FVII-alb, showing that SiaT activity was indeed limiting. When expressed in the NT3/4-KO+ST6GAL1-KI cell line, 90% and 84% of the complex antennae of FVII-alb and FVIII-BDD were sialylated, respectively and these values are comparable to those of plasma-derived versions of the proteins.<sup>48-50</sup> On FIX, 83% of the antennae were sialylated, which is lower than the approximately 95% for plasma-derived FIX but still higher than the approximately 70% on CHO cell-derived FIX.<sup>48,208</sup> Therefore, the sialic acid transfer rate seems to be the limiting factor for sialylation in HEK 293-F cells, at least in the absence of high GalNAc levels and for comparatively low expressed proteins such as highly complex coagulation factors.

## 5.5 Glyco-engineering can reduce *N*-glycan heterogeneity

Glyco-engineering reduced the complexity of the detected *N*-glycan patterns by abolishing GalNAc and by reducing antenna fucosylation as well as  $\alpha$ 2,3-sialylation. Thereby, the heterogeneity of *N*-glycans for all studied proteins—FVII-alb, FVIII-BDD and FIX—was reduced. Heterogeneity of therapeutic proteins is considered a risk for patients by regulatory authorities like the U.S. Food and Drug Administration, since different variants of the protein can have different biologic properties and consequentially negatively impact safety and efficacy.<sup>51,52</sup> To ensure comparable properties throughout the lifecycle of a product, authorities require thorough characterization of therapeutic proteins.<sup>52,266</sup> Thus, ensuring a low heterogeneity already in the development of the therapeutic protein, can positively impact patient safety, product efficacy and alleviate characterization efforts. Reducing *N*-glycan heterogeneity therefore is an additional benefit of the glyco-engineered cell lines, especially of the NT3/4-KO+ST6GAL1-KI cell line.

## 5.6 Glyco-engineered FVII-albumin binds less to ASGP-R and MR

The glyco-engineered FVII-alb variants bound weaker to ASGP-R and MR. This was in agreement with the detected changes in *N*-glycosylation and with previous reports. GalNAc sialylation and replacement with galactose or sialylated galactose reduced ASGP-R binding,<sup>30,61,63</sup> and lower levels of sulfated GalNAc or antennae fucose diminished MR binding.<sup>66-71,267</sup> Merely the decreased ASGP-R binding of FVII-alb from the NT3/4-KO+ST3GAL6<sub>sol</sub>-KI and the decreased MR binding of FVII-alb from the NT3/4-KO+ST6GAL1-KI cell lines cannot be explained by their *N*-glycosylation.

Of note, multiple examples show that the level of sialylation was not the sole determinant of ASGP-R binding. First, despite its slightly higher degree of sialylation, ASGP-R binding of FVII-alb from the wt+ST6GAL1-KI cell line was stronger than that of FVII-alb from the NT3/4-KO+ST3GAL6-KI cell line. This might be attributed to (i) the residual ASGP-R binding of sialylated GalNAc,<sup>268,269</sup> (ii) the higher affinity of non-sialylated GalNAc compared to galactose,<sup>62</sup> or (iii) of  $\alpha$ 2,6- compared to  $\alpha$ 2,3-linked sialic acids<sup>269</sup> towards the ASGP-R. Second, while fully sialylated FVII-alb from the NT3/4-KO+ST6GAL1-KI cell line, as expected, did not bind to the ASGP-R, NT3/4-KO+ST3GAL6-KI-derived FVII-alb did not require full sialylation to lose ASGP-R binding completely. Apart from the level of sialylation, the main difference between the two molecules was the type of sialic acid linkage—NT3/4-KO+ST3GAL6-KI: 60%  $\alpha$ 2,3-linked; NT3/4-KO+ST6GAL1-KI: 95%  $\alpha$ 2,6-linked—possibly indicating that the  $\alpha$ 2,3-linked sialic acids indeed bind less efficiently to the ASGP-R. After all, multiple studies showed that proteins carrying  $\alpha$ 2,6-linked sialic acids were cleared faster *in vivo* than proteins carrying  $\alpha$ 2,3-linked sialic acids,<sup>57,270-273</sup> albeit one study showed the opposite.<sup>156</sup> However, the fact that both FVII-alb variants do not bind the ASGP-R might also imply that even incomplete sialylation of FVII-alb is sufficient to abrogate ASGP-R binding. This might be facilitated by the strong reduction of ASGP-R binding caused by albumin fusion itself and could mean

that, beyond a specific level, increasing sialylation or altering the sialic acid linkage type does not impact ASGP-R binding further.

## **5.7 Glyco-engineered FVII-alb variants have improved pharmacokinetic properties**

Glycan receptors are widely conserved across mammalian species, particularly the MR and the ASGR1 subunit of the ASGP-R.<sup>274-276</sup> Human and rat MR and ASGR1 share 94% and 92% sequence similarity (determined with BLOSUM75) and the orthologs share similar ligand specificities.<sup>277,278</sup> Therefore, mammals are generally considered suitable models to study glycan-receptor-mediated clearance,<sup>279</sup> and the ASGP-R and MR binding study results—using recombinant human receptors—can be compared with those of the PK experiment in rats.

CHO cell-derived FVII and FVII-alb carry no GalNAc and more sialic acids in comparison to FVII and FVII-alb from wt HEK 293-F cells and BHK cell-derived FVII also carries more sialic acids in comparison to FVII from wt HEK 293-F cells.<sup>49</sup> Accordingly, the recoveries 5 min after intravenous injection were lower for the HEK than for the CHO or BHK cell-derived proteins.<sup>226,228</sup> However, as *N*-glycosylation of FVII-alb from NT3 and NT3/4-KO cells was similar to that from CHO cells their recoveries were comparable.<sup>49,226,228</sup>

Terminal half-life of glyco-engineered FVII-alb variants from NT3-KO and NT3/4-KO cells was nearly 2-fold longer compared to FVII-alb from wt HEK 293-F cells, which is in accordance with the altered *N*-glycosylation. Proteins with heterogeneous glycosylation are typically cleared from circulation in a biphasic manner, with a fraction of molecules cleared after minutes and another cleared over longer intervals. This reflects the presence of high and low-affinity ligands for clearance receptors among glycan structures.<sup>58,63,280</sup> FVII also follows this biphasic model<sup>55</sup> and thus the half-life calculated using the initial points of the FVIIa concentration curve—where high- and low-affinity ligands are present—is shorter than half-life calculated using later timepoints where only low-affinity ligands remain. Therefore, a comparison to literature studies, all of which use shorter intervals and earlier time points, was not possible. Hence, early half-life was additionally calculated with similar intervals compared to those studies (Table 21) and was found to be consistent.<sup>55,226-228</sup>

Due to the improved recovery and half-life, the AUC of FVII-alb from the NT3/4-KO cell line was 5.5-fold higher than that of NovoSeven®. Since FVII-alb from the NT3/4-KO+ST6GAL1-KI and NT3/4-KO+ST3GAL6-KI cell lines did not bind the ASGP-R and MR *in vitro*, these molecules might display even better PK properties. To address this hypothesis, a follow-up PK study with FVII-alb from these cell lines might provide additional data on the impact of  $\alpha$ 2,3- and  $\alpha$ 2,6-linked sialic acids on PK properties.

## **5.8 Fused albumin improves pharmacokinetic properties by reducing receptor binding**

Previous studies already showed that albumin fusion improves the half-life of therapeutic proteins and this was confirmed by the *in vivo* data.<sup>187,188</sup>

However, the strong decrease in ASGP-R and MR binding after albumin fusion observed *in vitro* was not described before. This decrease in receptor binding cannot be explained by changes in *N*-glycosylation since albumin is not glycosylated,<sup>200</sup> and accordingly did not contribute to the *N*-glycosylation of FVII-alb. It is more likely that steric hindrance accounts for this reduced binding. Due to its bulkiness, albumin can negatively impact the biologic activity of its fusion partners by blocking the active domain.<sup>187</sup> While this was not reported for FVII,<sup>226</sup> albumin might instead impede

the interaction between the receptors and FVII-alb *N*-glycans. In fact, both the ASGP-R and MR were shown to have the highest affinities towards oligosaccharides with more than two interaction partners.<sup>61,281–284</sup> However, FVII and FVII-alb mainly carry biantennary *N*-glycans and this means that the number of interaction partners on the *N*-glycan are limited to two (For example, an *N*-glycan with two terminal GalNAc residues carries two interaction partners for the ASGP-R, while a *N*-glycan with one terminal GalNAc and one terminal sialic acid only carries one interaction partner). Therefore, for efficient binding to ASGP-R or MR—needing three or more interaction partners—simultaneous access to both *N*-glycans might be necessary and this might be hindered by albumin fusion. In the PK rat experiment, this reduced binding is likely to be the reason for the improved recovery, since even those FVII-alb molecules with *N*-glycans with high affinity towards ASGP-R and MR are cleared at a slower rate compared to FVII without albumin fusion. A similar increase in recovery was also found by Weimer *et al.* and Zollner *et al.*,<sup>226,228</sup> but due to missing *N*-glycosylation data, the role of albumin remained unknown. Therefore, this here is the first study explaining this additional benefit of albumin fusion for the PK properties of FVII-alb.

## 5.9 Conclusion

The utility of the HEK 293-F expression system for therapeutic proteins was improved by glyco-engineering; specifically, by GalNAcT KO and SiaT KI. This virtually eliminated GalNAc incorporation on FVII-alb, FVIII-BDD, and FIX *N*-glycans and increased sialylation to levels comparable to the plasma-derived proteins. FVII-alb binding to clearance receptors decreased as a result, which in turn improved PK properties *in vivo*. Therapeutic proteins produced in the newly generated host cell lines combine the favorable PK properties of highly sialylated proteins with the benefits of fully human PTMs.

## 6 SUMMARY

Using human cell lines for the production of therapeutic proteins can be beneficial due to their ability to generate fully human post-translational modifications. HEK 293 cells are an efficient expression system with a record of approved therapeutic protein products. However, the presence of *N*-acetylgalactosamine, the low sialylation on *N*-glycans of recombinant HEK 293 cell-derived glycoproteins and the resulting efficient clearance via glycan receptors in patients—namely the asialoglycoprotein receptor and the mannose receptor—currently limits its use in therapeutic protein production.

To be able to produce recombinant proteins without *N*-acetylgalactosamine on their *N*-glycans, HEK 293-F clones featuring a functional KO of both the *B4GALNT3* and *B4GALNT4* genes were generated. Subsequently, to increase the sialylation, sialyltransferases *ST6GAL1* and *ST3GAL6* were overexpressed by gene knock-in. The model protein factor VII-albumin was expressed in these new host cell lines to evaluate the phenotypic changes induced by the described glyco-engineering. Furthermore, medium supplementation with *N*-acetylmannosamine and cytidine was tested to improve sialylation.

HEK 293-F cells with *B4GALNT3* and *B4GALNT4* knock-out produced factor VII-albumin devoid of *N*-acetylgalactosamine and sulfated *N*-acetylgalactosamine, with reduced antenna fucosylation and increased antennarity, bisecting *N*-acetylglucosamine as well as sialylation. Overexpression of *ST6GAL1* or *ST3GAL6* further increased sialylation and reduced antenna fucosylation, while sialylation was not affected by medium supplementation of sialic acid metabolism precursors *N*-acetylmannosamine and cytidine. Factor VII-albumin produced in the double *N*-acetylgalactosamine transferase knock-out cell line with simultaneous *ST6GAL1* knock-in showed a level of sialylation similar to that of plasma-derived factor VII and higher than that of factor VII from CHO or BHK cells. As a result, asialoglycoprotein and mannose receptor binding of glyco-engineered factor VII-albumin variants was abolished *in vitro* and pharmacokinetic properties were improved *in vivo*.

To determine whether the detected changes in *N*-glycosylation were specific for factor VII-albumin or whether the results are applicable to other proteins, B domain-deleted factor VIII and factor IX were expressed in the wild-type HEK 293-F cell line, the double *N*-acetylgalactosamine transferase knock-out clone and the double *N*-acetylgalactosamine transferase knock-out clone with *ST6GAL1* knock-in. Despite considerable differences in the *N*-glycosylation profiles of the three proteins, the effects of the applied glyco-engineering were largely comparable.

Thus, these new glyco-engineered cell lines are suitable for the expression of fully human therapeutic proteins with favorable *N*-glycosylation and improved pharmacokinetic properties.

## 7 ZUSAMMENFASSUNG

Für die Produktion von therapeutischen Proteinen mit humanen posttranslationalen Modifikationen stellen humane Zelllinien ein vorteilhaftes System dar. HEK 293-F Zellen sind ein effizientes Expressionssystem, das schon von regulatorischen Behörden zur Produktion von therapeutischen Proteinen zugelassen wurde. Allerdings sind *N*-Glykane von Proteinen, die in HEK 293 Zellen produziert werden, besetzt mit *N*-Acetylgalactosamin und tragen wenige Sialinsäuren, was in Patienten zum schnellen Abbau der Proteine durch Glykanrezeptoren wie dem Asialoglykoproteinrezeptor oder dem Mannose Rezeptor führt. Dadurch ist die Produktion von therapeutischen Proteinen in HEK 293 Zellen auf solche beschränkt, die diese Glykanstrukturen nicht tragen.

Um Proteine ohne *N*-Acetylgalactosamin produzieren zu können, wurden HEK 293-F Zellen, in denen die Enzyme B4GALNT3 und B4GALNT4 genetisch deaktiviert wurden, hergestellt. Um die Sialylierung zu erhöhen, wurden anschließend die Sialyltransferasen ST6GAL1 und ST3GAL6 durch eine Geninsertion überexprimiert. In den entstandenen Zelllinien wurde das Modellprotein Faktor VII-Albumin exprimiert und es wurden die phänotypischen Veränderungen analysiert, welche durch die angewandte Glyko-Optimierung induziert wurden.

HEK 293-F Zellen ohne funktionelles B4GALNT3 und B4GALNT4 stellten Faktor VII-Albumin ohne *N*-Acetylgalactosamin und sulfatiertem *N*-Acetylgalactosamin, mit reduzierter Antennenfukosylierung und mit erhöhter Antennarität, bisecting *N*-Acetylglukosamin und Sialylierung her. Die Überexpression von *ST6GAL1* oder *ST3GAL6* führte zu einer weiteren Erhöhung der Sialylierung und Reduzierung der Antennenfukosylierung. Dagegen hatte die Zugabe von *N*-Acetylmannosamin und Cytidin, Vorläufer des Sialinsäuremetabolismus, zum Kulturmedium keinen Effekt auf die Sialylierung. Faktor VII-Albumin, das in der Zelllinie ohne B4GALNT3- und B4GALNT4-Aktivität aber mit *ST6GAL1*-Überexpression hergestellt wurde, zeigte eine ähnlich hohe Sialylierung wie Faktor VII aus humanem Plasma und eine höhere als FVII aus CHO oder BHK Zellen. Glyko-optimierte Faktor VII-Albumin-Varianten zeigten eine reduzierte Bindung an den Asialoglykoproteinrezeptor und den Mannose Rezeptor *in vitro* und verbesserte pharmakokinetische Eigenschaften *in vivo*.

Um festzustellen ob die detektierten Änderungen der *N*-Glykosylierung spezifisch für Faktor VII-Albumin sind, oder ob die Ergebnisse auch auf andere Protein übertragbar sind, wurde ein Faktor VIII Molekül ohne B-Domäne und ein Faktor IX Molekül in Wildtyp HEK 293-F Zellen hergestellt, sowie in HEK 293-F Zellen ohne funktionelles B4GALNT3 und B4GALNT4 und in HEK 293-F Zellen ohne funktionelles B4GALNT3 und B4GALNT4 aber mit überexprimiertem *ST6GAL1*. Obwohl sich die *N*-Glykosylierung der drei Proteine grundlegend unterscheidet, waren die Veränderungen durch die angewendete Glyko-Optimierung in allen drei vergleichbar.

Die neuen, glyko-optimierten Zelllinien sind daher für die Herstellung von vollständig humanen Proteinen mit vorteilhafter *N*-Glykosylierung und verbesserten pharmakokinetischen Eigenschaften geeignet.

## 8 REFERENCES

1. Walsh G: Biopharmaceutical benchmarks 2014. *Nat Biotechnol* 32(10): 992–1000, 2014
2. Walsh G: Biopharmaceutical benchmarks 2018. *Nat Biotechnol* 36(12): 1136–45, 2018
3. Walsh G: Biopharmaceutical benchmarks 2010. *Nat Biotechnol* 28(9): 917–24, 2010
4. Farid SS: Process economics of industrial monoclonal antibody manufacture. *J Chromatogr B Analyt Technol Biomed Life Sci* 848(1): 8–18, 2007
5. Di Minno MN, Di MG, Di CM, Cerbone AM, Coppola A: Cost of care of haemophilia with inhibitors. *Haemophilia* 16(1): e190-e201, 2010
6. Chung CH, Mirakhur B, Chan E, Le Q-T, Berlin J, Morse M, Murphy BA, Satinover SM, Hosen J, Mauro D, Slebos RJ, Zhou Q, Gold D, Hatley T, Hicklin DJ, Platts-Mills TAE: Cetuximab-induced anaphylaxis and IgE specific for galactose-alpha-1,3-galactose. *N Engl J Med* 358(11): 1109–17, 2008
7. Ghaderi D, Taylor RE, Padler-Karavani V, Diaz S, Varki A: Implications of the presence of N-glycolylneuraminic acid in recombinant therapeutic glycoproteins. *Nat Biotechnol* 28(8): 863–7, 2010
8. Casademunt E, Martinelle K, Jernberg M, Winge S, Tiemeyer M, Biesert L, Knaub S, Walter O, Schroder C: The first recombinant human coagulation factor VIII of human origin: Human cell line and manufacturing characteristics. *Eur J Haematol* 89(2): 165–76, 2012
9. Sandberg H, Kannicht C, Stenlund P, Dadaian M, Oswaldsson U, Cordula C, Walter O: Functional characteristics of the novel, human-derived recombinant FVIII protein product, human-cl rhFVIII. *Thromb Res* 130(5): 808–17, 2012
10. Ben TH, Gonzalez DE, Barton NW, Zimran A, Kabra M, Lukina EA, Giraldo P, Kisinovsky I, Bavdekar A, Ben Dridi MF, Gupta N, Kishnani PS, Sureshkumar EK, Wang N, Crombez E, Bhirangi K, Mehta A: Velaglucerase alfa enzyme replacement therapy compared with imiglucerase in patients with Gaucher disease. *Am J Hematol* 88(3): 179–84, 2013
11. Wasley LC, Rehemtulla A, Bristol JA, Kaufman RJ: PACE/furin can process the vitamin K-dependent pro-factor IX precursor within the secretory pathway. *J Biol Chem* 268(12): 8458–65, 1993
12. Rehemtulla A, Roth DA, Wasley LC, Kuliopulos A, Walsh CT, Furie B, Furie BC, Kaufman RJ: In vitro and in vivo functional characterization of bovine vitamin K-dependent gamma-carboxylase expressed in Chinese hamster ovary cells. *Proc Natl Acad Sci U S A* 90(10): 4611–5, 1993
13. Grancha S, Navajas R, Maranon C, Paradela A, Albar JP, Jorquera JI: Incomplete tyrosine 1680 sulphation in recombinant FVIII concentrates. *Haemophilia* 17(4): 709–10, 2011
14. Bjorkman S: A commentary on the differences in pharmacokinetics between recombinant and plasma-derived factor IX and their implications for dosing. *Haemophilia* 17(2): 179–84, 2011
15. Durocher Y, Butler M: Expression systems for therapeutic glycoprotein production. *Curr Opin Biotechnol* 20(6): 700–7, 2009

16. Ghaderi D, Zhang M, Hurtado-Ziola N, Varki A: Production platforms for biotherapeutic glycoproteins. Occurrence, impact, and challenges of non-human sialylation. *Biotechnol Genet Eng Rev* 28(1): 147–76, 2012
17. Swiech K, Freitas MC de, Covas DT, Picanco-Castro V: Recombinant glycoprotein production in human cell lines. *Methods Mol Biol* 1258: 223–40, 2015
18. Gomes AR, Byregowda SM, Veeregowda BM, Balamurugan V: An Overview of Heterologous Expression Host Systems for the Production of Recombinant Proteins. *Adv Anim Vet Sc* 4(7): 346–56, 2016
19. Apweiler R, Hermjakob H, Sharon N: On the frequency of protein glycosylation, as deduced from analysis of the SWISS-PROT database. Dedicated to Prof. Akira Kobata and Prof. Harry Schachter on the occasion of their 65th birthdays. *Biochimica et Biophysica Acta (BBA) - General Subjects* 1473(1): 4–8, 1999
20. Wallick SC, Kabat EA, Morrison SL: Glycosylation of a VH residue of a monoclonal antibody against alpha (1---6) dextran increases its affinity for antigen. *J Exp Med* 168(3): 1099–109, 1988
21. Mimura Y, Sondermann P, Ghirlando R, Lund J, Young SP, Goodall M, Jefferis R: Role of oligosaccharide residues of IgG1-Fc in Fc gamma RIIb binding. *J Biol Chem* 276(49): 45539–47, 2001
22. Rajagopalan L, Organ-Darling LE, Liu H, Davidson AL, Raphael RM, Brownell WE, Pereira FA: Glycosylation regulates prestin cellular activity. *J Assoc Res Otolaryngol* 11(1): 39–51, 2010
23. Mimura Y, Church S, Ghirlando R, Ashton PR, Dong S, Goodall M, Lund J, Jefferis R: The influence of glycosylation on the thermal stability and effector function expression of human IgG1-Fc: properties of a series of truncated glycoforms. *Mol Immunol* 37(12-13): 697–706, 2000
24. Solá RJ, Al-Azzam W, Griebenow K: Engineering of protein thermodynamic, kinetic, and colloidal stability: Chemical Glycosylation with monofunctionally activated glycans. *Biotechnol Bioeng* 94(6): 1072–9, 2006
25. Leavitt R, Schlesinger S, Kornfeld S: Impaired intracellular migration and altered solubility of nonglycosylated glycoproteins of vesicular stomatitis virus and Sindbis virus. *J Biol Chem* 252(24): 9018–23, 1977
26. Tams JW, Vind J, Welinder, KG: Adapting protein solubility by glycosylation. N-glycosylation mutants of Coprinus cinereus peroxidase in salt and organic solutions. *Biochimica et biophysica acta* 1432(2), 1999
27. Galili U: The alpha-gal epitope and the anti-Gal antibody in xenotransplantation and in cancer immunotherapy. *Immunol Cell Biol* 83(6): 674–86, 2005
28. Lai JD, Swystun LL, Cartier D, Nesbitt K, Zhang C, Hough C, Dennis JW, Lillicrap D: N-linked glycosylation modulates the immunogenicity of recombinant human factor VIII in hemophilia A mice. *Haematologica* 103(11): 1925–36, 2018
29. Hotchkiss A, Refino CJ, Leonard CK, O'Connor JV, Crowley C, McCabe J, Tate K, Nakamura G, Powers D, Levinson A: The influence of carbohydrate structure on the clearance of recombinant tissue-type plasminogen activator. *Thromb Haemost* 60(2): 255–61, 1988

30. Seested T, Nielsen HM, Christensen EI, Appa RS: The unsialylated subpopulation of recombinant activated factor VII binds to the asialo-glycoprotein receptor (ASGPR) on primary rat hepatocytes. *Thromb Haemost* 104(6): 1166–73, 2010
31. Opdenakker G, van Damme J, Bosman F, Billiau A, Somer P de: Influence of carbohydrate side chains on activity of tissue-type plasminogen activator. *Proceedings of the Society for Experimental Biology and Medicine. Society for Experimental Biology and Medicine (New York, N.Y.)* 182(2): 248–57, 1986
32. Smedsrød B, Einarsson M: Clearance of tissue plasminogen activator by mannose and galactose receptors in the liver. *Thromb Haemost* 63(1): 60–6, 1990
33. Noorman F, Barrett-Bergshoeff MM, Rijken DC: Role of carbohydrate and protein in the binding of tissue-type plasminogen activator to the human mannose receptor. *Eur J Biochem* 251(1-2): 107–13, 1998
34. Stanley P, Taniguchi N, Aebi M: *In: Essentials of Glycobiology: N-Glycans*. 3rd ed., Cold Spring Harbor (NY), 2015
35. Sparrow LG, Lawrence MC, Gorman JJ, Strike PM, Robinson CP, McKern NM, Ward CW: N-linked glycans of the human insulin receptor and their distribution over the crystal structure. *Proteins* 71(1), 2008
36. Thaysen-Andersen M, Packer NH: Site-specific glycoproteomics confirms that protein structure dictates formation of N-glycan type, core fucosylation and branching. *Glycobiology* 22(11): 1440–52, 2012
37. Lee LY, Lin C-H, Fanayan S, Packer NH, Thaysen-Andersen M: Differential site accessibility mechanistically explains subcellular-specific N-glycosylation determinants. *Front Immunol* 5: 404, 2014
38. Suga A, Nagae M, Yamaguchi Y: Analysis of protein landscapes around N-glycosylation sites from the PDB repository for understanding the structural basis of N-glycoprotein processing and maturation. *Glycobiology* 28(10): 774–85, 2018
39. Harduin-Lepers A, Vallejo-Ruiz V, Krzewinski-Recchi M-A, Samyn-Petit B, Julien S, Delannoy P: The human sialyltransferase family. *Biochimie* 83(8): 727–37, 2001
40. Fiete D, Beranek M, Baenziger JU: Molecular basis for protein-specific transfer of N-acetylgalactosamine to N-linked glycans by the glycosyltransferases  $\beta$ 1,4-N-acetylgalactosaminyl transferase 3 ( $\beta$ 4GalNAc-T3) and  $\beta$ 4GalNAc-T4. *J Biol Chem* 287(34): 29194–203, 2012
41. Miller E, Fiete D, Blake NMJ, Beranek M, Oates EL, Mi Y, Roseman DS, Baenziger JU: A necessary and sufficient determinant for protein-selective glycosylation in vivo. *J Biol Chem* 283(4): 1985–91, 2008
42. Fiete D, Beranek M, Baenziger JU: Peptide-specific transfer of N-acetylgalactosamine to O-linked glycans by the glycosyltransferases  $\beta$ 1,4-N-acetylgalactosaminyl transferase 3 ( $\beta$ 4GalNAc-T3) and  $\beta$ 4GalNAc-T4. *J Biol Chem* 287(34): 29204–12, 2012
43. Stockell Hartree A, Renwick AGC: Molecular structures of glycoprotein hormones and functions of their carbohydrate components. *Biochem J* 287(3): 665–79, 1992



44. Dell A, Morris HR, Easton RL, Panico M, Patankar M, Oehninger S, Koistinen R, Koistinen H, Seppala M, Clark GF: Structural Analysis of the Oligosaccharides Derived from Glycodelin, a Human Glycoprotein with Potent Immunosuppressive and Contraceptive Activities. *J Biol Chem* 270(41): 24116–26, 1995
45. Hiraoka N, Misra A, Belot F, Hindsgaul O, Fukuda M: Molecular cloning and expression of two distinct human N-acetylgalactosamine 4-O-sulfotransferases that transfer sulfate to GalNAc beta 1->4GlcNAc beta 1->R in both N- and O-glycans. *Glycobiology* 11(6): 495–504, 2001
46. Vries T de, Srnka CA, Palcic MM, Swiedler SJ, van den Eijnden DH, Macher BA: Acceptor specificity of different length constructs of human recombinant alpha 1,3/4-fucosyltransferases. Replacement of the stem region and the transmembrane domain of fucosyltransferase V by protein A results in an enzyme with GDP-fucose hydrolyzing activity. *J Biol Chem* 270(15): 8712–22, 1995
47. Goh JB, Ng SK: Impact of host cell line choice on glycan profile. *Crit Rev Biotechnol* 38(6): 851–67, 2018
48. Gil G-C, Velander WH, van Cott KE: Analysis of the N-glycans of recombinant human Factor IX purified from transgenic pig milk. *Glycobiology* 18(7): 526–39, 2008
49. Böhm E, Seyfried BK, Dockal M, Graninger M, Hasslacher M, Neurath M, Konetschny C, Matthiessen P, Mitterer A, Scheiflinger F: Differences in N-glycosylation of recombinant human coagulation factor VII derived from BHK, CHO, and HEK293 cells. *BMC Biotechnol* 15: 87, 2015
50. Canis K, Anzengruber J, Garenaux E, Feichtinger M, Benamara K, Scheiflinger F, Savoy L-A, Reipert BM, Malisaukas M: In-depth comparison of N-glycosylation of human plasma-derived factor VIII and different recombinant products: from structure to clinical implications. *J Thromb Haemost* 16(8): 1592–603, 2018
51. Rosenlöcher J, Sandig G, Kannicht C, Blanchard V, Reinke SO, Hinderlich S: Recombinant glycoproteins: The impact of cell lines and culture conditions on the generation of protein species. *J Proteomics* 134: 85–92, 2016
52. Food and Drug Administration: *Guidance for Industry. Development of Therapeutic Protein Biosimilars: Comparative Analytical Assessment and Other Quality-Related Considerations*, 2019, Online: <https://www.fda.gov/media/125484/download>, Accessed: 2021
53. Morell AG, Gregoriadis G, Scheinberg IH, Hickman J, Ashwell G: The role of sialic acid in determining the survival of glycoproteins in the circulation. *J Biol Chem* 246(5): 1461–7, 1971
54. Basset C, Devauchelle V, Durand V, Jamin C, Pennec YL, Youinou P, Dueymes M: Glycosylation of immunoglobulin A influences its receptor binding. *Scandinavian journal of immunology* 50(6): 572–9, 1999
55. Appa RS, Theill C, Hansen L, Møss J, Behrens C, Nicolaisen EM, Klausen NK, Christensen MS: Investigating clearance mechanisms for recombinant activated factor VII in a perfused liver model. *Thromb Haemost* 104(2): 243–51, 2010
56. Baenziger JU: Beta1,4-N-Acetylgalactosaminyltransferase-3 (B4GALNT3) and Beta1,4-N-Acetylgalactosaminyltransferase-4 (B4GALNT4). In: *Handbook of Glycosyltransferases and Related Genes*, edited by Taniguchi N, Honke K, Fukuda M, Narimatsu H, Yamaguchi Y, Angata T, Tokyo, Springer Japan, 2014, pp 429–437

57. Chung C-Y, Wang Q, Yang S, Chough S, Seo Y, Cipollo JF, Balthasar JP, Betenbaugh MJ: The impact of sialylation linkage-type on the pharmacokinetics of recombinant butyrylcholinesterases. *Biotechnol Bioeng* 117(1): 157–66, 2020
58. Jones AJS, Papac DI, Chin EH, Keck R, Baughman SA, Lin YS, Kneer J, Battersby JE: Selective clearance of glycoforms of a complex glycoprotein pharmaceutical caused by terminal N-acetylglucosamine is similar in humans and cynomolgus monkeys. *Glycobiology* 17(5): 529–40, 2007
59. Mi Y, Fiete D, Baenziger JU: Ablation of GalNAc-4-sulfotransferase-1 enhances reproduction by altering the carbohydrate structures of luteinizing hormone in mice. *J Clin Invest* 118(5): 1815–24, 2008
60. Mi Y, Coonce M, Fiete D, Steirer L, Dveksler G, Townsend RR, Baenziger JU: Functional Consequences of Mannose and Asialoglycoprotein Receptor Ablation. *J Biol Chem* 291(36): 18700–17, 2016
61. Baenziger JU, Fiete D: Galactose and N-acetylgalactosamine-specific endocytosis of glycopeptides by isolated rat hepatocytes. *Cell* 22(2 Pt 2): 611–20, 1980
62. Baenziger JU, Maynard Y: Human hepatic lectin. Physicochemical properties and specificity. *J Biol Chem* 255(10): 4607–13, 1980
63. Mi Y, Lin A, Fiete D, Steirer L, Baenziger JU: Modulation of mannose and asialoglycoprotein receptor expression determines glycoprotein hormone half-life at critical points in the reproductive cycle. *J Biol Chem* 289(17): 12157–67, 2014
64. Su D, Zhao H, Xia H: Glycosylation-modified erythropoietin with improved half-life and biological activity. *Int J Hematol* 91(2): 238–44, 2010
65. Pontow SE, Kery V, Stahl PD: Mannose Receptor. In: *Molecular Biology of Receptors and Transporters - Receptors*, Elsevier, 1993, pp 221–244
66. Shepherd VL, Lee YC, Schlesinger PH, Stahl PD: L-Fucose-terminated glycoconjugates are recognized by pinocytosis receptors on macrophages. *Proc Natl Acad Sci U S A* 78(2): 1019–22, 1981
67. Largent BL, Walton KM, Hoppe CA, Lee YC, Schnaar RL: Carbohydrate-specific adhesion of alveolar macrophages to mannose-derivatized surfaces. *J Biol Chem* 259(3): 1764–9, 1984
68. Dong X, Storkus WJ, Salter RD: Binding and uptake of agalactosyl IgG by mannose receptor on macrophages and dendritic cells. *J Immunol* 163(10): 5427–34, 1999
69. Lee SJ, Evers S, Roeder D, Parlow AF, Risteli J, Risteli L, Lee YC, Feizi T, Langen H, Nussenzweig MC: Mannose receptor-mediated regulation of serum glycoprotein homeostasis. *Science* 295(5561): 1898–901, 2002
70. Fiete DJ, Beranek MC, Baenziger JU: A cysteine-rich domain of the "mannose" receptor mediates GalNAc-4-SO<sub>4</sub> binding. *Proc Natl Acad Sci U S A* 95(5): 2089–93, 1998
71. Liu Y, Chirino AJ, Misulovin Z, Leteux C, Feizi T, Nussenzweig MC, Bjorkman PJ: Crystal structure of the cysteine-rich domain of mannose receptor complexed with a sulfated carbohydrate ligand. *J Exp Med* 191(7): 1105–16, 2000

72. Leteux C, Chai W, Loveless RW, Yuen CT, Uhlin-Hansen L, Combarous Y, Jankovic M, Maric SC, Misulovin Z, Nussenzweig MC, Feizi T: The cysteine-rich domain of the macrophage mannose receptor is a multispecific lectin that recognizes chondroitin sulfates A and B and sulfated oligosaccharides of blood group Lewis(a) and Lewis(x) types in addition to the sulfated N-glycans of lutropin. *J Exp Med* 191(7): 1117–26, 2000
73. Huang L, Biolsi S, Bales KR, Kuchibhotla U: Impact of variable domain glycosylation on antibody clearance: an LC/MS characterization. *Anal Biochem* 349(2): 197–207, 2006
74. Millward TA, Heitzmann M, Bill K, Längle U, Schumacher P, Forrer K: Effect of constant and variable domain glycosylation on pharmacokinetics of therapeutic antibodies in mice. *Biologicals* 36(1): 41–7, 2008
75. Pipe SW, Montgomery RR, Pratt KP, Lenting PJ, Lillicrap D: Life in the shadow of a dominant partner: the FVIII-VWF association and its clinical implications for hemophilia A. *Blood* 128(16): 2007–16, 2016
76. Swystun LL, Ogiwara K, Rawley O, Brown C, Georgescu I, Hopman W, Labarque V, Male C, Thom K, Blanchette VS, Carcao MD, Lillicrap D: Genetic determinants of VWF clearance and FVIII binding modify FVIII pharmacokinetics in pediatric hemophilia A patients. *Blood* 134(11): 880–91, 2019
77. Scallon BJ, Tam SH, McCarthy SG, Cai AN, Raju TS: Higher levels of sialylated Fc glycans in immunoglobulin G molecules can adversely impact functionality. *Mol Immunol* 44(7): 1524–34, 2007
78. Chen R: Bacterial expression systems for recombinant protein production: E. coli and beyond. *Biotechnol Adv* 30(5): 1102–7, 2012
79. Nothhaft H, Szymanski CM: Protein glycosylation in bacteria: sweeter than ever. *Nat Rev Microbiol* 8(11): 765–78, 2010
80. Brooks SA: Appropriate Glycosylation of Recombinant Proteins for Human Use: Implications of Choice of Expression System. *Mol. Biotechnol.* 28(3): 241–56, 2004
81. Gemmill TR, Trimble RB: Overview of N- and O-linked oligosaccharide structures found in various yeast species. *Biochimica et Biophysica Acta (BBA) - General Subjects* 1426(2): 227–37, 1999
82. Dean N: Asparagine-linked glycosylation in the yeast Golgi. *Biochimica et biophysica acta* 1426(2), 1999
83. Gerngross TU: Advances in the production of human therapeutic proteins in yeasts and filamentous fungi. *Nat Biotechnol* 22(11): 1409–14, 2004
84. Lam JS, Huang H, Levitz SM: Effect of differential N-linked and O-linked mannosylation on recognition of fungal antigens by dendritic cells. *PloS one* 2(10): e1009, 2007
85. Gomord V, Fitchette A-C, Menu-Bouaouiche L, Saint-Jore-Dupas C, Plasson C, Michaud D, Faye L: Plant-specific glycosylation patterns in the context of therapeutic protein production. *Plant biotechnology journal* 8(5): 564–87, 2010
86. O'Neill MA, Darvill AG, Etzler ME, Mohnen D, Perez S: *In: Essentials of Glycobiology: Viridiplantae and Algae.* 3rd ed., Cold Spring Harbor (NY), 2015

87. Staudacher E, Altmann F, Wilson IB, März L: Fucose in N-glycans: from plant to man. *Biochimica et biophysica acta* 1473(1), 1999
88. Ailor E, Takahashi N, Tsukamoto Y, Masuda K, Rahman BA, Jarvis DL, Lee YC, Betenbaugh MJ: N-glycan patterns of human transferrin produced in *Trichoplusia ni* insect cells: effects of mammalian galactosyltransferase. *Glycobiology* 10(8): 837–47, 2000
89. Kim YK, Shin HS, Tomiya N, Lee YC, Betenbaugh MJ, Cha HJ: Production and N-glycan analysis of secreted human erythropoietin glycoprotein in stably transfected *Drosophila* S2 cells. *Biotechnol Bioeng* 92(4): 452–61, 2005
90. Hillar A, Jarvis DL: Re-visiting the endogenous capacity for recombinant glycoprotein sialylation by baculovirus-infected Tn-4h and DpN1 cells. *Glycobiology* 20(10): 1323–30, 2010
91. Tiemeyer M, Nakato H, Esko JD: *In: Essentials of Glycobiology: Arthropoda*. 3rd ed., Cold Spring Harbor (NY), 2015
92. Tangvoranuntakul P, Gagneux P, Diaz S, Bardor M, Varki N, Varki A, Muchmore E: Human uptake and incorporation of an immunogenic nonhuman dietary sialic acid. *Proc Natl Acad Sci U S A* 100(21): 12045–50, 2003
93. Harrison RL, Jarvis DL: Protein N-glycosylation in the baculovirus-insect cell expression system and engineering of insect cells to produce "mammalianized" recombinant glycoproteins. *Adv Virus Res* 68: 159–91, 2006
94. Hamilton SR, Gerngross TU: Glycosylation engineering in yeast: the advent of fully humanized yeast. *Curr Opin Biotechnol* 18(5), 2007
95. Karg SR, Kallio PT: The production of biopharmaceuticals in plant systems. *Biotechnol Adv* 27(6): 879–94, 2009
96. Estes S, Melville M: Mammalian cell line developments in speed and efficiency. *Adv Biochem Eng Biotechnol* 139: 11–33, 2014
97. Dumont J, Ewart D, Mei B, Estes S, Kshirsagar R: Human cell lines for biopharmaceutical manufacturing: History, status, and future perspectives. *Crit Rev Biotechnol* 36(6): 1110–22, 2016
98. Xu X, Nagarajan H, Lewis NE, Pan S, Cai Z, Liu X, Chen W, Xie M, Wang W, Hammond S, Andersen MR, Neff N, Passarelli B, Koh W, Fan HC, Wang J, Gui Y, Lee KH, Betenbaugh MJ, Quake SR, Famili I, Palsson BO, Wang J: The genomic sequence of the Chinese hamster ovary (CHO)-K1 cell line. *Nat Biotechnol* 29(8): 735–41, 2011
99. Grabenhorst E, Schlenke P, Pohl S, Nimtz M, Conradt HS: Genetic engineering of recombinant glycoproteins and the glycosylation pathway in mammalian host cells. In: *Glycotechnology*, edited by Berger EG, Clausen H, Cummings RD, Boston, MA, Springer US, 1999, pp 1–17
100. Zhang A, Potvin B, Zaiman A, Chen W, Kumar R, Phillips L, Stanley P: The gain-of-function Chinese hamster ovary mutant LEC11B expresses one of two Chinese hamster FUT6 genes due to the loss of a negative regulatory factor. *J Biol Chem* 274(15): 10439–50, 1999
101. Chou HH, Takematsu H, Diaz S, Iber J, Nickerson E, Wright KL, Muchmore EA, Nelson DL, Warren ST, Varki A: A mutation in human CMP-sialic acid hydroxylase occurred after the Homo-Pan divergence. *Proc Natl Acad Sci U S A* 95(20): 11751–6, 1998

102. Koike C, Uddin M, Wildman DE, Gray EA, Trucco M, Starzl TE, Goodman M: Functionally important glycosyltransferase gain and loss during catarrhine primate emergence. *Proc Natl Acad Sci U S A* 104(2): 559–64, 2007
103. Diaz SL, Padler-Karavani V, Ghaderi D, Hurtado-Ziola N, Yu H, Chen X, Brinkman-Van der Linden ECM, Varki A, Varki NM: Sensitive and specific detection of the non-human sialic Acid N-glycolylneuraminic acid in human tissues and biotherapeutic products. *PLoS One* 4(1): e4241, 2009
104. Hironaka T, Furukawa K, Esmon PC, Fournel MA, Sawada S, Kato M, Minaga T, Kobata A: Comparative study of the sugar chains of factor VIII purified from human plasma and from the culture media of recombinant baby hamster kidney cells. *J Biol Chem* 267(12): 8012–20, 1992
105. Bosques CJ, Collins BE, Meador JW3, Sarvaiya H, Murphy JL, Dellorusso G, Bulik DA, Hsu I-H, Washburn N, Sipsy SF, Myette JR, Raman R, Shriver Z, Sasisekharan R, Venkataraman G: Chinese hamster ovary cells can produce galactose-alpha-1,3-galactose antigens on proteins. *Nat Biotechnol* 28(11): 1153–6, 2010
106. Hokke CH, Bergwerff AA, van Dedem GW, van OJ, Kamerling JP, Vliegthart JF: Sialylated carbohydrate chains of recombinant human glycoproteins expressed in Chinese hamster ovary cells contain traces of N-glycolylneuraminic acid. *FEBS Lett* 275(1-2): 9–14, 1990
107. Déglon N, Aubert V, Spertini F, Winkel L, Aebischer P: Presence of Gal-alpha1,3Gal epitope on xenogeneic lines: implications for cellular gene therapy based on the encapsulation technology. *Xenotransplantation* 10(3): 204–13, 2003
108. Galili U: Anti-Gal: An abundant human natural antibody of multiple pathogeneses and clinical benefits. *Immunology* 140(1): 1–11, 2013
109. Padler-Karavani V, Yu H, Cao H, Chokhawala H, Karp F, Varki N, Chen X, Varki A: Diversity in specificity, abundance, and composition of anti-Neu5Gc antibodies in normal humans: Potential implications for disease. *Glycobiology* 18(10): 818–30, 2008
110. Berg EA, Platts-Mills TAE, Commins SP: Drug allergens and food--the cetuximab and galactose-alpha-1,3-galactose story. *Ann Allergy Asthma Immunol* 112(2): 97–101, 2014
111. Higashi H, Naiki M, Matuo S, Okouchi K: Antigen of "serum sickness" type of heterophile antibodies in human sera: Identification as gangliosides with N-glycolylneuraminic acid. *Biochem Biophys Res Commun* 79(2): 388–95, 1977
112. Merrick JM, Zadarlik K, Milgrom F: Characterization of the Hanganutziu-Deicher (serum-sickness) antigen as gangliosides containing n-glycolylneuraminic acid. *Int Arch Allergy Appl Immunol* 57(5): 477–80, 1978
113. Steinke JW, Platts-Mills TAE, Commins SP: The alpha-gal story: Lessons learned from connecting the dots. *The Journal of allergy and clinical immunology* 135(3): 589-96; quiz 597, 2015
114. Galili U, Repik PM, Anaraki F, Mozdzanowska K, Washko G, Gerhard W: Enhancement of antigen presentation of influenza virus hemagglutinin by the natural human anti-Gal antibody. *Vaccine* 14(4): 321–8, 1996
115. Hay CRM: The epidemiology of factor VIII inhibitors. *Haemophilia* 12 Suppl 6: 23-8; discussion 28-9, 2006

116. Ettingshausen CE, Kreuz W: Recombinant vs. plasma-derived products, especially those with intact VWF, regarding inhibitor development. *Haemophilia* 12 Suppl 6: 102–6, 2006
117. Lissitchkov T, Klukowska A, Pasi J, Kessler CM, Klamroth R, Liesner RJ, Belyanskaya L, Walter O, Knaub S, Bichler J, Jansen M, Oldenburg J: Efficacy and safety of simoctocog alfa (Nuwiq®) in patients with severe hemophilia A: a review of clinical trial data from the GENA program. *Therapeutic advances in hematology* 10, 2019
118. Leyte A, van Schijndel HB, Niehrs C, Huttner WB, Verbeet MP, Mertens K, van Mourik JA: Sulfation of Tyr1680 of human blood coagulation factor VIII is essential for the interaction of factor VIII with von Willebrand factor. *J Biol Chem* 266(2): 740–6, 1991
119. Woods AS, Wang H-YJ, Jackson SN: Sulfation, the up-and-coming post-translational modification: its role and mechanism in protein-protein interaction. *J Proteome Res* 6(3): 1176–82, 2007
120. Kumar SR: Industrial production of clotting factors: Challenges of expression, and choice of host cells. *Biotechnol J* 10(7): 995–1004, 2015
121. Zurlo G, Guo J, Takada M, Wei W, Zhang Q: New Insights into Protein Hydroxylation and Its Important Role in Human Diseases. *Biochim Biophys Acta* 1866(2): 208–20, 2016
122. Swiech K, Picanco-Castro V, Covas DT: Human cells: New platform for recombinant therapeutic protein production. *Protein expression and purification* 84(1): 147–53, 2012
123. Berkner KL: Expression of recombinant vitamin K-dependent proteins in mammalian cells: factors IX and VII. *Meth Enzymol* 222: 450–77, 1993
124. Suttie JW: Report of workshop on expression of vitamin k-dependent proteins in bacterial and mammalian cells Madison, Wisconsin, USA, April, 1986. *Thromb Res* 44(1): 129–34, 1986
125. Kannicht C, Ramstrom M, Kohla G, Tiemeyer M, Casademunt E, Walter O, Sandberg H: Characterisation of the post-translational modifications of a novel, human cell line-derived recombinant human factor VIII. *Thromb Res* 131(1): 78–88, 2013
126. Astermark J, Morado M, Rocino A, van den Berg HM, von DM, Gringeri A, Mantovani L, Garrido RP, Schiavoni M, Villar A, Windyga J: Current European practice in immune tolerance induction therapy in patients with haemophilia and inhibitors. *Haemophilia* 12(4): 363–71, 2006
127. Chapple SDJ, Crofts AM, Shadbolt SP, McCafferty J, Dyson MR: Multiplexed expression and screening for recombinant protein production in mammalian cells. *BMC Biotechnol* 6: 49, 2006
128. Butler M, Spearman M: The choice of mammalian cell host and possibilities for glycosylation engineering. *Curr Opin Biotechnol* 30: 107–12, 2014
129. Vink T, Oudshoorn-Dickmann M, Roza M, Reitsma JJ, de JRN: A simple, robust and highly efficient transient expression system for producing antibodies. *Methods* 65(1), 2014
130. Bylund L, Kytola S, Lui W-O, Larsson C, Weber G: Analysis of the cytogenetic stability of the human embryonal kidney cell line 293 by cytogenetic and STR profiling approaches. *Cytogenet Genome Res* 106(1): 28–32, 2004

131. Frattini A, Fabbri M, Valli R, Paoli E de, Montalbano G, Gribaldo L, Pasquali F, Maserati E: High variability of genomic instability and gene expression profiling in different HeLa clones. *Sci Rep* 5: 15377, 2015
132. Bandyopadhyay AA, O'Brien SA, Zhao L, Fu H-Y, Vishwanathan N, Hu W-S: Recurring genomic structural variation leads to clonal instability and loss of productivity. *Biotechnol Bioeng* 116(1): 41–53, 2019
133. World Health Organization: *Guidelines on the quality, safety, and efficacy of biotherapeutic protein products prepared by recombinant DNA technology: Replacement of Annex 3 of WHO Technical Report Series, No. 814*, World Health Organization, 2013
134. Fiete D, Mi Y, Oats EL, Beranek MC, Baenziger JU: N-linked oligosaccharides on the low density lipoprotein receptor homolog SorLA/LR11 are modified with terminal GalNAc-4-SO<sub>4</sub> in kidney and brain. *J Biol Chem* 282(3): 1873–81, 2007
135. Yan SB, Chao YB, van Halbeek H: Novel Asn-linked oligosaccharides terminating in GalNAc beta (1-->4)Fuc alpha (1-->3)GlcNAc beta (1-->. are present in recombinant human protein C expressed in human kidney 293 cells. *Glycobiology* 3(6): 597–608, 1993
136. Wedepohl S, Kaup M, Riese SB, Berger M, Dervedde J, Tauber R, Blanchard V: N-glycan analysis of recombinant L-Selectin reveals sulfated GalNAc and GalNAc-GalNAc motifs. *J Proteome Res* 9(7): 3403–11, 2010
137. Chin CL, Goh JB, Srinivasan H, Liu KI, Gowher A, Shanmugam R, Lim HL, Choo M, Tang WQ, Tan AH-M, Nguyen-Khuong T, Tan MH, Ng SK: A human expression system based on HEK293 for the stable production of recombinant erythropoietin. *Sci Rep* 9(1): 992, 2019
138. Smith PL, Skelton TP, Fiete D, Dharmesh SM, Beranek MC, MacPhail L, Broze GJ, Baenziger JU: The asparagine-linked oligosaccharides on tissue factor pathway inhibitor terminate with SO<sub>4</sub>-4GalNAc beta 1, 4GlcNAc beta 1,2 Mana alpha. *J Biol Chem* 267(27): 19140–6, 1992
139. Croset A, Delafosse L, Gaudry J-P, Arod C, Glez L, Losberger C, Begue D, Krstanovic A, Robert F, Vilbois F, Chevalet L, Antonsson B: Differences in the glycosylation of recombinant proteins expressed in HEK and CHO cells. *J Biotechnol* 161(3): 336–48, 2012
140. Yang Z, Wang S, Halim A, Schulz MA, Frodin M, Rahman SH, Vester-Christensen MB, Behrens C, Kristensen C, Vakhrushev SY, Bennett EP, Wandall HH, Clausen H: Engineered CHO cells for production of diverse, homogeneous glycoproteins. *Nat Biotechnol* 33(8): 842–4, 2015
141. Yamane-Ohnuki N, Kinoshita S, Inoue-Urakubo M, Kusunoki M, Iida S, Nakano R, Wakitani M, Niwa R, Sakurada M, Uchida K, Shitara K, Satoh M: Establishment of FUT8 knockout Chinese hamster ovary cells: an ideal host cell line for producing completely defucosylated antibodies with enhanced antibody-dependent cellular cytotoxicity. *Biotechnol Bioeng* 87(5): 614–22, 2004
142. Chung C-Y, Wang Q, Yang S, Yin B, Zhang H, Betenbaugh M: Integrated Genome and Protein Editing Swaps  $\alpha$ -2,6 Sialylation for  $\alpha$ -2,3 Sialic Acid on Recombinant Antibodies from CHO. *Biotechnol J* 12(2), 2017
143. Chai Y-R, Cao X-X, Ge M-M, Mi C-L, Guo X, Wang T-Y: Knockout of cytidine monophosphate-N-acetylneuraminic acid hydroxylase in Chinese hamster ovary cells by CRISPR/Cas9-based gene-editing technology. *Biochem Eng J* 161: 107663, 2020

144. Wong NSC, Yap MGS, Wang DIC: Enhancing recombinant glycoprotein sialylation through CMP-sialic acid transporter over expression in Chinese hamster ovary cells. *Biotechnol Bioeng* 93(5): 1005–16, 2006
145. Bork K, Reutter W, Weidemann W, Horstkorte R: Enhanced sialylation of EPO by overexpression of UDP-GlcNAc 2-epimerase/ManAc kinase containing a sialuria mutation in CHO cells. *FEBS Lett* 581(22): 4195–8, 2007
146. Grabenhorst E, Schlenke P, Pohl S, Nimtz M, Conradt HS: Genetic engineering of recombinant glycoproteins and the glycosylation pathway in mammalian host cells. *Glycoconj J* 16(2): 81–97, 1999
147. Fukuta K, Yokomatsu T, Abe R, Asanagi M, Makino T: Genetic engineering of CHO cells producing human interferon-gamma by transfection of sialyltransferases. *Glycoconj J* 17(12): 895–904, 2000
148. Yin B, Gao Y, Chung C-Y, Yang S, Blake E, Stuczynski MC, Tang J, Kildegaard HF, Andersen MR, Zhang H, Betenbaugh MJ: Glycoengineering of Chinese hamster ovary cells for enhanced erythropoietin N-glycan branching and sialylation. *Biotechnol Bioeng* 112(11): 2343–51, 2015
149. Ran FA, Hsu PD, Wright J, Agarwala V, Scott DA, Zhang F: Genome engineering using the CRISPR-Cas9 system. *Nature protocols* 8(11): 2281–308, 2013
150. Sugimoto I, Futakawa S, Oka R, Ogawa K, Marth JD, Miyoshi E, Taniguchi N, Hashimoto Y, Kitazume S: Beta-galactoside alpha2,6-sialyltransferase I cleavage by BACE1 enhances the sialylation of soluble glycoproteins. A novel regulatory mechanism for alpha2,6-sialylation. *J Biol Chem* 282(48): 34896–903, 2007
151. Dekkers G, Plomp R, Koeleman CAM, Visser R, Horsten HH von, Sandig V, Rispens T, Wuhrer M, Vidarsson G: Multi-level glyco-engineering techniques to generate IgG with defined Fc-glycans. *Sci Rep* 6: 36964, 2016
152. Weikert S, Papac D, Briggs J, Cowfer D, Tom S, Gawlitzek M, Lofgren J, Mehta S, Chisholm V, Modi N, Eppler S, Carroll K, Chamow S, Peers D, Berman P, Krummen L: Engineering Chinese hamster ovary cells to maximize sialic acid content of recombinant glycoproteins. *Nat Biotechnol* 17(11): 1116–21, 1999
153. Lin N, Mascarenhas J, Sealover NR, George HJ, Brooks J, Kayser KJ, Gau B, Yasa I, Azadi P, Archer-Hartmann S: Chinese hamster ovary (CHO) host cell engineering to increase sialylation of recombinant therapeutic proteins by modulating sialyltransferase expression. *Biotechnol Prog* 31(2): 334–46, 2015
154. Zhang P, Tan DL, Heng D, Wang T, Mariati, Yang Y, Song Z: A functional analysis of N-glycosylation-related genes on sialylation of recombinant erythropoietin in six commonly used mammalian cell lines. *Metab Eng* 12(6): 526–36, 2010
155. Jeong YT, Choi O, Son YD, Park SY, Kim JH: Enhanced sialylation of recombinant erythropoietin in genetically engineered Chinese-hamster ovary cells. *Biotechnol Appl Biochem* 52(Pt 4): 283–91, 2009
156. Bragonzi A, Distefano G, Buckberry LD, Acerbis G, Foglieni C, Lamotte D, Campi G, Marc A, Soria MR, Jenkins N, Monaco L: A new Chinese hamster ovary cell line expressing alpha2,6-



- sialyltransferase used as universal host for the production of human-like sialylated recombinant glycoproteins. *Biochim Biophys Acta* 1474(3): 273–82, 2000
157. Gupta SK, Shukla P: Gene editing for cell engineering: trends and applications. *Crit Rev Biotechnol* 37(5): 672–84, 2017
158. Smith JR, Maguire S, Davis LA, Alexander M, Yang F, Chandran S, French-Constant C, Pedersen RA: Robust, persistent transgene expression in human embryonic stem cells is achieved with AAVS1-targeted integration. *Stem cells (Dayton, Ohio)* 26(2): 496–504, 2008
159. Ocegüera-Yanez F, Kim S-I, Matsumoto T, Tan GW, Xiang L, Hatani T, Kondo T, Ikeya M, Yoshida Y, Inoue H, Woltjen K: Engineering the AAVS1 locus for consistent and scalable transgene expression in human iPSCs and their differentiated derivatives. *Methods* 101: 43–55, 2016
160. Ogata T, Kozuka T, Kanda T: Identification of an insulator in AAVS1, a preferred region for integration of adeno-associated virus DNA. *J Virol* 77(16): 9000–7, 2003
161. Kotin RM, Linden RM, Berns KI: Characterization of a preferred site on human chromosome 19q for integration of adeno-associated virus DNA by non-homologous recombination. *EMBO J* 11(13): 5071–8, 1992
162. Vcelar S, Melcher M, Auer N, Hrdina A, Puklowski A, Leisch F, Jadhav V, Wenger T, Baumann M, Borth N: Changes in Chromosome Counts and Patterns in CHO Cell Lines upon Generation of Recombinant Cell Lines and Subcloning. *Biotechnol J* 13(3): e1700495, 2018
163. He L, Winterrowd C, Kadura I, Frye C: Transgene copy number distribution profiles in recombinant CHO cell lines revealed by single cell analyses. *Biotechnol Bioeng*: 1713–22, 2012
164. Pilbrough W, Munro TP, Gray P: Intraclonal protein expression heterogeneity in recombinant CHO cells. *PLoS one* 4(12): e8432, 2009
165. Barnes LM, Bentley CM, Dickson AJ: Stability of protein production from recombinant mammalian cells. *Biotechnol Bioeng* 81(6): 631–9, 2003
166. Tharmalingam T, Barkhordarian H, Tejada N, Daris K, Yaghmour S, Yam P, Lu F, Goudar C, Munro T, Stevens J: Characterization of phenotypic and genotypic diversity in subclones derived from a clonal cell line. *Biotechnol Prog* 34(3): 613–23, 2018
167. Gu X, Wang DI: Improvement of interferon-gamma sialylation in Chinese hamster ovary cell culture by feeding of N-acetylmannosamine. *Biotechnol Bioeng* 58(6): 642–8, 1998
168. Baker KN, Rendall MH, Hills AE, Hoare M, Freedman RB, James DC: Metabolic control of recombinant protein N-glycan processing in NS0 and CHO cells. *Biotechnol Bioeng* 73(3): 188–202, 2001
169. Wong NSC, Wati L, Nissom PM, Feng HT, Lee MM, Yap MGS: An investigation of intracellular glycosylation activities in CHO cells: Effects of nucleotide sugar precursor feeding. *Biotechnol Bioeng* 107(2): 321–36, 2010
170. Almaraz RT, Tian Y, Bhattarcharya R, Tan E, Chen S-H, Dallas MR, Chen L, Zhang Z, Zhang H, Konstantopoulos K, Yarema KJ: Metabolic flux increases glycoprotein sialylation: Implications for cell adhesion and cancer metastasis. *Mol Cell Proteomics* 11(7): M112.017558, 2012

171. Bork K, Reutter W, Gerardy-Schahn R, Horstkorte R: The intracellular concentration of sialic acid regulates the polysialylation of the neural cell adhesion molecule. *FEBS Lett* 579(22): 5079–83, 2005
172. Freeze HH, Hart GW, Schnaar RL: *In: Essentials of Glycobiology: Glycosylation Precursors*. 3rd ed., Cold Spring Harbor (NY), 2015
173. Lee CA, Berntorp EE, Hoots WK: *Textbook of Hemophilia*, Oxford, UK, Wiley-Blackwell, 2010
174. Berntorp E, Shapiro AD: Modern haemophilia care. *Lancet (London, England)* 379(9824): 1447–56, 2012
175. Giansily-Blaizot M, Schved J-F: Recombinant human factor VIIa (rFVIIa) in hemophilia: mode of action and evidence to date. *Therapeutic advances in hematology* 8(12): 345–52, 2017
176. Santoro C, Quintavalle G, Castaman G, Baldacci E, Ferretti A, Riccardi F, Tagliaferri A: Inhibitors in Hemophilia B. *Seminars in thrombosis and hemostasis* 44(6): 578–89, 2018
177. Darby SC, Keeling DM, Spooner RJD, Wan Kan S, Giangrande PLF, Collins PW, Hill FGH, Hay CRM: The incidence of factor VIII and factor IX inhibitors in the hemophilia population of the UK and their effect on subsequent mortality, 1977-99. *J Thromb Haemost* 2(7): 1047–54, 2004
178. Lusher J, Ingerslev J, Roberts H, Hedner U: Clinical experience with recombinant factor VIIa. *Blood Coagul Fibrinolysis* 9(2): 119–28, 1998
179. Monroe DM, Hoffman M, Roberts HR: Platelets and thrombin generation. *Arterioscler Thromb Vasc Biol* 22(9): 1381–9, 2002
180. Kubisz P, Stasko J: Recombinant activated factor VII in patients at high risk of bleeding. *Hematology* 9(5-6): 317–32, 2004
181. Lindley CM, Sawyer WT, Macik BG, Lusher J, Harrison JF, Baird-Cox K, Birch K, Glazer S, Roberts HR: Pharmacokinetics and pharmacodynamics of recombinant factor VIIa. *Clin Pharmacol Ther* 55(6): 638–48, 1994
182. Agersø H, Brophy DF, Pelzer H, Martin EJ, Carr M, Hedner U, Ezban M: Recombinant human factor VIIa (rFVIIa) cleared principally by antithrombin following intravenous administration in hemophilia patients. *J Thromb Haemost* 9(2): 333–8, 2011
183. Bauer KA: Treatment of factor VII deficiency with recombinant factor VIIa. *Haemostasis* 26 Suppl 1: 155–8, 1996
184. Shapiro AD, Gilchrist GS, Hoots WK, Cooper HA, Gastineau DA: Prospective, randomised trial of two doses of rFVIIa (NovoSeven) in haemophilia patients with inhibitors undergoing surgery. *Thromb Haemost* 80(5): 773–8, 1998
185. Lusher JM, Roberts HR, Davignon G, Joist JH, Smith H, Shapiro A, Laurian Y, Kasper CK, Mannucci PM: A randomized, double-blind comparison of two dosage levels of recombinant factor VIIa in the treatment of joint, muscle and mucocutaneous haemorrhages in persons with haemophilia A and B, with and without inhibitors. rFVIIa Study Group. *Haemophilia* 4(6): 790–8, 1998

186. Konkle BA, Ebbesen LS, Erhardtsen E, Bianco RP, Lissitchkov T, Rusen L, Serban MA: Randomized, prospective clinical trial of recombinant factor VIIa for secondary prophylaxis in hemophilia patients with inhibitors. *J Thromb Haemost* 5(9): 1904–13, 2007
187. Rogers B, Dong D, Li Z, Li Z: Recombinant human serum albumin fusion proteins and novel applications in drug delivery and therapy. *Curr Pharm Des* 21(14): 1899–907, 2015
188. Sleep D, Cameron J, Evans LR: Albumin as a versatile platform for drug half-life extension. *Biochim Biophys Acta*: 5526–34, 2013
189. Golor G, Bensen-Kennedy D, Haffner S, Easton R, Jung K, Moises T, Lawo J-P, Joch C, Veldman A: Safety and pharmacokinetics of a recombinant fusion protein linking coagulation factor VIIa with albumin in healthy volunteers. *J Thromb Haemost* 11(11): 1977–85, 2013
190. Chaudhury C, Mehnaz S, Robinson JM, Hayton WL, Pearl DK, Roopenian DC, Anderson CL: The major histocompatibility complex-related Fc receptor for IgG (FcRn) binds albumin and prolongs its lifespan. *J Exp Med* 197(3): 315–22, 2003
191. Anderson CL, Chaudhury C, Kim J, Bronson CL, Wani MA, Mohanty S: Perspective-- FcRn transports albumin: relevance to immunology and medicine. *Trends Immunol* 27(7), 2006
192. Andersen JT, Dalhus B, Cameron J, Daba MB, Plumridge A, Evans L, Brennan SO, Gunnarsen KS, Bjørås M, Sleep D, Sandlie I: Structure-based mutagenesis reveals the albumin-binding site of the neonatal Fc receptor. *Nature communications* 3: 610, 2012
193. Eigenbrot C: Structure, function, and activation of coagulation factor VII. *Curr Protein Pept Sci* 3(3): 287–99, 2002
194. Brown MA, Stenberg LM, Stenflo J: Coagulation Factor Xa. In: *Handbook of proteolytic enzymes*. 3rd ed., edited by Rawlings N d., Salvesen G, Amsterdam, Acad. Press, 2013, pp 2908–2915
195. Kemball-Cook G, Johnson DJ, Tuddenham EG, Harlos K: Crystal structure of active site-inhibited human coagulation factor VIIa (des-Gla). *J Struct Biol* 127(3): 213–23, 1999
196. Jurlander B, Thim L, Klausen NK, Persson E, Kjalke M, Rexen P, Jørgensen TB, Østergaard PB, Erhardtsen E, Bjørn SE: Recombinant activated factor VII (rFVIIa): characterization, manufacturing, and clinical development. *Seminars in thrombosis and hemostasis* 27(4): 373–84, 2001
197. Fenaille F, Groseil C, Ramon C, Riandé S, Siret L, Chtourou S, Bihoreau N: Mass spectrometric characterization of N- and O-glycans of plasma-derived coagulation factor VII. *Glycoconj J* 25(9): 827–42, 2008
198. Bolt G, Kristensen C, Steenstrup TD: Posttranslational N-glycosylation takes place during the normal processing of human coagulation factor VII. *Glycobiology* 15(5): 541–7, 2005
199. Montacir O, Montacir H, Eravci M, Springer A, Hinderlich S, Mahboudi F, Saadati A, Parr MK: Bioengineering of rFVIIa Biopharmaceutical and Structure Characterization for Biosimilarity Assessment. *Bioengineering (Basel)* 5(1), 2018
200. Sheffield WP, Marques JA, Bhakta V, Smith IJ: Modulation of Clearance of Recombinant Serum Albumin by Either Glycosylation or Truncation. *Thromb Res* 99(6): 613–21, 2000

201. Orlova NA, Kovnir SV, Vorobiev II, Gabibov AG, Vorobiev AI: Blood Clotting Factor VIII: From Evolution to Therapy. *Acta naturae* 5(2): 19–39, 2013
202. Pipe SW: Functional roles of the factor VIII B domain. *Haemophilia* 15(6): 1187–96, 2009
203. Toole JJ, Pittman DD, Orr EC, Murtha P, Wasley LC, Kaufman RJ: A large region (approximately equal to 95 kDa) of human factor VIII is dispensable for in vitro procoagulant activity. *Proc Natl Acad Sci U S A* 83(16): 5939–42, 1986
204. Pittman DD, Alderman EM, Tomkinson KN, Wang JH, Giles AR, Kaufman RJ: Biochemical, immunological, and in vivo functional characterization of B-domain-deleted factor VIII. *Blood* 81(11): 2925–35, 1993
205. Bihoreau N, Veillon JF, Ramon C, Scohyers JM, Schmitter JM: Characterization of a recombinant antihemophilia-A factor (factor VIII-delta II) by matrix-assisted laser desorption/ionization mass spectrometry. *Rapid Commun. Mass Spectrom.* 9(15): 1584–8, 1995
206. Medzihradszky KF, Besman MJ, Burlingame AL: Structural characterization of site-specific N-glycosylation of recombinant human factor VIII by reversed-phase high-performance liquid chromatography-electrospray ionization mass spectrometry. *Anal. Chem.* 69(19): 3986–94, 1997
207. Bond M, Jankowski M, Patel H, Karnik S, Strang A, Xu B, Rouse J, Koza S, Letwin B, Steckert J, Amphlett G, Scoble H: Biochemical characterization of recombinant factor IX. *Semin Hematol* 35(2 Suppl 2): 11–7, 1998
208. Makino Y, Omichi K, Kuraya N, Ogawa H, Nishimura H, Iwanaga S, Hase S: Structural analysis of N-linked sugar chains of human blood clotting factor IX. *J Biochem* 128(2): 175–80, 2000
209. Mali P, Yang L, Esvelt KM, Aach J, Guell M, DiCarlo JE, Norville JE, Church GM: RNA-guided human genome engineering via Cas9. *Science* 339(6121): 823–6, 2013
210. Damerell D, Ceroni A, Maass K, Ranzinger R, Dell A, Haslam SM: The GlycanBuilder and GlycoWorkbench glycoinformatics tools: updates and new developments. *Biol Chem* 393(11): 1357–62, 2012
211. Gibson DG, Young L, Chuang R-Y, Venter JC, Hutchison CA, Smith HO: Enzymatic assembly of DNA molecules up to several hundred kilobases. *Nature methods* 6(5): 343–5, 2009
212. Rački N, Dreo T, Gutierrez-Aguirre I, Blejec A, Ravnikar M: Reverse transcriptase droplet digital PCR shows high resilience to PCR inhibitors from plant, soil and water samples. *Plant methods* 10(1): 42, 2014
213. Dobnik D, Spilsberg B, Bogožalec Košir A, Štebih D, Morisset D, Holst-Jensen A, Žel J: Multiplex Droplet Digital PCR Protocols for Quantification of GM Maize Events. *Methods Mol Biol* 1768: 69–98, 2018
214. Baker M: Digital PCR hits its stride. *Nature methods* 9(6): 541–4, 2012
215. Lin Y-C, Boone M, Meuris L, Lemmens I, van Roy N, Soete A, Reumers J, Moisse M, Plaisance S, Drmanac R, Chen J, Speleman F, Lambrechts D, van de Peer Y, Tavernier J, Callewaert N: Genome dynamics of the human embryonic kidney 293 lineage in response to cell biology manipulations. *Nature communications* 5: 4767, 2014

216. Kim S, Kim D, Cho SW, Kim J, Kim J-S: Highly efficient RNA-guided genome editing in human cells via delivery of purified Cas9 ribonucleoproteins. *Genome Res* 24(6): 1012–9, 2014
217. Varki A, Cummings RD, Aebi M, Packer NH, Seeberger PH, Esko JD, Stanley P, Hart G, Darvill A, Kinoshita T, Prestegard JJ, Schnaar RL, Freeze HH, Marth JD, Bertozzi CR, Etzler ME, Frank M, Vliegenthart JF, Lütke T, Perez S, Bolton E, Rudd P, Paulson J, Kanehisa M, Toukach P, Aoki-Kinoshita KF, Dell A, Narimatsu H, York W, Taniguchi N, Kornfeld S: Symbol Nomenclature for Graphical Representations of Glycans. *Glycobiology* 25(12): 1323–4, 2015
218. Ceroni A, Maass K, Geyer H, Geyer R, Dell A, Haslam SM: GlycoWorkbench: a tool for the computer-assisted annotation of mass spectra of glycans. *J Proteome Res* 7(4): 1650–9, 2008
219. Probst RJ, Lim JM, Bird DN, Pole GL, Sato AK, Claybaugh JR: Gender Differences in the Blood Volume of Conscious Sprague-Dawley Rats. *J Am Assoc Lab Anim Sci* 45(2): 49–52, 2006
220. Ouellette MM, McDaniel LD, Wright WE, Shay JW, Schultz RA: The establishment of telomerase-immortalized cell lines representing human chromosome instability syndromes. *Hum Mol Genet* 9(3): 403–11, 2000
221. Yamasaki K, Kawasaki S, Young RD, Fukuoka H, Tanioka H, Nakatsukasa M, Quantock AJ, Kinoshita S: Genomic aberrations and cellular heterogeneity in SV40-immortalized human corneal epithelial cells. *Invest Ophthalmol Vis Sci* 50(2): 604–13, 2009
222. Comelli EM, Head SR, Gilmartin T, Whisenant T, Haslam SM, North SJ, Wong N-K, Kudo T, Narimatsu H, Esko JD, Drickamer K, Dell A, Paulson JC: A focused microarray approach to functional glycomics: transcriptional regulation of the glycome. *Glycobiology* 16(2): 117–31, 2006
223. Inamori K-i, Willer T, Hara Y, Venzke D, Anderson ME, Clarke NF, Guicheney P, Bönnemann CG, Moore SA, Campbell KP: Endogenous glucuronyltransferase activity of LARGE or LARGE2 required for functional modification of  $\alpha$ -dystroglycan in cells and tissues. *J Biol Chem* 289(41): 28138–48, 2014
224. Uhler R, Popa-Wagner R, Kröning M, Brehm A, Rennert P, Seifried A, Peschke M, Krieger M, Kohla G, Kannicht C, Wiedemann P, Hafner M, Rosenlöcher J: Glyco-engineered HEK 293-F cell lines for the production of therapeutic glycoproteins with human N-glycosylation and improved pharmacokinetics. *Glycobiology*, 2021, doi: 1093/glycob/cwaa119
225. Wang J-R, Gao W-N, Grimm R, Jiang S, Liang Y, Ye H, Li Z-G, Yau L-F, Huang H, Liu J, Jiang M, Meng Q, Tong T-T, Huang H-H, Lee S, Zeng X, Liu L, Jiang Z-H: A method to identify trace sulfated IgG N-glycans as biomarkers for rheumatoid arthritis. *Nature communications* 8(1): 631, 2017
226. Weimer T, Wormsbächer W, Kronthaler U, Lang W, Liebing U, Schulte S: Prolonged in-vivo half-life of factor VIIa by fusion to albumin. *Thromb Haemost* 99(4): 659–67, 2008
227. Seested T, Appa RS, Christensen EI, Ioannou YA, Krogh TN, Karpf DM, Nielsen HM: In vivo clearance and metabolism of recombinant activated factor VII (rFVIIa) and its complexes with plasma protease inhibitors in the liver. *Thromb Res* 127(4): 356–62, 2011
228. Zollner S, Schuermann D, Raquet E, Mueller-Cohrs J, Weimer T, Pragst I, Dickneite G, Schulte S: Pharmacological characteristics of a novel, recombinant fusion protein linking coagulation factor VIIa with albumin (rVIIa-FP). *J Thromb Haemost* 12(2): 220–8, 2014

229. Jenkins N, Castro P, Menon S, Ison A, Bull A: Effect of lipid supplements on the production and glycosylation of recombinant interferon- $\gamma$  expressed in CHO cells. In: *Cell Culture Engineering 4: Improvements of Human Health*, edited by Buckland BC, Aunins JG, Bibila TA, Dordrecht, Springer Netherlands, 1995, pp 209–215
230. Kunkel JP, Jan DCH, Jamieson JC, Butler M: Dissolved oxygen concentration in serum-free continuous culture affects N-linked glycosylation of a monoclonal antibody. *J Biotechnol* 62(1): 55–71, 1998
231. Chee Fung Wong D, Tin Kam Wong K, Tang Goh L, Kiat Heng C, Gek Sim Yap M: Impact of dynamic online fed-batch strategies on metabolism, productivity and N-glycosylation quality in CHO cell cultures. *Biotechnol Bioeng* 89(2): 164–77, 2005
232. Lefloch F, Tessier B, Chenuet S, Guillaume J-M, Cans P, Goergen J-L, Marc A: Related effects of cell adaptation to serum-free conditions on murine EPO production and glycosylation by CHO cells. *Cytotechnology* 52(1): 39–53, 2006
233. Pacis E, Yu M, Autsen J, Bayer R, Li F: Effects of cell culture conditions on antibody N-linked glycosylation--what affects high mannose 5 glycoform. *Biotechnol Bioeng* 108(10): 2348–58, 2011
234. Costa AR, Withers J, Rodrigues ME, McLoughlin N, Henriques M, Oliveira R, Rudd PM, Azeredo J: The impact of cell adaptation to serum-free conditions on the glycosylation profile of a monoclonal antibody produced by Chinese hamster ovary cells. *New biotechnology* 30(5): 563–72, 2013
235. Fan Y, Jimenez Del Val I, Müller C, Wagtberg Sen J, Rasmussen SK, Kontoravdi C, Weilguny D, Andersen MR: Amino acid and glucose metabolism in fed-batch CHO cell culture affects antibody production and glycosylation. *Biotechnol Bioeng* 112(3): 521–35, 2015
236. Gotoh M, Sato T, Kiyohara K, Kameyama A, Kikuchi N, Kwon Y-D, Ishizuka Y, Iwai T, Nakanishi H, Narimatsu H: Molecular cloning and characterization of  $\beta$ 1,4- N -acetylgalactosaminyltransferases IV synthesizing N,N'-diacetyllactosediamine 1. *FEBS Lett* 562(1-3): 134–40, 2004
237. Sato T, Gotoh M, Kiyohara K, Kameyama A, Kubota T, Kikuchi N, Ishizuka Y, Iwasaki H, Togayachi A, Kudo T, Ohkura T, Nakanishi H, Narimatsu H: Molecular cloning and characterization of a novel human beta 1,4-N-acetylgalactosaminyltransferase, beta 4GalNAc-T3, responsible for the synthesis of N,N'-diacetyllactosediamine, galNAc beta 1-4GlcNAc. *J Biol Chem* 278(48): 47534–44, 2003
238. Roth J, Berger EG: Immunocytochemical localization of galactosyltransferase in HeLa cells: codistribution with thiamine pyrophosphatase in trans-Golgi cisternae. *J Cell Biol* 93(1): 223–9, 1982
239. Rabouille C, Hui N, Hunte F, Kieckbusch R, Berger EG, Warren G, Nilsson T: Mapping the distribution of Golgi enzymes involved in the construction of complex oligosaccharides. *J Cell Sci* 108: 1617–27, 1995
240. Lucocq JM, Berger EG, Warren G: Mitotic Golgi fragments in HeLa cells and their role in the reassembly pathway. *J Cell Biol* 109(2): 463–74, 1989

241. Nilsson T, Pypaert M, Hoe MH, Slusarewicz P, Berger EG, Warren G: Overlapping distribution of two glycosyltransferases in the Golgi apparatus of HeLa cells. *J Cell Biol* 120(1): 5–13, 1993
242. Ikehara Y, Sato T, Niwa T, Nakamura S, Gotoh M, Ikehara SK, Kiyohara K, Aoki C, Iwai T, Nakanishi H, Hirabayashi J, Tatematsu M, Narimatsu H: Apical Golgi localization of N,N'-diacetyllactosylamine synthase, beta4GalNAc-T3, is responsible for LacdiNAc expression on gastric mucosa. *Glycobiology* 16(9): 777–85, 2006
243. Green ED, van Halbeek H, Boime I, Baenziger JU: Structural elucidation of the disulfated oligosaccharide from bovine lutropin. *J Biol Chem* 260(29): 15623–30, 1985
244. Baenziger JU, Green ED: Pituitary glycoprotein hormone oligosaccharides: Structure, synthesis and function of the asparagine-linked oligosaccharides on lutropin, follitropin and thyrotropin. *Biochim Biophys Acta* 947(2): 287–306, 1988
245. Bergweff AA, Thomas-Oates JE, van Oostrum J, Kamerling JP, Vliegthart JFG: Human urokinase contains GalNAc  $\beta$ (1-4)[Fuc(1-3)]GlcNAc  $\beta$ (1-2) as a novel terminal element in N-linked carbohydrate chains. *FEBS Lett* 314(3): 389–94, 1992
246. Siciliano RA, Morris HR, McDowell RA, Azadi P, Rogers ME, Bennett HP, Dell A: The Lewis x epitope is a major non-reducing structure in the sulphated N-glycans attached to Asn-65 of bovine pro-opiomelanocortin. *Glycobiology* 3(3): 225–39, 1993
247. Kubyshkin A v., Fomochkina II, Petrosyan AM: THE IMPACT OF ALCOHOL ON PRO-METASTATIC N-GLYCOSYLATION IN PROSTATE CANCER. *Krim Z Eksp Klin Med* 8(4): 11–20, 2018
248. Huang H-H, Hassinen A, Sundaram S, Spiess A-N, Kellokumpu S, Stanley P: GnT1IP-L specifically inhibits MGAT1 in the Golgi via its luminal domain. *Elife* 4, 2015
249. Roth J, Taatjes DJ, Weinstein J, Paulson JC, Greenwell P, Watkins WM: Differential subcompartmentation of terminal glycosylation in the Golgi apparatus of intestinal absorptive and goblet cells. *J Biol Chem* 261(30): 14307–12, 1986
250. Koyota S, Ikeda Y, Miyagawa S, Ihara H, Koma M, Honke K, Shirakura R, Taniguchi N: Down-regulation of the alpha-Gal epitope expression in N-glycans of swine endothelial cells by transfection with the N-acetylglucosaminyltransferase III gene. Modulation of the biosynthesis of terminal structures by a bisecting GlcNAc. *J Biol Chem* 276(35): 32867–74, 2001
251. Lu J, Isaji T, Im S, Fukuda T, Kameyama A, Gu J: Expression of N-Acetylglucosaminyltransferase III Suppresses  $\alpha$ 2,3-Sialylation, and Its Distinctive Functions in Cell Migration Are Attributed to  $\alpha$ 2,6-Sialylation Levels. *J Biol Chem* 291(11): 5708–20, 2016
252. Nakano M, Mishra SK, Tokoro Y, Sato K, Nakajima K, Yamaguchi Y, Taniguchi N, Kizuka Y: Bisecting GlcNAc Is a General Suppressor of Terminal Modification of N-glycan. *Mol Cell Proteomics* 18(10): 2044–57, 2019
253. Narimatsu Y, Joshi HJ, Nason R, van Coillie J, Karlsson R, Sun L, Ye Z, Chen Y-H, Schjoldager KT, Steentoft C, Furukawa S, Bensing BA, Sullam PM, Thompson AJ, Paulson JC, Büll C, Adema GJ, Mandel U, Hansen L, Bennett EP, Varki A, Vakhrushev SY, Yang Z, Clausen H: An Atlas of Human Glycosylation Pathways Enables Display of the Human Glycome by Gene Engineered Cells. *Mol Cell* 75(2): 394-407.e5, 2019

254. Kumar R, Potvin B, Muller WA, Stanley P: Cloning of a human alpha(1,3)-fucosyltransferase gene that encodes ELFT but does not confer ELAM-1 recognition on Chinese hamster ovary cell transfectants. *J Biol Chem* 266(32): 21777–83, 1991
255. Sherwood AL, Upchurch DA, Stroud MR, Davis WC, Holmes EH: A highly conserved His-His motif present in alpha1--3/4fucosyltransferases is required for optimal activity and functions in acceptor binding. *Glycobiology* 12(10): 599–606, 2002
256. Toivonen S, Nishihara S, Narimatsu H, Renkonen O, Renkonen R: Fuc-TIX: a versatile alpha1,3-fucosyltransferase with a distinct acceptor- and site-specificity profile. *Glycobiology* 12(6): 361–8, 2002
257. Mollicone R, Moore SEH, Bovin N, Garcia-Rosasco M, Candelier J-J, Martinez-Duncker I, Oriol R: Activity, splice variants, conserved peptide motifs, and phylogeny of two new alpha1,3-fucosyltransferase families (FUT10 and FUT11). *J Biol Chem* 284(7): 4723–38, 2009
258. Paulson JC, Prieels JP, Glasgow LR, Hill RL: Sialyl- and fucosyltransferases in the biosynthesis of asparaginyl-linked oligosaccharides in glycoproteins. Mutually exclusive glycosylation by beta-galactoside alpha2 goes to 6 sialyltransferase and N-acetylglucosaminide alpha1 goes to 3 fucosyltransferase. *J Biol Chem* 253(16): 5617–24, 1978
259. Sewell R, Bäckström M, Dalziel M, Gschmeissner S, Karlsson H, Noll T, Gätgens J, Clausen H, Hansson GC, Burchell J, Taylor-Papadimitriou J: The ST6GalNAc-I sialyltransferase localizes throughout the Golgi and is responsible for the synthesis of the tumor-associated sialyl-Tn O-glycan in human breast cancer. *J Biol Chem* 281(6): 3586–94, 2006
260. Liu Y, Beyer A, Aebersold R: On the Dependency of Cellular Protein Levels on mRNA Abundance. *Cell* 165(3): 535–50, 2016
261. Huang G, Li Z, Li Y, Liu G, Sun S, Gu J, Kameyama A, Li W, Dong W: Loss of core fucosylation in both ST6GAL1 and its substrate enhances glycoprotein sialylation in mice. *Biochem J* 477(6): 1179–201, 2020
262. Jones MB, Teng H, Rhee JK, Lahar N, Baskaran G, Yarema KJ: Characterization of the cellular uptake and metabolic conversion of acetylated N-acetylmannosamine (ManNAc) analogues to sialic acids. *Biotechnol Bioeng* 85(4): 394–405, 2004
263. Keppler OT, Horstkorte R, Pawlita M, Schmidt C, Reutter W: Biochemical engineering of the N-acyl side chain of sialic acid: biological implications. *Glycobiology* 11(2): 11R-18R, 2001
264. Bork K, Horstkorte R, Weidemann W: Increasing the sialylation of therapeutic glycoproteins: The potential of the sialic acid biosynthetic pathway. *J Pharm Sci* 98(10): 3499–508, 2009
265. Kim EJ, Sampathkumar S-G, Jones MB, Rhee JK, Baskaran G, Goon S, Yarema KJ: Characterization of the metabolic flux and apoptotic effects of O-hydroxyl- and N-acyl-modified N-acetylmannosamine analogs in Jurkat cells. *J Biol Chem* 279(18): 18342–52, 2004
266. Food and Drug Administration: *GUIDANCE FOR INDUSTRY FOR THE SUBMISSION OF CHEMISTRY, MANUFACTURING, AND CONTROLS INFORMATION FOR A THERAPEUTIC RECOMBINANT DNA-DERIVED PRODUCT OR A MONOCLONAL ANTIBODY PRODUCT FOR IN VIVO USE*, 1996, Online: <https://www.fda.gov/media/77528/download>, Accessed: 2021
267. Pontow SE, Kery V, Stahl PD: Mannose Receptor. *Int Rev Cytol* 137, Part B: 221–44, 1993



268. Park EI, Manzella SM, Baenziger JU: Rapid clearance of sialylated glycoproteins by the asialoglycoprotein receptor. *J Biol Chem* 278(7): 4597–602, 2003
269. Park EI, Mi Y, Unverzagt C, Gabius H-J, Baenziger JU: The asialoglycoprotein receptor clears glycoconjugates terminating with sialic acid alpha 2,6GalNAc. *Proc Natl Acad Sci U S A* 102(47): 17125–9, 2005
270. André S, Unverzagt C, Kojima S, Dong X, Fink C, Kayser K, Gabius HJ: Neoglycoproteins with the synthetic complex biantennary nonasaccharide or its alpha 2,3/alpha 2,6-sialylated derivatives: their preparation, assessment of their ligand properties for purified lectins, for tumor cells in vitro, and in tissue sections, and their biodistribution in tumor-bearing mice. *Bioconjug Chem* 8(6): 845–55, 1997
271. André S, Unverzagt C, Kojima S, Frank M, Seifert J, Fink C, Kayser K, Lieth C-W von der, Gabius H-J: Determination of modulation of ligand properties of synthetic complex-type biantennary N-glycans by introduction of bisecting GlcNAc in silico, in vitro and in vivo. *Eur J Biochem* 271(1): 118–34, 2004
272. Unverzagt C, André S, Seifert J, Kojima S, Fink C, Srikrishna G, Freeze H, Kayser K, Gabius H-J: Structure–Activity Profiles of Complex Biantennary Glycans with Core Fucosylation and with/without Additional  $\alpha$ 2,3/ $\alpha$ 2,6 Sialylation: Synthesis of Neoglycoproteins and Their Properties in Lectin Assays, Cell Binding, and Organ Uptake †. *J Med Chem* 45(2): 478–91, 2002
273. Steirer LM, Park EI, Townsend RR, Baenziger JU: The asialoglycoprotein receptor regulates levels of plasma glycoproteins terminating with sialic acid alpha2,6-galactose. *J Biol Chem* 284(6): 3777–83, 2009
274. Spiess M, Lodish HF: Sequence of a second human asialoglycoprotein receptor: conservation of two receptor genes during evolution. *Proc Natl Acad Sci U S A* 82(19): 6465–9, 1985
275. Harris N, Super M, Rits M, Chang G, Ezekowitz RA: Characterization of the murine macrophage mannose receptor: demonstration that the downregulation of receptor expression mediated by interferon-gamma occurs at the level of transcription. *Blood* 80(9): 2363–73, 1992
276. Su Y, Bakker T, Harris J, Tsang C, Brown GD, Wormald MR, Gordon S, Dwek RA, Rudd PM, Martinez-Pomares L: Glycosylation influences the lectin activities of the macrophage mannose receptor. *J Biol Chem* 280(38): 32811–20, 2005
277. Park EI, Baenziger JU: Closely related mammals have distinct asialoglycoprotein receptor carbohydrate specificities. *J Biol Chem* 279(39): 40954–9, 2004
278. Martinez-Pomares L, Hanitsch LG, Stillion R, Keshav S, Gordon S: Expression of mannose receptor and ligands for its cysteine-rich domain in venous sinuses of human spleen. *Lab Invest* 85(10): 1238–49, 2005
279. Taylor ME, Drickamer K: Mammalian sugar-binding receptors: known functions and unexplored roles. *FEBS J* 286(10): 1800–14, 2019
280. Luo C, Chen S, Xu N, Wang C, Sai WB, Zhao W, Li YC, Hu XJ, Tian H, Gao XD, Yao WB: Glycoengineering of pertuzumab and its impact on the pharmacokinetic/pharmacodynamic properties. *Sci Rep* 7: 46347, 2017

281. Lee YC, Townsend RR, Hardy MR, Lönngrén J, Arnarp J, Haraldsson M, Lönn H: Binding of synthetic oligosaccharides to the hepatic Gal/GalNAc lectin. Dependence on fine structural features. *J Biol Chem* 258(1): 199–202, 1983
282. Weis WI, Drickamer K, Hendrickson WA: Structure of a C-type mannose-binding protein complexed with an oligosaccharide. *Nature* 360(6400): 127–34, 1992
283. Taylor ME, Drickamer K: Structural requirements for high affinity binding of complex ligands by the macrophage mannose receptor. *J Biol Chem* 268(1): 399–404, 1993
284. Roseman DS, Baenziger JU: The mannose/N-acetylgalactosamine-4-SO<sub>4</sub> receptor displays greater specificity for multivalent than monovalent ligands. *J Biol Chem* 276(20): 17052–7, 2001

**Parts of this dissertation were published in the following publication:**

224. Uhler R, Popa-Wagner R, Kröning M, Brehm A, Rennert P, Seifried A, Peschke M, Krieger M, Kohla G, Kannicht C, Wiedemann P, Hafner M, Rosenlöcher J: Glyco-engineered HEK 293-F cell lines for the production of therapeutic glycoproteins with human N-glycosylation and improved pharmacokinetics. *Glycobiology*, 2021, doi: 1093/glycob/cwaa119

## 9 ACKNOWLEDGEMENTS

I am most grateful to Prof. Dr. Mathias Hafner and Prof. Dr. Philipp Wiedemann for the opportunity to perform my doctoral thesis within the framework of the cooperation between the University of Heidelberg and the University of Applied Sciences Mannheim and for their support throughout the project.

I am also most grateful to Dr. Christoph Kannicht, Dr. Tobias Stuwe, Dr. Guido Kohla, and Dr. Maya Tiemeyer for the opportunity to work on this important and interesting project in collaboration with Octapharma Biopharmaceuticals.

I would like to express my very great appreciation to Dr. Julia Rosenlöcher, and especially Dr. Ruth Wagner for their outstanding scientific but also personal guidance and support in all facets of my doctoral thesis.

Assistance provided by Claudine Fisseau, Mario Kröning, Dr. Anja Brehm, and Dr. Paul Rennert with the glycan analytic and receptor binding experiments, and by Cathleen Wegmann, Melina Bitsch, Ulrike Bolz, Dr. Philipp Scheller, and Dr. Marko Kirtz with plasmid cloning, cell line generation and protein production is greatly appreciated.

I thank Ulrike Noller, Thomas Orlik, Marius Lechner, Julia Kaim, Janine Wöhlk, Dr. Annegrit Seifried, Dr. Madeleine Peschke, Dr. Tilo Schwientek, Dr. Lawrence Trawnicek, Dr. Barbara Solecka-Witulska, and Dr. Ronny Schmidt for providing me with the data of the PK rat experiment.

I would like to offer my special thanks to Dr. Markus Krieger for critically reviewing the manuscript and expanding my verbal skills through elaborate and often very entertaining commentary. I promise I will never again use the conjunctions *and* and *so* in conjunction.